Title

The Effect of Ethanol Addition to Gasoline on Low- and Intermediate-Temperature Heat Release under Boosted Conditions in Kinetically Controlled Engines

Author

Vuilleumier, David Malcolm

Publication Date

2016

Peer reviewed|Thesis/dissertation

The Effect of Ethanol Addition to Gasoline on Low- and Intermediate-Temperature Heat Release under Boosted Conditions in Kinetically Controlled Engines

By

David Malcolm Vuilleumier

A dissertation submitted in partial satisfaction of the

requirements for the degree of

Doctor of Philosophy

in

Engineering – Mechanical Engineering

in the

Graduate Division

of the

University of California, Berkeley

Committee in charge:

Professor Jyh-Yuan Chen, Chair

Professor Carlos Fernandez-Pello

Professor Enrique Iglesia

Summer 2016

Abstract

The Effect of Ethanol Addition to Gasoline on Low- and Intermediate-Temperature Heat Release under Boosted Conditions in Kinetically Controlled Engines

by

David Malcolm Vuilleumier

Doctor of Philosophy in Mechanical Engineering

University of California, Berkeley

Professor Jyh-Yuan Chen, Chair

The detailed study of chemical kinetics in engines has become required to further advance engine efficiency while simultaneously lowering engine emissions. This push for higher efficiency engines is not caused by a lack of oil, but by efforts to reduce anthropogenic carbon dioxide emissions, that cause global warming.

To operate in more efficient manners while reducing traditional pollutant emissions, modern internal combustion piston engines are forced to operate in regimes in which combustion is no longer fully transport limited, and instead is at least partially governed by chemical kinetics of combusting mixtures. Kinetically-controlled combustion allows the operation of piston engines at high compression ratios, with partially-premixed dilute charges; these operating conditions simultaneously provide high thermodynamic efficiency and low pollutant formation.

The investigations presented in this dissertation study the effect of ethanol addition on the low-temperature chemistry of gasoline type fuels in engines. These investigations are carried out both in a simplified, fundamental engine experiment, named Homogeneous Charge Compression Ignition, as well as in more applied engine systems, named Gasoline Compression Ignition engines and Partial Fuel Stratification engines. These experimental investigations, and the accompanying modeling work, show that ethanol is an effective scavenger of radicals at low temperatures, and this inhibits the low temperature pathways of gasoline oxidation. Further, the investigations measure the sensitivity of gasoline auto-ignition to system pressure at conditions that are relevant to modern engines. It is shown that at pressures above 40 bar and temperatures below 850 Kelvin, gasoline begins to exhibit Low-Temperature Heat Release. However, the addition of 20% ethanol raises the pressure requirement to 60 bar, while the temperature requirement remains unchanged.

These findings have major implications for a range of modern engines. Low-Temperature Heat Release significantly enhances the auto-ignition process, which limits the conditions under which advanced combustion strategies may operate. As these advanced combustion strategies are required to meet emissions and fuel-economy regulations, the findings of this dissertation may benefit and be incorporated into future engine design toolkits, such as detailed chemical kinetic mechanisms.

Dedication

This dissertation is dedicated to my family. First, to my mother, Beate, who instilled in me a love of learning. Second, to my father, Roger, who nurtured my curiosity for all things mechanical. Third, to my sister, Natalie, who inspires creativity when approaching problems. Finally, to my fiancée, Sarah, whose shining example has led my way.

Table of Contents

Chapter 1:

Perspectives on Combustion in the 21st Century and the continued need for studying Fuel-Engine interactions

I. Traditional Pollutants, Carbon Dioxide Emissions, and Global Warming:

The casual observer, after reading this dissertation, may question why this line of investigations has not previously been carried out, considering that internal combustion piston engines have been used for well over a century. Simply put, carbon dioxide emissions are the only reason we are now considering the problems of high-pressure, kinetically-controlled combustion. Prior to global interest in global warming, low-cost engines could be produced which achieved high load with low traditional emissions, with the only blemish on their records being compromised fuel economy. Now, regulations have forced interest in maintaining low traditional pollutant emissions, coupled with high power density and high efficiency, and this has led us to revisit many topics that were neglected through the last period of automotive malaise (e.g. 1980 – 2005).

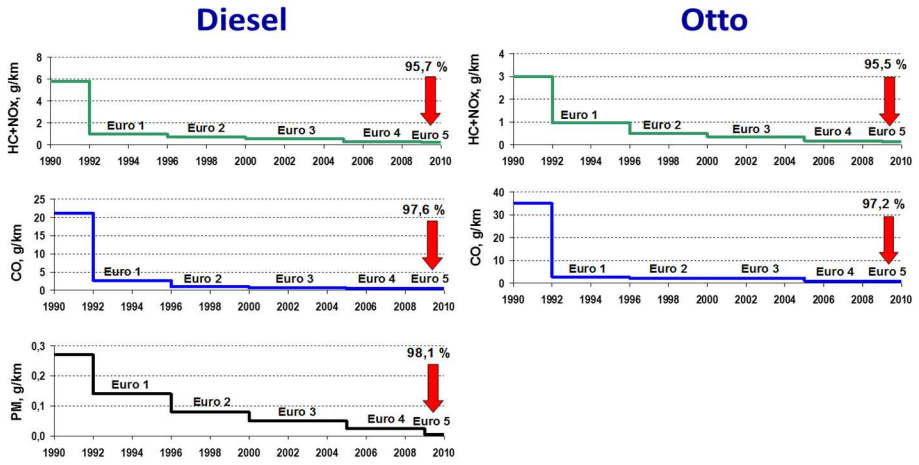

Figure 1.1: Emissions from diesel and spark-ignition vehicles at various stages of regulation, reprinted from [Mahalec 2013].

Emissions from automotive internal combustion engines were first regulated in 1961 when California mandated the use of positive crankcase ventilation to prevent blow-by gasses from reaching the atmosphere [CARB, 2016]. At this point and time, the primary vehicle emissions that regulators were concerned about were carbon monoxide (CO), particulate matter (PM), unburned hydrocarbons (UHC), sulfur dioxide (SO_2), and nitrogen dioxide (NO_2). Over the following fifty years, the automotive industry became highly skilled in reducing these emissions, first through changes made to the combustion process and later through the addition of catalytic processes to the exhaust system of automobiles. As seen in Figure 1.1, a modern vehicle will produce on the order of 5% of the emissions of an unregulated vehicle – and this has allowed a simultaneous increase in the number of automobiles as well as in the air quality [Mahalec 2013].

However, while traditional pollutants have been reduced to a small fraction of their previous values (on a mass/distance traveled basis), a new pollutant – anthropogenic carbon dioxide (CO_2) -- has triggered renewed focus on automobile emissions. A large body of evidence has reaffirmed the hypothesis that average global temperatures are rising due to the greenhouse effect, which is enhanced by the release of anthropogenic CO_2 into the atmosphere [IPCC 2014]. This is to say that the carbon cycle, in which CO_2 is consumed during photosynthesis, and then produced during the decomposition of plant matter, is not the problem. Instead, the problem lies in the extraction, combustion, and release of carbon that has been sequestered in the earth's crust [Smit 2014]. This carbon is typically in the form of petroleum, natural gas, or coal; after extraction the molecules are primarily used as fuel for combustion engines, either for stationary power generation or for transportation.

Transportation is a major source of CO_2 emissions, accounting for 23% of global CO_2 emissions in 2012 [IEA 2013]. Within transportation, approximately 75% of emissions come from over-the-road vehicles. Thus, with a global desire to reduce CO_2 emissions, transportation is a logical sector to tackle. This is especially pertinent due to the rapid industrialization of the developing world, which has resulted in the increased production of new vehicles, now totaling approximately 90 million vehicles per year [OICA 2016].

The reduction of CO_2 emissions from transportation can reasonably be achieved through at least two separate approaches. The first approach is to improve the fuel economy of vehicles. This can be achieved through increases in internal combustion engine efficiency, reduction of vehicle mass, electrification, or other similar strategies. These have been the primary approaches taken to meet the US CAFE regulations [NHTSA 2016], which are indirect regulations limiting carbon dioxide emissions from vehicles. The second approach to lowering overall vehicle CO_2 emissions is to lower the anthropogenic component of carbon in the fuel that the vehicle burns. This can be done in a number of ways. The most practiced method is to use biomass to create fuels; thus, the fuel is comprised solely of carbon that already was in the carbon cycle. An alternative method is to use renewable-derived electricity to synthesize a fuel, such as synthesizing molecular hydrogen from water via electrolysis. Yet another method is to produce hydrogen from fossil fuels via the syngas process and then sequester the CO_2.

It may be a useful thought experiment to attempt to assess which of the two pathways is a more effective method of reducing anthropogenic CO_2 emissions from transportation vehicles. Theoretically, lowering a fuel's anthropogenic carbon content has an overall greater potential to lower anthropogenic CO_2 emissions than increasing combustion or vehicle efficiency, as there is no fundamental limit on the amount that anthropogenic carbon can be removed from fuels, whereas this is not the case for combustion or vehicle efficiency. However, practically, it is so far difficult to produce the amount of fuel required globally without emitting anthropogenic carbon [Patzek 2005]. In the case of fuel production from biomass, photosynthetic efficiencies of on average 1% limit the total amount of energy that can be captured from the sun without devoting all arable land on the planet to producing fuel. However, reasonable fractions of biofuels can and are being produced; as of 2016, 10% of the gasoline sold in the U.S. was comprised of ethanol [EIA 2016]. However, even accounting for only 10% of the U.S. demand for gasoline, ethanol production has not been achieved without unintended consequences, such as globally shifting land use and deforestation, and detailed carbon counting must be performed to assess the real reduction in greenhouse gas emissions [Patzek 2005]. Alternatively, carbon sequestration may allow for fossil

fuels to be used without releasing anthropogenic CO_2, but no large-scale demonstration of this concept has been performed [Smit 2014].

Considering the problems of CO_2 and traditional pollutant emissions from transportation vehicles, the research in this dissertation contributes both to the improvement of combustion engine efficiency as well as the use of low-carbon fuels. This dissertation examines fuel-engine interactions that can enable or inhibit engine efficiency, as well as the effect of ethanol on gasoline-type fuels, and the subsequent effects on engine operation. These topics will be discussed in much greater detail in Sections VII and IX.

II. Convergence of Spark-Ignition and Diesel Engines:

a) Spark-Ignition Engines

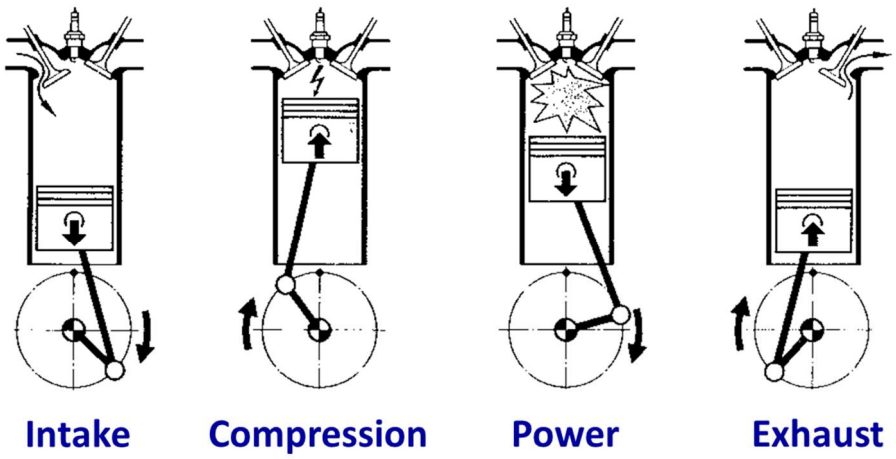

Figure 1.2: A schematic of the four strokes of the four-cycle Otto engine, reprinted from [Mahalec 2013].

Spark-Ignition (SI) engines, also known as Otto engines, are among the earliest form of internal-combustion piston engines, being developed by Etienne Lenoir in 1859 [Georgano 1985]. These engines burn a reasonably stoichiometric and homogeneous mixture of fuel and air via the propagation of a flame through the combustion chamber. This flame oxidizes the fuel, releasing the fuel's chemical energy, raising the temperature and thus the pressure of the system. The system pressure acts upon a moving surface, the piston, which is then converted from pressure-volume work into mechanical work. The SI engine's thermodynamic cycle is described by the Otto Cycle, and the stages of this cycle may be seen in Figure 1.2. Crucially, the Otto Cycle ideal thermodynamic efficiency is given by Eq. (**1.1**), where CR is the compression ratio, defined in

and raising the ratio of specific heats. Both of these parameters have some practical limits, as the increased efficiency is derived from higher compressed temperatures. In the case of SI engines, these higher temperatures lead to end-gas auto-ignition, which will be discussed further in the following paragraph [Heywood].

$$\eta_{thermodynamic} = 1 - \frac{1}{CR^{\gamma-1}} \qquad \textbf{Eq. (1.1)}$$

$$CR = \frac{V_1}{V_2} \qquad \textbf{Eq. (1.2)}$$

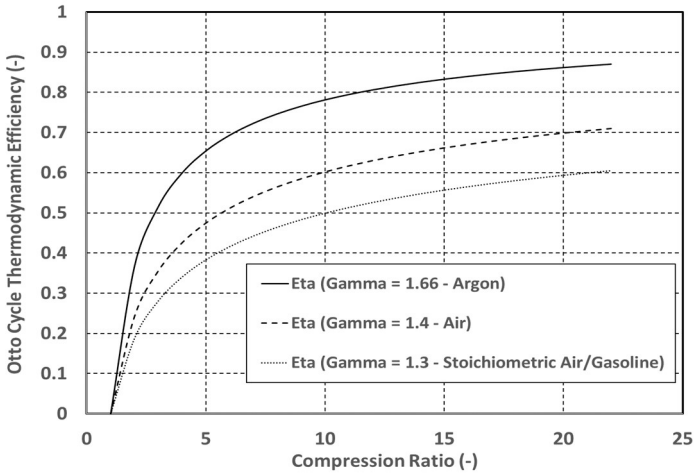

Figure 1.3: Thermodynamic efficiencies of the Otto Cycle for various combinations of Compression Ratio and specific heat ratio.

In practice, the SI engine burns a mixture that is near stoichiometric because this is required to effectively propagate a flame through a fuel-air mixture. Figure 1.4 illustrates this concept, showing that equivalence ratios near unity yield the highest flame propagation speeds, while significantly rich or lean mixtures result either in mixtures through which a flame is not able to propagate, or flame speeds less than half of those produced at stoichiometric conditions. The mixture is traditionally homogeneous, as this allows for simple methods of metering fuel into the system (via carburation, or later port-fuel-injection), as well as helping flame propagation. The power of the engine is modulated both through engine speed, as well as through throttling of the intake air mass. Throttling lowers the pressure, and consequently mass, of air and fuel at the beginning of the compression stroke, and this reduces the amount of chemical energy released during combustion. However, throttling results in the piston having to overcome a restriction during the intake stroke, and results in negative pressure-volume work, which reduces the efficiency of the engine; thus, throttling is undesirable.

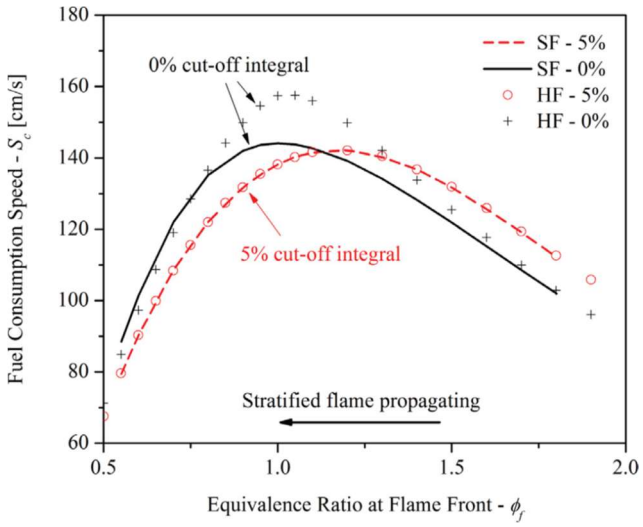

Figure 1.4: Predicted flame speeds versus equivalence ratio for homogeneous and stratified hydrogen-air flames, reprinted from [Shi 2016].

Returning attention to Eq. (**1.1**), it may be seen that two paths to raising the ideal efficiency of the system are available, and these paths are raising the compression ratio of the engine, or raising the specific heat ratio of the working fluid. The reason both of these changes raise the efficiency of the engine is that they both raise the temperature at the end of the compression stroke, allowing heat input to the system at a higher temperature. However, in the SI engine, raising the temperature at the end of the compression stroke is limited by fuel auto-ignition, which is referred to as "knocking." As discussed in Section V, fuel-oxidizer mixtures will auto-ignite if given sufficient residence time. By raising the system temperature, the residence time requirement for auto-ignition is shortened, and this induces knocking, which can be destructive to the engine. Thus, the efficiency of the SI engine is fundamentally limited by knocking.

As the SI engine is limited by knocking, but is still widely used, a great deal of research has been conducted on how to mitigate this problem, primarily with regards to the physical system. However, it must be noted that fuel chemistry has a large effect on auto-ignition, though this avenue of research has largely been ignored by the community since the removal of tetra-ethyl lead from gasoline in the 1970's, due to the focus on reducing traditional pollutants rather than raising thermodynamic efficiency. These goals, in the case of SI engines, may conflict with one another, as two of the key pollutants generated by the SI engine are oxides of nitrogen (NO and NO_2, abbreviated NO_x), which are produced through the thermal route. Therefore, as the compression ratio of the SI engine is increased, the peak cylinder temperature also increases, which will result in greater NO_x production during the closed cycle. A second primary research focus in SI engines is methods to avoid throttling the intake charge. The techniques developed to address these two major sources of inefficiency have driven SI engine development over the past two decades, and have resulted in three primary changes in the way an SI engine is constructed and operated.

First, SI engines have shifted the injection of fuel from the intake tract to the combustion chamber, in an effort to use the fuel latent heat of vaporization to cool the fuel-air mixture prior to the compression stroke. When the fuel is injected in the intake tract, a significant fraction of the fuel evaporates on a surface, and this draws the latent heat from this surface rather than from the

intake charge. By directly injecting the fuel into the open combustion chamber, the fuel evaporates while suspended in the oxidizer, lowering the charge temperature significantly. This reduction of temperature carries through the compression stroke and reduces knocking tendencies.

Second, SI engines are now commonly turbocharged, in an effort to limit throttling of the intake charge. Turbocharging is the act of compressing the incoming charge to increase the mass flow rate through the engine. The compression work is derived from waste exhaust enthalpy which is run through a turbine. Turbocharging allows the construction of a smaller engine for a given power level. With this smaller engine, throttling is reduced, and power modulation is effected via the level of turbocharging that is used.

Third, SI engines now commonly shift combustion late in the cycle to avoid knocking. As combustion is retarded relative to Top Dead Center (TDC), the peak temperature that the end-gas experiences decreases. This shift in combustion phasing is effected by altering the point at which the spark is triggered during the cycle. While shifting combustion phasing later in the cycle decreases efficiency, it is part of a broader overall strategy to increase efficiency, which is carried out in the following manner. Prior to two decades ago feedback control systems were limited to ensuring a stoichiometric mixture, and engine calibration and design was carried out with the requirement that the engine operate sufficiently far away from the knocking limit such that conditions were "safe," now engines can be designed to be operated at the knocking limit at all times, by the advent of sensors which measure knocking intensity and control algorithms which avoid it. This has allowed automakers to design engines with very high compression ratios, but which use combustion phasing retard to avoid knock under low-speed and high-load conditions which would have previously prohibited such a design. Thus, engines are designed with the knowledge that they are rarely called upon to provide full load, and most of their time is spent at part-load conditions, where higher compression ratios may be tolerated.

The implications for the three fundamental shifts in SI engine design is that SI engines now operate at higher pressures, lower temperatures, and with fuel-air charges that are less well-mixed. These changes have pushed SI engines closer to diesel engines in their design and operation and have impacts on how fuels are rated for SI engines, as discussed in Section IV.

b) Diesel Engines

The diesel engine is a widely used form of internal combustion engine, and in many respects similar to the SI engine. Where the diesel engine differs from the SI engine is the method in which fuel is introduced into the system and subsequently combusted. While the SI engine uses a premixed fuel-oxidizer charge which is then ignited at a single point by a spark plug, a diesel engine directly injects fuel into the combustion chamber, which then mixes with oxidizer, auto-ignites, and burns. Whereas in the SI engine the rate of combustion is determined by the rate of flame propagation, in the diesel engine combustion is limited by the rate of mixing between fuel and oxidizer. This is due to both the fuel used in diesel engines, which is highly reactive but of low volatility, and the conditions into which this fuel is injected, which are high ambient temperatures (> 850 K) and pressures (> 40 bar). Thus, as the fuel is injected, evaporates, and mixes with oxidizer, the chemical timescale is small relative to the physical timescale of the system.

The diesel engine is typically much more efficient than the SI engine for two reasons. The first reason is that because auto-ignition is required, rather than avoided, high compression ratios can be used, which raise the thermodynamic efficiency of the cycle, as seen in Eq. (**1.1** (note that for modern diesel engines the Otto Cycle now better reflects the diesel combustion process than the Diesel Cycle). Secondly, diesel engines do not require globally stoichiometric mixtures for operation, and so when partial load is required, less fuel is injected, but throttling is not applied to the intake air. By nearly eliminating pumping losses at part-load operation, the diesel engine becomes significantly more efficient than the SI engine under most operating conditions.

However, while the diesel engine is renowned for high efficiency due to the reasons discussed in the previous paragraph, it is also renowned for high emissions of NO_2 and PM [Heywood]. This is because in the diesel combustion process the fuel auto-ignites before it has fully mixed with oxidizer, leaving a "rich" mixture (excess fuel) at high temperatures, which forms soot. As further mixing occurs, the excess fuel is oxidized, but the high temperatures that are reached form NO_2 via the Zeldovich mechanism [Zeldovich]. A conceptual model of this process is depicted in Figure 1.5, which depicts the liquid diesel fuel jet emanating from the injector, the rich burn region, which is colored light-blue, the main soot formation region, in yellow, and the stoichiometric burning contour, in orange.

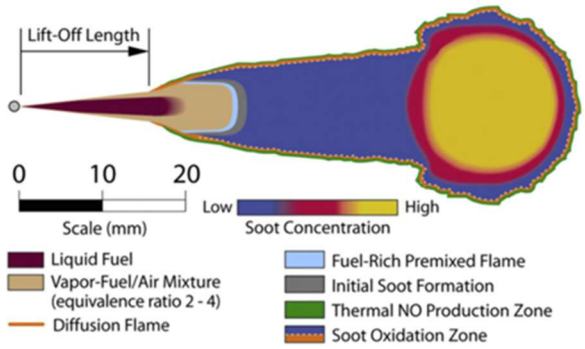

Figure 1.5: Conceptual model of diesel combustion, copied from Dec et. al. [Dec 1997].

Significant effort has been invested into reducing the formation of pollutants during the diesel combustion process. This has overshadowed efforts to improve diesel engine thermodynamic efficiency, as this efficiency is already typically quite high (approximately 44%) [Johanson 2016]. The efforts to reduce traditional pollutants have focused nearly exclusively on increasing the level of mixing between fuel and oxidizer prior to auto-ignition, in an effort to reduce both PM and NO_2 formation. There have been two primary avenues to achieve this. The first is through lowering the concentration of oxygen in the oxidizer by recycling exhaust gases; this process is termed exhaust gas recirculation (EGR). By reducing oxygen concentration, peak combustion temperatures are lowered, avoiding the formation of NO_2 [Heywood]. The second avenue has been to increase the fuel injection pressure, thereby increasing the velocity of the injected fuel, and increasing the mixing rate through additional shear and additional air entrainment into the turbulent jet [Heywood]. Increased fuel injection pressure has reduced the mixing time scale to the same order of magnitude as the chemical time scale, and allowed for more fuel premixing prior to ignition. The convergence of the mixing time scale and chemical time

scales have made the study and understanding of fuel oxidation and pyrolysis kinetics important in the design and research of diesel engines. In summary, the two primary methods of investigation into reducing diesel pollutant formation have brought the diesel engine closer to the SI engine, by creating a less heterogeneous mixture prior to the start of combustion.

III. Advanced Combustion Engines:

a) Homogeneous Charge Compression Ignition Engines

In addition to the research directed at SI and diesel engines, which has generally aimed at incremental improvement, a number of alternative combustion modes have been investigated, and these are termed Advanced Combustion Engines (ACE's). ACE's are often fully or partially kinetically-controlled. This means that fluid dynamics (either in the form of flame propagation in an SI engine or fuel-oxidizer mixing in a diesel engine) are not the dominant factor in auto-igniting the fuel-oxidizer mixture and controlling combustion phasing. Homogeneous Charge Compression Ignition (HCCI) engines take this concept to an extreme, by using a fully premixed charge that is compressed to the point of auto-ignition [Najt 1983]. The chemical kinetics that govern this auto-ignition process, discussed in Section V, determine at which point in the cycle the fuel-oxidizer mixture will auto-ignite, which is referred to as the combustion phasing. As there is only a narrow window of combustion phasings that are both safe and efficient, this process must be controlled via temperature, pressure, fuel concentration, or oxidizer concentration. Thus, the majority of research on HCCI engines has focused on methods to alter combustion phasing [Yao 2008].

The HCCI combustion process is in many respects similar to knocking in an SI engine. In both cases, a relatively homogeneous charge is compressed to the point of auto-ignition. To avoid the destructive pressure-oscillations that result from knocking, HCCI engines must utilize highly dilute charges [Saxena 2014]. However, being limited to dilute charges limits the maximum load of these engines. In order to achieve practical load levels, HCCI engines have been run with intake charge boosting systems, similar to diesel and SI engines [Saxena 2012]. However, this has been shown to have significant effects on the auto-ignition kinetics that are not fully understood or captured by current chemical kinetic mechanisms, and discussed in Section V. b) [Wolk 2015].

b) Partial Fuel Stratification in HCCI Engines

HCCI engines were quickly found to present problems achieving high-load operation [Saxena 2014]. This is due to their homogeneous nature; as the mixture is relatively homogeneous, the combustion occurs rapidly, typically over the span of 10 crank-angle degrees or less, or approximately 1.4 ms at 1200 RPM. While the homogenous charge and rapid combustion have significant benefits with regards to emissions and efficiency, this also rapidly releases the fuel's chemical energy into the working fluid, and if too much energy is added quickly, this causes destructive pressure oscillations termed ringing [Eng 2002].

$$\phi = \frac{Actual\ fuel\ mass}{Stoichiometric\ fuel\ mass} \qquad \textbf{Eq. 1.3}$$

A promising method to avoid ringing in HCCI engines is termed partial fuel stratification (PFS). This combustion mode is similar to HCCI in that it is fully kinetically-controlled, however

rather than using a fully homogeneous fuel distribution, a low level of stratification ($\phi = 0.4 \sim 0.65$, defined in

However, for PFS to function as an engine operating strategy, fuels must create a charge that ***sequentially*** auto-ignites. For sequential auto-ignition to occur, a fuel must exhibit low-temperature heat release under the chosen conditions of operation [Wolk 2014]. Fuels that do not exhibit low-temperature heat release under the chosen operating conditions will instead ignite uniformly, as the richer regions of the charge will be cooler than the leaner regions, due to a lower specific heat ratio of the fuel-oxidizer mixture in these regions, and the lower temperatures of the locally rich regions will essentially balance their higher fuel concentrations, creating a reactivity gradient with relatively equal weighting (on a per-mass basis) throughout [Wolk 2014].

REF

c) Gasoline Compression Ignition Engines

_Ref447356682 \h

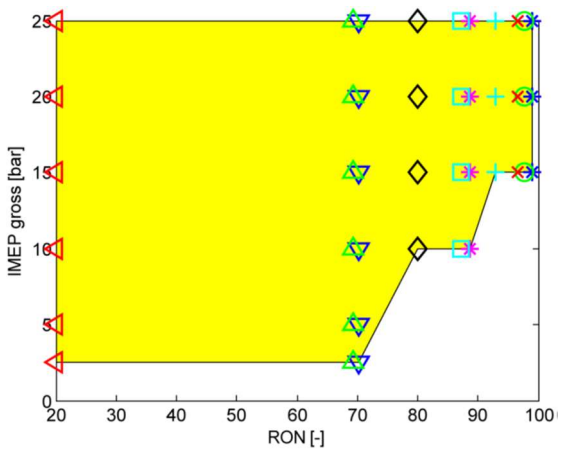

Figure 1.6: Load range of a Partially Premixed Combustion engine run with fuels of different RON levels, reprinted from [Borgqvist 2012].

Gasoline Compression Ignition (GCI) is an alternative form of low-temperature combustion to HCCI [Kalghatgi 2007]. GCI is similar to partial fuel stratification (PFS); it is primarily kinetically-controlled, though some mixing-controlled combustion may be present at high loads. The primary difference between PFS and GCI is the level of fuel stratification. While PFS strives to keep peak equivalence ratios below ~0.65, as this will prevent the formation of NO_2 and PM, GCI uses equivalence ratios up to ~2, which will form NO_2, but not PM. A primary benefit of allowing richer regions within the combustion chamber is the peak rates of heat release are further decreased, allowing higher loads without ringing. Equally important is that by allowing a wider range of equivalence ratios, control over combustion phasing may be achieved without requiring precise control of intake temperature, unlike HCCI or PFS engines.

\primary MECHANISM FOR GCI

One of the key challenges facing implementation of GCI engines is load range using existing fuels. Figure 1.6 plots the experimentally obtained load range using a GCI combustion strategy for a range of fuels spanning the octane scale. This figure indicates that high-octane fuels,

which are available commercially, create difficulties for a GCI engine attempting to reach low loads. Investigations into this topic have been made in [Kolodziej 2015], [Sellnau 2012], [Chang 2012], and [Borgqvist 2012]. Strategies to achieve lower loads have been demonstrated, including intake charge boosting (though this may require the use of a supercharger, rather than a turbocharger, due to the low exhaust enthalpy at low loads), injection strategy, exhaust rebreathing, and intake charge heating. However, these investigations have generally been approached from an engineering standpoint rather than a scientific one, and thus an understanding of the governing physics at these conditions is lacking from the literature. This topic is discussed further in Section VII. d), and is investigated both via experimentation and simulations in Chapter 5, which combines both empirical observations with theory to describe how fuel chemistry limits low-load GCI performance, and how fuel testing may be correctly used to predict low-load performance of gasoline-type fuels.

d) Low-Temperature Combustion Diesel Engines

In addition to the advanced combustion engine strategies discussed in the last three sections, yet another approach to low-temperature combustion is termed Low-Temperature Combustion (LTC) Diesel [Musculus 2013]. LTC Diesel is an operating strategy in which diesel fuel is injected into the combustion chamber well in advance of typical diesel combustion. This allows the fuel and oxidizer significantly more premixing time, which can dramatically reduce PM formation. However, as diesel fuel is very reactive, this requires significantly reducing the reactivity of the system; this is often achieved by using high (>25%) fractions of exhaust gas recirculation (EGR). The EGR has both a lower ratio of specific heats than air, which lowers compressed temperatures, and also a lower oxygen content, which further reduces system reactivity. However, this strategy has limitations, namely in that it is only possible to sufficiently reduce the system reactivity when low concentrations of fuel are present, and this makes high-load LTC Diesel operation nearly impossible. A positive aspect of the LTC Diesel approach to low-temperature combustion is that it works with production hardware and commercially available fuels, and is a combustion strategy currently used by manufacturers under certain engine operating conditions.

IV. Fuel Metrics:

a) Research Octane Number

The Research Octane Number (RON) is a measurement of fuel's tendency to auto-ignite in a SI engine [ASTM D2699 2015]. Section II. a) discusses the undesirable nature of auto-ignition in SI engines, due to the potential for severe engine damage. It was further noted that a number of factors influence the auto-ignition process in a SI engine, ranging from engine operating parameters (such as the physical engine, spark timing, intake pressure, intake temperature, engine speed, and mixture stoichiometry) to fuel characteristics (flame speed, ignition delay characteristics, and mixture specific heat ratio) [Heywood]. The RON test attempts to isolate the effect of engine operating parameters on fuel auto-ignition by fixing engine speed, inlet temperature, inlet pressure, air-fuel mixture stoichiometry, and spark timing [ASTM D2699 2015]; the conditions for these parameters are listed in Table 1.1. The RON test is conducted running the tested fuel under the fixed conditions listed above, and by raising the engine compression ratio until the knock intensity limit is reached. Mixtures of n-heptane and isooctane, which are called

Primary Reference Fuels (PRF's), with pure isooctane corresponding to PRF 100 and pure n-heptane corresponding to PRF 0, are then used to characterize the tested fuel. The PRF which requires the same compression ratio as the tested fuel to meet the same knock intensity gives the tested fuel its RON. Because of the low intake temperature used in the RON test, lower temperature, higher pressure conditions are realized by the system at the point of end-gas auto-ignition than in the Motor Octane Number test [Leppard 1990], which will be discussed in the following section.

Table 1.1: Limited Specifications for Research Octane Number (RON) and Motor Octane Number (MON) tests [ASTM D2699 2015, ASTM D2700 2015].

	RON	MON
Engine	CFR	
Engine Speed (RPM)	600	900
Inlet Pressure (bar)	1.01	1.01
Inlet Temperature (°C)	52	149
Inlet Temperature Measurement	Air	Air/Fuel
Mixture Stoichiometry	Maximum KI	
Spark Timing (°bTDC)	13	Varies
Fuel Delivery	Carburation	

b) Motor Octane Number

In addition to the RON test, a second octane test is in widespread use, the Motor Octane Number (MON) test [ASTM D2700 2015]. The MON test is similar to the RON test in many respects, using the same Cooperative Fuels Research (CFR) engine, and the same method of increasing compression ratio until a specific knock intensity is reached, and then comparing this compression ratio against the compression ratio needed to induce knocking in PRF mixtures. However, other operating parameters are altered from the RON test to emphasize high-temperature fuel reactivity. In the MON test, the inlet temperature is set to 149 °C rather than the 52 °C of the MON test. In addition, the mixture's residence time is decreased by increasing engine speed from 600 RPM to 900 PRM. The increase in engine speed and the increase in temperature change the dominant kinetic pathways from the low-temperature chain-branching pathway encountered in the RON test to the high-temperature beta-scission pathway that is key to a fuel's MON rating. The dominant fuel pathways leading to auto-ignition of hydrocarbon fuels under different temperature regimes are discussed in detail in Section V.

c) Fuel Sensitivity

Sections IV. a) and b) describe two different tests for determining fuel "quality" for a SI engine. Both tests measure the auto-ignition resistance of a fuel against that of PRF blends. However, it has been determined empirically that real fuels (rather than blends of pure components) often differ in their RON and MON ratings, and this is the underlying reason for

having two octane tests. The difference in a fuel's RON and MON ratings is referred to as Sensitivity (S), as seen in Eq. (1.4) [Heywood].

$$S = RON - MON \qquad \textbf{Eq. (1.4)}$$

Fuel sensitivity essentially describes the difference in behavior from a PRF [Leppard 1990]. A fuel that behaves like a PRF will have a sensitivity of zero, meaning that at both the RON and MON test conditions, the fuel's anti-knock resistance behaves the same as a single mixture of isooctane and n-heptane. While it may not seem plausible that a fuel made of hundreds of components could behave similarly to a binary blend, this is in fact the case for some fuels. Conversely, many fuels do not behave similarly to a single PRF in both the RON and MON test, leading to $|S| > 0$. In California, for instance, the emissions certification gasoline, which is somewhat representative of what is available on the open market, has a S of 7.5 [Halterman 2014]. While it is acknowledged that S is caused by differences in fuel auto-ignition chemistry, the mechanistic explanations for these differences are currently not well understood. As noted in Section V. d), detailed kinetic studies of gasoline type fuels have until recently been limited to fuel surrogates such as PRF's, and this has somewhat precluded the study of differences between PRF's and real fuels.

d) Anti-Knock Index

Due to real gasolines typically having $|S| > 0$, and the desire to rate fuels by a single metric, the Anti-Knock Index (AKI) was created. AKI is determined by averaging RON and MON values, as shown in Eq. (1.5).

$$AKI = \frac{(RON+MON)}{2} \qquad \textbf{Eq. (1.5)}$$

While AKI provides a single value for rating fuels, the value of this number has been repeatedly questioned, and this has led to the creation of alternative fuel tests and indexes. However, AKI is the metric that is used to rate commercial fuels in the United States.

e) Cetane Number

Octane tests have traditionally been used to quantify the knock-resistance of gasoline type fuels in SI engines. The corresponding test for diesel engines is the Cetane test [ASTM D613 2015], which gives the Cetane Number (CN) of a fuel. This test quantifies how readily a fuel auto-ignites in a diesel engine, which requires fuel auto-ignition to function, and thus a highly-ignitable fuel has traditionally been desirable. The Cetane test differs significantly from the Octane tests. While the Octane test premixes fuel and air prior to the combustion chamber, and Cetane test directly injects fuel into the combustion chamber, using a diesel, transport controlled combustion. This means that in the Cetane test, fuel evaporation, mixing, and auto-ignition are coupled, whereas in the Octane test, the primary factor is chemical ignition delay. Detailed conditions for the Cetane test may be found in **Table 1.2**.

The Cetane test determines the mixture of n-cetane and heptamethylnonane which gives the same test result as the fuel which is being rated. Rather than measuring knock intensity, the Cetane test measures ignition delay, specified as the number of crank angles that elapse between

the start of fuel injection and the start of combustion. In the Cetane test, the ignition delay is specified at 13 crank-angle degrees. To achieve this ignition delay, the compression ratio of the engine is changed. Thus, the mixture of n-cetane and heptamethylnonane which require the same compression ratio to achieve the 13 degree ignition delay as the rated fuel gives the rated fuel its cetane number, with CN=0 corresponding to behavior of heptamethylnonane and CN=100 corresponding to the behavior of n-cetane.

Table 1.2: Specified conditions for ASTM Cetane Test.

	Cetane
Engine	CFR
Engine Speed (RPM)	900
Inlet Pressure (bar)	1.01
Inlet Temperature (°C)	52
Inlet Temperature Measurement	Air
Mixture Stoichiometry	Varies
Fuel Flow Rate (ml/min)	13
Injection Timing (°bTDC)	13
Injection Pressure (bar)	103.4
Ignition Delay (°)	13
Fuel Delivery	Direct Injection

In addition to the Cetane engine test, the Derived Cetane Number, or DCN, may be determined through alternative methods [ASTM D7668 2015]. One such method is the Ignition Quality Tester (IQT), which uses a diesel injector to spray fuel into a preheated air, and which measures the ignition delay. The DCN from the IGT is well correlated to the CN, and offers the advantage of being a less complex test which requires less fuel than the CFR engine test.

f) Octane Index

Due to the shortcomings of the individual Octane ratings RON, MON, and AKI, alternative fuel ratings have been developed. The most widely used of these ratings is named Octane Index (OI) [Risberg 2003]. The Octane Index uses the RON and MON values of a fuel, coupled with engine and operating point specific information to predict a fuel's auto-ignition resistance under certain conditions. The OI may be calculated using Eq. (1.6), $\boldsymbol{S=RON-MON}$ **Eq. (1.4)**, and Eq. (1.7), where the parameter "$T_{COMP\ 15}$" in Eq. (1.7) is the average temperature of the charge at a pressure of 15 bar, while λ refers to the inverse of the equivalence ratio.

$$\boldsymbol{OI = RON + K \cdot S} \qquad \textbf{Eq. (1.6)}$$

$$K = 0.00497 \cdot T_{COMP\,15} - 0.135 \cdot \lambda - 3.67 \qquad \textbf{Eq. (1.7)}$$

Eq. (1.6) indicates that the OI uses RON as a baseline for fuel auto-ignition, and then either adds or subtracts the fuel sensitivity according to the K value. The K value is based on both the engine design and the specific operating condition. It may either be determined by Eq. (1.7), or by performing a least-squares regression on measured data for a range of fuels.

The OI was first created for use in characterizing fuel auto-ignition in HCCI engines, for which RON and MON were shown to only be effective in characterizing fuel under limited conditions [Risberg 2003]. The approach of incorporating engine operating conditions into the fuel rating has proven effective in better capturing auto-ignition behavior over a wide range of conditions; however, this requires additional information that limits the applicability of the rating. Specifically, as a consumer rating metric, it is unrealistic for consumers to perform calculations when deciding between a selection of fuels. However, as a research and development tool, the OI is useful as it allows worst-case scenarios to be constructed from a range of fuels available in the marketplace.

Though OI was created to address auto-ignition in HCCI engines, it has since been shown to be an effective method for predicting auto-ignition in spark ignition engines as well [Risberg 2016]. This is unsurprising, as SI engines, similar to HCCI engines, use a relatively homogeneous charge that, in knocking operation, is compressed to the point of auto-ignition.

g) Shortcomings of Current Fuel Metrics

While the RON, MON, and CN ratings have been very useful in describing fuels since the metrics' introductions over 60 years ago, they are beginning to show their limitations, as engines have undergone significant shifts in methods of operation. Simply put, it is quite telling that none of the three tests are performed under boosted intake pressure conditions, as both SI and diesel engines are now routinely operated under such conditions. In the case of the diesel engine, nearly every automotive, rail, ship, and large-scale power generation diesel engine sold in the past 20 years has been turbocharged or supercharged, and this has fundamentally changed the typical pressures during combustion. Secondly, common-rail direct injection systems have become standard on diesel engines, dramatically changing the pressure at which fuel is directly injected. The higher in-cylinder pressure and the higher injection pressure encountered in modern diesel engines has significantly altered the evaporation and mixing process during diesel combustion. In addition, the higher pressures will also have an effect on the kinetics of ignition. Finally, diesel engines are now run with up to seven separate fuel injection events, and this has further changed the environment into which fuel is injected. These changes in the way diesel engines are used are not reflected in the way that diesel fuels are rated.

A similar trend has occurred in SI engines. As noted in Section II. a), SI engines are now commonly turbocharged and use direct fuel injection. The turbocharging raises the operating pressure of the engine, while the direct-injection cools the air-fuel mixture, producing higher pressure and lower-temperature conditions. Additionally, the direct-injection typically leaves some level of fuel stratification, which may affect the combustion process, as demonstrated in [Shi 2016] and [Sjöberg 2006]. Finally, for knock-limited conditions, extreme spark timing retard is

now common, further leading to lower-temperature and longer residence-time charge conditions. All of these factors have altered modern SI engines further and further away from the operating points that were chosen for the RON and MON tests, and which were relevant for engines 60 years ago. Further, it has been shown that the change in SI operating conditions is in fact material, such that that neither RON nor MON ratings individually describe knock-resistance at highly boosted conditions [Kalghatgi 2014].

While SI and diesel engines have drifted from the conditions at which the RON, MON, and CN tests were created, low-temperature combustion engines face a more challenging problem – they typically rely on a range of conditions to force auto-ignition. These conditions may vary significantly in temperature, pressure, fuel concentration, and oxygen concentration. Thus it is very difficult to devise a single metric or test to characterize a fuel which may have different sensitivities to each parameter. A number of new fuel indexes for HCCI have been proposed, however only OI has shown to be effective across a wide range of conditions [Kalghatgi 2014], and even OI has not been shown to work under every situation [Truedsson 2014].

V. Auto-Ignition of Fuels in Engines

a) High-Temperature Pathway

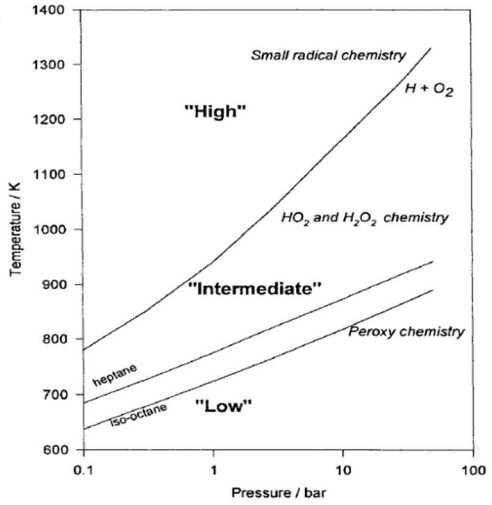

Figure 1.7: Regime diagram for different temperature ranges of combustion chemistry, reprinted from [Piling 1997].

Hydrocarbon auto-ignition kinetics can be split into three regimes: a high-temperature regime, a low-temperature regime, and an intermediate temperature regime [Piling 1997]. These regimes are schematically indicated in Figure 1.7, along with their dominant classes of chemical reactions. The effect of these different regimes of combustion chemistry on auto-ignition of hydrocarbons may be seen in Figure 1.8 [Mehl 2015]. Figure 1.8 plots the time required for auto-ignition of isooctane at different temperatures. It may be seen that Figure 1.8 has three distinct trends. In Figure 1.8, the high-temperature regime is on the left hand side of the figure, in this case corresponding to temperatures above 850 K. The intermediate-temperature region is found in the center of the figure, displaying negative-temperature coefficient (NTC) behavior, which is discussed in Section V. c). Finally, the low-temperature region is located on the right hand side of

Figure 1.8, and discussed in Section V. b). These three temperature regions correspond to three distinct pathways for fuel oxidation, that are depicted in Figure 1.9, and that are discussed in their respective sections.

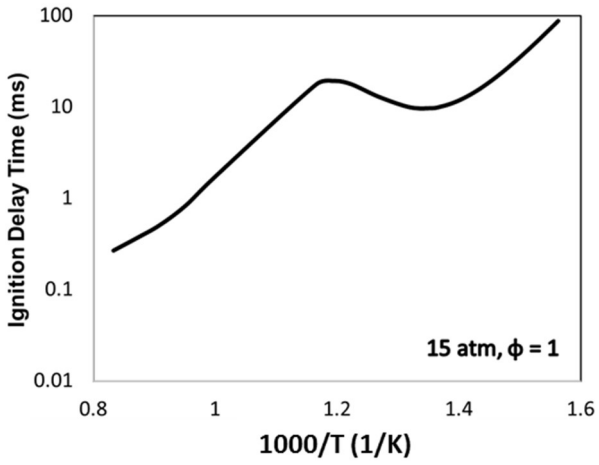

Figure 1.8: Ignition delay curve for isooctane at 15 atm and an equivalence ratio of unity, reprinted from [Mehl 2015].

High-temperature combustion chemistry is typically characterized by decomposition of the hydrocarbon, followed by oxidation. The high-temperature pathway can be seen at the top of Figure 1.9, where the fuel radical is formed by hydrogen abstraction either via molecular oxygen or a hydroxyl radical, then decomposed by beta-scission. This process of decomposition continues with the help of the chain branching reaction $H + O_2 \rightarrow OH\cdot + O\cdot$ until the fuel molecule is reduced to a collection of small radicals and intermediates, such as $CH\cdot$, CO, $OH\cdot$, $CH_3\cdot$, and $O\cdot$. These small radicals continue reacting to form the products H_2O and CO_2 via the reactions $CO + OH\cdot \rightarrow CO_2 + H\cdot$ and $H\cdot + O_2 \rightarrow OH\cdot + O\cdot$. High temperature chemistry is the final step in the auto-ignition process; this process is complete once the chain branching reaction of $H + O_2 \rightarrow 2\ OH\cdot$ begins, typically at temperatures near 1200 K [Westbrook 2007]. However, the quasi-stable intermediate species hydrogen peroxide will thermally decompose at temperatures near 1000K, thus the Though high-temperature chemistry is required for auto-ignition, it is typically the step with the least variability, as evidenced by the collapse of ignition delay behavior for various hydrocarbons at high temperatures, as seen in Figure 1.10; there are typically much greater differences among the low- and intermediate-temperature chemistries of hydrocarbons.

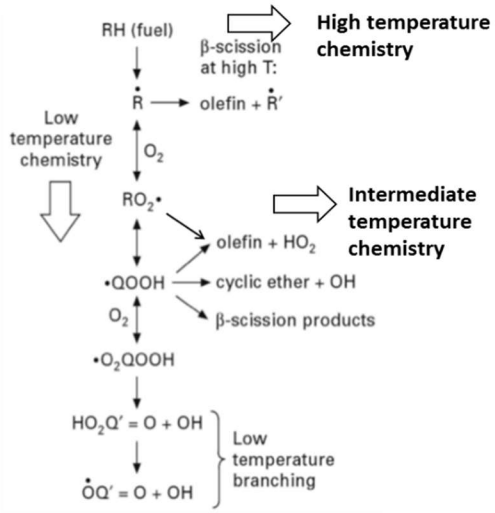

Figure 1.9: Dominant reaction pathways for high-temperature, intermediate-temperature, and low-temperature oxidation of hydrocarbon fuels, reprinted from [Curran 1998].

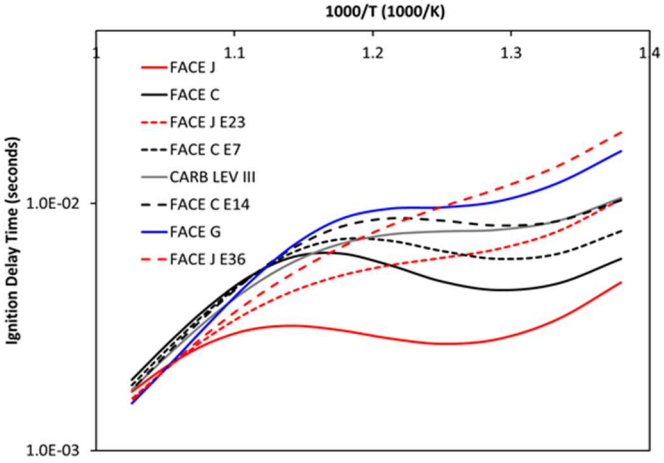

Figure 1.10: Ignition delays for a selection of gasoline-type fuels at 25 bar pressure and an equivalence ratio of unity.

b) Low-Temperature Pathway

Low-temperature chemistry is highly important to the auto-ignition process of hydrocarbons in combustion engines; this is due to the accelerating effect that low-temperature chemistry has on auto-ignition [Westbrook 2016]. Similar to high-temperature chemistry, there are chain-branching pathways at low temperatures. However, in contrast to high-temperature chemistry, low-temperature chemistry first oxidizes the fuel molecule and then decomposes the fuel molecule, rather than decomposing the fuel molecule and then oxidizing, such as in the high-temperature pathway.

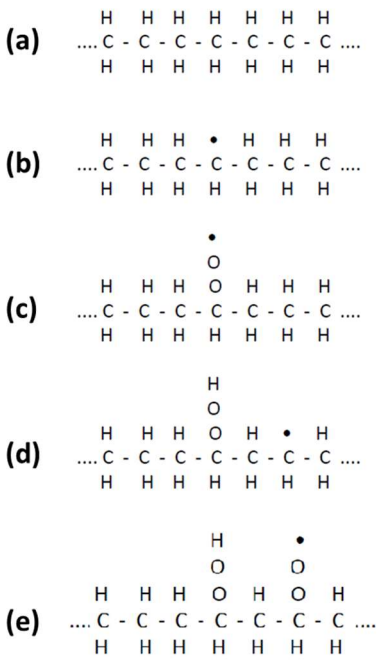

Figure 1.11: Chemical structures of alkane derived radicals during the low-temperature oxidation pathway, reprinted from [Westbrook 2016].

The low-temperature pathway may be seen in Figure 1.9. The first step, as in the high-temperature pathway, is the hydrogen abstraction from fuel, which is shown in Figure 1.9 (b). The following step is oxygen addition to the fuel radical to form the alkylperoxy radical, seen in Figure 1.9 (c); the first oxygen addition step has been shown to be sensitive to oxygen concentration, and likely underlies the pressure sensitivity of hydrocarbon reactions in engines [Mehl 2009]. Following oxygen addition is the isomerization to the hydroperoxyalkyl radical, shown in Figure 1.9 (d). The hydroperoxyalkyl radical leads to a second oxygen addition to form the hydroperoxyalkylperoxy radical, shown in Figure 1.9 (e). After the formation of the hydroperoxyalkylperoxy radical, this highly oxygenated radical will decompose to form a ketohydroperoxide and OH·. The ketohydroperoxide further decomposes to form two radicals, the carbonyl radical and another hydroxyl radical, thus branching the radical chain.

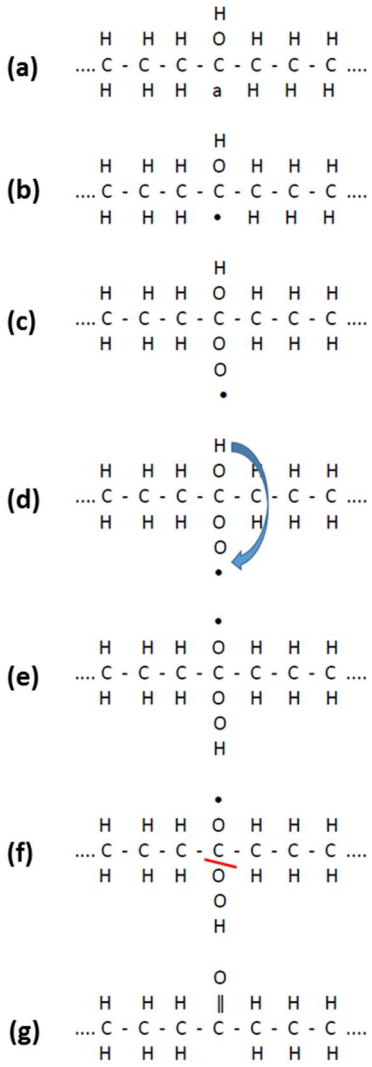

Figure 1.12: Low-temperature oxidation pathway of alcohol fuels, reprinted from [Westbrook 2016].

However, certain conditions must be met for this low-temperature pathway to be active. The first condition is fuel radical formation, as the following O_2 additions rely on the presence of fuel radicals. Fuel radical formation is generally not a limiting step except in the case of highly branched alkanes that are surrounded by methyl groups. Secondly, and more often a limiting case, is the availability of a sufficiently long saturated carbon chains to allow for the isomerization and second oxygen addition steps. In the range of common gasoline components, these chains may be severed by methyl group placement, double bond placement, or hydroxyl group placement along the chain. In the case of the double-bond of olefinic fuels, the electron delocalization of the double bond increases the reverse rate of the oxygen addition to the point at which the ketohydroperoxide forming pathway is no longer favored [Westbrook 2016]. In the case of alcohols, the hydroxyl group causes the alpha-hydrogen to be abstracted preferentially, leading to molecular oxygen addition to this site, as shown in Figure 1.12 (b) and (c). Isomerization shifts the radical site from the oxygen addition site to the hydroxyl group, to form a hydroperoxy group, shown in Figure 1.12

(d) and (e). This hydroperoxy group is abstracted from the fuel radical, leaving an aldehyde, shown in Figure 1.12 (f) and (g), and disrupting the chain branching pathway. Thus, the alcohol will effectively scavenge radicals from the system at low temperatures, by offering a preferential radical formation that leads to chain termination. A similar chain-termination pathway exists at low-temperatures for benzylic species as well. These various chain termination pathways stemming from the placement of hydroxyl groups, methyl groups, or double bonds serve as a reminder that molecular structure is at least equally important to chain length in hydrocarbon fuels.

c) Intermediate Temperature Pathway

In addition to the high- and low-temperature pathways, which both lead to chain branching, there also exists intermediate temperature pathways, which lead to chain propagation or to the formation of stable intermediates, but not to chain branching [Piling 1997]. This divergent behavior from the low- and high-temperature pathways results in the negative temperature coefficient (NTC) behavior that may be seen in Figure 1.8, via the formation of stable intermediates and the corresponding chain termination. Also, the intermediate temperature pathway is responsible for intermediate temperature heat release [Mehl 2012], which is utilized to run late-phasing HCCI combustion, and this will be further discussed in Section III. a), while investigations into the chemical nature of intermediate temperature heat release will be presented in Chapter 4 of this dissertation.

The intermediate temperature pathway can essentially be described as an alternative to the low-temperature pathway; the intermediate temperature pathway still begins with hydrogen abstraction followed by oxygen addition for the fuel radical. However, either prior to or after the isomerization to the hydroperoxyalkyl radical, and rather than undergoing the second oxygen addition, the fuel radical will deviate from the low-temperature pathway, as shown in Figure 1.9. The alternative pathways shown in Figure 1.9 make up the primary intermediate temperature pathways. The intermediate temperature pathways consist of conversion of the alkylperoxy radical and the hydroperoxyalkyl to stable olefinic species and HO_2, or beta-scission of the hydroperoxyalkyl radical, or formation of a cyclic ether and a hydroxyl radical from the hydroperoxyalkyl radical [Curran 1998]. Thus, the intermediate temperature pathway represents a middle ground between the multiple oxidation steps of the low-temperature pathway, and the fast pyrolysis of the high-temperature pathway.

d) Chemical Kinetic Mechanisms

Chemical kinetic mechanisms are a type of chemistry model used in simulating the dynamic chemical behavior of a system. Kinetic mechanisms describe the concentration dynamics of a system typically using Arrhenius rates and the species ordinary differential equation written in the form seen in Eq. (8). The chemical system is described by specifying the stoichiometric factors, the pre-exponential factor, activation energy, and thermal dependence for each chemical reaction that is relevant to the system.

$$\frac{d\,[c_i]}{dt} = k_j * \left[c_j\right]^n * [c_k]^m + \cdots = \left(A_j\, T^{n_j}\, e^{-\frac{E_{a_j}}{RT}}\right) * \left[c_j\right]^n * [c_k]^m + \cdots \qquad \textbf{Eq. (8)}$$

Kinetic mechanisms for fuel oxidation and pyrolysis may be constructed in varying levels of detail. Those with the least detail use a single global reaction rate which approximates the

detailed system. However, as our questions become more detailed, our predictions must become more detailed as well. It has been shown that a much higher level of detail is needed to describe the combustion of hydrocarbon fuels [Wolk 2015]. Current state-of-the-art kinetic mechanisms for use in modeling the combustion of a single hydrocarbon fuel molecule with seven carbon atoms will use on the order of 4,000 species and 10,000 elementary steps [Mehl 2011 Kin.]. Many of the elementary steps containing low molecular weight species, such as OH, HO_2, CH, and generally all species containing four carbons or less, are not specific to a single fuel molecule. This is highly advantageous, because real gasoline-type fuels are not comprised of a single molecular component, but by hundreds of components. While it is currently impractical to model each component, an approach to this problem has often been to use a small number of surrogate components to represent the fuel. The current state-of-the-art gasoline mechanism uses four-thousand species and ten-thousand elementary steps to model the combustion of 7 gasoline surrogate components [Mehl 2011 Kin.]. As the number of surrogate components for gasoline has increased from one component (isooctane) to two components (isooctane and n-heptane) to seven components, a greater number of fuel properties have been able to be matched by the kinetic surrogates, including C/H ratio, ignition delay profiles, compositions by class of hydrocarbon, and average molecular weight.

Kinetic mechanisms created for modeling combustion are now under-constrained in terms of infinite number of reasonable rate parameters that may be used in a kinetic mechanism and the small number of measured experimental results for the oxidation a given fuel. Thousands of activation energies, thousands of pre-exponential factors, and thousands of sets of thermodynamic data (e.g. NASA polynomials) are required to be specified for a reaction mechanism with thousands of species and tens of thousands of elementary steps. As the majority of these species are highly unstable, and because the majority of the elementary steps involve two unstable species that are difficult to synthesize, the majority of the individual rates and the majority of the thermodynamic data remains unmeasured. Luckily, these parameters may be calculated using various levels of theory. However, because many of the partially oxidized or partially decomposed fuel molecules contain a significant number of atoms, only low levels of theory are affordable or available for calculating rate constants and thermodynamic properties. These calculations are typically accurate to an order of magnitude, leaving room for a significant amount of tuning to be performed on a large number of elementary steps. These uncertainties are compounded over a reaction pathway, further raising the system uncertainty.

Kinetic mechanisms are typically tuned to meet parameters measured in fundamental combustion experiments. However, the number of parameters measured is quite low. For a given well-characterized fuel, such as isooctane or n-heptane, it is typical for ignition delay experiments to have been performed. These experiments rapidly compress a fuel-oxidizer mixture to a temperature (650 K – 1200 K) and pressure (3 bar – 50 bar) condition and measure the time required at this condition for ignition to occur. This generates a response curve, as seen in Figure 1.8. However, this curve is far from sufficient to constrain a large mechanism. Evidence of unconstrained mechanisms exists in the evolution of the Lawrence Livermore National Laboratory (LLNL) detailed n-heptane mechanism. First published in 1998, this mechanism reproduced experimentally measured ignition delay times over a range of conditions [Curran 1998]. However, over the following ten years some speciation data was published from experiments such as jet-stirred reactors. This new speciation data lead to a significant revision of the mechanism in 2011,

as the original mechanism incorrectly predicted the formation and consumption of key stable intermediates, such as formaldehyde [Mehl 2011].

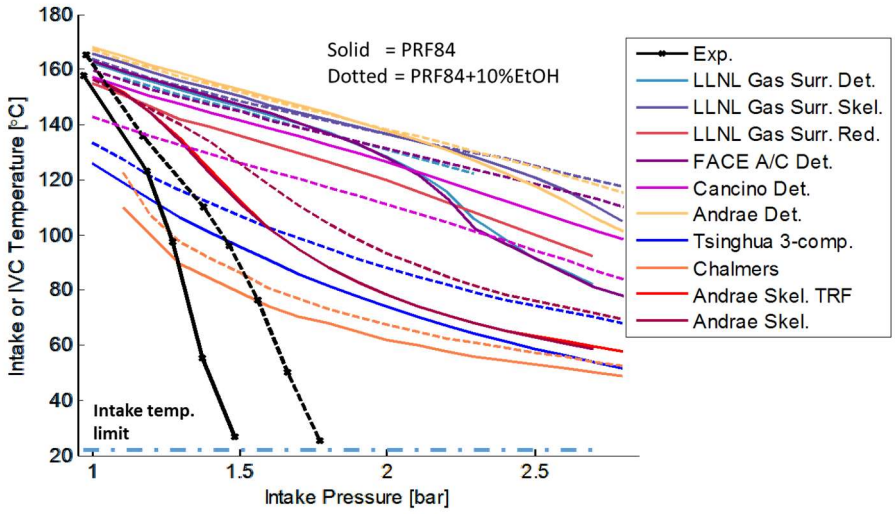

Figure 1.13: Experimental conditions needed to achieve auto-ignition in a homogeneous charge compression ignition engine (black), compared to simulated conditions for 10 chemical kinetic mechanisms (colored), reprinted from [Wolk 2015].

In addition to the speciation problems that mechanisms face, overall ignition delay predictions are still insufficient for simulating engine combustion, due to the sub-millisecond accuracy that is required for this task. While ignition delay predictions by mechanisms often appear accurate when plotted on a log-log scale, this can mask their performance when simulating systems that are highly sensitive to overall ignition delay, such as kinetically-controlled engines [Wolk 2015]. Figure 1.13 provides a comparison between measured and predicted temperature and pressure combinations which produce a constant ignition delay in a homogeneous charge compression ignition (HCCI) engine. The predicted conditions are all seen to vary substantially from the experimental conditions at high intake pressures, though the predictions approximately match the experiment at low intake pressures. The predictions are made by ten recently published mechanisms representing the current state of the field. While these mechanisms generally predict ignition delays well in fundamental experiments, especially when plotted on a log-log scale, their performance is not sufficient for predictive modeling of engine combustion. While a 10% error in predicted ignition delay may be imperceptible when plotted on a log-log scale, in an engine, this 10% error in the simulation can either change the mode of combustion, or prevent combustion from occurring. This fidelity requirement when simulating engines simultaneously highlights the difficulties faced by predictive modeling while reinforcing the need for experimentation. To reiterate, as our questions become more detailed, operating at the boundary of kinetic regimes, our predictions must become more detailed as well.

VI. Common Classes of Gasoline Fuel Components and their Ignition Chemistry

Gasoline composition is commonly described by the fractions of the following classes of molecules: (n)-paraffins, iso-paraffins, olefins, naphthenes, and aromatics; the abbreviated for

these classes is termed “Piona”. In addition to the hydrocarbon classes, it is also common to report the oxygenate fraction of the gasoline. The sections below provide brief descriptions of the Piona hydrocarbon classes and their general influence on the system’s reactivity.

a) iso-Paraffins

iso-Paraffins are a key class of hydrocarbons for gasoline fuel, as they represent the “ideal” gasoline species, isooctane, which is a commonly used surrogate for gasoline, or one component of a two-component gasoline surrogate. iso-Paraffins are highly branched saturated hydrocarbons. The branches are formed by methyl groups which are attached to the main carbon chain. These methyl groups have high activation energy barriers to hydrogen abstraction (two- to four-times the activation energies of secondary and tertiary sites, respectively) [Curran 2002]. This limits the radical pool within the system, and lowers the system reactivity. Further, depending on the site of the initial hydrogen abstraction, the branched nature of the molecule may inhibit the isomerization steps described in Section V. b), further reducing the reactivity of the fuel at low temperatures.

b) n-Paraffins

n-Paraffins are another key class of hydrocarbons found in gasoline, and they represent the “lowest-quality” gasoline fuel, as they have strong tendencies to auto-ignite under engine-relevant conditions. This class of hydrocarbons also provides the second gasoline surrogate species, n-heptane, which are used in two component gasoline surrogates termed Primary Reference Fuels (PRF’s). Their structure is that of a saturated carbon chain with no branching, and their combustion chemistry is characterized by strong tendencies for the low-temperature chemistry pathways due to high rates of hydrogen abstraction and no inhibitions to isomerization from the alkylperoxy radical to the hydroperoxyalkyl radical [Curran 1998]. This uninhibited low-temperature pathway leads to high reactivity in engines, which for gasoline type fuels is undesirable, and this has earned n-paraffins their “low-quality” moniker.

c) Olefins

Olefinic compounds are characterized by their unsaturated carbon atoms and allylic C-H bonds. While olefinic compounds appear in real gasolines, they typically are not included in gasoline surrogates. However, olefins are now being incorporated into chemical kinetic mechanisms for gasoline oxidation, as they can comprise on the order of 10% (by mole) of real gasolines (see Fig. 3 in Chapter 5 for compositions of real gasolines) [CRC 2014].

The carbon-carbon double-bond results in four weakly-bound allylic hydrogens that serve as the primary abstraction sites during fuel radical formation, as shown in Figure 1.14 (a) and (b) [Westbrook 2016]. As discussed in Section V. b), the radical site adjacent to the carbon-carbon double bond becomes a site of oxygen addition at low temperatures (Figure 1.14 (c)). However, as the hydrogen atom was loosely bonded at this site, so is the molecular oxygen, due to electron delocalization, and the low temperature pathway does not generally continue to the isomerization step, reducing the tendency of the olefin for low temperature heat release.

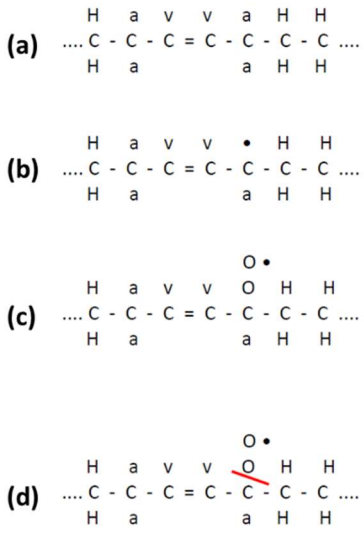

Figure 1.14: Low-temperature oxidation pathway for olefinic molecules reprinted from [Westbrook 2016].

d) Naphthenes

Cycloalkanes are another class of hydrocarbons that are commonly found in gasoline type fuels, and yet they typically are found in mole fractions of less than 20%, and are neither extremely reactive or knock-resistant, like n-heptane or isooctane, respectively [CRC 2014]. Thus, they are not found in fuel surrogates, though similar to olefins, they are now being included as species in chemical kinetic mechanisms.

Cyclohexane is the commonly-used surrogate for naphthenes in chemical kinetic mechanisms [Mehl 2011 Kin.]. At low temperatures, cyclohexane reactivity is similar to an alkane; first, a hydrogen is abstracted from the fuel molecule, and secondly, the fuel radical undergoes oxygen addition. The oxygen addition step results in four likely isomers, with approximately 60% opening the ring and then following the n-alkane low-temperature combustion scheme [Simmie 2003]

e) Aromatics

Aromatic compounds are commonly found in gasoline, and have a significant influence on gasoline combustion, leading to their inclusion in realistic gasoline surrogates. These surrogates are termed Toluene Reference Fuels (TRF's). They are mixtures of n-heptane, isooctane, and toluene. Aromatic hydrocarbons are characterized by resonantly stabilized six-member rings. Toluene, the commonly used surrogate for the class, has a methyl group attached to this ring.

The presence of the resonantly stabilized ring significantly alters combustion chemistry. Rather than following the hydrogen abstraction and multiple oxygen addition and isomerization steps of low-temperature alkane chemistry, toluene reactions at low temperatures rarely lead to chain branching [Westbrook 2016]. Hydrogen abstraction from the ring can terminate in the

formation of a cresol, benzyl alcohol, bibenzyl, or ethyl benzyl, as shown in Figure 1.15. In contrast, the primary route for opening the ring and decomposition of the fuel molecule is via abstraction of a methyl group hydrogen, which can then lead to benzaldehyde via reactions with atomic oxygen or $\cdot HO_2$. The benzaldehyde then undergoes radical abstraction leading to benzoyl radicals, followed by decomposition to the phenyl radical via loss of carbon monoxide. Next, oxygen addition to the phenyl radical gives phenoxy radicals, which may then decompose to yield cyclopentadienyl radicals These cyclopentadienyl radicals may terminate in cyclopentadiene, or undergo an oxygen addition, giving cyclopentadional radicals, which finally lead to the opening of the ring. However, the undoubtedly weary reader will note that this pathway (which is shown in Figure 1.8) is much more tedious than even the multiple oxygen addition pathways of alkanes. Thus, aromatic species generally exhibit minimal low-temperature reactivity, reducing the global reactivity of nearly all gasoline mixtures, hence their use in increasing auto-ignition resistance of gasoline.

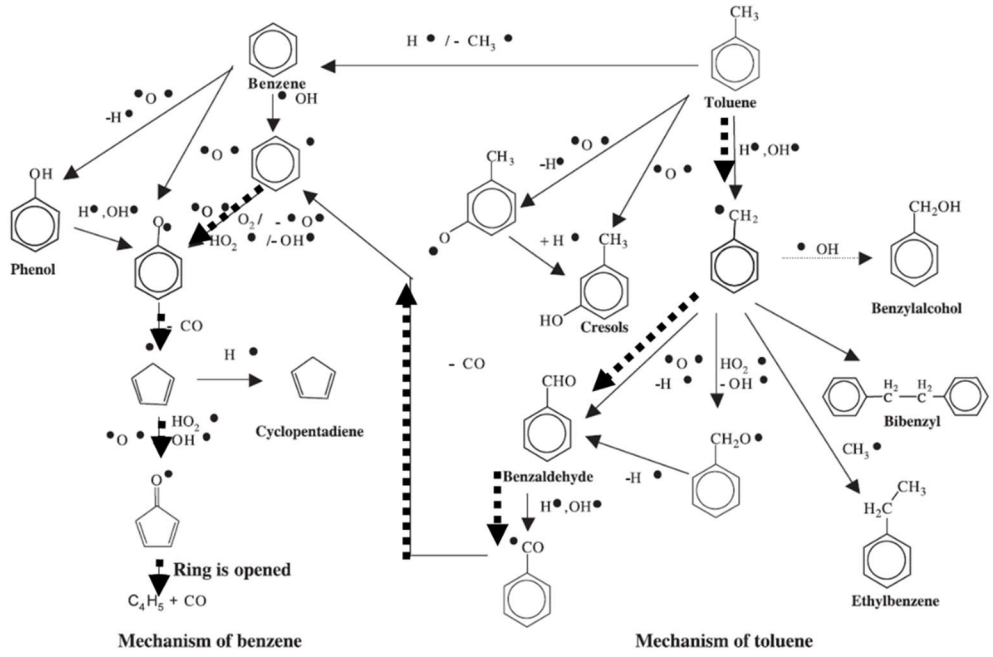

Figure 1.15: Reaction mechanism for toluene and benzene reprinted from [Brezinsky 1986].

f) Ethanol

While ethanol is not a traditional gasoline compound, it now (by mandate) comprises 10% of our gasoline in the United States [NHTSA 2016]. Though this is on the same order as olefins or naphthenes, ethanol has a significantly larger impact on physical and chemical properties of fuels than either of these other two classes of hydrocarbons, and thus its inclusion is a requirement for the combustion modeling of gasolines which contain ethanol [Marinov]. At the low- and intermediate-temperatures which are key to the auto-ignition process, ethanol significantly inhibits low-temperature chain branching in hydrocarbons. As will be demonstrated in Chapter 3, ethanol's primary effect on the auto-ignition process is the scavenging of hydroxyl and HO_2 radicals. These two radicals react with ethanol fuel radicals to form stable species such as hydrogen peroxide or

water. This behavior is in contrast to ethanol's high-temperature reactivity, which is higher than many typical gasoline hydrocarbons, due to the single required unimolecular thermal (beta-scission) decomposition at these high temperatures. However, the low-temperature radical scavenging effects have a larger impact on auto-ignition under most engine-relevant situations, especially at high pressures in which the low-temperature pathways of alkanes are active.

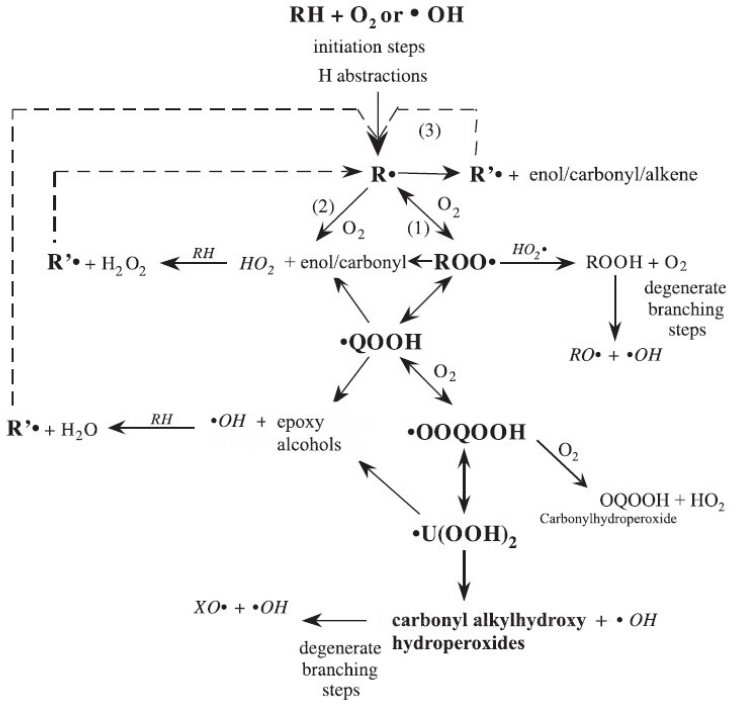

Figure 1.16: Reaction mechanism for alcohol combustion reprinted from [Battin-Leclerc 2008] and [Sarathy 2014].

VII. Knowledge Gaps Inhibiting Effective Modeling and Implementation of Kinetically-controlled Engines

a) Transition of Gasoline Fuels to Low-Temperature Heat Release Regime under Boosted Conditions

The transition of gasoline fuels from single-stage heat release to dual-stage heat release has been shown to have significant effects on the auto-ignition behavior of the fuel. However, the transition from single-stage to dual-stage heat release behavior is neither well characterized by experiments, nor well predicted by chemical kinetic mechanisms (see Figure 1.13). Thus, the experimental efforts presented in Chapter 2 of this dissertation to characterize gasoline's Low-Temperature Heat Release transition were missing from the literature and timely, considering the current interest in boosted Advanced Combustion Engines.

b) Effect of Ethanol Addition to Gasoline on Auto-Ignition at Boosted Conditions

Although ethanol has been blended in gasoline for many years, insufficient research into its blending effects with gasoline exists in the literature. This is evidenced by, among other factors, a significant initiative by the Department of Energy, involving 7 National Laboratories, to study the effects of ethanol, and additional biofuel, blending in gasoline [DOE 2016]. Until 2016, emissions certification tests for light-duty gasoline vehicles used certification gasolines that did not contain any ethanol. Further, the two most widely used gasolines for research, EPA EEE, and RD387, both contain no ethanol. These factors highlight the need for a better understanding of the effects of ethanol addition to gasoline under conditions which are relevant to modern SI and kinetically-controlled engines and this topic is the focus of Chapter 3 of this dissertation.

c) Heat Producing Potential of Intermediate Temperature Pathways

Intermediate temperature combustion pathways have been shown to provide sufficient heat release to stabilize combustion under high-load HCCI conditions [Mehl 2012]. However, the activation of these pathways has only been demonstrated using fuels which are capable of low-temperature chain branching behavior, such as alkanes, while fuels that do not exhibit significant low-temperature chemistry, such as ethanol, have not been shown to exhibit Intermediate Temperature Heat Release. The interactions between alkanes and ethanol under conditions which may generate Intermediate Temperature Heat Release has not been thoroughly investigated prior to the work presented in Chapter 3 of this dissertation.

d) Characterization of the Low-Load Gasoline Compression Ignition (GCI) ignition process

Low-load operation of GCI engines using commercially available fuel has been a challenge for research groups which are developing said engines [Sellnau 2013, Kolodziej 2015]. While engineering solutions have been applied to allow low-load GCI engine operation, these investigations have focused on solving the problem rather than understanding it. Therefore, while systems have been developed to allow low-load GCI operation under certain conditions, there is little broad understanding of how changes to the fuel affect the low-load performance. This topic is investigated in Chapter 5 of this dissertation.

e) Characterization of Fuels for Kinetically-controlled Engines

Kinetically-controlled engines typically effect auto-ignition of fuels via significantly different temperature, pressure, fuel concentration, and oxidizer concentration levels than traditional spark-ignition (SI) or diesel engines. Thus, it is unsurprising that the fuel "quality" metrics which have been established for SI and diesel engines, namely Research Octane Number, Motor Octane Number, and Cetane Number, do not well describe the auto-ignition of fuels in kinetically-controlled engines. The lack of correspondence between fuel auto-ignition in an engine and a single metric has been shown repeatedly, in [Kalghatgi 2003], as well as [Shibata 2007] and [Truedsson 2014]. However, a method of quantifying ignition behavior under advanced-engine conditions is critical to the implementation of kinetically-controlled engines, due to the considerable range of fuel variability in the marketplace, both with regard to hydrocarbon composition and with regard to ethanol content. While new fuel metrics have been proposed, they have yet to be tested under Gasoline Compression Ignition of Partial Fuel Stratification conditions or under boosted conditions with gasoline-ethanol mixtures.

f) Interaction of the Combustion and Engine System in a Partial Fuel Stratification Engine

As discussed in Section III. b), Partial Fuel Stratification (PFS) is a new combustion concept that has been demonstrated to raise the high-load limit of HCCI engines while retaining

high efficiency and low emissions [Yang 2011]. The mechanisms underlying the efficacy of PFS operation have been investigate in [Wolk 2014]. PFS has demonstrated high levels of performance in a single-cylinder engine, in which intake boosting, intake preheating, and exhaust gas recirculation are simulated, such as provided by external sources. However, no studies have been made which address the feasibility of creating the desired intake conditions using the system exhaust enthalpy.

VIII. The Influence of Ethanol Addition to Gasoline Type Fuels at Engine-Relevant Conditions

a) Current and Future Ethanol Utilization

In the United States, ethanol has been added to gasoline in significant fractions for over a decade, after ethanol was mandated to displace certain volumes of gasoline by the Energy Policy Act of 2005 [EPA 2013] and later by the Energy Independence and Security Act of 2007 [GPO 2007]. The intent of adding ethanol to gasoline was to reduce foreign oil reliance and reduce carbon emissions from fossil fuels. The efficacy of this reasoning and implementation will not be discussed in this dissertation, but the effect on the resultant gasoline-ethanol blends will be investigated and thoroughly discussed.

The 2005 and 2007 mandates have resulted in the widespread sale of gasoline containing 10% ethanol by volume (E10) [NHTSA 2016]. Due to the mandates being on an absolute volume basis, rather than a percentage of overall fuel use, the required amount of ethanol in gasoline has not yet been met. Thus, there is a possibility of shifting to E15 or E20 gasoline in the future.

b) Influence on SI Engine Knocking

Ethanol has traditionally been added to gasoline as an anti-knock agent. Ethanol's RON of 109, MON of 91, and AKI of 100 mean that it is generally less knock prone than consumer grade gasoline [Foong 2014]. Thus, the introduction of significant fractions of ethanol to gasoline feedstock typically increases the fuel octane rating. However, though ethanol has been used as a fuel and fuel additive for decades, the reasons for the ethanol knock resistance are still not well understood, contributing to the engine community revisiting ethanol-gasoline blending interactions [Sluder 2016, Stein 2012, Leone 2014, Foong 2014]. Ethanol blending in gasoline has traditionally not been well understood because ethanol has multiple mechanisms with which to reduce knocking, however these mechanisms vary with temperature and are non-linear with volumetric blending.

As discussed in Section VI. f), ethanol is a potent radical scavenger at low temperatures, converting OH to H_2O and HO_2 to H_2O_2; this behavior contributes to its high RON rating. However, at high temperatures, typically above 1000 K, ethanol is chemically more reactive than many common gasoline hydrocarbons, and this contributes to its significantly lower MON rating [Foong 2014]. In addition to its chemical effects on ignition delay, ethanol also provides significant knock resistance via evaporative cooling. Ethanol's heat of vaporization of 38.56 kj/mol is comparable to that of heptane, at 36.57 kj/mol [NIST 2016]. However, because of ethanol's lower number of carbon atoms per molecule and hydroxyl group, a higher number of moles of ethanol are needed to form a stoichiometric mixture, when compared to C7 and C8 alkane gasoline components. Thus, ethanol's heat of vaporization effect on the mixture becomes approximately 5

times the evaporative cooling effect of gasoline for a given mixture stoichiometry, which for stoichiometric conditions results in a temperature reduction of approximately 15 Kelvin for gasoline evaporation and approximately 75 Kelvin for ethanol evaporation. While this evaporative cooling effect is significant in reducing knocking, it is only captured by the MON test, which specifies an intake air temperature after fuel addition and evaporation [ASTM D2700 2015]; conversely, the RON test specifies an air temperature before fuel mixing and evaporation [ASTM D2699 2015].

The final significant effect of ethanol on knocking is highly nonlinear blending behavior with gasolines, and with individual hydrocarbons. Ethanol has been shown to have nonlinear volumetric blending (with respect to RON, MON, and overall reactivity) [Foong 2014]. This is not necessarily counterintuitive, as ethanol has a much higher molar density than typical gasoline hydrocarbons, and thus volumetric blending leads to nonlinear changes in mole fraction of the mixture. However, what is surprising is that the blending behavior of ethanol may have opposite effects for different blending components. In [Foong 2014], it was shown that ethanol has "synergistic" blending properties with isooctane. This means that the measured RON and MON of mixtures can be higher than the RON or MON of either pure component. This behavior is reversed for ethanol blending with toluene; here, "antagonistic" blending occurs, with blends of some ethanol-toluene mixtures exhibiting lower measured RON and MON values than either pure component. This behavior is still not well understood, though it is naturally of great interest to the kinetics community. In gasoline, the fraction of toluene is typically lower than the other hydrocarbon components, and thus ethanol nearly always raises the RON and MON values of commercial gasoline blends. However, these opposing effects with different classes of hydrocarbons are a source of confusion for the applied engine community over the influence of ethanol on knocking in SI engines [Sluder 2016].

In summary, the primary effects of ethanol addition to gasoline – radical scavenging at low temperatures, high reactivity at high temperatures, significant charge cooling when evaporation occurs in a fuel-oxidizer mixture, and non-linear synergistic and antagonistic blending effects – can result in ethanol having drastically different levels of effectiveness in reducing knocking in SI engines, depending on the base gasoline blend, the engine hardware (injection location and strategy), and the engine operating conditions (charge temperature-pressure history and residence time).

c) Influence of Ethanol on Low- and Intermediate-Temperature Chemistry

The influence of ethanol addition on low- and intermediate-temperature chemistry at engine relevant conditions is thoroughly investigated in this dissertation, with Chapters 3, 4, and 5 being partially or fully devoted to this topic.

The heat release behavior of fuels has gained considerable interest in recent years, due to the realization that this behavior can have an outsized effect on the auto-ignition process [Dec 2007, Mehl 2012]. Whereas in ignition delay experiments it is typical to see distinct low-temperature, negative temperature coefficient (NTC), and high-temperature behavior for gasoline and its pure components, this has not always been the case in engine experiments. This is due to the different conditions to which fuels are subjected in fundamental and engine experiments.

Linking heat release analysis from an engine to fuel chemistry was not practical until the advent of the HCCI engine. This is because in SI and diesel engines, fuel stratification and fluid

dynamics govern the combustion process, rather than chemical kinetics. However, researchers of HCCI engines, which have far fewer physical (transport/mixing) effects influencing the combustion process, established links between fuel heat release behavior and overall reactivity [Saxena 2014]. Fuels burned in HCCI engines were divided into fuels that displayed two-stage heat release, meaning both LTHR and high-temperature heat release (HTHR), and fuels which only displayed HTHR. The primary fuel associated with LTHR was n-heptane, and it was used as a fuel for HCCI engines due to its ability to easily be brought to conditions which caused auto-ignition. Conversely, gasoline, ethanol, methane, and methanol became known for their single-stage heat release behavior.

However, after the advent of boosted HCCI engines it was discovered that intake pressure could change the heat release behavior of gasoline [Dec 2007]. It was also found that heat release behavior could affect the performance of HCCI engines, and knowledge of a fuel's heat release behavior, specifically low- and intermediate-temperature heat release (ITHR), could enable highly-efficient combustion strategies [Mehl 2012, Saxena 2014]. Despite underpinning key HCCI operating strategies, little effort was made to study in detail the effect of gasoline composition and ethanol addition on LTHR and ITHR. Chapter 2 of this dissertation first characterizes the heat release behavior of primary reference fuels over a range of intake pressures as a baseline, specifically measuring the intake pressure required to induce LTHR. Then, Chapter 3 assesses the effect of ethanol addition to both a primary reference fuel and to real gasolines on heat release behavior over the same boost pressure range as in Chapter 2. Building on this work, Chapter 5 tests a wider range of gasoline compositions with a wider range of ethanol contents, and assess the interactions between different classes of hydrocarbons, both neat and blended with ethanol. Also demonstrated in Chapter 5 are the effects of ethanol blending and LTHR on low-load operation of a GCI engine, which has not previously been assessed.

d) Influence on Low-Load GCI Operation

Section III. c) introduced the GCI engine and the challenges facing its implementation. One of the primary challenges for these engines is effective operation over the full-load range using fuels available in the marketplace. Figure 1.6 shows the load range of an experimental GCI engine, and the missing load range on the right hand side of the figure indicates that achieving stable GCI operation with marketplace fuels (RON 90+) is challenging at low-loads. Approaches have been demonstrated to allow GCI operation with low-loads, such as exhaust rebreathing, late injection timing, and altered injector spray pattern [Sellnau 2012, Kolodziej 2015]. However, these studies have not considered or assessed the effect of fuel variability on these results. In the United States, ethanol content in gasoline may vary seasonally and regionally. In addition, it is possible that the average ethanol content in gasoline may increase in the future, with discussions of E15 and E20 use already occurring, and E15 approved for sale by the EPA [EPA 2016]. In Chapter 3 it will be shown that ethanol content significantly inhibits LTHR in gasoline type fuels. Considering the temperature-pressure conditions achieved by a GCI engine at low-loads, it is likely the low-temperature chemistry has a significant, if not dominant, influence on the auto-ignition process. This will be highly sensitive to fuel composition, especially ethanol content, and investigations into this previously uninvestigated subject are presented in Chapter 5.

IX. Fuel Characterization and the use of an HCCI Engine as a Reactor

As discussed in Section II, both SI and diesel engines are now operated at conditions that significantly deviate from their historical usage. This usage generally corresponds to higher cylinder pressure (due to turbocharging), more dilute operation (due to EGR), with different levels of fuel stratification (less, in the case of diesel engines, and more, in the case of SI engines). Further, as discussed in Section IV, this has created a divergence between standard operating conditions and the conditions at which fuels are currently evaluated. This divergence has led to questions regarding appropriate methods to quantify the auto-ignition behavior, or "quality," of fuels, particularly at boosted conditions. Chapter 2 demonstrates that one of the major effects of boosted conditions on gasoline type fuels is the triggering of Low-Temperature Heat Release (LTHR). This dissertation demonstrates LTHR dramatically changes the conditions required for stable operation of the engine. Further, Chapter 5 demonstrates that LTHR behavior is not well captured by the current gasoline fuel ratings, RON and MON. Thus, the possibility of using a boosted HCCI engine to characterize fuels at high intake pressure conditions is evaluated in Chapter 5.

Considering an HCCI engine for gasoline fuel evaluation, one of the primary disadvantages of an HCCI based test is that fuel physical properties, such as density, viscosity, and volatility would not be captured. However, these properties are also not captured by the RON and MON tests, and are generally less important than fuel kinetic effects for fuels which have significant resistance to auto-ignition, as long ignition-delay times leave ample time for mixing of fuel and oxidizer. A second disadvantage is the inability of running an HCCI engine at stoichiometric conditions without oxidizer dilution. A significantly lean or dilute mixture is different than the mixture found in a spark-ignition engine. However, it is likely representative of the fuel-oxidizer mixture that will be found in future Advanced Combustion Engines.

Now considering the advantages of an HCCI engine for gasoline fuel evaluation, the first advantage is the wide range of pressures and temperatures that may be achieved. These temperatures and pressures range from unboosted-SI levels to pressure levels not yet used in production SI engines, but currently encountered in research engines. Secondly, an HCCI test would reduce the specificity of the test. The current RON and MON tests rely on compression of the end-gas by the burned zone to induce knock. This conflates flame speed with the temperature-pressure conditions required to induce auto-ignition. The use of an HCCI engine test would reduce the number of compounding effects on the auto-ignition process, while still retaining the basic dynamic pressure-temperature history that is imposed by a piston engine. An evaluation of this concept and its applicability to GCI engines is demonstrated in Chapter 5.

X. The Influence of Intake Charge Conditions and Injection Timing on Combustion, Engine Performance, and Emissions of a Partial Fuel Stratification Engine

Fuel-engine interactions are not only limited to either enabling or inhibiting a combustion strategy; these interactions will also influence the degree to which an operating strategy may be implemented. However, while the combustion performance of the engine is of key importance, optimization of this system may come at the expense of other key engine systems, such as the

turbocharging system or heat-exchanger systems. Chapter 6 of this dissertation examines in detail an operating point for a partial-fuel stratification combustion strategy. This chapter examines the tradeoffs between combustion system performance and the intake charge preparation which is a prerequisite for this performance. It is demonstrated in this chapter that many permutations of the same operating condition (of injection timing and strategy, intake temperature, intake pressure, and exhaust gas recirculation levels) may have similar combustion system performance, but these permutations on the same operating condition may significantly influence system performance by altering the turbocharger efficiency, and consequently the system pumping losses. In addition, it is shown that similar combustion system performance does not necessarily correspond to similar emissions performance, highlighting the sensitivity of low-temperature combustion strategies to small disturbances.

In addition to system performance, the stability of this system is also assessed in this work. The effect of small changes in fuel injection timing on combustion phasing is assessed, as well as small changes in injected fuel mass. These parameters are found to have sufficient authority to effect significant changes over combustion phasing.

Finally, analysis was performed on the exhaust enthalpy to determine the range of system boundary conditions (ambient temperatures) that would allow the engine system to prepare the intake air to the optimal conditions that were identified in an earlier portion of the study. It was found that the engine system could function properly at the specified operating point for ambient temperatures ranging from -70 °C to 70 °C.

XI. Introduction to Chapters Two through Six

The following five chapters detail investigations that have been performed on the effects of intake pressure on low- and intermediate-temperature chemistry pathways in engines, the effects of ethanol addition on said pathways, and the influence of these pathways on emerging combustion systems such as Gasoline Compression Ignition of Partial Fuel Stratification.

Chapter 2: Chapter 2 investigates the heat release behavior of gasoline surrogates (Primary Reference Fuels) in a Homogeneous Charge Compression Ignition engine. The heat release behavior and pressure sensitivity of each fuel is linked to its composition. Zero-dimensional chemical kinetic modeling is performed to determine the key kinetic pathways leading to low-temperature heat release an auto-ignition. High-octane Primary Reference Fuels are found to be sensitive to intake temperature, with conditions 0.4 bar above atmospheric pressure triggering low-temperature heat release for PRF 85.

Chapter 3: Building on the work presented in Chapter 2, Chapter 3 investigates the differences between the auto-ignition and heat release behavior of gasoline surrogates and real gasolines (produced from refinery streams), both at naturally aspirated and boosted intake pressure conditions. In addition, the effect of ethanol blending on low-temperature heat release is investigated. Ethanol is found to suppress low-temperature heat release, requiring additional intake pressure to achieve similar heat release behavior. This was found, through kinetic modeling, to be due to the radical scavenging effect of ethanol, postponing the buildup of OH and HO_2 radical pools.

Chapter 4: Chapter 4 details fundamental engine and kinetic modeling investigations into intermediate temperature heat release in a Homogeneous Charge Compression Ignition engine. Mixtures of ethanol and normal-heptane are used as fuels; kinetic modeling was performed with greater confidence due to the use of pure components. Intermediate temperature heat release was found to be pressure sensitive, with the main heat-producing reactions being reactions between ethanol fuel radicals ($R\cdot$) and molecular oxygen (O_2) or hydroxyl radicals ($OH\cdot$) to form hydroperoxyl radicals (HO_2) or water (H_2O), respectively.

Chapter 5: Building on the investigations described in Chapters 2 through 4, this chapter investigates the influence of a gasoline's Piona composition and low-temperature heat release behavior on its low-load performance in a Gasoline Compression Ignition engine. The influence of low-temperature heat release was assessed using gasoline compression ignition experiments to measure the minimum achievable load with each fuel. Homogeneous Charge Compression Ignition engine experiments were performed to measure the low-temperature heat release behavior of each fuel. Gasoline Compression Ignition performance was compared to low-temperature heat release behavior, as well as Research Octane Number, Motor Octane Number, Anti-Knock Index, and Octane Index. Only the fuel's low-temperature heat release and Octane Index were found to be good indicators of low-load Gasoline Compression Ignition engine performance. This information, coupled with analysis from zero-dimensional chemical kinetic simulations, indicated that low-temperature heat release controls the auto-ignition process under Gasoline Compression Ignition conditions. Further, the influences on low-temperature heat release of various classes of fuel components, including ethanol, were investigated. While ethanol was found to effect the greatest suppression of low-temperature heat release, aromatic compounds also inhibited the low-temperature chemistry pathways.

Chapter 6: While combustion system performance underpins overall engine performance, the combustion system cannot be optimized independent of the engine system, as desired intake and exhaust conditions may require significant degradation of the total cycle efficiency. Chapter 6 investigates these tradeoffs in the manner described in Section X of Chapter 1.

Chapter 2:

Exploration of Heat Release in a Homogeneous Charge Compression Ignition Engine with Primary Reference Fuels

This article was presented at the 2013 Society of Automotive Engineers (SAE) Powertrains, Fuels, and Lubricants Conference.

David Vuilleumier, Hatem Selim, Robert W. Dibble, Mani Sarathy

I. Abstract

This study utilizes homogeneous charge compression ignition HCCI engine experiments to characterize fuel effects on Low Temperature Heat release (LTHR) and Intermediate Temperature Heat Release (ITHR) of different primary reference fuel mixtures (PRF). Experiments varied intake pressure from naturally aspirated to 1.8 bar boosted conditions, equivalence ratio from ϕ=0.3 to 0.4, and a variety of different fuel mixtures (PRF 85 to PRF 100). The engine experiments were used to guide single-zone HCCI simulations, using detailed chemical kinetic mechanisms comprising PRF mixtures. The experiments revealed important trends related to pre-ignition reactions in blends of isooctane and n-heptane. As previous research has found, the pre-ignition reactions seen in these mixtures have a high sensitivity to pressure. Intake pressures below 1.4 bar showed no LTHR and minimal ITHR for all of the fuels tested, while pressures of 1.4 bar and above showed varying onsets of LTHR based on mixture composition. It was also found that significant increases in ITHR were coupled with increases in LTHR. Simulated heat release profiles of different PRF mixtures were examined and compared with the experimental results. The simulations results showed good agreement with the experiments for different fuels at low pressures. However, at higher pressures, the expected LTHR and ITHR profiles at the given experimental conditions were not observed. Sensitivity analysis was conducted to identity the fuel mixtures and pressures needed for to exhibit similar heat release profiles as the experiments. The simulation results were used to identify the dominant reaction pathways contributing to ITHR under various conditions.

II. INTRODUCTION

Homogeneous Charge Compression Ignition (HCCI) engines operate with high efficiencies and with low oxides of nitrogen emissions when compared to spark ignited (SI) engines due to burning highly dilute charges and not requiring throttling. However, due to knocking caused by short combustion duration, HCCI engines have difficulty achieving high power densities required of automotive engines [Eng 2002, Dec 2009 Proc.]. It has been shown that delayed combustion timing coupled with boosting and higher equivalence ratios can allow high power outputs in HCCI engines, as the piston expansion after top dead center (TDC) reduces the peak pressure rise rate of the burning charge [Sjöberg 2007, Sjöberg 2004, Saxena 2011, Dec 2010]. In addition, for higher power output conditions, moderate to late combustion timing has been shown to increase overall efficiency through reduced heat losses, though this is dependent on retaining high combustion efficiency [Saxena 2013].

While late combustion timing is at times critical to HCCI operation, combustion phasing in HCCI is heavily influenced by Low Temperature Heat Release (LTHR) and to a lesser extent Intermediate Temperature Heat Release (ITHR). LTHR is a term that describes the first stage heat release in dual stage heat release fuels; it is termed LTHR because it typically occurs in HCCI engines at temperatures ranging from 600 K to 800 K, though this range is fuel and operating condition dependent [Westbrook 2007]. ITHR is a term that describes heat released between the end of LTHR and the start of main combustion (here referred to as High Temperature Heat Release, or HTHR). ITHR is characterized by a low rate of heat release (ROHR) that transitions into HTHR. Because the ROHR typically does not drop before the start of HTHR, ITHR is more difficult to define and to quantify than LTHR, though ITHR typically occurs in the temperature range of 950 – 1050 K [Sjöberg 2007], and the key reactions contributing to ITHR have been identified for multiple fuels [Mehl 2012, Vuilleumier 2013]

LTHR typically releases heat during the compression stroke, raising charge temperature prior to TDC and therefore advancing ignition [Westbrook 2007, Shibata 2005, Tanaka 2003]. In addition, LTHR creates a radical pool that can both enable ITHR and advance HTHR. ITHR has been shown to release heat in the TDC region, and the heat release between TDC and HTHR reduces or eliminates the temperature drop that would be created by the piston descending after TDC. By providing a more stable temperature in the TDC region, ITHR has been linked to greater combustion stability with late firing, allowing CA50's of up to 16° ATDC [Dec 2010].

While LTHR and ITHR are able to improve certain aspects of HCCI combustion, such as combustion stability and intake temperature requirements, there are possible negative effects of these phenomena as well. LTHR can advance combustion phasing thereby causing or increasing knocking under certain conditions, such as high power output [Shibata 2005]. In addition, heat released by LTHR prior to TDC degrades the efficiency of the engine, as part of the fuel's chemical energy is released during the compression stroke. Negative effects of ITHR have not been thoroughly investigated, though it is possible that ITHR could have the same negative effects as LTHR under certain conditions.

Previous experimental work on PRF blends in HCCI engines has shown that LTHR occurs for most PRF blends, even those with relatively high isooctane content [Shibata 2005]. It has also been demonstrated that a given PRF mixture will show more LTHR in an HCCI engine than gasoline for a given octane rating, due to the LTHR inhibitors that are found in gasoline [Shibata 2005]. ITHR has been shown to occur in PRF 80, increasing the late firing limit of HCCI [Sjöberg 2007]. ITHR often occurs in cases where LTHR is significant, however previous work has shown that significant LTHR is not necessary for ITHR, but rather a radical pool generated by low temperature chemistry [Dec 2010, Vuilleumier 2013].

Hwang and co-workers [Hwang 2008] examined HCCI autoignition both experimentally and numerically. They found that PRF80 was the only tested fuel to have LTHR; however, in order to match the experimental results a PRF40 detailed chemical kinetic model was used numerically. Mehl and co-workers [Mehl 2009] also numerically investigated LTHR profiles of PRF80 in HCCI using a single-zone model and an updated detailed gasoline reaction mechanism. Their results revealed that a PRF68 detailed chemical kinetic model successfully simulated the experimental data.

This study seeks to further the understanding of the interplay between LTHR and ITHR in gasoline surrogates, develop a better understanding of the pressure dependency of pre-ignition reactions, and explore the fuel chemistry effects that change the magnitude of ITHR and LTHR in HCCI engines.

III. METHODS

a) Experimental Methods

A four-cylinder 1.9L Volkswagen TDI engine was used in this study, as previously described in [Saxena 2011, Vuilleumier 2013]. This study fired only cylinder 4 of the engine. Cylinder 4's intake and exhaust systems are separate from the other 3 cylinders, to allow this cylinder to function without interference from the other cylinders. The engine is driven by an electric motor at a speed of 1800 RPM. The engine has had the following modifications to provide a better platform for HCCI combustion:

1) The original deep-bowl pistons have been replaced with 17:1 CR bathtub-bowl pistons.
2) Combustion chambers are fitted with AVL QH33D water-cooled quartz piezoelectric pressure transducers installed in the original diesel injector port.
3) The custom intake manifold has been fitted with port fuel injection.
4) Fuel is fed to the injectors by a nitrogen-pressurized tank maintained at 45 PSI.
5) Fuel injection is controlled by a custom NI/Labview based system.
6) Fuel flow is measured via change in scale measurements over time.
7) Equivalence ratio is measured via automotive-type wide-band lambda sensors installed in the exhaust manifolds with a precision of ± 0.015.
8) Intake air is pressurized by a 100 HP compressor with a 6 m^3 surge tank, and controlled by a pressure regulator.
9) A Kulite XTEL 190(M) piezoresistive pressure sensor with a precision of ± 2% measures intake pressure near the intake valve with crank-angle resolution.
10) Temperatures in the intake and exhaust system are measured using K-Type thermocouples with a precision of ± 2 Kelvin.

Figure 2.1 shows a schematic of the engine used in this study.

The data was collected at stable, non-transient, engine operating points, with constant intake conditions (temperature, pressure, and equivalence ratio). Each test point was replicated once to check for consistency in results. For each of these test points several parameters were measured and recorded, the most important of which include the in-cylinder pressure, the intake temperature, the exhaust temperature, the equivalence ratio, and the mass of fuel injected.

In-cylinder pressure was measured at intervals of every 0.25° with each pressure measurement being triggered by the signal from a crankshaft encoder. For each test point, 300 consecutive thermodynamic cycles were measured and recorded. Equivalence ratio is controlled via a feedback control system using the wideband lambda sensor in the exhaust manifold and fuel injection pulse width control.

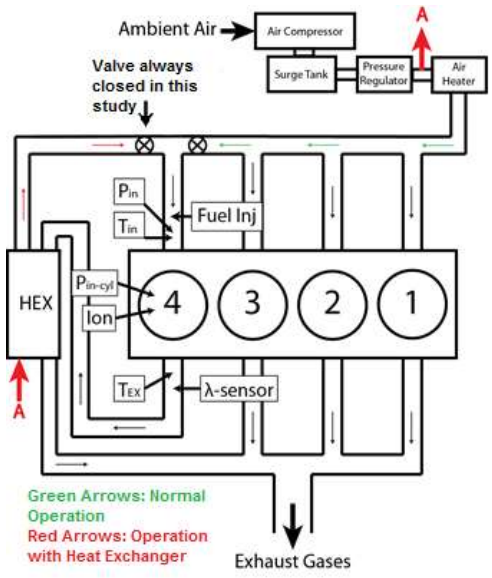

Figure 2.1. Schematic of engine, including intake system, exhaust system, and key sensors.

To calculate engine parameters such as blow by, wall heat loss (Woschni model [Woschni 1967]), pressure loss across the intake valve, and intake valve closure (IVC) temperature were calculated using a cycle simulation of the engine in AVL Boost [AVL 2013], as in [Shibata 2005]. The abovementioned values were determined by the comparison of measured and calculated motored pressure traces of all the conditions used in firing cycles. For the blow by and wall heat calibration factor special attention was paid on the expansion part of the cycle. With the calibrated model the IVC temperature is calculated for all different intake conditions.

Post-processing of the measured data was performed to calculate the ROHR and in-cylinder temperature profiles. The process used in this study was the same as used in [Vuilleumier 2013]. The basis for the calculation was the average pressure trace of three hundred consecutive cycles. Before averaging, the pressure of each individual cycle was smoothed by using a Savitzki-Golay filter with 19 points [Savitzki 1964]. The calculation of ROHR was made by a procedure described in [Heywood 1988]. The ROHR model included blow by and wall heat losses. The wall heat losses are calculated with a Woschni model and use calibration factors determined from cycle simulation calculations. The thermodynamic properties of the mixture were calculated by using NASA polynomials of the species in the mixture. The calculation assumes the cylinder mixture during the compression stroke is comprised of fuel, air and residual gases. The amount of residual gases was calculated by the cycle simulation calculation. After combustion, during expansion, the cylinder mixture is comprised of combustion products that would be formed from the initial mixture if complete combustion is assumed. The change from initial mixture to combustion products happens during combustion and it is assumed that this change is proportional to the Vibe [Vibe 1970] combustion profile with assumed start and end of combustion. The process is iterative which means that after calculation of ROHR the start and end of combustion are calculated and used as new assumptions. The iteration is ended when the assumed start and end of combustion are equal to the calculated ones. In-cylinder temperature is calculated by using the ideal gas equation and calculated profiles of mass, volume and composition during the closed cycle.

Table 2.1: General engine parameters.

Compression Ratio	17:1
Displacement	.474 L
Bore	79.4 mm
Stroke	95.5 mm
Rod Length	144 mm
Coolant Temperature	95 °C
Oil Temperature	100 °C
Fuel Injection	Port Fuel Injection
Fuel Pressure	45 PSI
No. of Valves	2
IVO	2 °bTDC
IVC	47.5 °aBDC
EVO	47.5 °bBDC
EVC	8 °aTDC

b) Simulation Methods

Simulations of HCCI engine were conducted and compared with the experimental results. The detailed chemical reaction mechanism developed for gasoline fuels by Lawrence Livermore National Laboratory (LLNL) **[**Mehl 2012, Mehl 2011, LLNL Surrogate 2013] was used. Simulations were conducted using single-zone HCCI simulator provided in the CHEMKIN-PRO software [Chemkin 2013], wherein the entire charge (air and fuel) is assumed to be thermodynamically uniform. Even though this approximation does not match the actual case, it has been widely used by multiple research groups when modeling HCCI engines [Hwang 2008, Silke 2009, Naik 2005**]**. The reason being is that the single-zone model can give considerable details about the chemical kinetics of HCCI combustion with low computational cost. For all simulations, the CA50 was maintained constant at 6 degrees ATDC in coherence with the experimental work. The simulations were performed under adiabatic conditions. In order to maintain similar pressure rise rate history in the numerical simulations, compression ratio was set to be 16.75:1; while the actual compression ratio of the engine was approximately 17:1. The equivalence ratio was kept constant at 0.4 under all conditions. While simulations of HCCI engines are typically performed under adiabatic conditions [Tsujimura 2011, Dec 2004], maintaining CA50 constant between the experimental and numerical analyses is not common. The common assumption that compensates for using a single-zone model is matching $CA10_{experimental}$ with the $CA50_{numerical}$. This emanates from the assumption that, realistically, 20% of the charge, referred to as the "ignition core", will be under adiabatic conditions, hence 10% of heat released experimentally corresponds to 50% of heat released numerically **[**Silke 2009**]**. However, using this approach typically does not successfully capture the combustion details for the same PRF. This is

credited to the fact that, the abovementioned assumption advances the combustion phasing, which typically cannot be mimicked by the available reactions mechanisms. In addition, this approach requires changes in the simulation parameters such as cylinder volume and inlet pressure in order to efficiently simulate the volume and partial pressure of 20% of the charge in experiments. This was evident in previous findings, where the authors had to use significantly higher n-heptane composition to achieve the same experimental behavior (e.g., PRF40 simulates PRF80 [Hwang 2008], and PRF54 simulates PRF80 [Mehl 2009]). While matching the simulated CA50 with the experimental CA10 is a logical practice, we do not believe this is the ideal method to study the effects of various fuel mixtures on heat release profiles. Instead, we decided to maintain the same CA50 between the experiments and the simulations, and to determine the change in inlet parameters to qualitatively study the experimentally observed trends. This numerical approach started with simulations of the experimental results under the same inlet conditions. Heat release rate profile was analyzed and LTHR and ITHR regions were identified. Secondly, parametric studies were conducted in order to pinpoint the role of pivotal parameters on the heat release profile. Specifically, effects of PRF composition and inlet pressure were considered.

IV. RESULTS AND DISCUSSION

a) Experimental Results

Experiments were conducted at a variety of intake pressures and at two equivalence ratios, for 4 PRF blends. These conditions are presented in Table 2.2. Pressure traces collected during the experiments are presented in Figure 2.2 and in the Appendix Figures A1-A3, while the associated calculated temperature profiles are presented in Figure 2.3 and Appendix Figures 2.4-2.6. The pressure traces show that as intake pressure is increased from 1.0 bar to 1.6 bar, TDC pressures increase from approx. 37 bar to approx. 61 bar. The calculated temperature profiles show that HTHR at 1.0 bar starts between 1075 K and 1125 K, with PRF 85 requiring to lowest temperature and PRF 100 requiring the highest temperature. As intake pressure is increased to 1.6 bar, HTHR begins at lower temperatures: from 925 K for PRF 90, to 1025 K for PRF 100.

Table 2.2. Range of conditions tests.

Intake Pressure	1.0 – 2.0 bar
Equivalence Ratio	ϕ = 0.3 - 0.4
Fuels	PRF 85 - PRF 100
CA 50	6 °aTDC
Engine Speed	1800 RPM

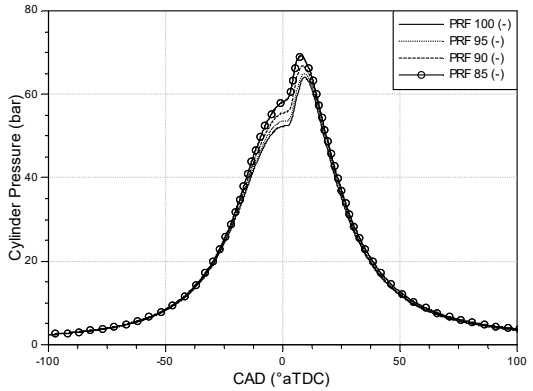

Figure 2.2. Pressure traces for various fuels at 1.4 bar intake pressure, ϕ = 0.4, and CA50 = 6 °aTDC.

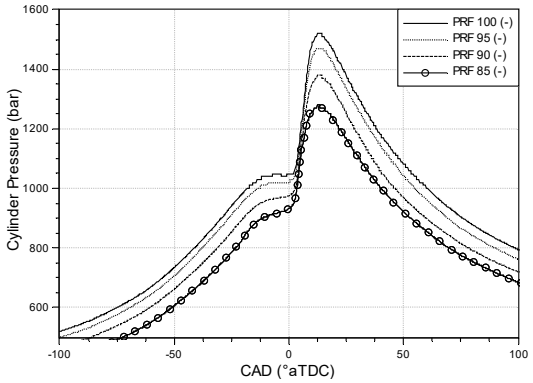

Figure 2.3. Temperature profiles for various fuels at 1.4 bar intake pressure, ϕ = 0.4, and CA50 = 6 °aTDC.

Figures 2.4 and 2.5 and Appendix Figures 7 and 8 show heat release rates for a range of intake pressures and PRF blends, and these are the same conditions for which pressure and temperature profiles were presented in Figures 2.2 and 2.3, and Appendix Figures 1 through 6. Because equivalence ratio was held constant rather than fuel energy, and intake temperatures changed to achieve constant combustion phasing for fuels with varying reactivity, the mass of fuel injected and therefor the fuel energy injected changes from trace to trace. To compensate for this, the heat release rates that are presented have been scaled by the total fuel energy injected in a given cycle, to allow fair comparison of the heat release rates among different fuels for similar conditions. Figures 2.6 through 2.9 show the same heat release profiles, but magnified to focus on the LTHR and ITHR regions. While the HTHR profiles are generally similar among the different cases, the LTHR and ITHR regions show more significant changes. Throughout the data, trends are seen with changing fuel fractions of n-heptane and isooctane, with changing intake pressure, and with changing equivalence ratio.

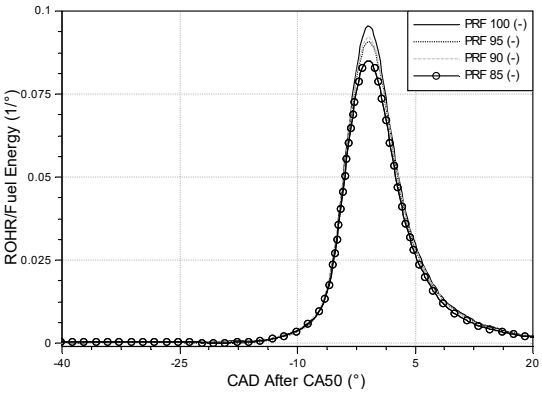

Figure 2.4. Heat release profiles for various fuels at 1.0 bar intake pressure, ϕ = 0.4.

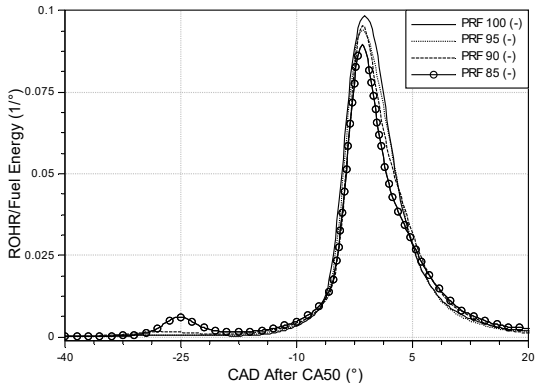

Figure 2.5. Heat release profiles for various fuels at 1.4 bar intake pressure, ϕ = 0.4.

Significant differences in LTHR and ITHR are seen as intake pressure increases. Figure 2.6 shows that at 1.0 bar intake pressure (absolute) for ϕ = 0.4, minimal differences are seen in the LTHR and ITHR regions for the different fuels. However, as intake pressure increases to 1.4 bar (Figure 2.8) with the same equivalence ratio, PRF 85 shows LTHR and increased ITHR. At the same pressure, PRF 90 shows the beginnings of LTHR as well as enhanced ITHR, and PRF 95 now shows more ITHR than PRF 100. This trend continues as intake pressure increases to 1.6 bar (Figure 2.9): PRF 85 now produces enough LTHR that the required intake temperature to maintain constant combustion phasing is below ambient temperature, while PRF 90 shows more LTHR than at 1.4 bar intake pressure, and PRF 95 shows a small amount of LTHR and increased ITHR. These results indicate that higher intake pressures increase the low-temperature reactivity of PRF blends, while not significantly altering the HTHR profiles. Ultimately, while intake pressures are a convenient way to describe the experiments that were performed, the pressures during the LTHR and ITHR region are likely more important to note when comparing engines with different compression ratios. In this case, the TDC pressures changed from approx. 37 bar (at 1.0 bar intake pressure, unreacted), to approx. 52 bar (at 1.4 bar intake pressure, unreacted), to approx. 61 bar (at

1.6 bar intake pressure, unreacted). This indicates that for the equivalence ratios tested, the shift in fuel chemistry to produce LTHR and ITHR in significant quantities occurs in the 40-50 bar range.

In addition to the pressure effect on LTHR and ITHR, a fuel effect is visible in these results. With the test engine's compression ratio of 17:1, increased n-heptane fractions resulted in increased LTHR and ITHR at and above 1.4 bar intake pressure. At 1.6 bar intake pressure the fuel sensitivity increased, with larger changes in the heat release profile observed for each 5% addition of n-heptane, when compared to 1.0 bar or 1.4 bar intake pressure. 1.0 bar intake pressure produced minimal differences between the heat release profiles for the four fuels tested; however n-heptane fractions greater than 15% were not tested, and it is likely that larger changes in the PRF number would have resulted in LTHR.

At 1.4 bar intake pressure, experiments at two equivalence ratios (ϕ= 0.3, 0.4) were run to test the effect of equivalence ratio on LTHR and ITHR. Comparisons of Figures 2.7 and 2.8 show that the lower equivalence ratio results in less LTHR and ITHR. These results demonstrate that ITHR is sensitive to both pressure and equivalence ratio, with more ITHR occurring with higher amounts of either variable.

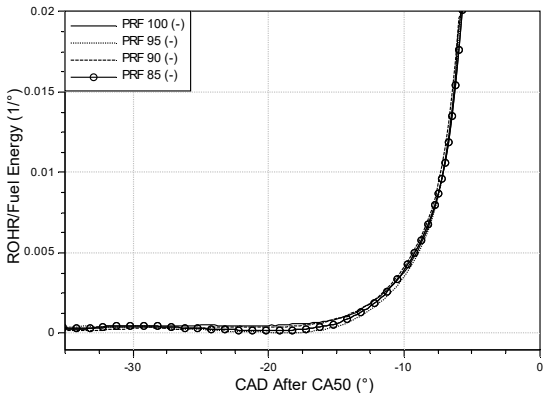

Figure 2.6. Magnified heat release profiles for various fuels at 1.0 bar intake pressure, ϕ = 0.4, and CA50 = 6 °aTDC.

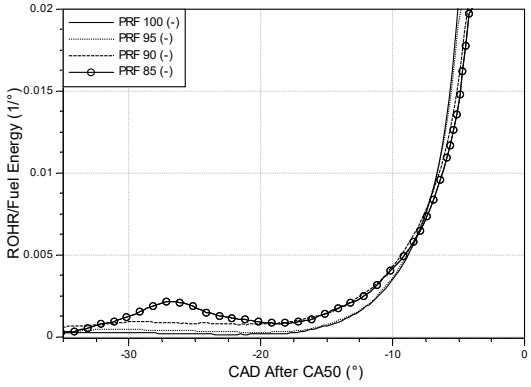

Figure 2.7. Magnified heat release profiles for various fuels at 1.4 bar intake pressure, ϕ = 0.3, and CA50 = 6 °aTDC.

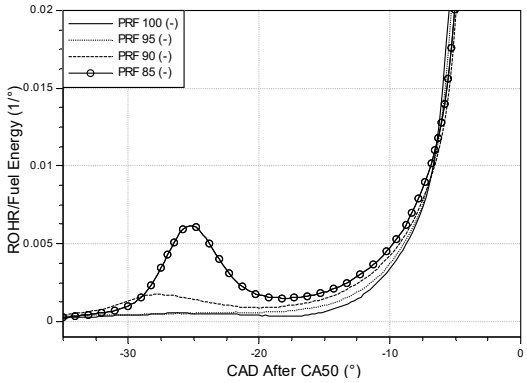

Figure 2.8. Magnified heat release profiles for various fuels at 1.4 bar intake pressure, ϕ = 0.4, and CA50 = 6 °aTDC.

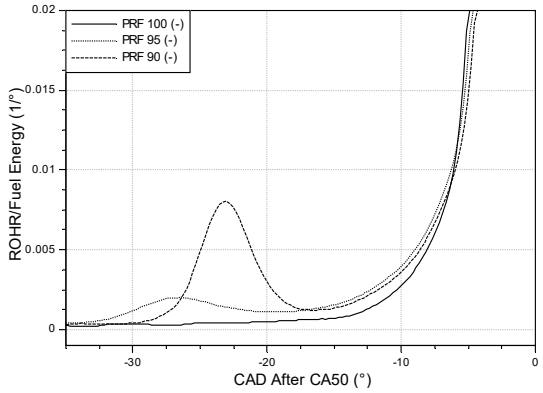

Figure 2.9. Magnified heat release profiles for various fuels at 1.6 bar intake pressure, ϕ = 0.4, and CA50 = 6 °aTDC.

Pressure, coupled with LTHR and ITHR, had a large effect on intake temperature requirements to maintain a constant combustion phasing, as seen in Figure 2.10. PRF 100, which showed no LTHR behavior in the pressure range that was tested, did show an increase in ITHR and overall reactivity as intake pressure increased, and this resulted in intake temperature requirements which decreased by 70° C, as intake pressure increased from 1.0 bar to 1.6 bar. However, the effect was larger for cases that not only increased ITHR, but also LTHR. PRF 95's intake temperature dropped 117 ° C, while PRF 90's intake temperature dropped 146° C. In both of these cases, the largest drop in intake temperatures occurred with the onset of LTHR. This is likely due to the dual effects of the charge heating and increased radical pool provided by LTHR. The increased radical pool also increases ITHR and overall fuel reactivity.

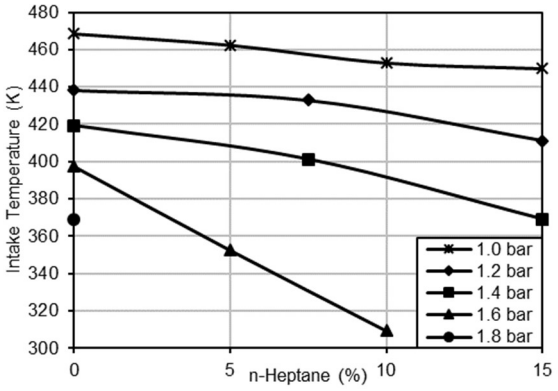

Figure 2.10. Intake temperatures required to maintain constant combustion phasing of CA50 = 6 °aTDC for various PRF blends and intake pressures.

b) Modeling Results

The modeling started with numerical simulations of the experimental results under adiabatic conditions. A constant CA50 has been maintained for all cases at 6 °aTDC. The primary reference fuel composition changed between 100-85 at different intake pressures of 1-2 bar, while the equivalence ratio was kept constant at 0.4. The inlet temperature for each inlet fuel mixture and/or pressure condition was changed so as to maintain constant CA50.

100% isooctane

Figure 2.11 presents the heat release profiles of PRF100 with different intake pressures. The temperature after TDC until combustion takes place was roughly constant at 1000 K for all cases. The numerical results successfully captured ITHR profiles at high intake pressures. Absence of LTHR was expected due to the low reactivity of the mixture (100% isooctane). The trends obtained from the numerical results agree qualitatively with the obtained experimental findings; however, a higher inlet pressure was required in the simulations to achieve the same increase in ITHR.

95% isooctane, 5% n-heptane

Heat release profiles under different intake pressures are depicted in Appendix Figure 2.9**.** Similar to the previous case, PRF95 gives a prominent increase in ITHR with an increase in intake pressure. However, it did not show any cool flame behavior under the experimentally examined conditions. This agrees with the obtained experimental results, but again a higher inlet pressure is needed to achieve the same increase in ITHR as the experiments.

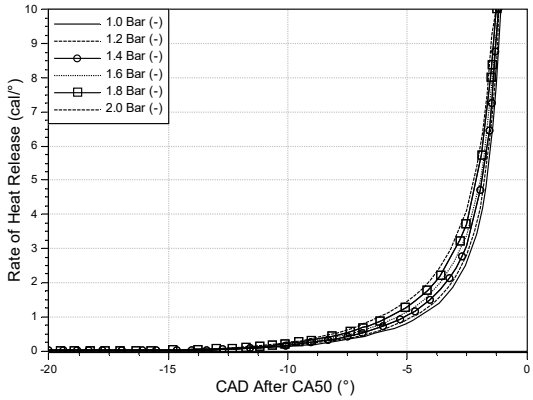

Figure 2.11. Simulated heat release profiles for PRF100 under different inlet pressures, constant CA50 = 6 deg, ϕ = 0.4.

90% isooctane, 10% n-heptane

Similar to the previous cases, ITHR was observed at intake pressures higher than 1 bar for PRF90 fuel. However, the concentration of n-heptane was not high enough to trigger the occurrence of LTHR, as shown in Appendix Figure 2.10. Again, these results agree qualitatively with the presented experimental data.

85% isooctane, 10% n-heptane

Figure 2.12 depicts heat release profiles of PRF85 at different intake pressures. The results showed poor agreement in comparison with the experimental results. Absence of any LTHR was evident in the simulations unlike the experimental results where significant LTHR was obtained at 1.4 bar intake pressure. This is due to several reasons: i.) the low reactivity of the reaction mechanism cannot capture low-temperature chemistry as well as high-temperature chemistry, and ii) the use of a single-zone model considers the entire charge as a lumped mixture wherein homogeneity dilutes the charge, whereas in the experiments local fuel-rich as well as fuel-lean spots exist (i.e., fuel stratification). Moreover, neglecting the residuals effect, which can create local hot pockets (i.e., thermal stratification), poses an important role.

Figure 2.13 shows the change in inlet temperature needed to maintain same combustion phasing at different PRF compositions as well as inlet pressure. The results showed consistent decrease in the required inlet temperature with the increase of n-heptane composition due to its higher reactivity at lower temperatures. Similarly, increase in inlet pressure required decrease in inlet temperature so as to avoid advanced firing.

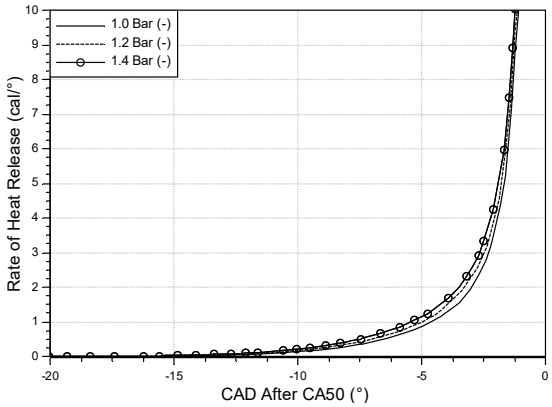

Figure 2.12. Simulated heat release profiles for PRF85 under different inlet pressures, constant CA50 = 6 °aTDC, ϕ = 0.4.

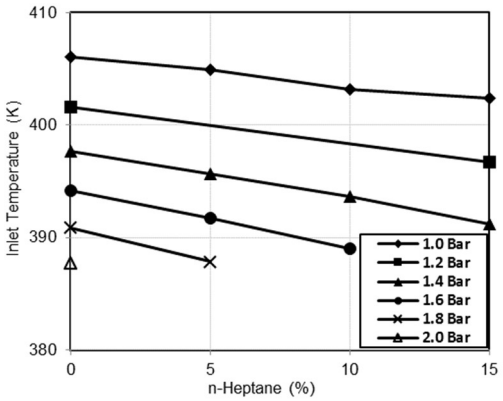

Figure 2.13. Required inlet temperature in simulations to maintain constant combustion phasing, CA50 = 6 °aTDC, at ϕ = 0.4, with various intake pressures.

<u>Effect of PRF Composition and Inlet Pressure</u>

In this section, we investigate sensitivity of the combustion heat release to inlet pressure and PRF composition. We chose PRF85 at 1.4 bar intake pressure as our baseline case and then investigated the effect of the inlet pressure as well as fuel composition on heat release profiles while maintaining CA50 at 6 degrees ATDC.

Figure 2.14 represents heat release profiles of PRF85 at wide range of intake pressures. The results showed continuous increase in ITHR between intake pressures of 1.4 up to 2 bar where a minimal LTHR was observed. However, significant LTHR was obtained beyond 2 bar. Consequently, we can conclude that higher intake pressures (2.2 bar) are required to achieve the experimental results (1.4 bar) due to the abovementioned reasons. On the other hand, Figure 2.15 shows the decrease in inlet temperature heat release so as to keep constant combustion phasing. One can see higher rate of decrease in the required temperature at 2.2 bar where the LTHR starts to have a significant role. Subsequently, lower inlet temperature is required to retard the CA50.

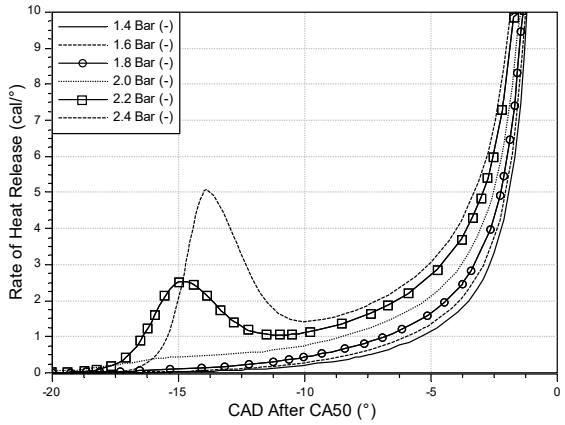

Figure 2.14. Simulated heat release profiles of PRF85 at different pressures, CA50 = 6 °aTDC, and ϕ = 0.4.

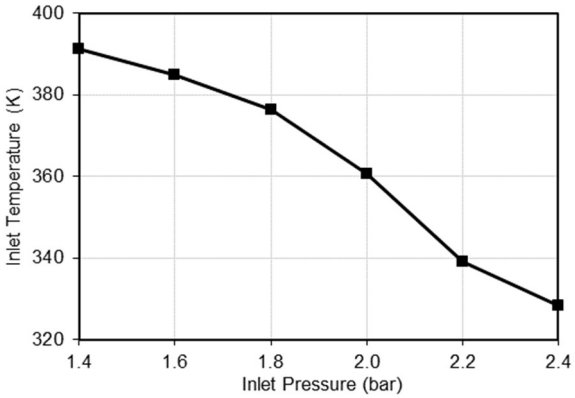

Figure 2.15. Required inlet temperature for PRF85 at different pressures to maintain CA50 at 6 °aTDC with ϕ = 0.4.

Change in PRF composition at the same intake pressure did not give a significant effect on the heat release profiles up to PRF75, as shown in Figure 2.16. No LTHR was observed, and the increase in ITHR was marginal. However, at 30% n-heptane significant increase in ITHR was attained, and LTHR started to take place. Effect of LTHR was reflected on the required inlet temperature to maintain constant CA50. As shown in Figure 2.17, substantial decrease in the required inlet temperature was observed for PRF70 where the onset of LTHR was observed.

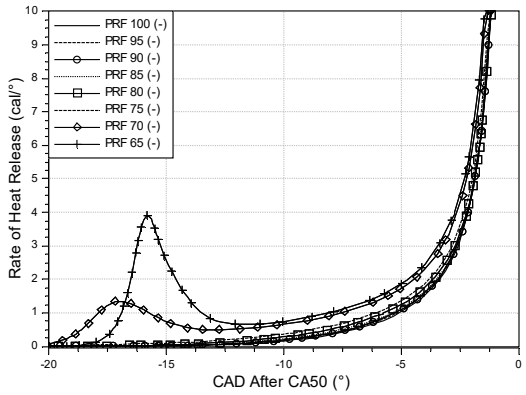

Figure 2.16. Heat release rate for different PRF compositions at 1.4 bar intake pressure with ϕ = 0.4 and CA50 = 6 °aTDC.

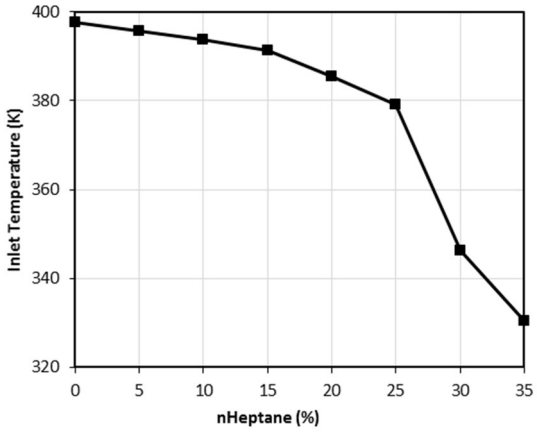

Figure 2.17. Required inlet temperature for different PRF compositions with the same inlet pressure, 1.4 bar, to maintain CA50 at 6 °aTDC with ϕ = 0.4.

<u>Reaction Path Analysis</u>

This section discusses the reaction kinetics of LTHR numerically. Two cases of the previously presented parametric studies are included. Case 1 represents the LTHR due to high intake pressure (PRF 85 and 2.2 bar) and Case 2 discusses the LTHR due to high n-heptane concentration (PRF70, 1.4 bar intake pressure). This study presents the major elementary reactions responsible for the LTHR and the major exothermic elementary reactions that contribute in the heat release in the LTHR zone.

Combustion in the LTHR region starts with hydrogen abstraction from n-heptane and/or isooctane (RH) to form alkyl radical (R). The formed alkyl radical then adds molecular oxygen and follows a series of low temperature reaction sequences that eventually form stable compounds such as ketones and cyclic ethers and release hydroxyl radicals. Details of the chemistry of PRF combustion and low temperature chain branching chemistry are given elsewhere [12, 25]. Appendix Figures 2.11 through 2.13 depict the reaction rate of elementary reactions responsible for the abovementioned series of reactions in Case 1. Results are only presented for n-heptane combustion, while isooctane is expected to follow the same reaction pathways. One can clearly

see that OH and HO_2 are the most dominant radicals in the hydrogen abstraction stage. Different isomerization reactions take place for the alkylperoxy radical (RO_2) as shown in Appendix Figure 2.12, to form hydroperoxyalkyl (QOOH) radicals. The QOOH radicals then either reacts to form a cyclic ether plus release OH or adds another molecular oxygen to form an intermediate (O_2QOOH) that rapidly decomposes to OH radicals and ketones, as shown in Appendix Figure 2.13. Figure 2.18 presents exothermic elementary reactions that contribute considerably to the LTHR. Net heat release by each reaction was integrated over the LTHR zone and normalized by the total LTHR. The highest heat release is contributed by isooctane reactions. This seems to be counter-intuitive since n-heptane is responsible for initiation of the LTHR. However, the high composition of isooctane in the fuel mixture, 85%, results in this high heat release contribution by isooctane reactions. Formation of HO_2 radical via hydrogen peroxide reaction with oxygen poses a pivotal role in the LTHR. In addition, radical-radical reactions have a prominent contribution into the LTHR such as reactions 4 and 7, and this also highlights the role of OH.

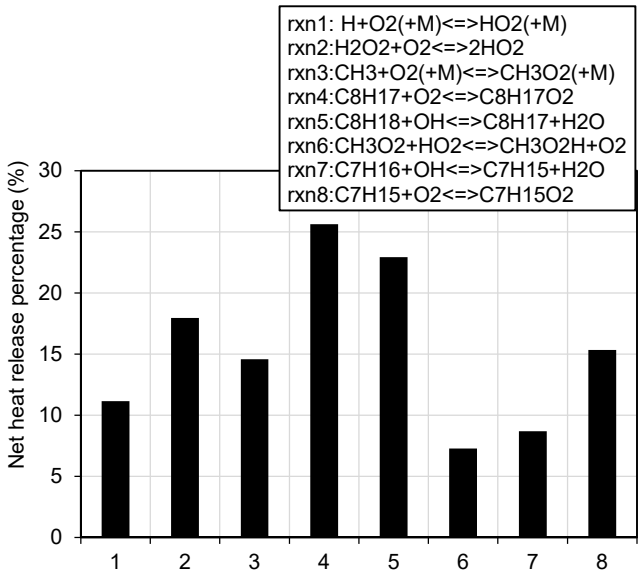

Figure 2.18. Net heat release by elementary reactions as a percentage of the total LTHR, PRF85 at 2.2 bar intake pressure, CA50 = 6 °aTDC, and ϕ = 0.4.

Appendix Figures 14 through 16 describe the reaction rate of main elementary reactions responsible for the LTHR onset in PRF70 fuel at 1.4 bar intake pressure. No remarkable changes were observed in terms of reaction rate trends or magnitude as compared to Case 1. Figure 2.19 depicts the net heat release by several elementary reactions. Comparing the trends obtained from both cases allows several conclusions to be obtained. Firstly, in Case 2 n-heptane reactions releases more heat than the isooctane reactions, even though n-heptane composition is 30%. It is also the major trigger of the low temperature combustion. Heat release by reactions 2 and 3 contribute less than in Case 1 which was conducted at higher pressures. This can be attributed to the fact reactions 2 and 3 are pressure dependent and accelerate at higher pressures. Thus, increasing the pressure in Case 1 has a considerable effect on accelerating these reactions and their contribution to LTHR.

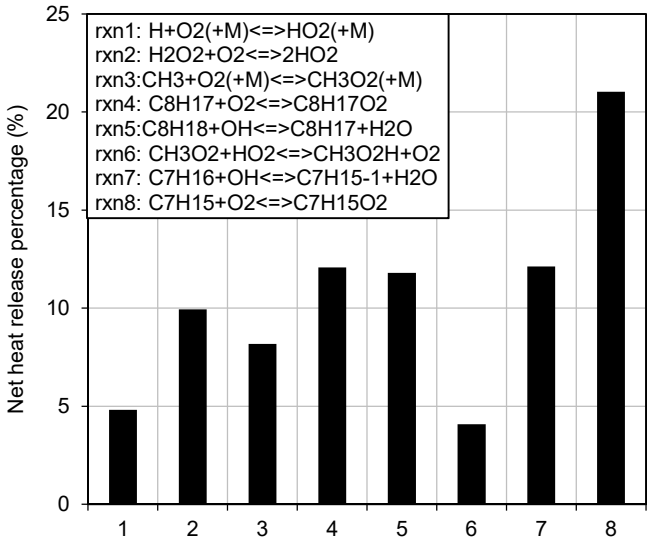

Figure 2.19. Net heat release by reactions as a percentage of the total LTHR, PRF70 at 1.4 bar intake pressure, CA50 = 6 °aTDC, and ϕ = 0.4.

V. SUMMARY/CONCLUSIONS

This paper has used engine experiments and chemical kinetic simulations to better understand the relationship between fuel composition and heat release characteristics in HCCI engines. PRF 100 through PRF 85 have been tested in an HCCI engine, and it has been found that PRF 100 does not produce LTHR for intake pressures between 1.0 bar and 1.6 bar, but it does produce increasing amount of ITHR as intake pressure is increased. Also, PRF 95 through PRF 85 produce LTHR once a critical intake pressure has been reached. This intake pressure decreases as the PRF number decreases. Finally, LTHR and ITHR are shown to be ϕ sensitive, with higher ϕ's leading to higher amounts of LTHR and ITHR.

Experimental results were numerically simulated using single-zone model of CHEMKIN-PRO software under adiabatic conditions; reaction mechanism developed by Lawrence Livermore National Laboratory (LLNL) has been used. The results showed good agreement with the experimental data for lower intake pressures. However, at an intake pressure of 1.4 bar and PRF85, unlike experimental data, numerical simulations failed to attain the LTHR profiles. Parametric studies were implemented to identify the effect of inlet pressure as well as PRF composition on heat release profiles. The results showed that LTHR started to take place at an intake pressure of 2 bar and above for PRF85. On the other hand, PRF70 was required to attain LTHR at 1.4 bar. Chemical kinetics analysis showed the reaction rates of pivotal elementary reactions within the LTHR zone. In addition, the highest net heat release rates per elementary reactions were identified within the cool flame. The major exothermic reactions were found to include OH and HO_2 radicals as well as alkyl radials released into the reaction pool after hydrogen abstraction.

VI. DEFINITIONS AND ABBREVIATIONS

ϕ	equivalence ratio
°aBDC	degrees after bottom dead center
°bBDC	degrees before bottom dead center
°aTDC	degrees after top dead center

°bTDC	degrees before top dead center
CA10	crank angle at which 10% of the heat has been released
CA50	crank angle at which 50% of the heat has been released
CAD	crank angle degrees
HCCI	homogenous charge compression ignition
HTHR	high temperature heat release
ITHR	intermediate temperature heat release
LTHR	low temperature heat release
PRF	primary reference fuel
ROHR	rate of heat release
RPM	revolutions per minute
TDC	top dead center

Chapter 3:

Investigation of the influence of intake pressure and fuel composition on Low-Temperature Heat Release in a gasoline fueled HCCI engine

This article is being prepared for submission to the journal Fuel.

David Vuilleumier, Nour Atef, Goutham Kukkadapu, Ben Wolk, Darko Kozarac, Samveg Saxena, Robert Dibble, Mani Sarathy

Abstract:

Advanced Combustion Engines (ACE's) have been shown to both reduce combustion related emissions as well as increase overall thermal efficiency of piston engines. ACE's typically rely on partially premixed or fully premixed charges that are autoignited through compression ignition. The autoignition timing is often kinetically-controlled. A critical factor in the autoignition of gasoline type fuels is the amount of low-temperature and intermediate-temperature heat release (LTHR & ITHR) that occurs, as this heat release elevates the charge temperature prior to autoignition. It has been observed that at lower intake pressures gasoline behaves as a single-stage heat release fuel, while at higher intake pressures gasoline behaves as a two-stage heat release fuel. However, the conditions at which this transition occurs have not been thoroughly investigated.

This paper experimentally investigates the conditions under which gasoline transitions from a single-stage heat release fuel to a dual-stage heat release fuel as intake pressure is increased. These experiments were performed in a single-cylinder HCCI engine fueled with two research-grade gasolines, FACE A and FACE C. These gasolines were tested neat, and with 10% (by volume) ethanol addition, and with 20% ethanol addition. In addition, these results were compared to results previously obtained for PRF 84, and additional results for PRF 84 with 10% and 20% ethanol addition are also presented. The experiments revealed that there was no measurable difference between the onset of LTHR for the three fuels, FACE A, FACE C, and PRF 84. However, as ethanol was added to these fuels, the onset of LTHR shifted from 1.4 bar intake pressure to 2.2 bar intake pressure (for 20% ethanol addition).

I. Introduction:

Homogeneous Charge Compression Ignition (HCCI) engines fundamentally rely on the autoignition of a fuel-oxidizer mixture for operation [Aceves 2001]. Therefore, it is critical to understand the auto-ignition behavior of any fuel used in an HCCI engine, so that the conditions for auto-ignition of the fuel-oxidizer mixture can be developed in the engine at the appropriate part of the cycle. Further, other advanced engine concepts, such as Gasoline Compression Ignition [Ciatti 2013, Sellnau 2012] and Partially Premixed Compression Ignition [Kalghatgi 2007, Lewander 2009], also feature an auto-ignition process that partially controls the combustion behavior. Understanding the auto-ignition of fuels in these engines is critical to their operation; however, due to the highly inhomogeneous mixture found in these other advanced engine concepts, the HCCI engine is a more suitable system for studying fuel auto-ignition.

In an HCCI engine, two types of auto-ignition are typically encountered [Tanaka 2003, Sjöberg 2007]. In general, fuels with low reactivity, such as isooctane or methane, will ignite in a single stage; upon reaching a certain temperature and pressure, the fuel will autoignite, rapidly combusting and releasing all of the fuel's chemical energy [Aceves 2000 HCCI, Vuilleumier 2013 Exp.]. In contract, highly reactive fuels, such as n-heptane, will typically display a two-stage autoignition process, in which heat is released at low temperatures (typically on the order of 1% to 5% of the fuel's chemical energy) [Vuilleumier 2013 Exp.], which is termed Low-Temperature Heat Release (LTHR), followed by the main auto-ignition event, which releases the majority of the fuel's chemical energy. These two behaviors of auto-ignition in the HCCI engine can be separated by whether a fuel does or does not produce LTHR under a set of operating conditions.

LTHR has been shown to depend on both fuel and conditions. In [Dec 2007], it is shown that a given Primary Reference Fuel (PRF) can display either no LTHR behavior at low intake pressures and high engine speeds, or display LTHR at high intake pressures and low engine speeds. This behavior was further explored in [Vuilleumier 2013 Exp.]. The LTHR behavior was found to be sensitive to fuel composition (ratio of isooctane to n-heptane), intake pressure, engine speed (residence time), and exhaust-gas recirculation (charge composition). In [Vuilleumier 2013 Exp.], it is shown that as intake pressure of the engine is increased such that a fuel transitions from displaying no LTHR to some LTHR, the fuel's resistance to auto-ignition diminishes greatly, and the engine operating conditions needed to maintain constant combustion phasing change significantly.

In [Pitz 2008], the LTHR behavior of PRF combustion in an HCCI engine was investigated in an HCCI engine using chemical where kinetic modeling. A particular focus of this study was the intake pressure sensitivity of the fuel. This pressure sensitivity was shown to be dependent on O_2 addition reactions in the fuel's low-temperature chemistry pathways, specifically $R+O_2 = RO_2$ and $QOOH + O_2 = O_2QOOH$.

Previoused investigations into LTHR in high-octane fuels have focused on PRF's or traditional gasolines. However, interactions between alcohols and various gasoline components; such as alkanes, alkenes, and aromatic species; or blends of components, have not been thoroughly explored. This study investigates the autoignition sensitivity of two gasoline blends and one primary reference fuel to intake pressure. In addition, the effects of adding ethanol to these gasolines and to the gasoline surrogate (PRF 85) are studied by adding 10% and 20% ethanol by volume to the three base fuels. The investigations were carried out with both experiments and modeling. Experimentally, the investigations were performed by conducting an intake pressure sweep of each fuel to measure at which intake pressure the fuel begins to display LTHR while running in HCCI operation. The HCCI engine experiments are supported by RCM experiments in which ignition delay times were measured for the fuels, under conditions similar to those encountered in the engine. Then, RCM measurements were used to test the chemical kinetic mechanism, which in turn was used to simulate the HCCI engine experiments, probing the effects of fuel composition and intake pressure on the auto-ignition process and LTHR occurrence.

II. Experimental Methods:

c) Engine

All engine experiments were performed using a single cylinder of a of a 4-cylinder VW TDI engine, modified extensively for HCCI operation. These modifications include the addition

of pressure transducers and thermocouples in the intake and exhaust tracts, the additions of in-cylinder pressure sensing, intake and exhaust tracts separated from the other 3 cylinders for the cylinder of interest, the addition of port-fuel injection, the additions of oxygen sensors and a gas sampling port in the exhaust, and custom shallow-bowl pistons. A more detailed description of the modifications can be found in [Saxena 2011]. A schematic of the experimental setup can be found in Figure 3.17, while engine specifications may be found in Table 3.3.

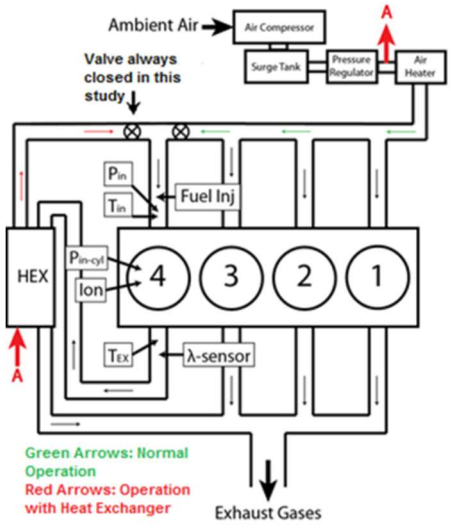

Figure 3.17: A representative schematic of the experimental engine.

For each engine operating point, an intake pressure, fuel, charge equivalence ratio, and combustion phasing (defined as the crank angle at which 50% of the total heat is released, or CA50) are specified, and the intake temperature is adjusted to attain the correct CA50. Thus, for less reactive conditions, a higher intake temperature is required to achieve a fixed CA50, and for more reactive conditions a lower intake temperature will be required.

Table 3.3: Key engine parameters.

Engine Parameters			
CR	17:1	Fuel Injection	PFI
Disp.	.474 L	Fuel Pressure	45 PSI
Bore	79.4 mm	No. of Valves	2
Stroke	95.5 mm	IVO	2 °bTDC
Con. Rod	144 mm	IVC	47.5 °aBDC
Coolant Temp.	95 °C	EVO	47.5 °bBDC
Oil Temp.	100 °C	EVC	8 °aTDC

At each engine operating point the in-cylinder pressure is measured for 300 cycles. In addition, each operating point is measured twice to ensure repeatability. The rate of heat release (ROHR) for each engine operating point is calculated from the in-cylinder pressure traces. These 300 pressure traces are first filtered, using a Savitzky-Golay filter of 19 points, and then averaged. The calculation of the ROHR is made in a manner described in [Heywood 1988]. This method accounts for both wall heat losses via a Woschni model [Woschni 1967], mass loss due to blow-by, changing specific heat ratios of the gas due to both temperature change as well as gas composition change from reactants to products (calculated from NASA thermodynamic tables).

All constants in the model were tuned using motoring pressure traces and a cycle simulation model in AVL BOOST, as described in [AVL 2013]. In addition to the ROHR, the in-cylinder mass-averaged temperature is calculated using the ideal gas model. A more detailed description of the calculation methods can be found in [Vuilleumier 2013 Int.].

In this study, nine fuels were compared. Three base fuels were used, FACE A, FACE C, and PRF 84. Specifications on these fuels can be found both in Figure 3.18, as well as in [x]. Six additional fuels were created by blending each of the three base fuels with two levels of ethanol—10% and 20% ethanol by volume. Unfortunately, problems with the experimental apparatus prevented measurements of neat PRF 84, though PRF 84 + 10% ethanol and + 20% ethanol were unaffected. PRF 85 data that was originally presented in [Vuilleumier 2013 Exp.] has been provided for comparison.

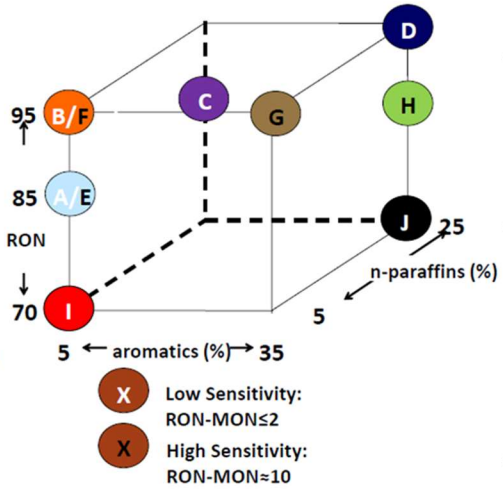

	FACE A	FACE C	PRF 84
RON	83.5	84.7	84
MON	83.6	83.6	84
Sensitivity	-0.1	1.1	0
H/C ratio	2.29	2.27	2.26
Avg. mol. wt.	97.8	97.2	112.0
Hydrocarbon Type, liquid mol%[1]			
n-alkanes	13.2	28.6	17.6
iso-alkanes	83.7	65.1	82.4
Aromatics	0.3	4.4	0.0
Alkenes	0.4	0.4	0.0
Cycloalkanes	2.4	1.5	0.0

[1] Determined by DHA (ASTM D6733 and D6730)

Figure 3.18: FACE A and C gasoline fuel specifications [Cannella 2014], and their surrogate, PRF 84.

d) RCM

The rapid compression machine (RCM) data in this study was generated by the University of Connecticut RCM. The RCM facility has previously been described in detail in [Sarathy 2015]. The University of Connecticut RCM employs a pneumatically driven creviced piston that hydraulically arrested and locked, with a compression time of roughly 30 ms. The pressure measurement is taken with a Kistler 6125C pressure transducer, and the signal is amplified using a Kistler 5010B charge amplifier. The compressed temperature and pressure are altered via uncompressed pressure and compression ratio (which is varied via changes to the stroke and the clearance volume), while uncompressed temperature was held constant at 333 K. All mixtures of fuel and air were prepared in a stainless steel chamber separate from the RCM, and allowed sufficient mixing time to ensure homogeneity.

The ignition delay times of six fuels were measured during the course of this study, for temperatures ranging from 632 to 745 K, at 20 and 40 bar pressures. The six fuels used were FACE A, FACE C, PRF 84, and the E10 blends of these three fuels. Both first stage and total ignition delays were determined from the measured pressure traces, using the time from the end of the compression stroke to the local maximum pressure derivative for each stage of the pressure rise (first stage, where applicable, and main pressure rise). To ensure repeatability, a minimum of five

samples were taken at each condition to create a single reported data point; this reported data point is the measured value closest to the mean of the experiments. All reported points have standard deviations less than 10% of the mean value.

e) 0-D Chemical Kinetic Modeling of Engine Experiments

The HCCI engine experiments were simulated using a 0D multi-zone model (coupled homogeneous batch reactors) created in Chemkin Pro [Chemkin 2008]. A Chemkin model was used rather than a CFD model to allow the use of detailed chemical kinetic mechanisms when simulating reacting cases. This model was created in the following manner:

First, RANS CFD simulations of the experimental engine were carried out for non-reacting (motoring) cases to determine the temperature distribution at TDC for a given intake pressure and temperature. At TDC, the charge was divided into 20 zones, such that the maximum temperature in each zone varied by 10 Kelvin (except in the highest and lowest temperature zones, which had small mass fractions < 5%). These results were used to create a Chemkin multi-zone model. The model was created such that the average temperature and pressure of the model mimicked the CFD results during the compression and expansion strokes, as can be seen in Figure 3.19. The 20 zones in the Chemkin model use the same mass fractions as the 20 groupings from the CFD work. The relative heat transfer rates have been scaled to give the same temperature distribution at TDC as in the CFD results. The model acceptably reproduced the in-cylinder temperature distribution predicted by the CFD simulation for both high and low intake pressures (1.0 bar to 2.2 bar), with high and low intake temperatures (~ 175 C to ~ 30 C), respectively.

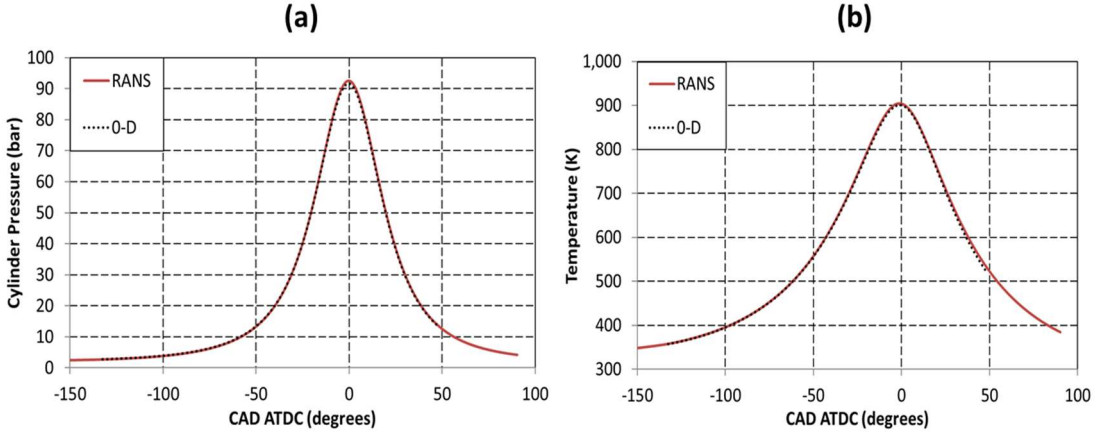

Figure 3.19: Comparisons of pressure (a) and average temperature (b) profiles for RANS and 0-D models at 2.2 bar intake pressure under a non-reacting condition.

III. Results and Discussion:

e) Engine

An HCCI engine was used to evaluate the autoignition properties of nine gasoline-type fuels. These fuels were composed of three base fuels (FACE A, FACE C, and PRF 84), and blends of these fuels with ethanol at 10% and 20% by volume. Figure 3.20 plots the intake temperatures required to maintain constant combustion phasing for each fuel at a given intake pressure. By

holding combustion phasing constant at a fixed engine speed, the effective ignition delay of the fuel-oxidizer charge is held constant. Thus, the required intake temperature indicates a fuel's overall reactivity at a given set of conditions, relative to the other tested fuels. Further, the intake temperature, and the change in required intake temperature with intake pressure, is also indicative of the type of heat release behavior the fuel is exhibiting. This will be discussed further after the presentation of Figure 3.20.

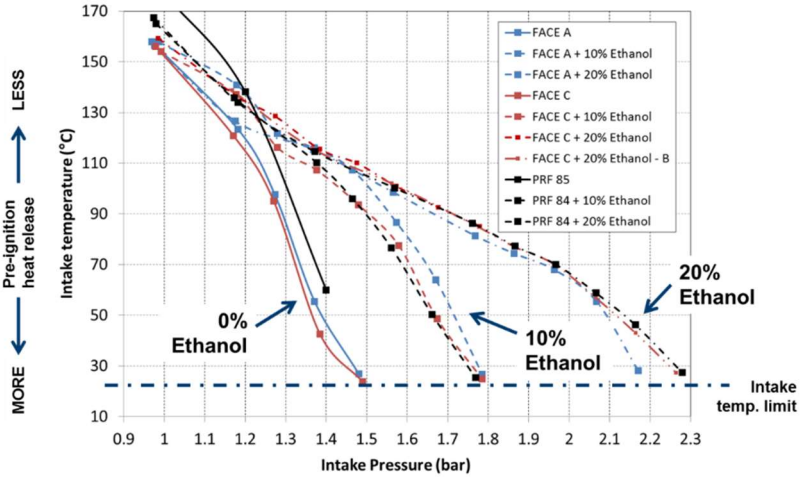

Figure 3.20: Required intake temperature to maintain constant combustion phasing (6° ATDC) over a range of intake pressures for 9 different fuels.

Figure 3.20 shows that at low intake pressures, all fuels behave similarly in terms of reactivity; as seen in Figure 3.21 (a), the fuels also showed similar ROHR behavior. As intake pressures increase, all fuels show increases in reactivity; however, the behavior of the fuels is clearly affected by the amount of ethanol that has been added. In the case of the neat fuels, as the intake pressure increases beyond 1.3 bar, a significant increase in reactivity is noted, which corresponds to the onset of LTHR. Figure 3.21 (b) shows that at 1.4 bar intake pressure the neat fuels display LTHR whereas the 10% and 20% ethanol fuels display single-stage heat release. In the case of the fuels containing 10% ethanol, increased intake pressure resulted in a linear increase in reactivity until a critical intake pressure was achieved. Upon reaching this critical intake pressure, 1.8 bar in the case of the 10% ethanol fuels, the 10% ethanol fuels began to exhibit LTHR and ITHR, as seen in Figure 3.21 (C). Finally, the fuels containing 20% ethanol exhibited a linear increase in reactivity until intake pressures of 2.2 bar were exceeded, again corresponding to the onset LTHR and ITHR, as seen in Figure 3.21 (d). From this data, the correlation between LTHR and reactivity is clear: LTHR increases the autoignition potential of the fuel significantly. Also, the onset of LTHR increases the fuel's reactivity more than an equivalent pressure increase in a region of single-stage autoignition behavior. These shifts in heat release behavior and reactivity can be seen in Figure 3.20, in which the required intake temperature for constant combustion phasing is plotted against intake pressure. For each fuel, two auto-ignition regimes exist: a low-intake pressure regime lacking LTHR, and a high-pressure regime in which the fuel exhibits LTHR. Both regimes resulted in linear relationships between intake pressure and the intake temperature required for constant combustion phasing; however the slope of the intake-pressure/intake-temperature relationship varied across the two regimes, with greater sensitivity to intake pressure in the high-pressure regime in which LTHR is exhibited.

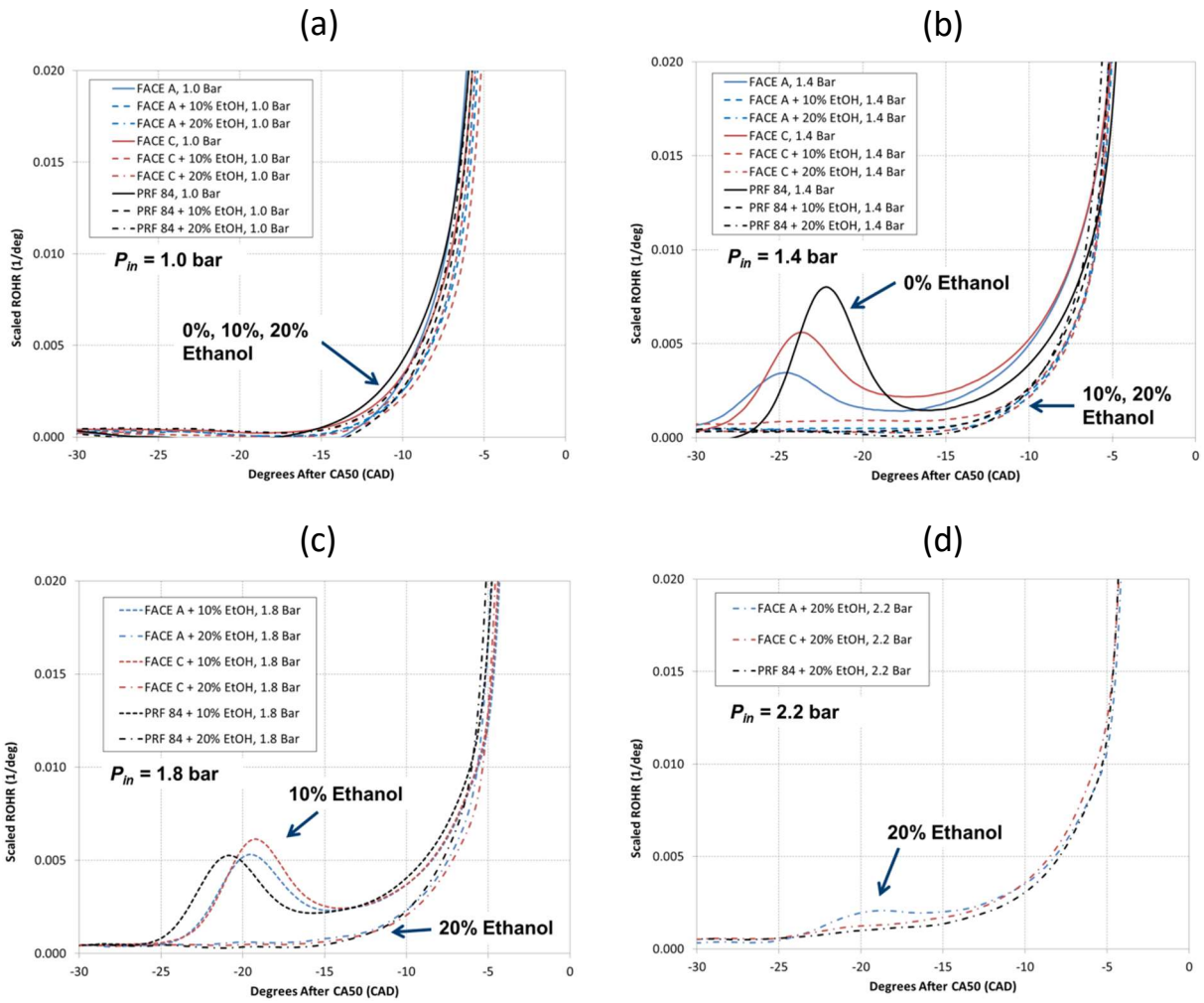

Figure 3.21: Heat release profiles in the LTHR and ITHR regions for the 9 fuels tested (where possible) at different intake pressures, ranging from 1.0 bar (a) to 2.2 bar (d).

Figure 3.21 (a) – (d) plots measured heat release traces for the nine tested fuels at four different intake pressures. The three gasolines, PRF 84, FACE A, and FACE C, behave similarly for a given level of ethanol addition, with FACE A being slightly less reactive than FACE C, despite the relatively significant differences in their compositions. This indicates that under these conditions, the octane number is a relatively good metric of autoignition behavior.

Interestingly, at low intake pressures, all fuels, regardless of their ethanol content, exhibited similar heat release behavior and required intake temperatures. This is surprising, as the fuels with ethanol added will have higher octane numbers and will be generally less reactive (as seen in the RCM data presented below) than the neat fuels. This indicates that at lower load conditions, the octane number of the fuel is not a good indicator of its reactivity in the HCCI engine.

Heretofore all experimental results have been obtained with a combustion phasing of 6 dATDC. In addition to this phasing, measurements were performed at 4 dATDC, 8 dATDC, and 10 dATDC. These sweeps revealed that when using intake temperature to control combustion phasing, the amount of LTHR can be affected due to the changes in the temperature history during

the compression stroke. Figure 3.22 shows the conditions under which LTHR begins to occur with significant magnitude. Due to engine operability limits, the full space of LTHR cannot be explored, however the outline of LTHR's limits on the high-temperature and low-pressure boundary can be seen. For the residence time encountered when running at 1800 RPM, pressure must exceed approximately 30 bar while the charge temperature is below approximately 850 kelvin for LTHR to occur for the neat fuels. When 10% ethanol is added, a pressure of approximately 45 bar must be exceeded prior to the temperature surpassing 875 kelvin. Finally, in the case of 20% ethanol addition, the pressure must exceed 65 bar while the temperature is below 900 kelvin.

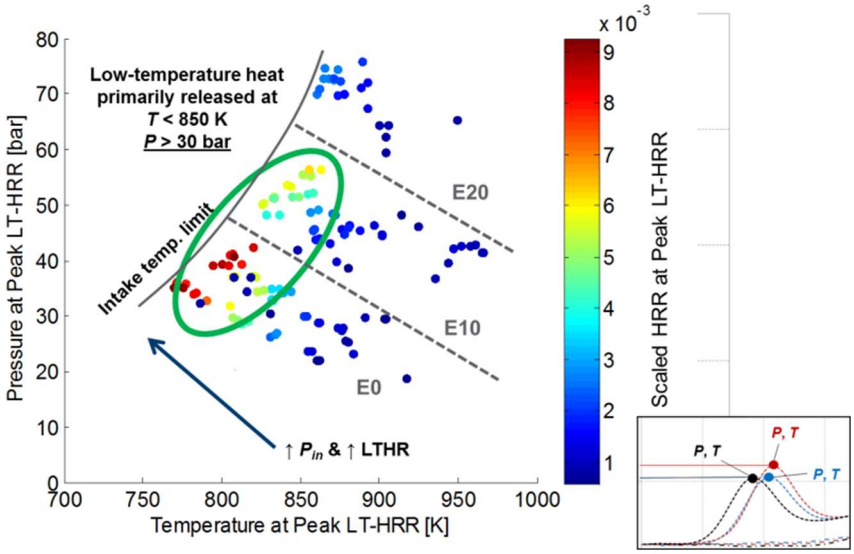

Figure 3.22: Temperature and pressure of peak LTHR for all fuels and conditions tested.

f) RCM Experiments and Simulations

To support the HCCI engine experiments, to provide more fundamental data on the fuels and fuel mixtures, and to determine the suitability of a PRF surrogate for the two tested FACE fuels, experiments were performed in a rapid compression machine (RCM) at both low (20 bar) and high (40 bar) pressure, with FACE C, FACE C, PRF 84, and +10% ethanol mixtures of these fuels. The RCM experiments measured both the first stage (LTHR) and second stage (HTHR) ignition delays.

As seen in Figure 3.23 (a), total ignition delays among the three base fuels were quite similar at 20 bar compressed pressure. However, the ethanol addition to the three fuels caused some slight differences between PRF 84 and FACE A and FACE C, with PRF 84 being slightly less reactive in the Negative Temperature Coefficient (NTC) region than FACE A or FACE C. The first stage ignition delays at 20 bar, as seen in Figure 3.23 (b), showed the opposite trend to the total ignition delays; all fuels behaved similarly with 10% ethanol, which neat there was some variance, with PRF 84 consistently displaying the shortest delay times prior to the first stage heat release. At the 20 bar condition, all six fuels exhibited significant NTC behavior in the measured temperature range.

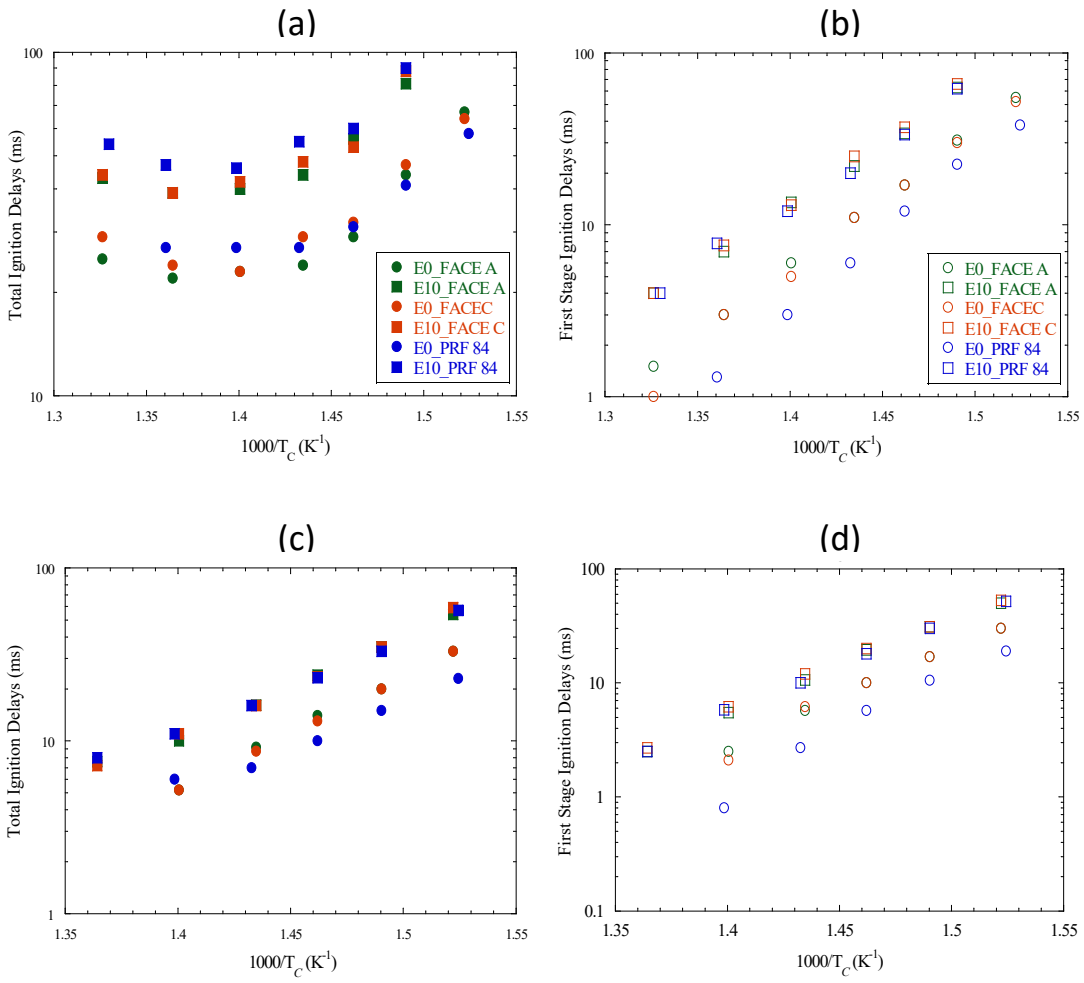

Figure 3.23: Total Ignition Delays and First Stage Ignition Delays for 6 different fuels as measured in a Rapid Compression Machine at two different pressures; 20 bar for (a) and (b) and 40 bar for (c) and (d).

By increasing the pressure of the system to 40 bar, significant changes in ignition delay behavior are seen. First considering the overall ignition delays at this condition, which are seen in Figure 3.23 (c), it may be seen that the fuels no longer exhibit NTC behavior in the measured temperature range. However, this is likely due to shifting of the NTC region to a higher temperature range. Next, Figure 3.23 (c) shows nearly identical ignition delays for the three E10 fuels at 40 bar, while the three E0 fuels show nearly identical behavior, with PRF 84 slightly more reactive than the two FACE gasolines. Considering the first stage ignition delays which are shown in Figure 3.23 (d), neat PRF 84 has a slightly shorter first stage ignition delay than FACE A and C. However, once ethanol is added, the first stage ignition delays for all three E10 fuels are indistinguishable.

Figure 3.23 (a) – (c) shows that while PRF 84 deviated from the ignition delay behavior exhibited by FACE A and C under certain conditions, similar first-stage and overall ignition delay times were observed under most conditions. This generally-good agreement between the fuels indicates that PRF 84 is a suitable surrogate for FACE A and C. Cases where the behavior diverges are during ethanol addition at low pressures (20 bar), and in the timing of the first stage heat

release. This is similar to the behavior observed in the engine, in which the PRF 84 + 10% ethanol and + 20% ethanol exhibited nearly identical behavior to FACE A and FACE C with the same volume fractions of ethanol. While these results are reassuring in the use of PRF's as gasoline surrogates, it must be noted that both FACE A and FACE C have essentially no sensitivity, as shown in Figure 3.18. Further, FACE A and FACE C both are comprised primarily of n-alkanes and iso-alkanes, similar to a PRF. However, this is not true of all gasolines, which may contain higher fractions of aromatic compounds, cyclo-alkanes, or olefinic compounds, all of which may behave less similarly in their auto-ignition chemistry to a PRF.

g) HCCI Engine Simulations

Chemical kinetic simulations were performed to elucidate underlying causes of the fuel's sensitivity to ethanol addition and boosted intake pressures. The chemical kinetic simulations were performed using a 0-D multi-zone chemical kinetic model included with the commercial software Chemkin Pro, using a kinetic mechanism by Cai et. al. [Cai 2015]. The Cai mechanism contains oxidation schemes for two fuel components, isooctane and n-heptane, and is intended for use in simulating combustion of PRF's. Figure 3.24 shows that the previously described multi-zone model coupled with the Cai mechanism qualitatively reproduces the heat release behavior found in HCCI engines; this is significantly better agreement than could be obtained with a single-zone model.

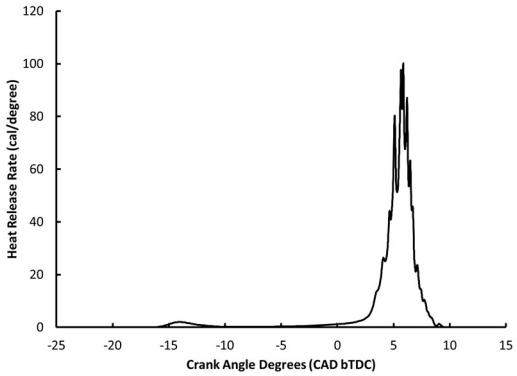

Figure 3.24: Simulated HCCI ROHR at 2.7 bar intake pressure and φ = 0.4 for PRF 84 using a 20-zone model.

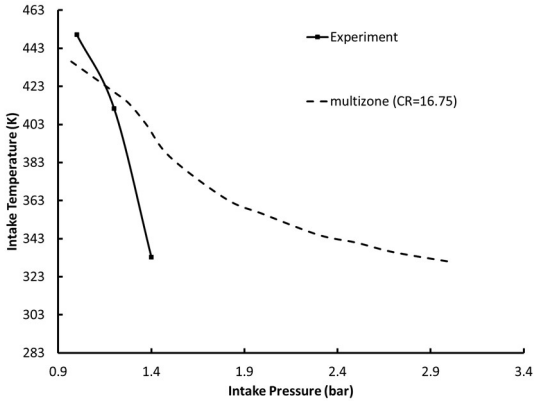

Figure 3.25: Experimental and simulated intake temperatures required for constant combustion phasing (6° ATDC) at various intake pressures for PRF 84.

Figure 3.25 shows the required intake temperatures to maintain constant combustion phasing for the experiment and the model. While the results differ significantly in a qualitative sense, qualitatively they both show a region with less intake temperature sensitivity at lower intake pressures followed by higher intake pressure sensitivity at higher intake pressures. Figure 3.26 shows the heat release behavior predicted by the model. Here it can be seen that the model predicts LTHR for intake pressures above 1.5 bar. This is reasonably similar to the results obtained experimentally.

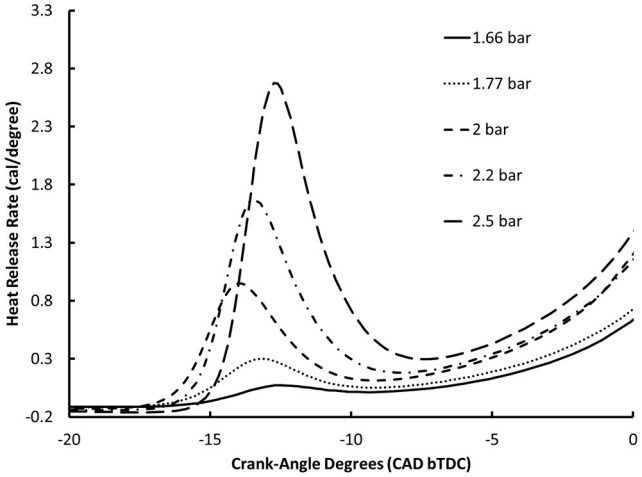

Figure 3.26: Simulated ROHR profiles for PRF 84 at various intake pressures during the LTHR and ITHR phases of the HCCI combustion process.

To better understand the effects of ethanol addition to gasoline on LTHR and the effects of LTHR on HCCI combustion, a detailed analysis was performed at a specific engine operating point with two different fuel blends. This engine operating point was 1.8 bar intake pressure, an equivalence ratio of 0.4, combustion phasing of 6° ATDC, with PRF 84 and PRF 84 + 10% ethanol. At this condition, the model predicted significant LTHR for PRF 84, and no LTHR for PRF 84 + 20% ethanol. Figure 3.27 shows the average charge temperature and heat release rate in the LTHR region for the two cases. It can be seen that while LTHR elevates the temperature of the PRF 84 case, the charge temperature is not elevated sufficiently to reach the temperature of the PRF 84 + 10% ethanol case, which exhibits no LTHR at this condition. The difference in charge temperature after LTHR has occurred indicated that the increased reactivity due to LTHR is primarily a chemical effect rather than a thermal effect, though both factors contribute to the increased reactivity. As seen in Figure 3.28, after LTHR the PRF 84 has a high rate of production (ROP) relative to PRF 84 + 20% ethanol. Also, the conversion of n-heptane during LTHR is quite high. This leads to the formation of a large radical pool during LTHR which lowers the temperature for the start of high temperature heat release (HTHR). In the case of PRF 84 + 20% ethanol, the ethanol acts as a radical sink which both inhibits LTHR and reduces the size of the radical pool prior to hot ignition. This can be seen in Figure 3.29, which shows the consumption of active radicals by ethanol. Finally, the addition of ethanol dilutes the n-heptane in the mixture, which further reduces the system reactivity.

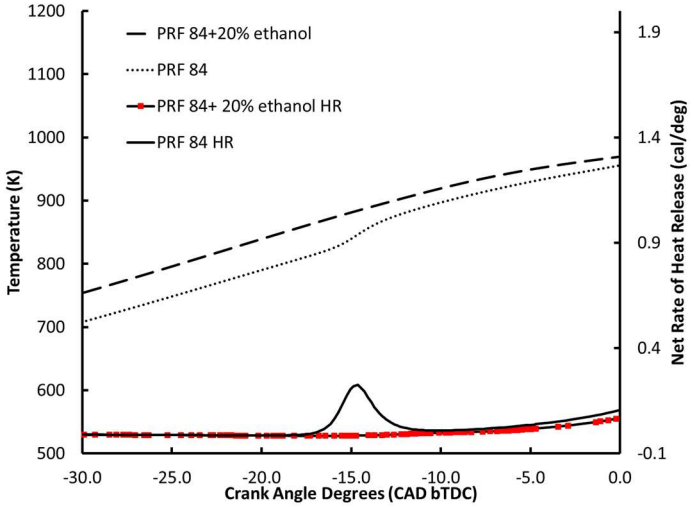

Figure 3.27: Simulated temperature and ROHR profiles for PRF 84 and PRF 84 + 20% ethanol at 1.8 bar intake pressure.

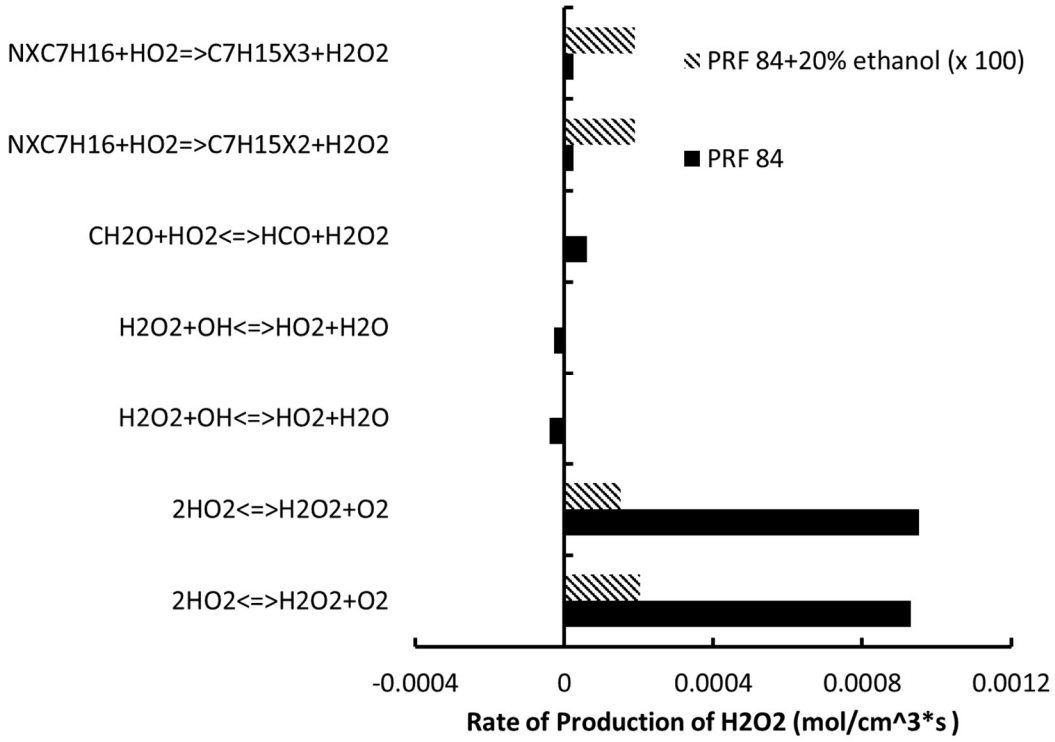

Figure 3.28: Simulated H2O2 ROP and ethanol radical consumption in the ITHR phase at 1.8 bar intake pressure with PRF 84 and PRF 84 + 20% ethanol.

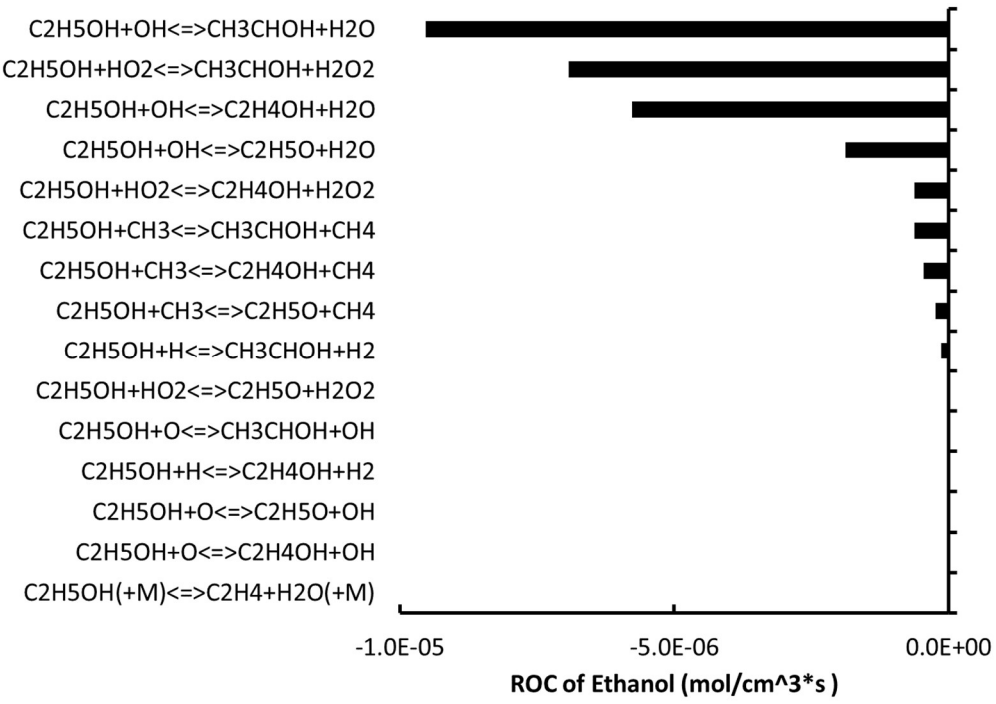

Figure 3.29: Simulated radical consumption by ethanol during the ITHR phase at 1.8 bar intake pressure with PRF 84 + 20% ethanol.

IV. Conclusions:

In this paper, the Low-Temperature Heat Release (LTHR) behavior of gasoline, and gasoline-ethanol blends, is explored in an HCCI engine, an RCM, and through zero-dimensional chemical kinetic models. A key focus of these investigations is the transition of a fuel from single-stage to dual-stage heat release in an engine, with increased intake pressure. The conclusions from each section of the investigation are presented below:

a) Engine

1. At low intake pressures and equivalence ratios and moderate engine speeds, gasoline exhibits single-stage heat release when burned in an HCCI combustion system.
2. As intake pressure is increased, gasoline begins to exhibit Low Temperature Heat Release.
3. Ethanol addition to gasoline increases the pressure at which the onset of LTHR begins.
4. The primary reference fuel and two FACE gasolines behaved similarly, but not identically, both neat and with ethanol addition.
5. Low Temperature Heat Release significantly changes the intake temperature required to maintain constant combustion phasing. This is both a thermal and a chemical effect.

b) RCM

6. FACE A, C, and PRF 84 have similar first stage and total ignition delays.
7. PRF 84 is an acceptable surrogate for FACE A and C both neat and with ethanol addition

c) HCCI Engine Simulations

8. LTHR, while having both thermal and chemical effects on ignition delay, primarily encourages ignition through a boosted radical pool.
9. Ethanol acts as a radical sink, both reducing LTHR magnitude and delaying ignition.

Chapter 4:

Intermediate temperature heat release in an HCCI engine fueled by ethanol / n-heptane mixtures: an experimental and modeling study

This study appeared as an article in Combustion and Flame in 2014.

David Vuilleumier, Darko Kozarac, Marco Mehl, Samveg Saxena, William J. Pitz, Robert W. Dibble, Jyh-Yuan Chen, S. Mani Sarathy

I. Abstract

This study examines intermediate temperature heat release (ITHR) in homogeneous charge compression ignition (HCCI) engines using blends of ethanol and n-heptane. Experiments were performed over the range of 0%-50% *n*-heptane liquid volume fractions, at equivalence ratios 0.4 and 0.5, and intake pressures from 1.4 bar to 2.2 bar. ITHR was induced in the mixtures containing predominantly ethanol through the addition of small amounts of *n*-heptane. After a critical threshold, additional *n*-heptane content yielded low temperature heat release (LTHR). A method for quantifying the amount of heat released during ITHR was developed by examining the second derivative of heat release, and this method was then used to identify trends in the engine data. The combustion process inside the engine was modeled using a single-zone HCCI model, and good qualitative agreement of pre-ignition pressure rise and heat release rate was found between experimental and modeling results using a detailed n-heptane/ethanol chemical kinetic model. The simulation results were used to identify the dominant reaction pathways contributing to ITHR, as well as to verify the chemical basis behind the quantification of the amount of ITHR in the experimental analysis. The dominant reaction pathways contributing to ITHR were found to be H-atom abstraction from n-heptane by OH and the addition of fuel radicals to O_2.

II. Introduction and Background

Homogeneous charge compression ignition (HCCI) engines combine characteristics of both spark-ignition (SI) and compression-ignition (CI) engines. Like spark-ignition engines, a premixed fuel-in-air charge is used to enable cleaner combustion with low soot and particulate matter emissions. Similar to CI engines, a high operating efficiency is attained since throttle valves are not used for power output control and the charge is ignited through compression ignition. The use of a premixed charge with compression ignition, however, causes high heat release and pressure rise rates leading to ringing (high amplitude in-cylinder pressure fluctuations, which can damage the engine and lower the operating efficiency) [Eng 2002]. To prevent these excessive heat release rates, charge dilution is used through lean equivalence ratios or high exhaust gas recirculation (EGR) rates. However, excessive charge dilution causes low power output. One effective strategy to allow high HCCI power output is to introduce more fuel (i.e., less charge dilution) while using highly delayed combustion timing, later than 8 degrees after top dead center (°aTDC), to prevent excessive ringing [Sjöberg 2007, Sjöberg 2004, Saxena 2011, Saxena 2013, Dec 2010]. Recent research [Dec 2010, Yang 2010, Mehl 2012] has shown that fuels that exhibit a moderate pre-ignition heat release occurring near top dead center (TDC), like gasoline or higher

alcohols, are highly conducive for enabling delayed combustion timing. This characteristic heat release behavior is distinct from the more commonly known low temperature heat release (LTHR) [Tanaka 2003, Dec 2009], presenting in most cases a single stage ignition. Moreover, the in-cylinder temperatures associated with the pre-ignition heat release are typically too high to allow the chemistry responsible for the traditional low temperature branching mechanisms responsible for the LTHR. For these reasons, this combustion regime has been defined as intermediate temperature heat release (ITHR).

ITHR allows the in-cylinder charge temperature to continue rising after top dead center where piston expansion would normally cause the charge to cool down prior to hot ignition, thus it enables more delayed combustion timing, as late as 19 °aTDC if sufficient ITHR is available [Dec 2010]. The resulting delays in combustion timing attained using ITHR allow improved performance of HCCI engines because of less heat loss, lower ringing intensity, and the ability to achieve high power output while maintaining high efficiency and low NO_x emissions. For example, indicated mean effective pressures ($IMEP_g$) of 16.34 bar for gasoline [Dec 2010] and 18.1 bar for E10 [Dec 2010] have been demonstrated using delayed combustion timing in prior studies.

Although ITHR has been shown to be an important part of sustaining high-load HCCI operating points, it has not been extensively studied. ITHR has been demonstrated to be a fuel and operating condition dependent phenomenon; ethanol does not exhibit ITHR, while iso-pentanol and gasoline exhibit increasing amounts of ITHR as intake pressure is increased [Dec 2010, Yang 2010]. Hydrobate, a low octane refinery stream, shows a combination of LTHR and ITHR [Yang 2012]. Detailed kinetic models with simplified engine simulations have been previously used to investigate the chemical origins of ITHR [Mehl 2012, Hwang 2008, Tsujimura 2011, Saisirirat 2010]. Highly simplified engine models with strong emphasis on the chemical aspects were able to reproduce all the features of the heat release observed in the experiments. These early studies helped in identifying some common mechanisms behind the onset of the intermediate temperature heat release, such as the presence of a weak low temperature branching chemistry followed by methyl radical formation and oxidation to CO. The formation of HO_2 radicals also was found to play a key role in the development of the ITHR regime. Based on these findings, the absence of ITHR in ethanol was explained by the lack of the low temperature branching chemistry for this fuel. In the case of gasoline, the real fuel's complexity makes it difficult to be completely confident in detailed reaction pathway analysis of surrogate fuels. For this reason, blends of ethanol and n-heptane are utilized in this study of ITHR.

To the authors' knowledge, inducing ITHR in a relatively non-reactive fuel by the addition of a highly reactive fuel has not yet been studied. This study explores strategies for inducing ITHR in HCCI engines while operating with fuels that typically show little pre-ignition reactions. Several fuel mixtures consisting predominantly of ethanol with small fractions of n-heptane are studied to determine if small amounts of a highly reactive fuel can be used to induce sufficient amounts of ITHR to enable significant delays in combustion timing.

The use of blends of ethanol/n-heptane in HCCI engines have previously been explored [Saisirirat 2010, Lu 2006, Saisirirat 2011, Lü 2007, Olsson 2001, Yates 2012, Kamio 2007], but primarily from the point of view of dual-fuel control strategies, and thus focus on CA50 shifts caused by varying fuel blends rather than changes in heat release rate (HRR) at a constant CA50.

In addition, there is very little HCCI engine data from ethanol/n-heptane blends that are primarily composed of ethanol, as most previous work has focused on high n-heptane fractions. Studies investigating the possible use of E85as a fuel in HCCI engines have been undertaken, sometimes using an E85 surrogate and sometimes using standard E85, but these investigations have not focused on the study of ITHR and it is unclear from the presented rate of heat release (ROHR) curves whether ITHR occurs in these mixtures [Andrae 2009, Dahl 2011]. The effect of ethanol addition to n-heptane on low-temperature heat release (LTHR) has been studied in [Lü 2007, Kamio 2007]. It has been found that ethanol addition to n-heptane decreases LTHR. Other studies have shown that pure ethanol does not show two-stage heat release [Sjöberg 2010], and it is well known that pure n-heptane shows two-stage ignition [Curran 1998]. The occurrence of ITHR in ethanol/n-heptane blends has not been previously presented. However, our close examination of HRR curves from [Saisirirat 2011] indicates that ITHR behavior may be seen in ethanol/n-heptane blends. Co-oxidation of ethanol/n-heptane blends have been explored in only a small number of fundamental combustion experiments [Dagaut 2010]. Jet stirred reactor (JSR) data has been collected mixtures of ethanol/n-heptane (20/80 and 50/50 mol%) and successfully modeled in [Saisirirat 2011, Haas 2009]. Experimental flow reactor data of an E85 surrogate containing ethanol/n-heptane has been presented in [Haas 2009] and the experimental results have been successfully simulated, finding that at low temperatures n-heptane radical generation drives ethanol oxidation. No ITHR behavior has been observed in such fundamental combustion experiments because they were not designed with the goal of studying ITHR. van Lipzig et al. were the first to measure laminar flame speeds of ethanol/n-heptane (50/50 vol%) using the heat flux burner method [Lipzig 2011].

This study examines the ITHR behavior of various ethanol/n-heptane blends in an HCCI engine. Previous fundamental work has shown that engines can be used to study fuel chemistry effects on the evolution of heat release [Sjöberg 2007, Tsujimura 2011, Zhang 2009, Zhang 2010, Zhang 2012]. The study is comprised both of experimental and numerical results, with a focus on changes to the HRR profile, dominant chemical reactions, and intake temperature requirements for constant combustion phasing. The study includes several steps. First, experimental results are collected from the HCCI engine operating with well-defined mixtures of ethanol and n-heptane. Second, the results are then processed with the emphasis on analysis of ROHR and ITHR. Finally, a representative engine model with detailed chemical kinetics is employed to analyze the chemistry responsible for ITHR.

III. Methodologies

a) Experimental

A four-cylinder 1.9L Volkswagen TDI engine was used in this study. Specifications for this engine are provided in Table 4.1. In this study, only cylinder 4 was fired, and its intake and exhaust streams have been isolated from the other cylinders. The experimental engine is similar to the one used in prior HCCI studies [Saxena 2014], and all experiments were conducted at 1800 RPM. The engine includes significant modifications for enabling and enhancing HCCI combustion. The original deep-bowl pistons with a compression ratio of 19.5:1 in the Volkswagen TDI engine are replaced with relatively flat 17:1 pistons for reduced heat loss. Each cylinder is equipped with an in-cylinder quartz piezoelectric, water-cooled, pressure transducer (AVL QH33D) which is installed in the diesel fuel injector port. Port fuel injectors are installed in a custom intake manifold, and the fuel injection is controlled using a custom injection control system

constructed using solid-state relays and control signals generated from a National Instruments/Labview system. Fuel pressure is provided by a nitrogen-pressurized fuel tank mounted on a scale. Fuel flow is measured via the change in scale measurements over time, with a precision of ± 7% at the lowest fuel flow rates used in this study. Equivalence ratio is monitored using wide-band lambda sensors installed in the exhaust manifolds with a precision of ± 0.015. Cylinder 4's exhaust is routed separately to prevent sensor contamination from the non-firing cylinders. The stock turbocharger is removed, and an external 100 HP compressor with a 6 m^3 surge tank is used in providing intake air at boosted pressure. A pressure regulator is installed after the surge tank to simulate the effects of a supercharger or turbocharger. Intake pressure is measured using a Kulite XTEL 190(M) piezoresistive pressure sensor with a precision of ± 2%. This sensor allows a crank-angle resolved measurement of intake pressure near the intake valve, and is used to set the absolute level of the AVL QH33D in-cylinder pressure sensor at the beginning of each engine cycle. Temperatures are measured in the intake manifold and the exhaust manifold as shown in Fig. 4.1 using K-Type thermocouples with a precision of ± 2 Kelvin.

Table 4.1: Experimental engine specifications.

Engine Parameters	
Compression Ratio	17:1
Displacement	.474 L
Bore	79.4 mm
Stroke	95.5 mm
Rod Length	144 mm
Coolant Temperature	95 °C
Oil Temperature	100 °C
Fuel Injection	PFI
Fuel Pressure	45 PSI
No. of Valves	2
IVO	2 °bTDC
IVC	47.5 °aBDC
EVO	47.5 °bBDC
EVC	8 °aTDC

The data was collected at stable, non-transient, engine operating points, with constant intake conditions (temperature, pressure, and equivalence ratio). Each test point was replicated once to check for consistency in results. For each of these test points several parameters were measured and recorded, the most important of which include the in-cylinder pressure, the intake temperature, the exhaust temperature, the equivalence ratio, and the mass of fuel injected.

In-cylinder pressure was measured at intervals of every 0.25° with each pressure measurement being triggered by the signal from a crankshaft encoder. For each test point, 300 consecutive thermodynamic cycles were measured and recorded. Equivalence ratio is controlled using a feedback control system using the wideband lambda sensor in the exhaust manifold and fuel injection pulse width control.

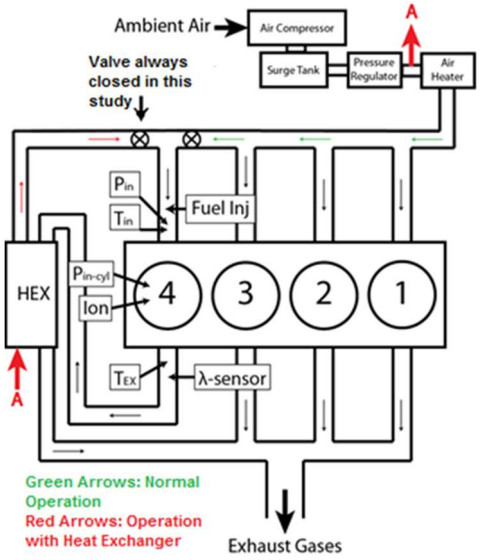

Figure 4.1: Schematic of engine, including intake system, exhaust system, and key sensors.

The calculation of ROHR that will be described later is very sensitive to initial and boundary conditions. Therefore, in order to verify the measured data and to calculate values that were not measured, a cycle simulation model of the engine was made. The model was made in AVL Boost [AVL Boost 2013] and was used in the calculation of blow by, wall heat calibration factor, pressure loss across the intake valve, actual compression ratio and intake valve closure (IVC) temperature. The cycle simulation model incorporated the cylinder geometry which included the full valve lift profiles, and intake and exhaust ports. The intake pressure was set to be equal to the measured absolute intake pressure, which is crank angle resolved, and the intake temperature was set to the measured average intake temperature. The exhaust boundary conditions were equal to measured average pressure and temperature. The model used a Woschni [Woschni 1967] heat transfer model with an additional constant calibration factor. The relevant above mentioned values were determined by the comparison of measured and calculated motored pressure traces of all the conditions used in firing cycles. For the blow by and wall heat calibration factor, special attention was paid on the expansion part of the cycle. For determination of compression ratio and intake valve pressure loss, the important factor is the peak motoring pressure. With the calibrated model the IVC temperature is calculated for all different intake conditions.

Post-processing of the measured data was performed to calculate the ROHR and in-cylinder temperature profiles. The basis for the calculation was the average pressure trace of three hundred consecutive cycles. Before averaging, the pressure of each individual cycle was smoothed by using a Savitzki-Golay filter with 19 points [Savitzky 1964]. The calculation of ROHR was

made by a procedure described in [Heywood 1988]. The ROHR model included blow by and wall heat losses. The wall heat losses are calculated with a Woschni model and use the calibration factor determined from cycle simulation calculations. The thermodynamic properties of the mixture were calculated by using NASA polynomials of the species in the mixture. The cylinder mixture during compression is comprised of fuel, air and residual gases. The amount of residual gases was calculated by the cycle simulation calculation. After combustion, during expansion, the cylinder mixture is comprised of combustion products that would be formed from the initial mixture if complete combustion is assumed. The change from initial mixture to combustion products happens during combustion and it is assumed that this change is proportional to the Vibe [Vibe 1970] combustion profile with assumed start and end of combustion. The process is iterative which means that after calculation of ROHR the start and end of combustion are calculated and used as new assumptions. The iteration is ended when the assumed start and end of combustion are equal to the calculated ones. In-cylinder temperature is calculated by using the ideal gas equation and calculated profiles of mass, volume and composition during the closed cycle. For clarity, a flowchart of the experimental and numerical procedures is presented in Fig. 4.2.

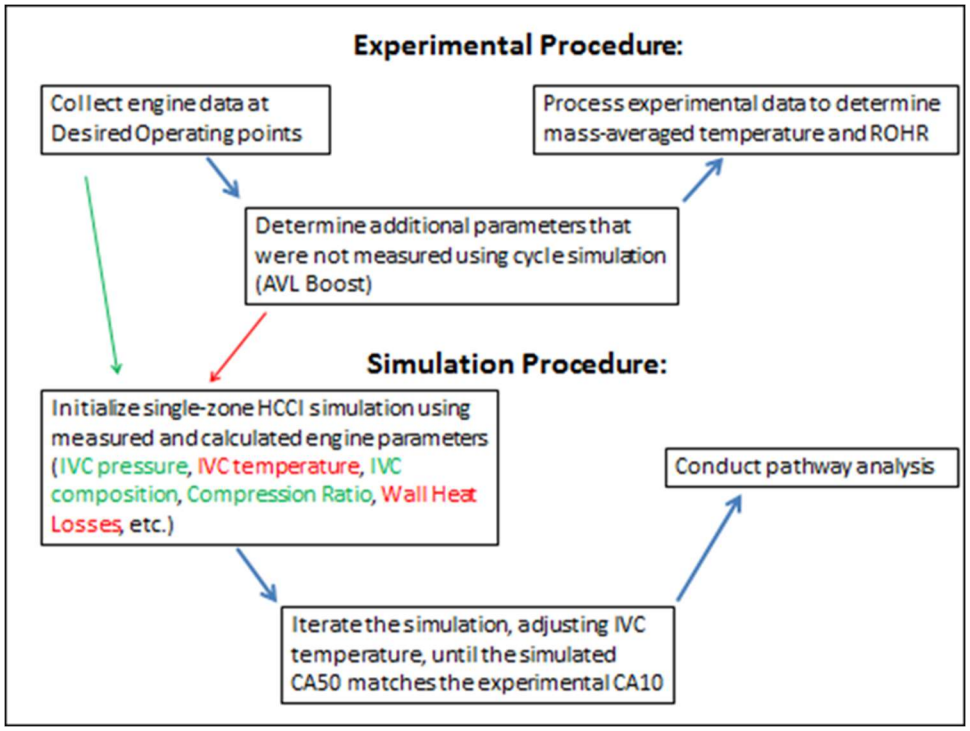

Figure 4.2: A flowchart of the experimental and simulation procedures

b) Chemical Kinetic Modeling

The chemical kinetic mechanism that was used to study the HCCI combustion of ethanol/n-heptane mixtures was developed at the Lawrence Livermore National Laboratory. The detailed chemical kinetic mechanism for n-heptane [LLNL 2013, Mehl 2011] was developed in a hierarchical manner, and therefore includes detailed chemistry for ethanol combustion. The LLNL mechanism was chosen because of its ability to reproduce fundamental combustion behavior of n-

heptane under a wide variety of conditions, as shown in [Curran 1998, Mehl 2011, Mehl 2009]. Briefly, the core C_0-C_4 mechanism was developed by NUI Galway and is described further in [Johnson 2009, Moc 2009]. The ethanol sub-mechanism is largely based on the original work of Marinov et al. [Marinov 1999]. The goal of this study is not to develop a new detailed chemical kinetic model for ethanol combustion, although we recognize this as an active area of research with advances being made regularly.

The purpose of this section is to assess the capability of the selected LLNL model to predict the combustion behavior of ethanol/n-heptane blends in an HCCI engine. This is accomplished by first validating the model against fundamental experimental data from Dagaut et al. [Dagaut 2010] for oxidation of ethanol/n-heptane blends in a jet-stirred reactor (JSR). This is similar to the approach taken by Saisirirat et al. [Saisirirat 2011] in their JSR and HCCI engine study of ethanol/n-heptane blends. We were unable to find fundamental ignition data on heptane/ethanol mixtures in shock tubes or rapid compression machines for model validation. The CHEMKIN PRO [Chemkin 2013] transient perfectly stirred reactor code was used to compare the kinetic model against jet stirred reactor data at ethanol/n-heptane 50/50 mol% mixture, 10 atm, $\phi = 0.5$, and a range of temperatures between 500-1200 K [Dagaut 2010]. A 50/50 mol% and equivalence ratio of 0.5 was selected because this is closest to the conditions of the HCCI engine used in this study. Fig. 4.3 presents the comparison of simulated and experimental concentration profiles. The model predicts the profiles of major product species CO, CO_2, and H_2O within a factor of 1.5 at all temperatures. The reactivity of n-heptane is slightly over predicted at all temperatures, while the reactivity of ethanol is under predicted below 800 K and well predicted at higher temperatures. This level of agreement for the fuel reactivity and major products species is similar to the level of agreement presented by Dagaut et al. [Dagaut 2010] using their chemical kinetic model. The minor species ethylene (C_2H_4), methane (CH_4), formaldehyde (CH_2O), ethane (C_2H_6), and hydrogen (H_2) are well predicted by the model, while propene (C_3H_6), 1-butene (C_4H_8-1), and 1-pentene (C_5H_{10}-1) are predicted within a factor of 2. Simulations were also conducted to compare against data at $\phi = 1.0$ and for ethanol/n-heptane 80/20 mol% mixtures [Dagaut 2010], and similar levels of agreement were obtained, but are not presented here. Based on these results, we believe that the present chemical kinetic model is appropriate for conducting simulations of ethanol/n-heptane blends under HCCI conditions.

The HCCI single cylinder engine is simulated using the CHEMKIN PRO [Chemkin 2013] single zone model. The model integrates the ODE system corresponding to the chemical and thermal evolution of a closed homogeneous system under an imposed volume history reproducing the engine cycle. This kind of model aims to simulate the autoignition process in the core of the fuel/air mixture. The single zone HCCI model enables the use of detailed chemical kinetic models with which we can investigate the chemical reactions contributing to heat release. LES engine simulations can assess the effect of these inhomogeneities, but are much more laborious and computationally intensive than single-zone calculations. As the focus of this study is to better understand ITHR, which occurs prior to HTHR, Multizone HCCI simulations were not used, as this type of simulation was devised to improve prediction of HTHR characteristics and emissions [Flowers 1999, Aceves 2000]. Therefore the use of a Multizone simulation in this study, in which the focus is on heat release prior to main ignition, would only result in an analysis of the core zone of the simulation, which would have the highest temperature and the only significant kinetic activity prior to HTHR. This is essentially analogous to use of a single zone model, as was used in

this study. In this paper, we have chosen a simplified, single-zone approach that allows us to reproduce many of the trends seen in the experiments.

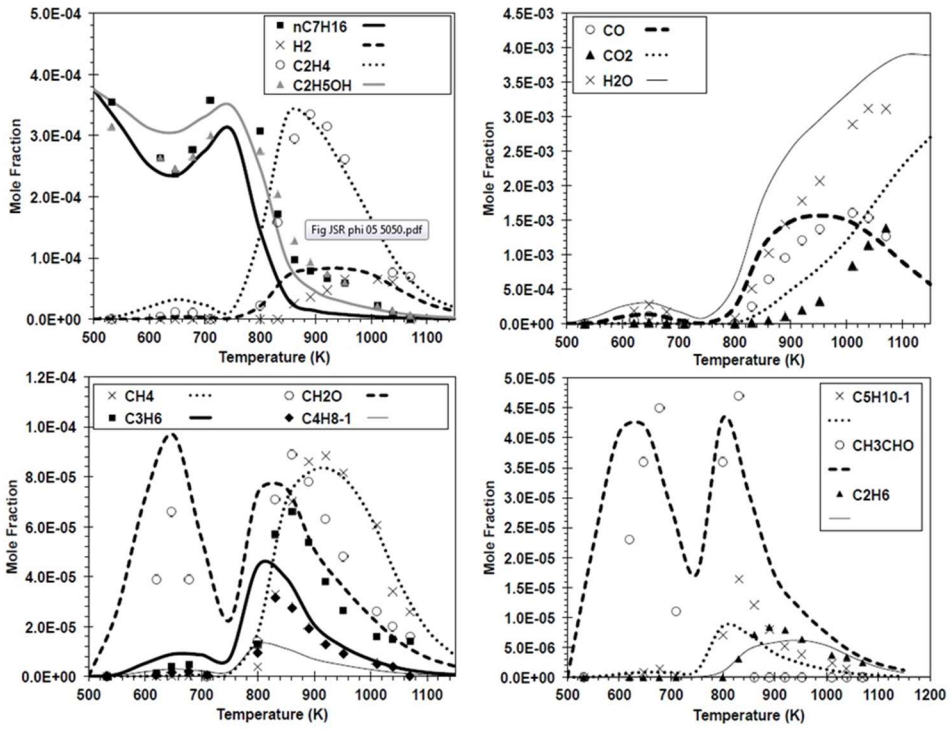

Figure 4.3: Species mole fraction profiles for ethanol/n-heptane (50/50 mol% mixture) oxidation versus reactor temperature in a JSR at 10 atm, τ = 0.7 s and ϕ = 0.5. Experimental data (symbols) are compared to calculations (lines).

In order to reproduce the in-cylinder pressure during the compression stroke, a slightly reduced compression ratio (CR) has been adopted wherein the model assumes a CR of 16.75 while the nominal geometric CR is approximately 17. Heat losses were also accounted for and were directly estimated from the experiments using the Woschni model [Woschni 1967]. With the reduced compression ratio and heat losses, the model has a good agreement with experimental motoring pressure traces, shown in Fig. 4.4. This combined strategy of using a reduced compression ratio and heat losses ensures a good match of the pressure history across the whole compression stroke mimicking the effect of the blow-by and the heat exchange up to the ignition event. After the ignition the single zone model cannot follow the more gradual pressure rise measured by the experiments, which is caused by temperature and composition inhomogeneity.

The simulations targeted the ignition timing obtained in the experiments by varying the temperature at the crank angle corresponding to the IVC for each fueling and boost pressure condition. The experimental ignition timing has been defined as the 10% burn point (CA10) and this value was compared with the 50% burn point (CA50) of the single zone simulation. The rationale for the different definition of the ignition time in the experiment and the model has been analyzed by Sjöberg et al. [3], wherein it is stated that the model reproduces the conditions obtained in the core of the charge which, experimentally, correspond to about 20% of the whole air/fuel

mixture. Thus, the 10% burn point corresponds to the consumption of 50% of the adiabatic core mass.

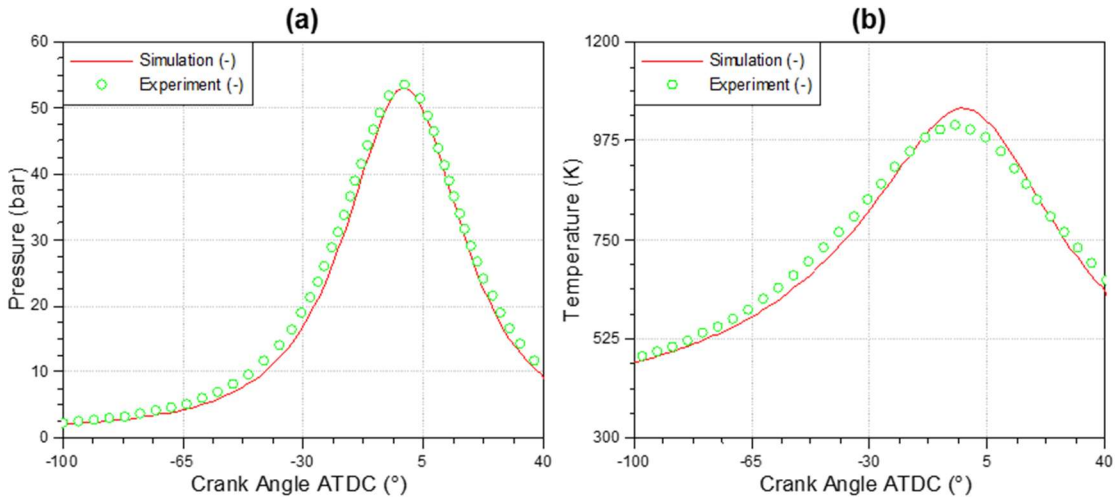

Figure 4.4: A comparison of simulated and experimental motoring (no fuel injected) pressure (a) and temperature (b) traces, with intake conditions of 1.4 bar and 388 Kelvin.

IV. Results and Discussion

a) Engine Results

Table 4.2 lists the engine operating conditions that were used during the tests. The intake pressure, n-heptane fuel fraction, and equivalence ratio were varied while the CA50 was held constant at approximately 10 °aTDC in all cases. Figure 4.5 (a) shows typical engine pressure traces for a fuel-sweep at 1.8 bar intake pressure, while Fig. 4.5 (b) shows the corresponding in-cylinder temperature traces calculated from post processing the measured data. The pressure traces in Fig. 4.5 (c) vary near TDC due to multiple factors, including differences in the specific heat ratio of the gasses due to the different intake temperatures used to match CA50, differences in the amount of heat release due to ITHR differences between different runs, as well as slight IVC pressure differences caused by varying amounts of pressure drop across the intake valve that correspond with intake charge temperature. Figure 4.6 (a, c) shows the Rates of Heat Release (ROHR) traces, for various fuel blends at fixed intake pressure (1.8 bar) and equivalence ratio (ϕ = 0.4). These traces have all been shifted slightly (less than 1 crank-angle degree), to align their CA50s at 10 °aTDC, and allow better comparisons between traces. Also, the traces have been divided by total energy released over the cycle, to provide better comparisons across fuel blends that contain different amounts of energy, and this will be hereafter referred to as the scaled ROHR. In these traces, a progression of ITHR with increasing n-heptane fraction can be seen, starting with minimal or no ITHR in the pure ethanol case, and increasing from there.

Table 4.2 - Engine operating conditions

Variables	Range	Fixed Conditions	Value
Intake Pressure	1.4 bar – 2.2 bar	Engine Speed	1800 RPM
N-Heptane Liquid Volume Fraction	0.0 – 0.5	Internal EGR	~ 4%
ϕ	0.4 – 0.5	Coolant Temperature	95 C

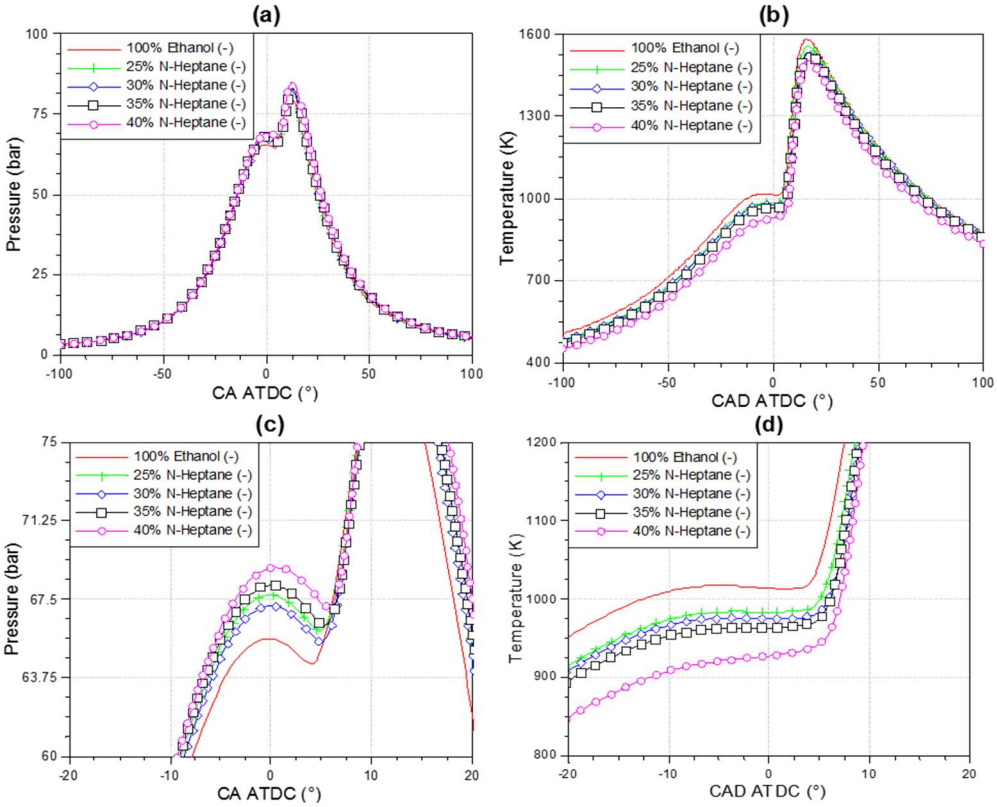

Figure 4.5: Experimental in cylinder pressure (a) and average temperature (b) traces at constant intake pressure (1.8 bar), equivalence ratio (ϕ = 0.4), and combustion phasing (CA50 ≈ 10 °aTDC), for a variety of ethanol/n-heptane blends. The fuel component fractions are denoted by percent liquid volume. Portions (c) and (d) are magnified versions of (a) and (b) to allow closer inspection of the TDC region.

As the n-heptane liquid volume percentage increases from 0% to 40%, the ITHR increases with n-heptane content. These results suggest that if fuel (e.g. ethanol) does not exhibit ITHR in an HCCI engine, ITHR can be produced by adding a more reactive fuel component (e.g. n-heptane). This same trend is seen in Fig. 4.6 (b, d), which shows ROHR traces for 2.2 bar intake pressures. In this case, however, the highest n-heptane percentage, 40%, generates a small amount of low-temperature heat release, in addition to ITHR. With the 2.2 bar case, the following progression can be observed: a transition from no ITHR, seen with pure ethanol, to some ITHR, seen with small n-heptane fractions, to small amounts of LTHR, seen in the 40% n-heptane trace. The first two stages of this progression were observed at all pressures and equivalence ratios that were run in this study, while the distinct LTHR presence was only observed at 2.2 bar. However,

it is theorized that since LTHR and ITHR both show pressure sensitivity and fuel sensitivity, then if fuel blends with higher n-heptane fractions were run in the engine at lower pressures, the same LTHR behavior would emerge. The beginnings of LTHR can be seen at 1.8 bar and 40% n-heptane, which has much more ITHR than the 35% n-heptane at the same pressure, as well as at 2.2 bar and 35% n-heptane. The key difference between the 1.8 bar 40% trace and the 2.2 bar 35% when compared against the lower fuel fractions is the earlier onset of heat release that corresponds better with the LTHR temperature range than with the observed ITHR temperature range. This indicates that the transition from pure ITHR to a mix of ITHR and LTHR has already begun in the traces of 2.2 bar 35% and 1.8 bar 40%.

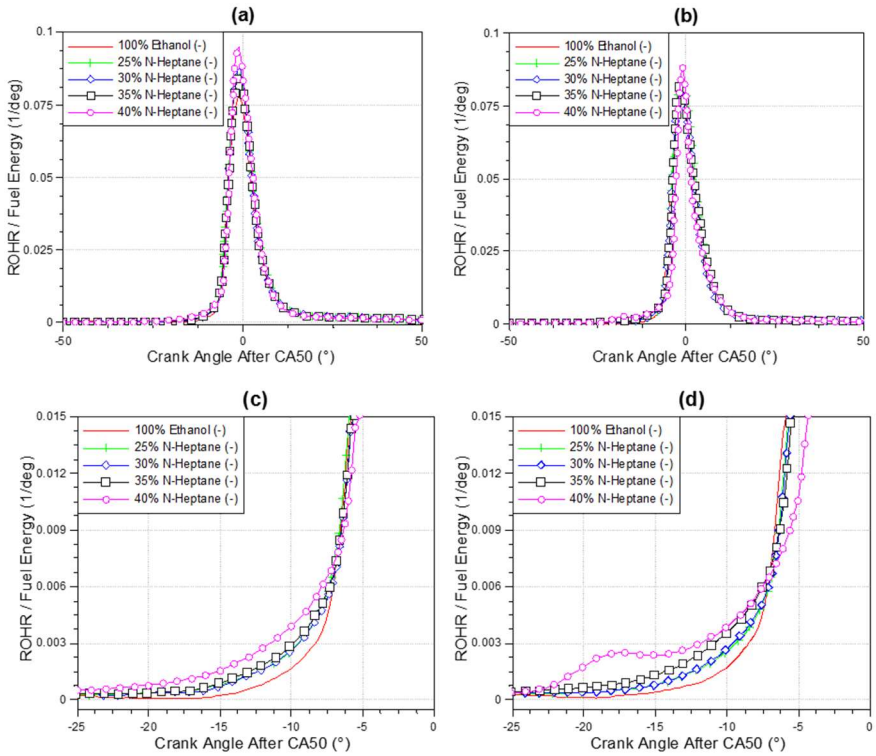

Figure 4.6: Heat release rates at constant intake pressure (a, c – 1.8 bar; b, d – 2.2 bar), equivalence ratio (ϕ = 0.4), and combustion phasing (approximately 10 °aTDC). The traces have all been aligned so that CA 50 occurs at zero degrees on the x-axis. The unaligned CA50's deviated by ± 0.8 degrees.

ITHR's effect on in-cylinder temperature can be seen in the top-dead-center (TDC) region of Fig. 4.5(b), where higher n-heptane volume fractions, and the corresponding increases in ITHR, help keep the in-cylinder temperature from decreasing during the end of the compression stroke and the beginning of the expansion stroke, prior to hot ignition. The effect of the ITHR could also be seen in the stability of the combustion and in intake temperature requirements. As seen in Fig. 4.7, as n-heptane percentage increases, the coefficient of variation (CoV) IMEP decreases. This decrease in CoV IMEP corresponds with increased ITHR. However, as the n-heptane fraction is increased past a certain limit, the CoV IMEP begins to increase. Interestingly, this increase corresponds to the beginning of LTHR behavior. Trends in intake temperature requirements for maintaining a constant CA50 were also apparent. Mixtures with a higher percentage of n-heptane, and therefore more ITHR or LTHR, required lower intake temperatures to maintain a constant

combustion phasing. The influence of equivalence ratio on the required intake temperature can also be seen in Fig. 4.8; the higher equivalence ratio case of $\phi = 0.5$ results in a more rapid drop in intake temperatures as the n-heptane fraction is increase than in the $\phi = 0.4$ case, and this trend is caused by higher amounts of ITHR. Figure 4.7 highlights the importance of understanding the causes of ITHR behavior, and using this knowledge to influence control strategies of HCCI, as more ITHR and LTHR may not always be beneficial to stable engine operation. ITHR appears to lower the CoV IMEP of the engine near the late firing operational limit. Therefore it is important to operate the engine under conditions that enhance ITHR. However, since LTHR corresponds to an increase in the engine's CoV IMEP, the conditions under which high ITHR but little LTHR exist are important. As noted in [Sjöberg 2011], ITHR extends the late firing limit of HCCI, and therefore as this limit is approached, additional ITHR should increase combustion stability. However, the decrease in stability that was encountered as LTHR began to appear was unexpected. The test conditions with LTHR relied on this behavior to elevate TDC temperatures sufficiently to cause autoignition. One possible explanation for the increasing CoV IMEP is that small changes in LTHR magnitude from cycle to cycle varied TDC temperature suitably to cause partial misfire in some cases. Alternatively, it is also possible that the addition of n-heptane to ethanol causes the blended fuel to become more phi-sensitive [Dec 2011]. This would cause locally rich fuel-air mixtures to ignite early and induce early ignition of the entire fuel-air charge. The added phi sensitivity of the fuel may add to the cyclic variations that are common in HCCI engines due to small amounts of internal exhaust gas recirculation (EGR) or small variations in fueling, as small cycle-to-cycle variations in mixture will cause larger changes in combustion timing than a less phi-sensitive mixture would. It is also possible that the reduced intake temperatures used to match combustion phasing with the LTHR cases contributed to the decreased stability through the reduction in TDC temperatures for these cases. However, to better understand and explain these effects, new experiments that target this trend are needed.

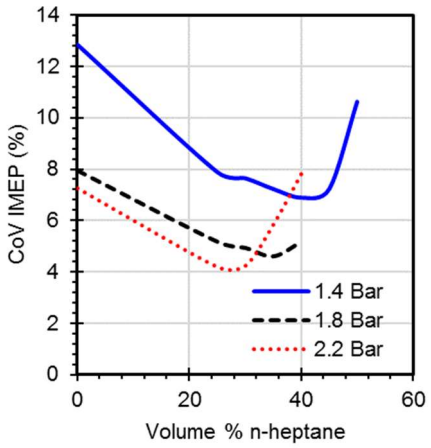

Figure 4.7: IMEP Coefficient of Variation for various fuel blends, at constant equivalence ratio and combustion phasing.

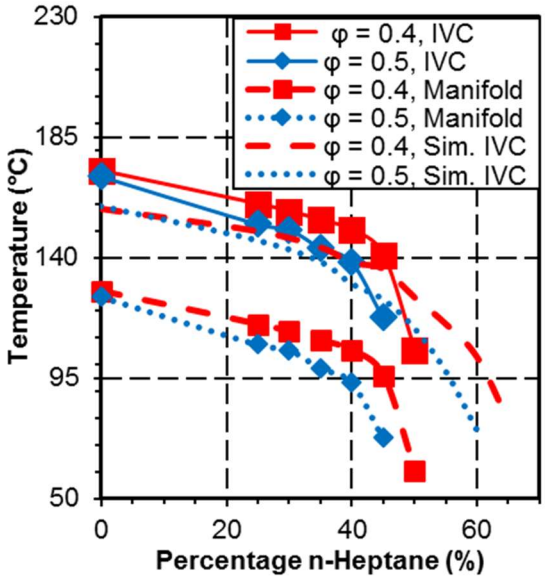

Figure 4.8: Experimental (markers) and simulated (dashed lines) intake valve closure (IVC) and intake manifold temperatures for various fuel blends and equivalence ratios. The intake pressure (1.4 Bar) and combustion phasing (CA50=10 °aTDC) have been held constant.

b) Modeling Results

As described in the methods section, the experimental IVC temperatures were calculated using AVL Boost. In the engine simulations the intake temperatures were adjusted (shown in Fig. 4.8) to match the combustion phasing of the experiments. The Boost simulations showed that for this engine, IVC temperatures are higher than intake temperatures. This result may seem counterintuitive; however, the Boost simulation shows that the compression of the gasses in the combustion chamber by the piston, as the intake valve is still closing, raises the charge temperature relative to the intake temperature, and this effect outweighs the heat losses of the intake charge through the intake port and across the intake valve. Figure 4.8 shows a comparison of the experimental intake temperatures and the temperatures required by the simulation to match combustion phasing. A complete list of initial conditions used in the simulations is provided in Table 4.3.

While an exact reproduction of the experimental temperatures is not achieved, the trends of the experiment are matched well with a small offset, both in the slope of the decreasing IVC temperatures, as well as the inflection that occurs due to the onset of LTHR when the n-heptane percentage is increased above 40%. The heat release traces from the simulations are shown in Fig. 4.9. Figure 4.8 and Fig. 4.9 show that the simulations are able to reproduce the key trends of the experiments. Figure 4.8 shows that the experiments and the simulations both require a decrease in intake temperature to maintain constant combustion phasing as the n-heptane fraction increases. Fig. 4.8 also shows that higher equivalence ratios require lower intake temperatures, except in the case of pure ethanol. Figure 4.9 shows that the experiments (a) and simulations (b) show similar increases in the magnitude of ITHR as the n-heptane fraction is increased. However, the simulation is not perfect, and while the trends of the experiments are preserved, the simulations are found to be less sensitive to the addition of n-heptane than the experiments. This is chiefly observed in Fig.

8, where the experimental IVC temperature drops dramatically with the addition of roughly 40% n-heptane, whereas the simulation requires 50% n-heptane for a similar effect.

Table 4.3: Initial Conditions used in chemical kinetic simulations.

Case	Initial Pressure (bar)	Initial Temperature (K)	Air Composition	Equivalence Ratio	Fuel Mole Fraction N-Heptane	Fuel Mole Fraction Ethanol
2.2 Bar, 100% Ethanol	2.36	415.15	21% Oxygen, 79% Nitrogen	0.4	0	1
2.2 Bar, 25% N-Heptane	2.38	396.45	21% Oxygen, 79% Nitrogen	0.4	0.1167	0.8832
2.2 Bar, 45% N-Heptane	2.475	361.15	21% Oxygen, 79% Nitrogen	0.4	0.245	0.755
2.2 Bar, 55% N-Heptane	2.475	336.15	21% Oxygen, 79% Nitrogen	0.4	0.3264	0.6736

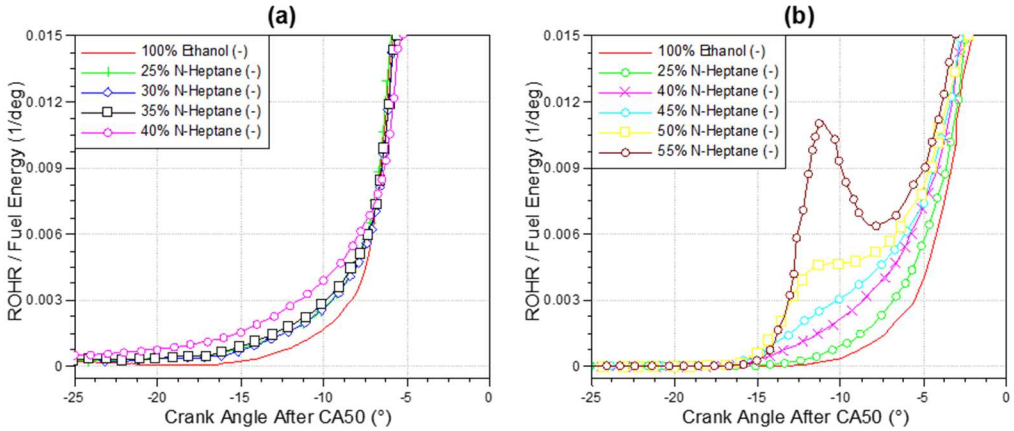

Figure 4.9: A comparison of experimental (a) and simulated (b) heat release rates for constant combustion phasing, intake pressure (1.8 bar), and equivalence ratio (ϕ = 0.4) at various mixture of ethanol/n-heptane (liquid volume fractions). The traces have been shifted so that the CA50 occurs at 0 degrees.

The simulation allowed an exploration of conditions that were not possible in the engine. Specifically, the addition of higher n-heptane fractions was examined computationally because these higher n-heptane fractions are not possible to test with the current experimental setup, as they would require intake temperatures below ambient. According to the simulation (Fig. 4.9), these higher n-heptane fractions would produce significant LTHR, which experimental data suggests may increase the CoV IMEP (Fig. 4.7).

c) Reaction Pathways Contributing to Heat Release

The analysis presented up to this point has established that the simulations performed with detailed chemical kinetic modeling are able to reproduce the experimentally observed heat release behavior. Thus, the simulations can be used with some confidence to elucidate the chemical nature of ITHR behavior via analysis of important reaction pathways. In addition, the chemical reactions distinguishing no ITHR, increasing ITHR, and transition to LTHR as a function of ethanol/n-heptane fuel mixture fraction can be identified.

Prior to proceeding with the detailed chemical analysis, the entire data set of simulated heat release curves was analyzed in order to select a subset that represent the different heat release behaviors noted above. Figure 4.10 displays four operating points at 2.2 bar with distinguishing heat release profiles that allow for comparison across fuel mixture fractions. These heat release profiles are representative of experimentally observed behavior; however, operating conditions do not match exactly due to the differences between simulations and experiments noted in the previous section. Once representative conditions were chosen, the key heat producing reactions during the ITHR period were determined. These reactions are shown in Fig. 4.11, which presents the dominant reactions contributing to the heat release rate at 8 degrees before CA50 in the three cases that provide the best insight into ITHR. The timing of 8 degrees before CA50 was chosen because it lies within the LTHR/ITHR window and a notable change in heat release rate can be observed at various ethanol/n-heptane blend ratios (see Fig. 4.10). A reaction path analysis was done with the goal of identifying the contribution of each fuel component to ITHR. To enable this analysis, a modified version of the ethanol/n-heptane chemical kinetic model was created wherein carbon atoms from n-heptane are labeled "C" while carbon atoms from ethanol are labeled "c". Thus, the ancestry of smaller molecules and each fuel component's contribution to heat release generated by smaller molecule oxidation can be identified. For example, the species formaldehyde labeled as "CH_2O" comes from n-heptane (nC_7H_{16}), whereas the same species labeled as "cH_2O" comes from ethanol (c_2H_5OH). This modeling approach is analogous to experimental isotopic labeling of reactant molecules to track atoms through a reaction network [Mack 2005]. The results of this analysis, displayed in Fig. 4.11, show the most important reactions contributing to heat release rate. The reactions corresponding to species derived from n-heptane (carbon labeled "C") are given on the upper half of the bar chart and the reactions corresponding to ethanol (carbon labeled "c") are on the lower half. Because of carbon labeling scheme, the same reactions appear on both the top and bottom of the graph. Note that the reactions displayed in Fig. 4.11 are reversible reactions, so they are written in the exothermic direction to clearly identify the direction corresponding to heat release. Figure 4.11 reports only reactions that contribute to the positive (exothermic) terms to focus attention on heat release rate.

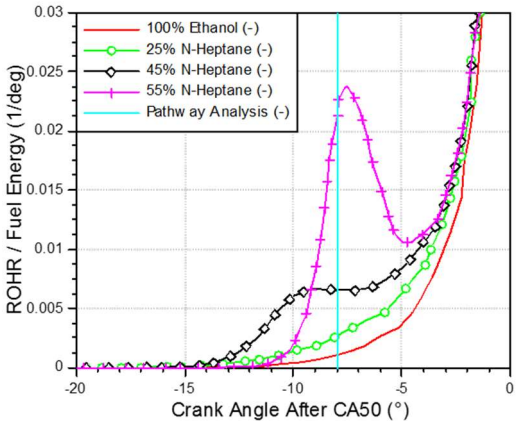

Figure 4.10: Simulated rate of heat release (ROHR) as a function of crank angle degrees after CA50 for various n-heptane/ethanol mixtures at 2.2 bar intake pressure and an equivalence ratio of 0.4.

To supplement the information in Fig. 4.11 on individual reactions, the heat release rate from various reaction groups relative to engine crank angle are presented in Fig. 4.12. The reactions are grouped based on the number of carbon atoms in the oxidized species, namely C1-C2, c1-c2, C3-C4, and C7. Again, "C1-C2" denotes species with carbon derived from n-heptane, and "c1-c2" is for species with carbon derived from ethanol. This method of presenting heat release by various reaction groups is similar to that used by Hwang, Dec, and Sjoberg [13]. They explain that primary heat-releasing reactions are correlated with the number of carbons in the hydrocarbon species undergoing partial oxidation to generate heat. Reactions containing small molecules with zero, one, and two carbon atoms (C0, C1-C2, and c1-c2) generate heat at different times and magnitudes than hydrocarbons with three and four carbon atoms (e.g., C3-C4), which in turn display different trends than larger hydrocarbons (e.g., C7 for n-heptane) [13]. In this way, the contribution to heat release at different CA (e.g., LTHR, ITHR, and HTHR) ensuing from the oxidation of various hydrocarbons sizes is clearly presented.

As previously discussed, the 100% ethanol simulation at 2.2 bar shows no LTHR or ITHR. Examining Fig. 4.11, the dominant reaction pathways contributing to the heat release rate are the hydrogen abstraction from ethanol by OH radicals and subsequent R + O_2 reactions (i.e., R is a hydroxyethyl radical), most notably the concerted elimination reaction leading to acetaldehyde and HO_2. Other reaction pathways that contribute less to heat release in this window are the oxidation reactions of H, cH_3, HcO, and cH_3O_2 radicals and the recombination of HO_2 to form H_2O_2. It is interesting to note that although the formation of H_2O_2 is exothermic, the subsequent H_2O_2 decomposition to two OH radicals is endothermic. When 25% of n-heptane is blended with ethanol, there is an increase in the magnitude of ITHR at 8 degrees before CA50 (Fig. 4.10). In this case, reactions involving n-heptane and its associated heptyl radicals contribute to the increased heat release rate, wherein hydrogen abstraction by OH radicals and subsequent R + O_2 leading to RO_2 (i.e., R is a heptyl radical) are important. However, significant increases are also seen in a number of ethanol reactions, specifically those associated with the oxidation of small radicals, such as reactions involving cH3, cH2O, and HcO. The heat release caused by reactions producing HO_2 also increases in this case. The production of HO_2 from 1-hydroxyethyl radicals is exothermic, but simultaneously decreases the overall reactivity of the system by inhibiting OH

production. Figure 4.12 (b) shows that while n-heptane reactions play a significant role in the heat release rate during ITHR for the 25% n-heptane case, ethanol reactions c1-c2 still comprise the largest single group of heat producing reactions.

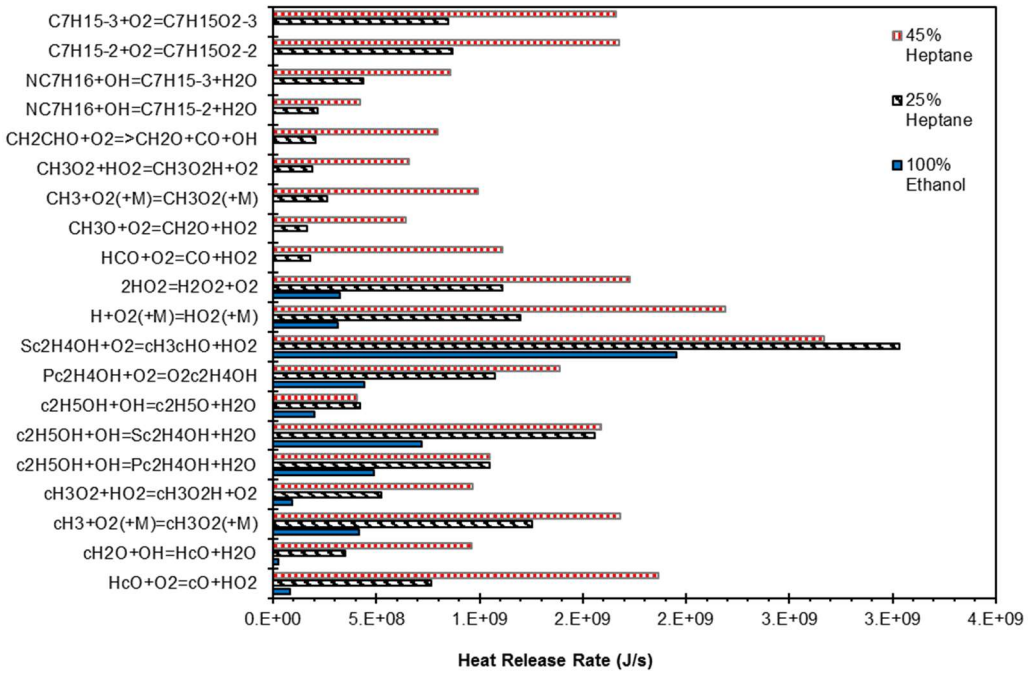

Figure 4.11: Contributions of important reactions towards total heat release rate for various n-heptane/ethanol mixtures at 2.2 bar intake pressure and 8 degrees before CA50 (with CA50 occurring at approx. 6 °aTDC).

As the blended volume % of n-heptane increases to 45%, a more prominent ITHR behavior is observed in Fig. 4.10. This is correlated with an increase of both heptane oxidation reactions and most ethanol oxidation reactions as shown in Fig. 4.11. However, the increase in the n-heptane oxidation reactions is greater than the increase in ethanol oxidation reactions, and consequently, as seen in Fig. 4.12 (c), more of the ITHR with this fuel combination is derived from n-heptane. A trend towards increased oxidation of small radicals from n-heptane is evident. The oxidation of the 1-hydroxyethyl radical to form acetaldehyde and HO_2 diminishes its contribution to heat release, most likely because the oxygen preferentially oxidizes the heptyl radicals that are now present in larger concentrations. Thus, the inhibitory effects of the 1-hydroxyethyl plus O_2 reaction are being reduced. The oxidation of small radicals from ethanol also increases, but the magnitude of the increase is less than the increases for n-heptane derived radicals. An interesting observation is the increasing heat release contribution via oxidation of the ethanol-derived small molecules HcO and cH_2O as n-heptane is added. This indicates that n-heptane addition is increasing the conversion of ethanol to HcO and cH_2O, such that their subsequent oxidation releases heat in the ITHR regime. These trends are also witnessed in Fig. 4.12 (c), which highlights the increased importance of C1-C2 reactions from n-heptane. Finally, no increase is seen in the hydrogen abstraction from ethanol, likely due to the decreased ethanol content in the fuel blend.

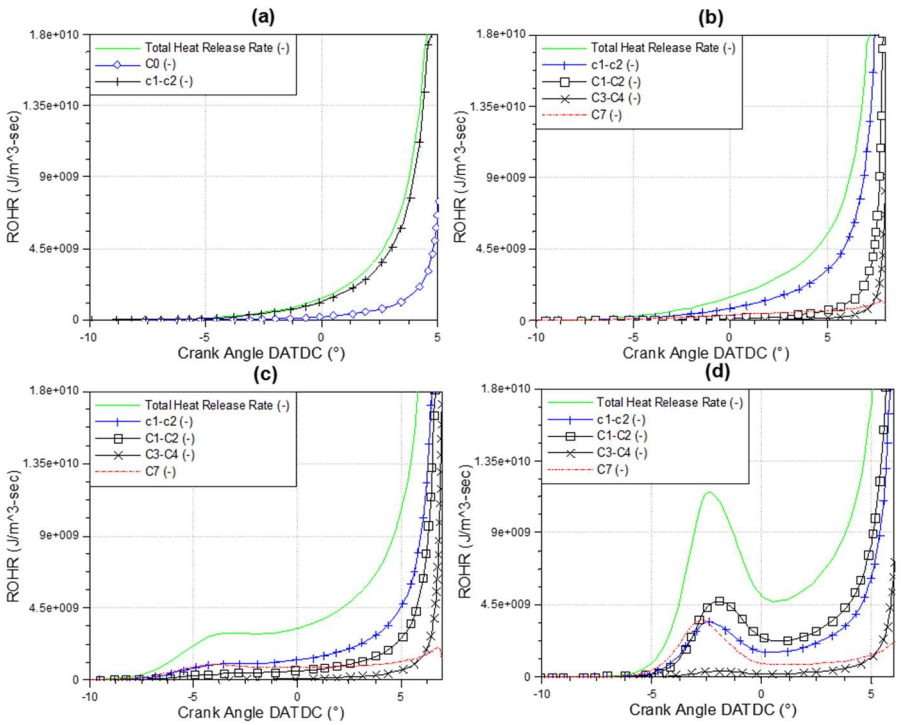

Figure 4.12: Simulated heat release rates for (a) 100% ethanol, (b) 25% n-heptane, (c) 45% n-heptane, and (d) 55% n-heptane with intake pressure of 2.2 bar and equivalence ratio of 0.4. In addition to the global heat release rate, the rates of various reaction groups are plotted as well. Reactions using ethanol carbon are denoted with "c," while reactions using n-heptane carbon are denoted with "C."

A shift from ITHR to LTHR behavior is observed when the n-heptane fraction increases to 55%. Figure 4.12 (d) shows that this change corresponds to an increase in importance of n-heptane derived C1-C2 reactions, but increases in heat release among all reaction groups are observed, including ethanol. This highlights the importance the ethanol plays in all mixture fractions that were tested; even with high n-heptane percentages displaying a heat release mode not seen in pure ethanol, ethanol oxidation plays a significant part in the overall heat release rate. However, when the n-heptane concentration crosses a threshold, a transition from ITHR to LTHR is observed. This can be attributed to the decreased importance of 1-hyroxyethyl plus O_2 reaction, which has the characteristic of inhibiting low temperature reactivity.

Reaction Pathways Contributing to OH Radical Production

The previous section discussed the reaction pathways contributing to heat release. This section aims to further investigate the reactions contributing to the overall reactivity of the system by analyzing the reaction pathways leading to OH radical production and consumption. Figure 4.13 (a-d) presents the reaction groups (e.g., C0, C1-C2, c1-c2, C3-C4, and C7) which contribute to OH radical rate of production (ROP) as a function of CAD in a similar manner as presented previously for the heat release analysis. A positive ROP value denotes OH radical production and a negative ROP value denotes consumption; the OH net ROP is also presented. For all blends of ethanol and n-heptane, the net ROP is always near zero until the main ignition event. This is

because any OH produced in the LTHR and ITHR regions is quickly consumed via the oxidation of fuel, smaller hydrocarbons, and C0 species. The net effect of this OH production and consumption is evolution of heat that drives the ignition and combustion process. With 100% ethanol, there is minimal OH production in the LTHR and ITHR region (e.g., -10 to -2 CAB after CA50) coming from decomposition of c0 and c1-c2 species. Figure 4.14 shows that most of the OH is consumed via H-atom abstraction reactions from the ethanol. With 25% n-heptane, there is again minimal OH production/consumption in the LTHR and ITHR region, which explains the lack of heat release at these conditions. The addition of n-heptane appears to contribute to overall OH radical activity primarily in the region immediately prior to the main ignition event via C7, C3-C4, and C1-C2 reactions, but reactions of ethanol and its derivatives are still the primary species involved in OH production/consumption. With 45% and 55% n-heptane additions, there is an increase in heat release in the LTHR and ITHR regions, and it becomes clear that OH production/consumption in this region also increases. Reactions from n-heptane (C7) are responsible for producing OH via low-chain branching reactions, and the OH radicals are subsequently consumed by H-atoms abstractions from both fuels, n-heptane and ethanol. This is further evidence that the addition of highly reactive n-heptane generates the radical pool necessary to consume the less reactive ethanol.

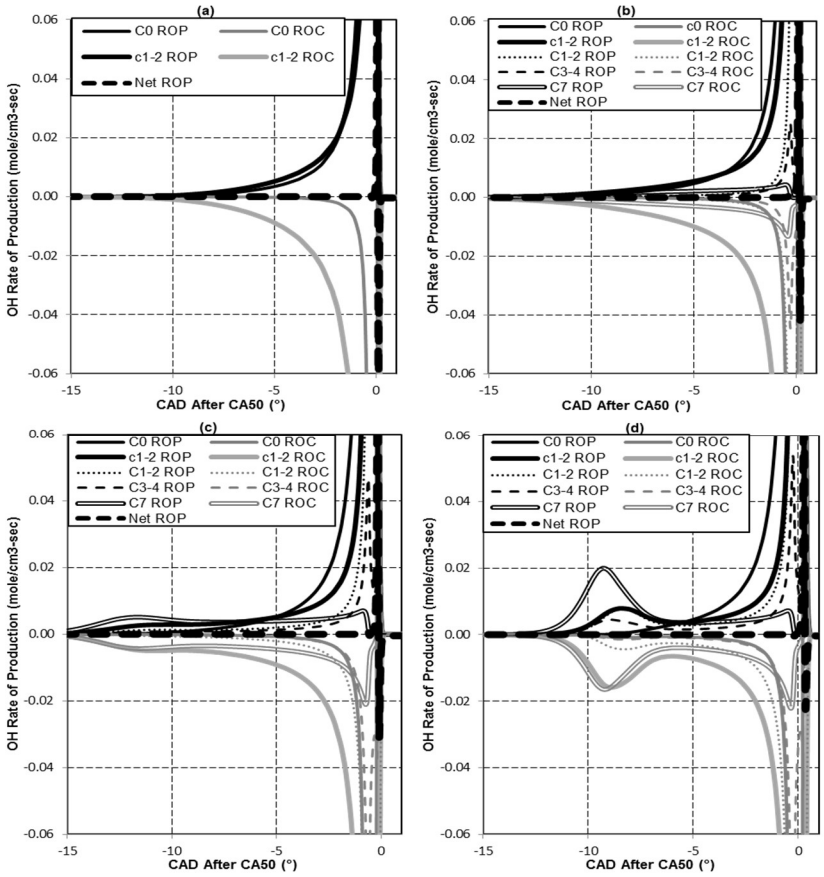

Figure 4.13: Simulated OH rate of production and rate of consumption for various reaction groups, for the cases of 100% ethanol (a), 25% n-heptane (b), 45% n-heptane (c), and 55% n-heptane (d) at 2.2 bar intake pressure and $\phi = 0.4$.

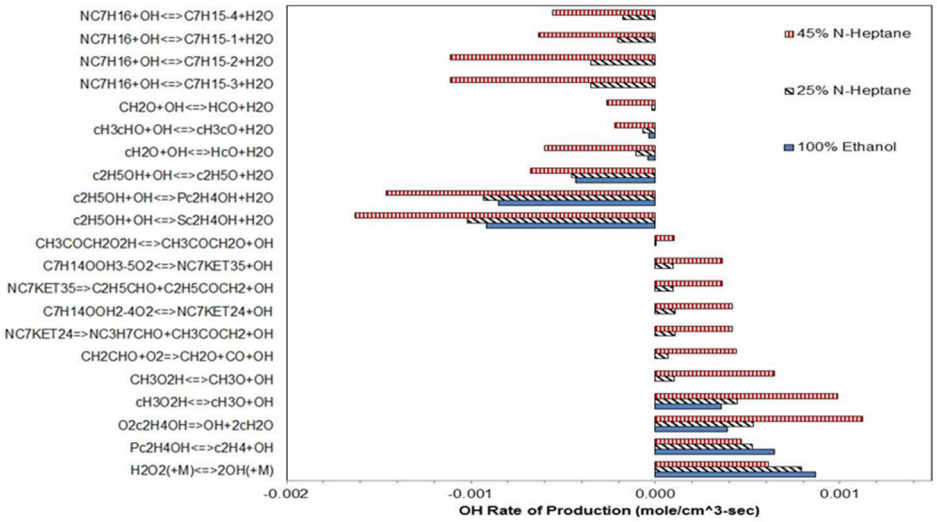

Figure 4.14: Simulated OH rate of production for top OH producing and consuming reactions for various fuels at 2.2 bar intake pressure and $\phi = 0.4$.

d) Quantification of ITHR

Thus far, the statements made in this paper regarding the magnitude of ITHR are all qualitative because, as of yet, no concrete method to quantify the amount of heat released during ITHR has been proposed. In this paper three potential methods of ITHR quantification will be explained with their advantages and disadvantages, namely, a temperature based method, a ROHR based method, and a ROHR derivative based method. In addition, one potential chemical marker of ITHR will be discussed. All the methods that are explained below are methods for defining the boundaries of when ITHR occurs, so that the cumulative heat release between the boundaries can be determined.

e) Temperature based method

One potential method of quantification of ITHR is by assigning a temperature range to ITHR, and determining the amount of heat released between the two temperature boundaries. This method relies on the assumption that ITHR can only occur within a prescribed temperature range. However, this study has found that such a temperature based prescription is not valid. Figure 4.15 plots ROHR against simulated in-cylinder temperature, and this figure shows that while general statements about an ITHR temperature range can be made, the starting and ending temperatures cannot be precisely defined across different conditions. This temperature method may work well if ITHR always occurred within a specific temperature window and was not bounded by high-temperature heat release (HTHR); however, if the maximum temperature of the ITHR window is too high, then the cumulative heat release during ITHR can be vastly over estimated because the ROHR during HTHR is much higher than it is during ITHR.

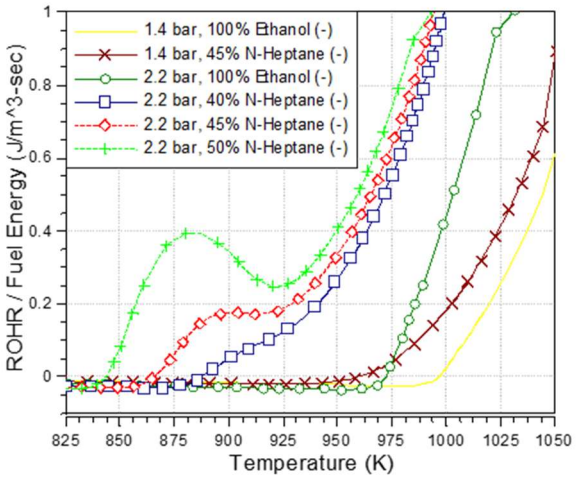

Figure 4.15: Simulation results of rate of heat release traces for various conditions, plotted against in-cylinder temperature.

f) ROHR based method

Another potential method of quantification is summing all of the heat release that occurs below a certain scaled ROHR and assigning this as ITHR. Examination of Fig. 4.6 shows that by taking an arbitrary scaled ROHR, such as 0.006 (1/deg), to be the cutoff for ITHR, each increase in n-heptane fraction will yield a higher amount of energy that is quantified as ITHR by this method of quantification. While this method will approximate the amount of ITHR, this method has no fundamental basis. For example, we have already shown that ITHR is linked to a certain set of chemical reactions that are not intrinsically limited to producing heat at certain rates, and therefore this is an arbitrary measure that likely could not be applied across engines, or even fuels.

g) ROHR derivative based method

The third method of quantification that was examined was using the derivative of the scaled ROHR to find ITHR boundaries. This method sums the heat release up to a point where the ROHR starts to change suddenly, as determined by the derivative of the ROHR. This method attempts to bridge the gap between engine data and fundamental principles, as modeling shows that the sudden change in ROHR is indicative of a shift in the dominant reaction chemistry. By using this criterion as a boundary condition for ITHR, quantification can be achieved using common engine data, and this method can be tied to the cause of ITHR, offering a non-arbitrary measure of a chemical phenomenon. We found that using a value of 0.004 ($1/deg^2$) as the upper limit for ITHR would reliably find the visually appropriate "end" of ITHR that corresponds to the switch in dominant heat-producing reactions.

The basic ROHR derivative method described above was further supplemented in order to provide accurate results across the range of conditions and fuels that were explored in these experiments. A key addition to the derivative of ROHR method deals with the exclusion of LTHR from the summing of heat release. This is an important issue, as ITHR may comprise on the order of 5% of the heat release, and LTHR may also be on the same order. In certain engine conditions

and with certain fuels, prior to ITHR there could be a significant amount of LTHR. In the results of ROHR this would be presented as a second peak which occurs before the peak caused by HTHR. Therefore, the calculation of ITHR cannot use the beginning of the cycle as an initial point but rather has to find a point where LTHR ends and ITHR begins. Transition from LTHR to ITHR is visually characterized by the valley in the ROHR curve (negative temperature coefficient region) and therefore the start of ITHR is defined as the minimum point in this valley. This is confirmed via chemical analysis of the simulations as the point at which formaldehyde begins to accumulate and when the LTHR reactions have nearly stopped.

To reiterate the method of ITHR calculation explicitly, the end of ITHR is found by finding the crank angle at which the derivative of the ROHR exceeds 0.004 ($1/deg^2$), starting from the maximum derivative of the ROHR and working towards the start of combustion. From this point, the start of ITHR is found by identifying the point at which the 2nd derivative of the heat release is equal to zero between the LTHR peak and the ITHR end point. If two-stage ignition is not present, the start of ITHR is taken to be the start of combustion. Once the starting and ending points of ITHR are established, the ROHR is integrated between these two points to determine the total amount of heat released during the ITHR period. An example of how this method functions on a test case can be seen in Fig. 4.16.

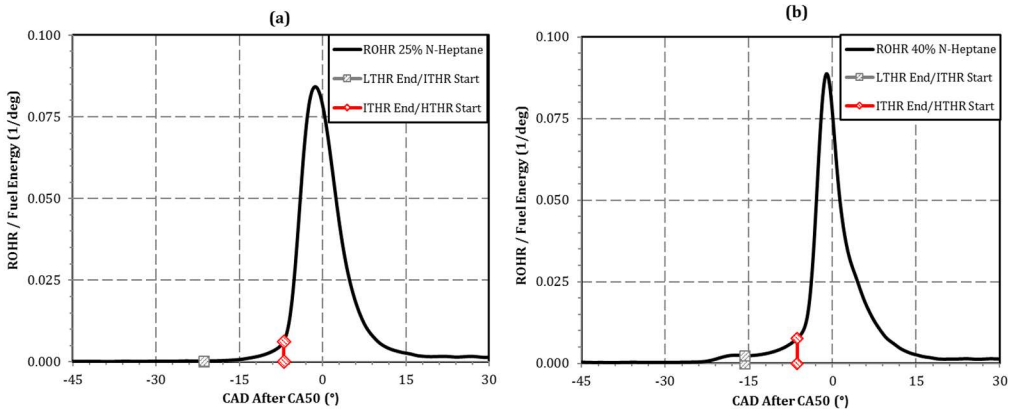

Figure 4.16: An example of the boundaries of LTHR/ITHR and ITHR/HTHR found by the derivative ROHR method in the cases of 2.2 bar intake pressure, ϕ=0.4, (a) 25% N-Heptane and (b) 40% N-Heptane.

The use of this ROHR derivative method with a LTHR cutoff to find the boundaries of ITHR yielded very reasonable results, both in terms of what we would expect when visually assessing HRR's, and also when comparing to the start and end of ITHR as determined by the simulated chemistry. This good performance was observed across the range of conditions that were explored in the present experiments. The levels of ITHR calculated by the derivative of ROHR method can be seen in Fig. 4.17. This figure highlights the three types of ITHR behavior that is seen when inspecting HRR profiles. Cases with minimal or no ITHR, such as when burning pure ethanol, will yield a result of below 2% of the total heat release, due to the continuity of the ROHR, which forces the HRR to pass through the lower and upper boundaries used in this method. Cases with a small amount of ITHR, which in these experiments correspond to n-heptane percentages between 25% and 45% depending on intake pressure, are found to have ITHR comprising 2-3%

of the total heat release. And for cases with significant ITHR, which correspond to n-heptane percentages between 35% and 50%, ITHR comprises roughly 5% of the total heat release.

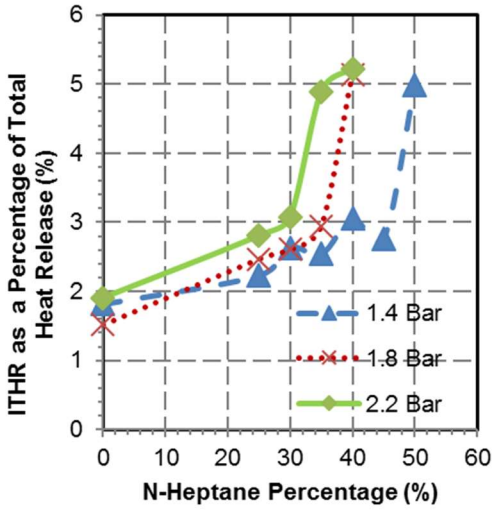

Figure 4.17: ITHR percentage of total heat release for various fuel blends and intake pressures, with constant equivalence ratio of 0.4 and combustion phasing of CA50 = 10 °aTDC. Values are calculated using derivative of ROHR method.

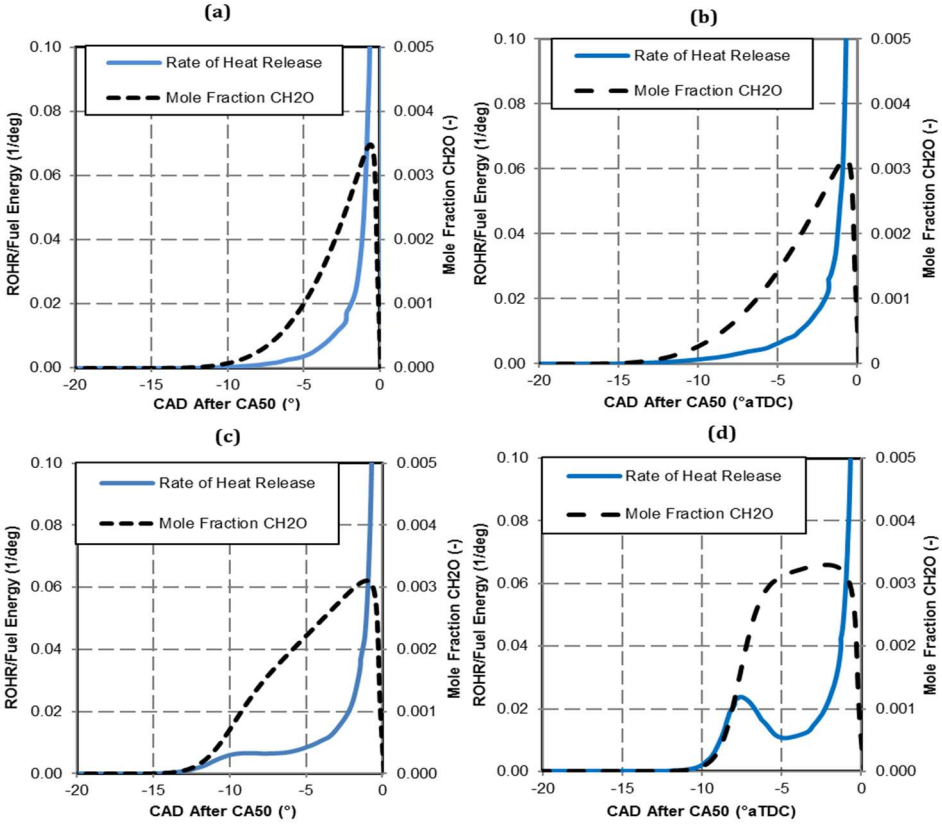

Figure 4.18: Simulated molar concentration of Formaldehyde in the ITHR region, for 2.2 bar intake pressure, ϕ = 0.4, for four fuels: 100% ethanol (a), 25% n-heptane (b), 45% n-heptane (c), and 55% n-heptane (d). The scaled ROHR is plotted for reference.

In addition to quantifying ITHR from ROHR data, an effort was made to determine if any chemical markers exist for ITHR, which could be used by experimentalists who are studying this phenomenon. With this in mind, a number of simulated species concentrations were assessed for their correspondence to ITHR. It was found that formaldehyde began to accumulate at the start of ITHR in heat release cases that feature no LTHR. In cases with LTHR, formaldehyde is primarily accumulated during LTHR, but production continues during ITHR. In both cases, the majority of the time formaldehyde is present in a significant concentration is during the ITHR period, as formaldehyde is quickly consumed during HTHR. This behavior is shown in Fig. 4.18. This simulated behavior agrees with the results of [16], in which formaldehyde was found grow in concentration during ITHR. The presence of formaldehyde during ITHR may make it a useful marker for ITHR in experiments that can measure formaldehyde.

V. Additional Considerations and Future Work

This paper has utilized a simple single-zone HCCI model to help elucidate the underlying chemical kinetics relating to ITHR. The use of such a model does not constitute an engine simulation, but rather a simulation of the chemical process that occurs in the combustion chamber. In this sense, the simulation could be improved by simulating the flows of air and fuel into the combustion chamber, and accounting for fluid dynamic effects in the combustion chamber. However, the simulation of these factors would likely not significantly alter the results that have been obtained for the portion of the cycle that is of interest in this study – the crank angle space occupied by LTHR and ITHR. Studies have shown that chemical kinetics are the key factor in determining HCCI heat release characteristics [Flowers 2002, Jun 2003], and while mutli-zone models will produce better agreement between the simulation and the experiment during HTHR, the single-zone model used in this study qualitatively reproduced the heat release characteristics of LTHR and ITHR. With these factors in mind, the decision to utilize a single-zone model with detailed kinetics rather than a multi-zone model or an LES simulation with reduced kinetics was made.

The inputs to the chemical-kinetic simulations consisted only of air and fuel. This neglects the internal gas recirculation (IGR), which on this engine is very low, due to positive valve overlap. It is calculated that the maximum IGR for this engine is on the order of 4%. Therefore, having large concentrations of species that influence combustion at the start of the cycle would require extremely high concentrations of these species at the end of the previous cycle. As the engine experiments used in this study were conducted at stable operating points, the chance of incomplete combustion products being present in appreciable quantities during the next cycle is low, and qualitative agreement between the chemical kinetic simulations and the engine experiments was achieved without attempting to account for trace amounts of residual species. However, to verify that incomplete combustion products that could be present would not have a significant effect on the heat release characteristics, a set of simulations was run in which 100 PPM of CO and 100 PPM of CH_2O were added to the fuel and air mixture. The results of these simulations can be seen in Fig. 4.19. These results demonstrate that the addition of these species does not impact the rate of heat release characteristics to a large degree. With regards to the rate of heat release, the primary effect is the advancing or delaying of HTHR, depending on the case. These results agree with the

results presented in [Machrafi 2008], which show that significantly higher concentration of residual species, such as CO and CH_2O, are needed to significantly impact HCCI combustion.

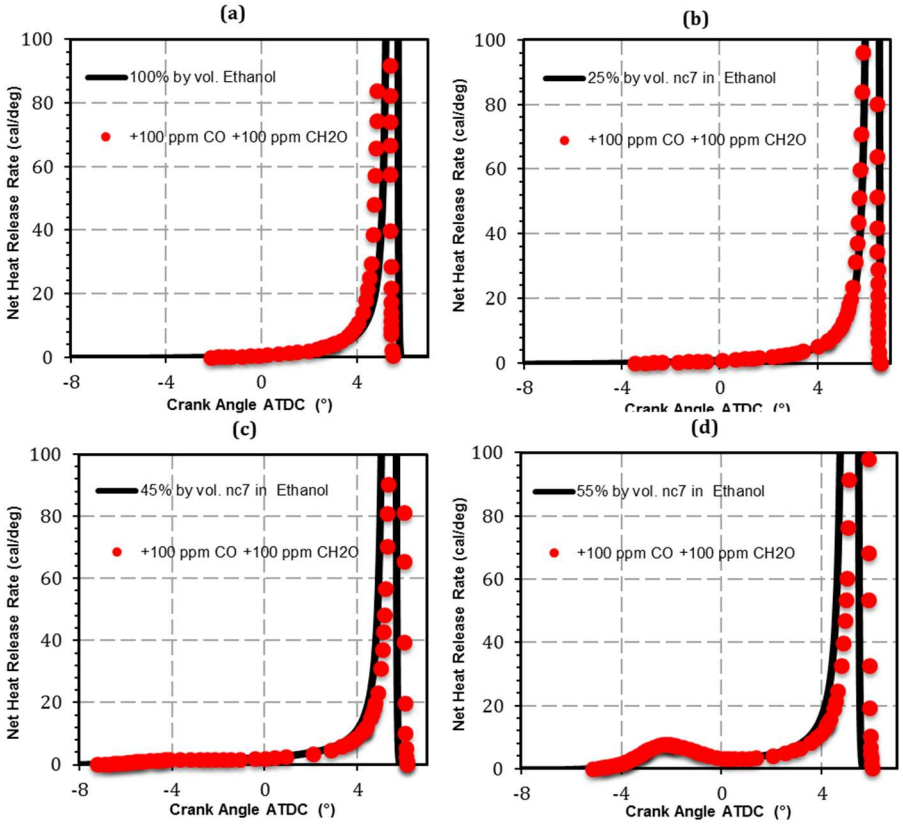

Figure 4.19: Effects of the addition of common incomplete combustion products on HCCI ROHR for the cases of 2.2 bar intake pressure, 100% ethanol (a), 25% n-heptane (b), 45% n-heptane (c), 55% n-heptane (d), and ϕ=0.4.

In this paper an HCCI engine has been used to study the chemical kinetics of ITHR. The engine was chosen as the experimental basis for this study because ITHR has thus far only been observed in engines. However, the engine is not the ideal experiment to study the chemistry underlying ITHR, and therefore the authors hope that this work will encourage other researchers utilizing fundamental experiments to examine conditions that may yield ITHR. The study of ITHR in fundamental experiments could provide useful validation data for detailed chemical kinetic models that predict ITHR, such as the one used in this study, and advance the understanding of ITHR considerably.

VI. Conclusions

This paper has combined engine experiments of mixtures of ethanol and smaller amounts of n-heptane in a boosted HCCI engine with chemical kinetic simulations to explore ITHR behavior in engines. The simulations, once verified against experimental results, were used to elucidate the dominant chemical reactions and pathways that control ITHR. Finally, the results of the experiments and the simulations were used to develop a method to quantify the amount of heat

release that can be classified as ITHR from experimental engine data. The following are the main findings of this paper:

1. ITHR can be induced in a fuel that does not exhibit ITHR behavior through the addition of small amounts of a second fuel that has high low-temperature reactivity.
2. As the addition of the highly reactive fuel is increased, ITHR will increase, and eventually LTHR will be triggered.
3. Increased ITHR lowers the engine's CoV IMEP and intake temperature requirements, while the onset of LTHR corresponds to a rise in CoV IMEP and further lowering of intake temperature requirements.
4. ITHR can be qualitatively simulated using detailed kinetic models in a simple single-zone HCCI model.
5. At the conditions studied here, ITHR is driven both by ethanol and n-heptane oxidation reactions.
6. The blending of n-heptane to pure ethanol results in a dramatic increase in ITHR due to hydrogen abstraction from n-heptane by OH radicals and the addition of heptyl radicals to O_2.
7. The derivative of ROHR method of ITHR quantification can accurately predict the beginning and end of ITHR from basic engine data. By using a threshold of 0.004 (1/ deg^2), the end of ITHR is predicted. The start of ITHR is taken to be the low point in the valley between the LTHR peak and the HTHR, or the start of combustion in cases where no two-stage ignition is present. The total heat released during ITHR can be calculated by integrating the HRR between the starting and ending points of ITHR.
8. Simulations show formaldehyde accumulation during the LTHR and ITHR periods, agreeing with the findings in [Dec 2008]. This suggests that formaldehyde can be used as a chemical marker for the occurrence of ITHR.

Chapter 5:

The effects of fuel composition and ethanol content on lowest stable load in a Gasoline Compression Ignition engine: An Experimental and Modeling Study

This article is in preparation for submission to Fuel.

David Vuilleumier, Frithjof Schwerdt, Diego Bestel, Marco Mehl, Alex Frank, Robert Dibble, Mani Sarathy

Abstract:

Gasoline Compression Ignition (GCI) engines are a potential practical implementation of LTC, combining low emissions, high efficiency, and control of combustion phasing. However, when using a GCI operation strategy, fuel choice and engine compression ratio are often a compromise between the ability to achieve auto-ignition at low loads, and the ability to achieve sufficient premixing and combustion duration at high loads. This study investigates the effects of fuel composition on low-load performance of a GCI engine. To achieve this, 7 fuel blends were created, achieving 3 different Anti-Knock Index (AKI) levels – 85 AKI, 88 AKI, and 91 AKI. At each AKI level, multiple fuels with different levels of ethanol were present. Each fuel's low-load performance was evaluated by measuring the lowest achievable stable load at 3 different intake pressures (1.05 bar, 1.23 bar, 1.40 bar), and a wide range of injection timings (15 - 40 crank-angle degrees before Top-Dead-Center -- CAD bTDC). The minimum loads of the various fuels ranged from 0.1 bar indicated mean effective pressure (IMEP) to 4.8 bar IMEP.

Corresponding Homogeneous Charge Compression Ignition (HCCI) experiments were conducted to better understand the GCI minimum-load experimental results. The HCCI experiments measured the auto-ignition behavior, and more specifically the Low-Temperature Heat Release (LTHR) behavior of the 7 fuels over a range of intake pressures. The Research Octane Number (RON), Motored Octane Number (MON), AKI, Octane Index (OI), and LTHR behavior of each fuel were compared to the GCI low-load results. MON and AKI were found to be poor predictors of low-load performance, while RON correlated reasonably well. However, OI and LTHR behavior offered superior correlation to RON, indicating the importance of a fuel's sensitivity, and LTHR behavior. Calculated ignition delays corresponded well with the observed trends in both the GCI and HCCI engines. This data also showed the LTHR suppression by ethanol and toluene.

I. Introduction:

In an era of tightening emissions regulations, especially carbon dioxide (CO_2), high-efficiency engines are sought to reduce the carbon emissions of over-the-road vehicles. This desire for highly efficient engines has resulted in a great deal of research of compression ignition engines, due to their inherent tolerance to higher compression ratios than spark ignition (SI) engines, and the corresponding rise in efficiency that accompanies higher compression ratios [Heywood 1988]. However, to avoid the high traditional pollutant emissions of diesel engines, particulate matter (PM) and oxides of nitrogen (NO_x), Low Temperature Combustion (LTC) has been extensively

studied [Yao 2009]. The purest form of LTC, homogeneous charge compression ignition (HCCI) [Najt 1983], has been found to be generally impractical for automotive use, due to the difficulty of controlling a fully kinetically governed system, and difficulties in achieving high-load operation of an HCCI engine. However, various alternative strategies for LTC have arisen, such as Partially Premixed Compression Ignition (PPCI) [Kalghatgi 2007], Reactivity Controlled Compression Ignition (RCCI) [Splitter 2010], and Low-Temperature Combustion Diesel (LTC Diesel) [Musculus 2013]. These strategies typically use some amount of fuel stratification to achieve both a wider load range and a greater degree of control over combustion phasing than HCCI engines.

One particularly promising strategy for achieving LTC is Gasoline Compression Ignition (GCI) [Ciatti 2013, Sellnau 2012]. This strategy directly injects gasoline into the combustion chamber, and relies on the high resistance to autoignition afforded by conventional high-RON gasoline to allow the charge to partially premix, resulting in dilute conditions under which LTC can occur. Because the fuel is directly injected, the local equivalence ratios throughout the cylinder can be altered based on intake conditions, allowing control of combustion phasing and combustion noise [Shahlari 2013] / ringing intensity [Eng 2003]. GCI has been shown to offer high efficiency and low engine-out emissions over a variety of conditions [Sellnau 2015]. However, two key challenges for GCI engines are low-load operation and fuel variability.

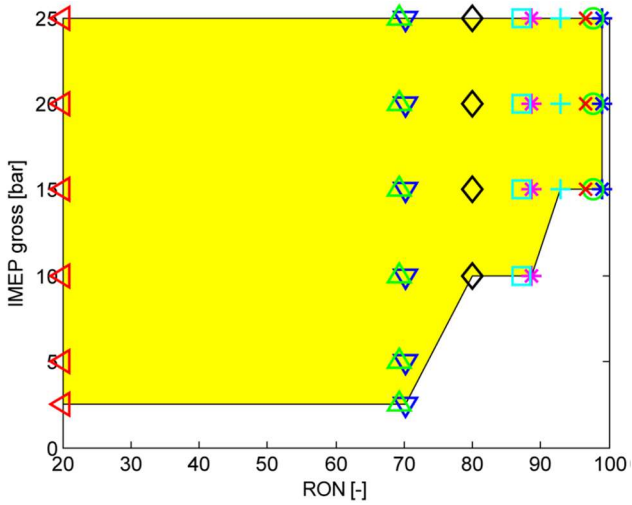

Figure 5.1: Load range of a Partially Premixed Combustion engine run with fuels of different RON levels, reprinted from [Borqvist 2012].

Low-load operation is challenging for GCI engines because at low loads, a very small mass of fuel is injected into the combustion chamber. This small mass of fuel, coupled with the long ignition delay of gasoline, results in low local equivalence ratios that are difficult to ignite. Further, at low loads, intake pressure is typically reduced to near-ambient levels [Kolodziej 2014], as exhaust enthalpy is low, making it difficult to drive a compressor via a turbocharger. Various strategies have been developed in an attempt to overcome these challenges, such as exhaust rebreathing, late direct injection timing, and intake boosting through supercharging. While these strategies have been successful at increasing the load range of GCI engines, they have not eliminated challenges at low loads [Sellnau 2015, Ciatti 2015]. These challenges can be seen in Fig. 5.1 [Borqvist 2012], which depicts the load range for a GCI engine with a range of gasoline-type fuels. This figure illustrates the difficulty in achieving low-load GCI operation with low-

reactivity fuels by showing the limitations that were encountered with a particular experimental setup.

Fuel variability is a challenge faced by all combustion systems that are at least partially governed by chemical kinetics. Fuel composition can vary significantly from refinery to refinery, and this results in a measurable range of fuel properties, such as molecular composition that in turn affects the Research Octane Number (RON) and Motor Octane Number (MON) and strength of the pathways governing these two fuel parameters, as well as homogeneous ignition delays times. This range of properties has been shown to affect LTC and GCI combustion systems by altering the conditions that result in a fuel-oxidizer mixture's auto-ignition. Considering the gasoline fuel regulations in California, aromatic species have a limit of comprising 22% of gasoline by weight [CARB 2013]; this may have a significant effect on the final properties of the gasoline, specifically with regards to fuel sensitivity.

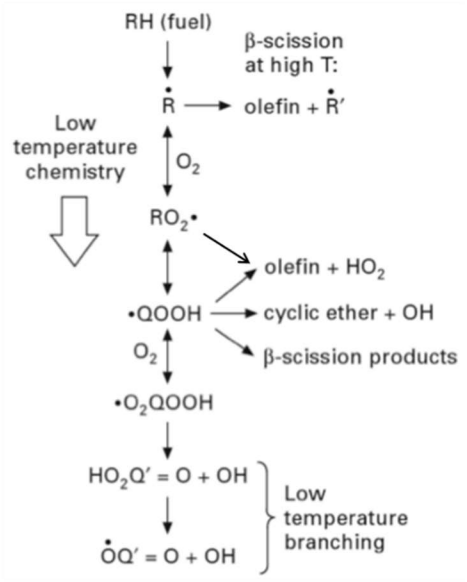

Figure 5.2: Dominant reaction pathways for high-temperature, intermediate-temperature, and low-temperature oxidation of hydrocarbon fuels, reprinted from [Curran 1998].

This study investigates the effects of fuel composition and its Low-Temperature Heat Release (LTHR) behavior on GCI low-load performance, using GCI engine experiments, HCCI engine experiments, and 0-D chemical kinetic simulations. To carry out this study, a palette of 7 fuels was assembled, primarily using the gasoline Fuels for Advanced Combustion (FACE) as base stocks, and blending with ethanol to meet certain Anti-Knock Index (AKI) levels. In this study, the effects of AKI and ethanol content are studied parametrically, while other gasoline components and properties are varied, though not independently. The LTHR behavior of each fuel was assessed in an HCCI engine. LTHR has been shown to significantly alter the ignition behavior of gasoline fuels, especially under elevated intake pressure (boosted) conditions. This study assesses whether LTHR may have a similar effect on low-load GCI combustion, which is in many ways similar to HCCI combustion, with dilute charges that can be difficult to ignite.

The dominant kinetic pathway for LTHR is shown in Fig. 5.2 [Curran 1998]. It may be seen from this figure that the O_2 addition and subsequent isomerization lead to chain branching at low-temperatures (typically below 850 Kelvin). Ethanol has previously been shown to inhibit low-temperature chemistry through radical scavenging [Vuilleumier 2016], primarily of OH and HO_2 radicals. While the radical scavenging of ethanol significantly reduces the system reactivity at higher intake pressure that induce LTHR in gasoline, at lower intake pressures ethanol addition has minimal effect. The effect of LTHR suppression by ethanol is assessed throughout this study.

II. Experimental Methods:

a) Fuels

Seven fuels were used in the course of this study. Their names, as well as ethanol, paraffin, iso-paraffin, olefin, naphthene, and aromatic (E-Piona) content can be found in Fig. 5.3, and detailed hydrocarbon analysis can be found in [Cannella 2014]. Three of the fuels were derived from FACE fuels and are labeled FACE C, FACE J, and FACE G. FACE gasolines were created so that certain fuel properties (RON, Aromatic content, n-paraffin content, and sensitivity) could be varied parametrically. A detailed explanation of FACE fuel selection and properties may be found in [Cannella 2014].

The three FACE base fuels for this study, FACE G (95 RON), FACE C (85 RON), and FACE J (70 RON) were blended with ethanol to achieve specific AKI levels (85, 88, and 91 AKI), as shown in Fig. 5.4. In addition to the blends of FACE C, J, and G, a fourth fuel was used as well; Haltermann CARB LEV III – Regular Octane certification fuel (CARB LEV III), which has an AKI rating of 87. CARB LEV III is the current certification gasoline for vehicle emissions tests in California. Examination of Fig. 5.3 reveals that FACE J, FACE G, and CARB LEV III all have high fractions of aromatic compounds, but significantly different AKI levels (Fig. 5.4). Conversely, FACE C is much more similar in composition to a Primary Reference Fuel (PRF), with 95% of the components either n-paraffins or iso-paraffins. The fuels used in this study were chosen for their ability to match certain AKI levels (84.5, 87.7, 91) with similar sensitivities while varying ethanol content significantly.

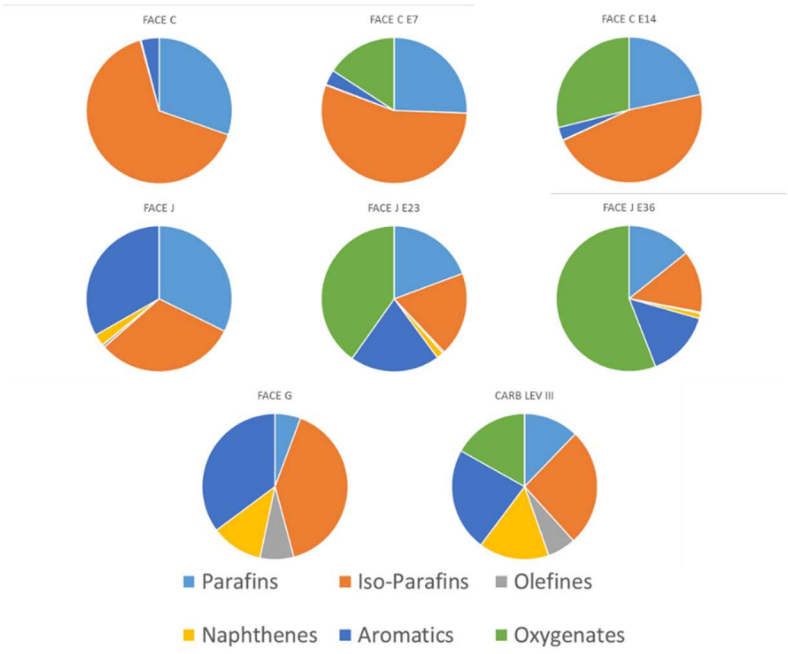

Figure 5.3: E-Piona compositions of blended and pure fuels [Cannella 2014].

Figure 5.4 shows the AKI levels of the 7 fuels against their ethanol content (note that neat FACE J was not used in this study). It can be seen that at each AKI level (84.5, 87.7, and 91 AKI), at least two ethanol contents were represented with ethanol content of the blends ranging from 0% to 36%. The RON and MON values for the mixtures presented here were not measured, but RON/MON data for FACE gasolines blended with ethanol were available from [Cannella 2014] in the case of FACE C and FACE G, by specifications sheet for CARB E10, and by an industrial partner for FACE J.

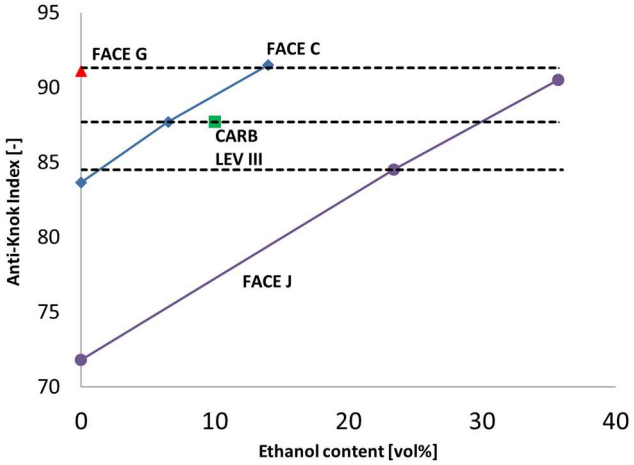

Figure 5.4: Ethanol content vs. Anti-Knock Index of tested fuels [Cannella 2014].

Table 5.1: Measured RON, MON, and AKI values of the seven fuels used in this study. Measurements from [Cannella 2014], specifications sheet, or industrial testing.

Fuel	RON	MON	AKI
FACE C	84.7	83.6	84.2
FACE C E7	89.3	86.2	87.7
FACE C E14	94.3	88.7	91.5
FACE J E23	88.4	80.6	84.5
FACE J E36	95.8	84.8	90.3
CARB E10	91.0	83.4	87.7
FACE G	96.5	85.8	91.2

a) GCI and HCCI Engine Experiments

GCI and HCCI engine experiments were carried out on a modified Volkswagen (VW) 2.0 liter displacement engine. The 4-cylinder engine was modified for use as a single-cylinder research engine by isolating the intake and exhaust tracts of a single cylinder; the three other cylinders were motored. A schematic of this engine can be seen in Fig. 5.5, which depicts the airflow system of the experimental engine. In addition to the isolated intake and exhaust systems, other modifications to this engine include a low heat transfer shallow-bowl piston with CR of 16.5:1, in-cylinder pressure sensing via a glowplug mounted AVL GH14D sensor, intake pressure sensing via a Kulite XTEL 190(M) sensor, an intake-air heater, and lastly, gaseous and liquid port fuel injectors (PFI) mounted in the intake tract. A Micro-Motion Coriolis flow meter was used to measure intake airflow, while a scale was used to measure liquid fuel flow. Finally, an external compressor was used to provide intake pressure above atmospheric conditions. The HCCI experiments utilized the PFI system run at 4 bar fuel pressure to provide a homogeneous charge, while the GCI experiments used the common-rail injection system run at 400 bar fuel pressure to directly inject fuel; the primary difference between these two combustion modes is the manner in which fuel is delivered to the engine.

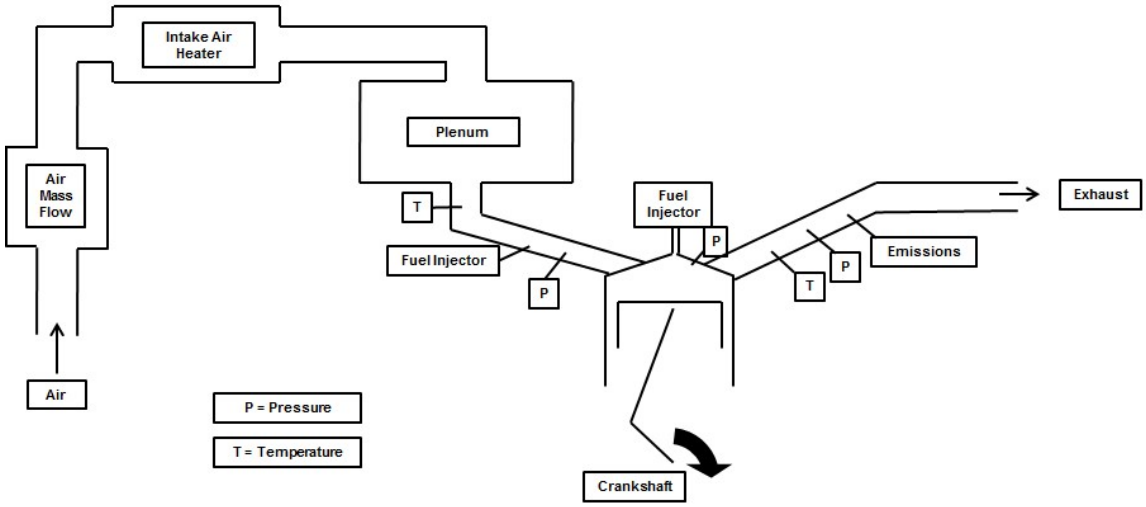

Figure 5.5: Schematic of the airflow tract for the experimental engine used in this study.

Table 5.2: Experimental conditions and engine specifications.

	GCI Operating Conditions	HCCI Operating Conditions
Engine Speed (RPM)	850	1000
Intake Temperature (°C)	45	45 - 130
Intake Pressure (bar)	1.05, 1.23, 1.4	1.0 - 1.8
Injection Type	DI	PFI
Injection Timing (dBTDC)	10 - 40	Closed Valve
Injection Pressure (bar)	400	4
External EGR Rate (%)	0	0
Coolant Temperature (°C)	105	
Compression Ratio (-)	16.5	
IVO (°bTDC)	20	
IVC (°bTDC)	140	
EVO (°aTDC)	140	
EVC (°aTDC)	8	
No. of Valves	4	
Bore (mm)	81	
Stroke (mm)	95.5	
Connecting Rod Length (mm)	144	

The GCI lowest-load experiments were carried out in the following manner. First, a stable mid-load operating point was established at a fixed engine speed, injection pressure, EGR rate, intake temperature, and intake pressure (see Table 5.2 for detailed conditions). Then, as depicted in Fig. 5.6, the injection duration was decreased until the stability threshold of a standard deviation

of 0.15 bar IMEP was exceeded. Thus, the minimum amount of fuel which could achieve stable combustion was measured, as well as the corresponding load. After determining the minimum load at a given injection timing, the start of injection (SOI) timing was advanced by 5 CAD, and the process was repeated for SOI's ranging from 10 CAD bTDC to 40 CAD bTDC, such that a minimum load was found for each fuel at each intake pressure.

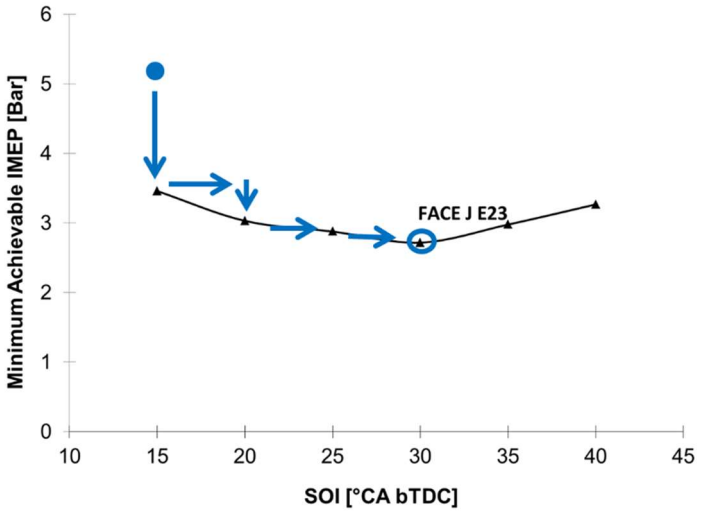

Figure 5.6: Example of the procedure used to measure minimum load for the GCI engine.

The HCCI engine experiments were performed similarly to those performed in [Vuilleumier 2016 Inves.]. At each intake pressure, starting from naturally aspirated (1.0 bar), the intake temperature required to achieve combustion phasing of 6 CAD aTDC was measured for a fixed equivalence ratio (0.3) and EGR rate (0%). This procedure was performed for each fuel, and the intake pressure was increased in 0.2 bar increments until an ambient intake temperature was reached.

The experimental results were post-processed using a procedure first described in [Vuilleumier 2013]. Briefly, the pressure measurements from 300 consecutive cycles were filtered with a 19-point Savitzki-Golay filter, before being averaged. The mass-averaged cylinder temperature was calculated from the ideal gas law, considering both changing trapped mass (due to blow-by losses and direct injection), as well as varying specific gas constant (due to temperature and composition changes), which was calculated for each time-step from JANAF tables. The rate of heat release (ROHR) was calculated from the general method described in [Heywood 1988]. The ROHR model considered wall heat losses via the Woschni model [Woschni 1967], as well as blow-by losses and changing specific heat ratios, as previously described. To accurately model the cylinder charge composition during the period of combustion, the ROHR is solved iteratively, with the new combustion profile used to determine the change of species. The iteration ends when the ROHR profile converges with the profile of changing species due to combustion.

b) 0-D Chemical Kinetic Modeling of Engine Experiments

Chemical kinetic simulations were carried out to help elucidate the experimental portions of this study. Homogeneous 0-D ignition delays were computed for the 7 tested mixtures to qualitatively compare the ignition delays. The ignition delays were calculated using the commercial software Chemkin Pro [Chemkin 2008] coupled with Lawrence Livermore National

Laboratory's Gasoline chemical kinetic mechanism [Mehl 2011] and a well-mixed constant-volume reactor model. Surrogates for the gasoline mixtures were the same as described in [Sarathy 2015], and are reprinted in Table 5.3.

Table 5.3: Compositions of surrogate mixtures used to compute ignition delays.

Surrogate Components (mol. %)									
Fuel	Isooctane	n-Heptane	Toluene	n-Butane	iso-Pentane	2-methyl-Hexane	Cyclo hexane	Cyclo pentane	Ethanol
FACE C	56	11	3	17	8	5	0	0	0
FACE C E7	47	9	3	14	7	4	0	0	16
FACE C E14	40	8	2	12	6	4	0	0	29
FACE J	31	32	33	0	0	0	0	4	0
FACE J E23	19	19	20	0	0	0	0	2	40
FACE J E36	14	14	15	0	0	0	0	2	56
FACE G	38	8	31	0	0	0	9	14	0
CARB LEV III	50	20	14	0	0	0	0	0	16

III. Results and Discussion:

a) GCI Lowest Stable Load

GCI lowest-load experiments were carried out in the manner described in section 2.b, under the conditions listed in Table 5.2, and with the fuels listed in Table 5.1. Figure 5.7 plots the lowest achievable load for each fuel at each intake pressure. This figure shows that as the intake pressure is increased, the minimum stable load decreases for all tested fuels. This is not altogether intuitive, as increased intake pressures result in globally leaner mixtures. However, the increased reactivity of the fuel at higher pressures, and the ability to create locally stoichiometric mixtures through injection strategy, outweighs the decrease in global equivalence ratio.

It may also be seen from Fig. 5.7 that the fuel's AKI level is not an effective indicator of low-load GCI performance. It can be seen that there is significant overlap in performance between the 85 AKI fuels and the 88 AKI fuels. Further, the 91 AKI fuels show a significant spread in achievable load, though no overlap with the other AKI levels. It can also be seen that at a given AKI level, higher ethanol content fuels generally achieve higher minimum loads under GCI conditions. However, this rule does not hold in the case of FACE C E14, so the ethanol content is not the only factor influencing the GCI performance of the tested fuels.

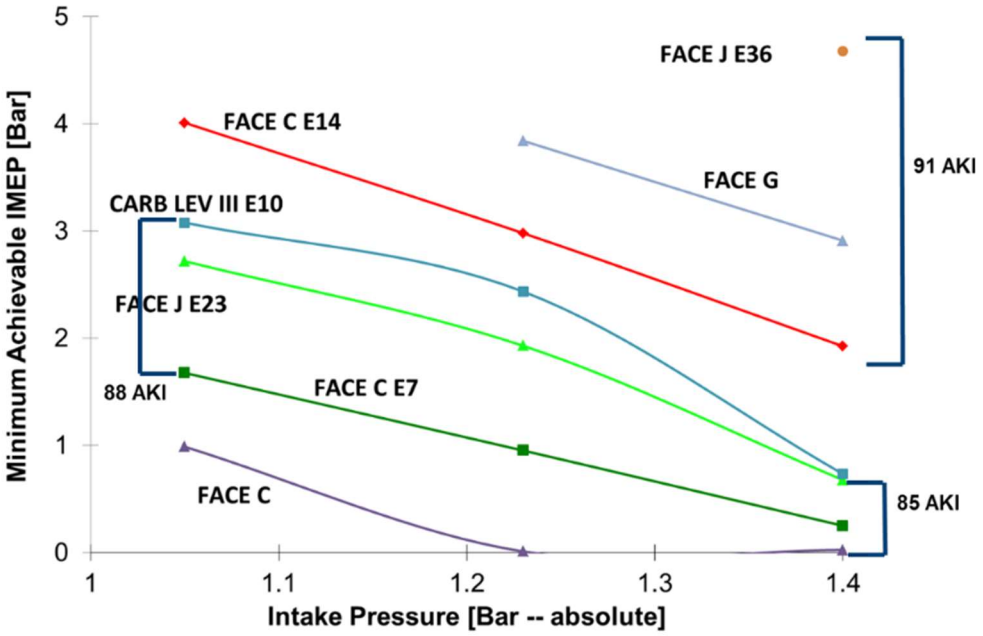

Figure 5.7: Minimum load level achieved for the 7 fuels tested in the GCI engine, at three intake pressure levels. Fuels are labeled individually, while AKI levels of the fuels are indicated by brackets and labels.

As noted above, the overall mixture stoichiometry decreased as intake pressure was increased. However, this is not to say that local equivalence ratio at the point of ignition decreased, as direct-injection timing was not fixed, and was optimized for peak reactivity. Figure 5.8 provides qualitative insight into local equivalence ratio by plotting the optimal injection timing against intake pressure for each tested fuel. From this figure, it can be seen that the optimal SOI timing retards with increased intake pressure, except in the case of FACE G. The optimal SOI timing is a balance between providing the most time for the fuel-air mixture to auto-ignite and maintaining a mixture of sufficient local richness as the mixing process between air and fuel proceeds. It can be seen from Fig. 5.7 that the fuel which achieved the lowest loads, FACE C, also required the most retarded injection timing, while the fuels with higher minimum loads, and consequently a greater mass of fuel injected per cycle, typically required more advanced injection timing. The primary outlier to this trend was FACE J E36, which required significantly delayed injection timing relative to other fuels with similar load, namely FACE G and FACE C E14.

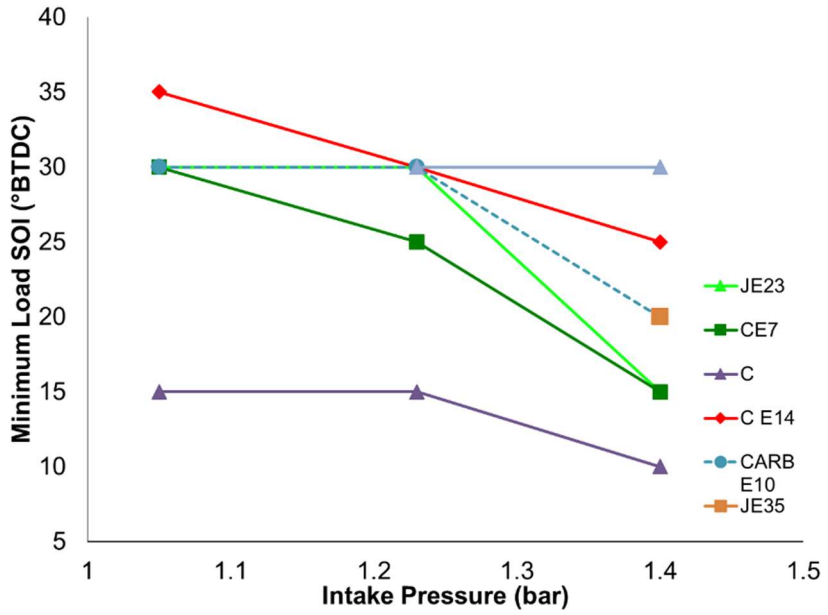

Figure 5.8: Start of Injection timings used to achieve minimum load for the 7 fuels tested in the GCI engine.

b) HCCI Low-Temperature Heat Release

HCCI engine experiments were performed to elucidate the mechanisms behind the GCI experimental results. Each of the seven fuels were tested for their LTHR onset intake pressure at fixed engine speed, combustion phasing, and equivalence ratio, using the procedure described in 3.b and similar to those in [Vuilleumier 2013 Exp., Vuilleumier 2016 Inves.]. The LTHR onset intake pressure, henceforth referred to as critical pressure, is the lowest intake pressure observed to induce LTHR in the tested fuel. LTHR has previously been observed to begin occurring at intake pressures between 1.4 – 1.8 bar for PRF mixtures between 85 – 100 [Vuilleumier 2013 Exp.]. The transition from single stage heat release behavior (no LTHR) to dual-stage heat release behavior (LTHR present) for a gasoline type fuel can be seen in Fig. 5.9. Figure 5.9 plots the rate of heat release profile in the region near TDC, prior to hot ignition, for FACE C E14 at four intake pressure. The transition from single-stage to dual-stage heat release behavior is depicted in the region of -20 CAD aCA50, in which the heat release rate for 1.5 bar intake pressure deviates from the other three traces. This transition from single-stage to dual-stage heat release corresponds well with the change in slope seen in intake temperature – intake pressure relationship of FACE C E14 shown in Fig. 5.10. This figure plots the intake temperature required for constant combustion phasing at each intake pressure tested for each fuel. As the change in slope seen in Fig. 5.10 is related to the onset of LTHR for a given fuel, the critical intake pressure for each fuel may be seen in this figure.

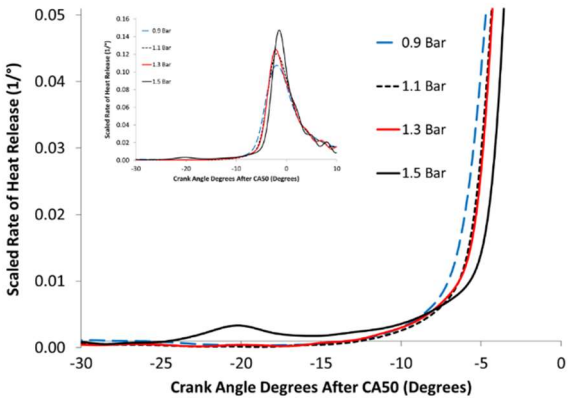

Figure 5.9: Magnified Rate of Heat Release traces for FACE C E14 at four intake pressures.

Figure 5.10 provides an overview of a fuel's auto-ignition behavior in an HCCI engine. It can be seen that at low intake pressures, the fuels generally behave similarly to one another, with differences in required intake temperature of approximately 15 °C. Conversely, at higher intake pressures, once some of the fuels have begun to exhibit LTHR, the difference in required intake temperatures may span over 50 °C. Practically, this limits engine operation with these fuels to lower intake pressures, as cooling of the intake charge to sub-ambient conditions is generally impractical. The difference in behavior among the fuels at high and low intake pressures highlight the extreme pressure sensitivity of gasoline type fuels in the pressure range at which they transition from single to dual-stage heat release behavior.

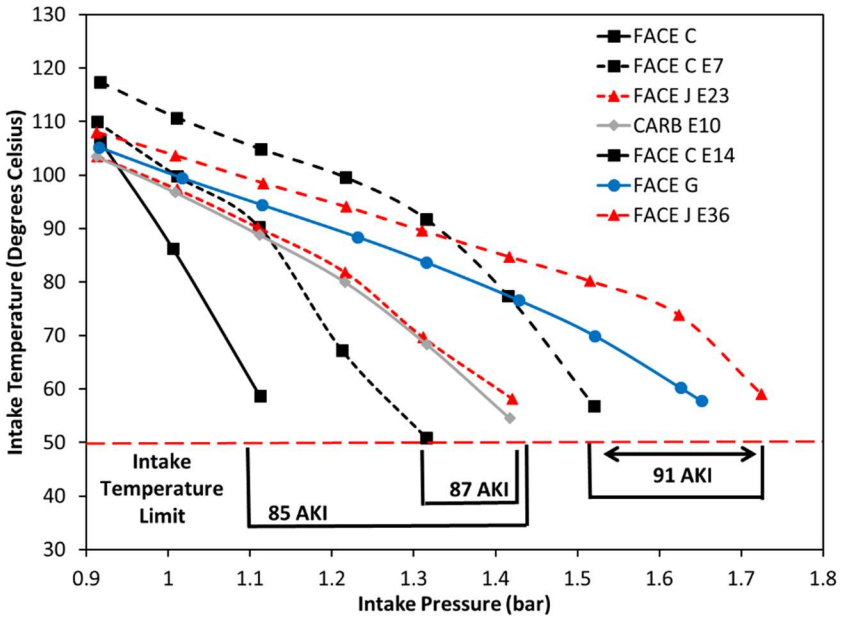

Figure 5.10: Intake temperatures required for constant combustion phasing (6 °aTDC) at constant equivalence ration (ϕ = 0.3).

In addition to observing the transition from single- to dual- stage heat release behavior, it may also be seen from Fig. 5.10 that as in the case of the GCI experiments, in the HCCI experiments AKI does not accurately describe the reactivity of the fuels. This is true both at naturally aspirated conditions, in which the fuels behave relatively similarly to one another, and at boosted conditions, in which the AKI rating does not correspond well to the onset of LTHR and the significant increase in reactivity that accompanies this transition. It can also be seen from Fig. 5.10 that the 85 and 88 AKI fuels exhibit an overlap in reactivity, while the 91 AKI fuels are less reactive. Finally, the higher ethanol content fuels at a given AKI level generally transition to LTHR at a higher intake pressure than fuels with less ethanol, though there is an exception to this in the case of FACE C E14. These trends will be discussed further in Sections III c) and III a) below.

c) RON, MON, AKI, OI and LTHR Dependence

As noted in section III a) and III b), the AKI ratings of the fuels were poor descriptors of each fuel's low-load GCI performance, as well as their HCCI reactivity. To assess which fuel metric provided the best description of low-load GCI performance, the following fuel metrics were assessed: RON [ASTM D2699 2015], MON [ASTM D2700 2015], AKI, Octane Index (OI) [Risberg 2003], and a newly proposed measurement technique, Low-Temperature Heat Release Critical Pressure.

While RON, MON, and AKI are well known, OI is less well known and deserves a brief description. In addition, LTHR has not previously been used as a descriptor of fuel performance, and the method used in this paper to quantify fuels by the LTHR behavior requires explanation. OI is calculated with Eq. (5.1) [Risberg 2003]. The "K" parameter in Eq. (5.1) may either be calculated through Eq. (5.3) [Risberg 2003], or via a regression from experimental data. In this case, a "K" value of -1.13 was calculated from Eq. (5.3), and this was found to be the optimal K value for the GCI operating conditions. The parameter "$T_{COMP\ 15}$" in Eq. (5.3) is the average temperature of the charge at a pressure of 15 bar, while λ refers to the inverse of the equivalence ratio. Discussion on the selection and use of these parameters can be found in [Risberg 2003].

$$OI = RON + K \cdot S \qquad \textbf{Eq. (5.1)}$$

$$S = RON - MON \qquad \textbf{Eq. (5.2)}$$

$$K = 0.00497 \cdot T_{COMP\ 15} - 0.135 \cdot \lambda - 3.67 \qquad \textbf{Eq. (5.3)}$$

LTHR was also used in an attempt to describe the fuels, due to the large effect LTHR has on auto-ignition in an HCCI engine. The method for using LTHR as a fuel descriptor was as follows. Each fuel was run in the HCCI engine from naturally-aspirated conditions through boosted conditions until the minimum achievable intake temperature was reached (limited by the experimental apparatus). The first intake pressure at which LTHR was observed in the ROHR trace (defined as a deviation of the heat release from zero, greater than the assumed margin of error of the calculation, in the LTHR region) was denoted as the critical pressure for LTHR under these test conditions. This critical pressure was then used as a fuel metric in a similar way to RON or MON, in this case by comparing the minimum achievable load with the LTHR critical pressure.

Once fuel metrics were established, the lowest-load GCI data was used to assess the suitability of each fuel metric for quantifying low-load GCI performance. This was done by determining the R^2 value for the best-fit 2nd order polynomial for each fuel metric at each GCI intake pressure. An example of this process is depicted in Fig. 5.11, which plots the measured lowest achievable load in the GCI experiment against the Octane Index values for the seven tested fuels. This figure also depicts the best-fit 2nd order polynomial and the resultant R^2 value for this fuel metric-load combination; R^2 values for all metric-load combinations may be found in Table 5.4.

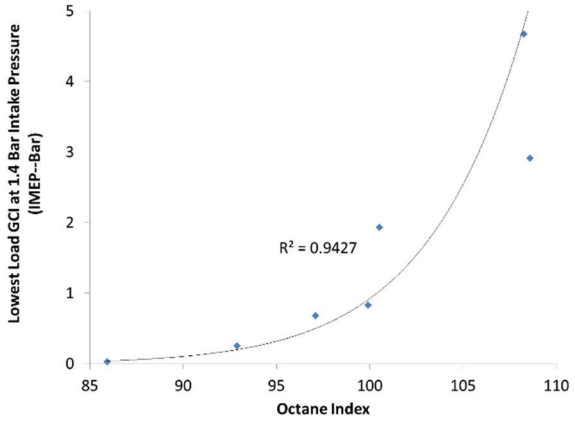

Figure 5.11: Correlation, including best-fit line, between Octane Index and GCI minimum load for each fuel at 1.4 bar intake pressure.

Table 5.4, which characterizes the correlation between a fuel metric and low-load GCI performance, shows that the AKI value of a fuel does not correspond particularly well with its low-load GCI performance, as is indicated by the low R^2 values for the best-fit polynomials between AKI and the three sets of GCI experiments. The reason for the poor performance of AKI is explained by evaluating RON and MON as descriptors of low-load GCI performance. While RON correlates relatively well to low-load performance, it can be seen in Table 5.4 that MON has nearly no correlation with low-load GCI performance. However, this is not to imply that MON does not contain information for assessing fuel performance at these conditions. This can be seen in the OI R^2 values. The OI combines the information from both the RON and the MON test, but not simply by averaging, but rather by assigning an operating-point determined multiplier to the difference between RON and MON. Under the GCI conditions that were tested in this paper, the OI index improves upon the prediction of operating performance offered by the RON test. Finally, the measured LTHR critical pressure was also found to correlate very well with the low-load performance offered by each fuel. Both the LTHR critical pressure method and the OI method of assessing fuels yielded essentially identical performance.

Table 5.4: R^2 values for best-fit lines between various fuel rating metrics and measured minimum load in GCI lowest-load experiments.

	Correlation w/GCI Lowest-Load 1.4 Bar	Correlation w/GCI Lowest-Load 1.23 Bar	Correlation w/GCI Lowest-Load 1.05 Bar
AKI	$R^2 = 0.63$	$R^2 = 0.67$	$R^2 = 0.56$
RON	$R^2 = 0.89$	$R^2 = 0.93$	$R^2 = 0.84$
MON	$R^2 = 0.09$	$R^2 = 0.18$	$R^2 = 0.53$
OI	$R^2 = 0.94$	$R^2 = 0.98$	$R^2 = 0.97$
LTHR	$R^2 = 0.95$	$R^2 = 0.97$	$R^2 = 0.98$

Table 5.5 lists the RON, MON, AKI, and OI values for four common fuel components. Two of the listed components, isooctane and n-heptane, each have, by definition, the same values for RON and MON, which in turn leads to the same values for AKI and OI. The difference between RON and MON, as seen in Eq. 5.2, is named sensitivity (S). The two other molecules listed in Table 5.5 have high sensitivity values (the reasons for this will be discussed in the next section, but are related to the lack of low-temperature branching in these fuels). These high sensitivity values lead to large discrepancies between the four metrics. Thus, when a fuel is comprised of high concentrations of ethanol or toluene, and the operating point of interest results in a negative K value, the OI value will diverge significantly from the AKI value. This has significance for markets in which fuels are sold by AKI, as the results of this paper show that fuels with the same AKI level can have significantly different performance in an advanced combustion engine. However, as the OI has also been shown to be relatively effective in predicting low-load GCI performance, it does allow for limiting cases to be determined from fuel specifications in specific marketplaces.

Table 5.5: Octane rating values for common fuel components. OI is calculated with K = -1.13.

Blending Components	RON	MON	AKI	OI
Ethanol	109	90	99	130
Toluene	121	107	114	137
Iso-Octane	100	100	100	100
N-Heptane	0	0	0	0

a) 0-D Simulated Ignition Delays

Fundamental ignition delay calculations were made in order to better understand the relationships between low-load GCI auto-ignition, HCCI auto-ignition, and the four octane metrics

previously described. Figure 5.12 plots the ignition delays for FACE C, FACE J, and FACE J E36 at 20 bar pressure, an equivalence ratio of unity, and over a range of temperatures that encompass the high-, intermediate-, and low-temperature regimes. FACE C and FACE J both have essentially no sensitivity – this means that they behave similarly to primary reference fuels (PRF's) in terms of knock resistance. While knock resistance is made up of a number of factors, including laminar flame speeds, heat of vaporization, and specific heat ration of a fuel-air stoichiometric mixture, a fuel's auto-ignition behavior is typically the primary factor in knock resistance. Thus, fuels that have a Sensitivity equal to zero will typically display very similar ignition delay behavior to primary reference fuels. PRF's typically exhibit a significant negative temperature coefficient (NTC) region behavior. This NTC behavior can be seen in Fig. 5.12 for FACE J and FACE C. Conversely, FACE J E36 shows minimal NTC behavior, and correspondingly has a relatively high sensitivity. This indicates that FACE J E36 performs dissimilarly to a single PRF across engine operating conditions, and it can be seen from Fig. 5.12 that FACE J E36's ignition delay behavior is most likely the cause, as there is a significant difference between the ignition delay behavior of FACE J E36 and all of the PRF blends.

Figure 5.12 helps explain the links between LTHR, Octane, and kinetics. Figure 5.12 shows the reduction in reactivity in the low-temperature regime that is caused by ethanol blending, even with a relatively reactive fuel such as FACE J. The resulting blend, FACE J E36, exhibits minimal NTC behavior in the intermediate-temperature regime. The NTC behavior displayed by alkanes is representative of the transition from the low-temperature pathway indicated in Fig. 5.2 to the intermediate temperature pathway shown in the same figure. Fuels such as ethanol, toluene, or FACE J E36, which do not display significant NTC behavior, also do not exhibit significant levels of LTHR in an HCCI engine. The minimal NTC behavior of FACE J E36 is due to the lack of low-temperature chain-branching that occurs in the fuel; without significant chain-branching pathways, the formation of stable intermediates does not result in a marked reduction in reactivity.

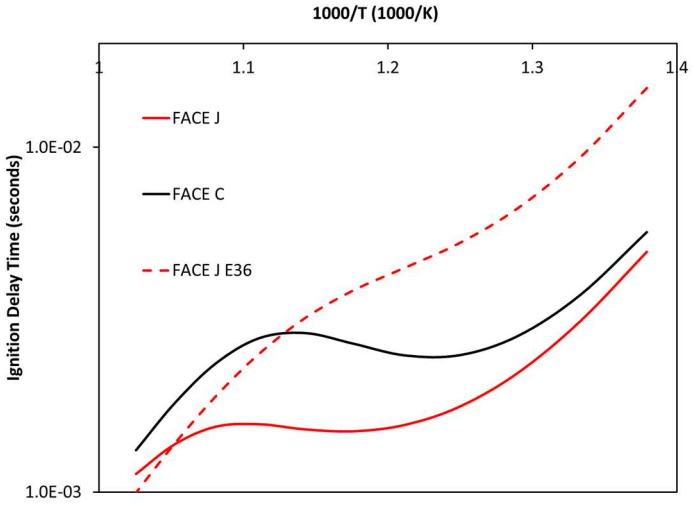

Figure 5.12: Calculated ignition delay times for FACE J, FACE J E36, and FACE C at 40 bar pressure and an equivalence ratio of unity.

Figure 5.12 shows calculated ignition-delay times for three fuels with an AKI rating of approximately 85: PRF 85, FACE C, and FACE J E23. As previously discussed, while FACE C and FACE J E23 have a similar AKI rating, they behave quite differently in both the GCI engine

and the HCCI engine, and have different RON and MON ratings. Figure 5.12 shows the significant similarity in ignition-delay behavior between PRF 85 and FACE C, and this similarity is reflected in their similar AKI, RON, and MON ratings (see Table 5.1 for measured values of FACE C; PRF 85 has RON and MON values of 85 by definition). Conversely, the difference in ignition-delay behavior between FACE C and FACE J E23 is also depicted in Fig. 5.12. This figure shows that FACE J E23 exhibits lower reactivity than FACE C in the low-temperature regime and higher reactivity than FACE C in the high-temperature regime. This ignition-delay behavior is reflected in the RON and MON ratings of FACE J E23, which has a lower MON rating than FACE C, indicating higher reactivity at high-temperature, and a higher RON rating than FACE C, indicating lower reactivity at low-temperature. Therefore, the sensitivity of a fuel, or the difference between RON and MON, may be related to the difference in the strength of the low-temperature oxidation pathway of a given fuel, and consequently the magnitude of NTC behavior of a given fuel, relative to a primary reference fuel. The lack of low-temperature reactivity of highly-sensitive fuels relative to less sensitive fuels may be seen both in Fig. 5.11 and in Fig. 5.12, in which the two most sensitive fuels in these figures, FACE J E36 and FACE J E23, respectively, deviate from the low-temperature auto-ignition behavior of less sensitive fuels.

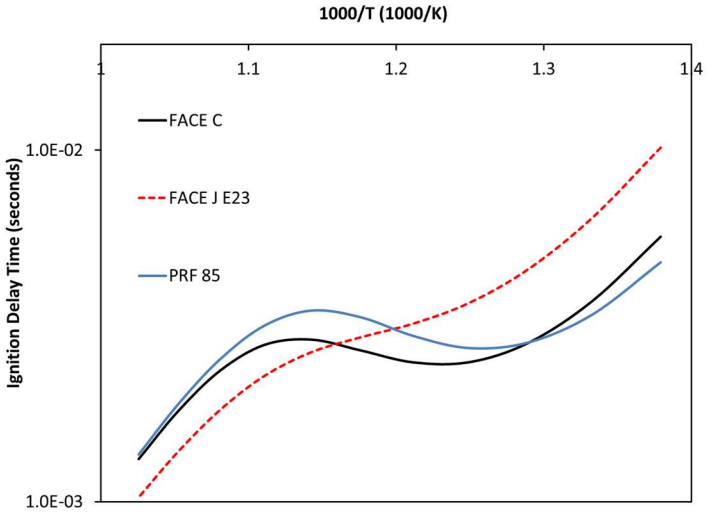

Figure 5.13: Calculated ignition delay times for FACE C, FACE J E23, and PRF 85. All calculations made at 40 bar pressure and an equivalence ratio of unity.

It is well known [Simmie 2003, Battin-Leclerc 2008] that the high-temperature ignition delay properties of hydrocarbon fuels are quite similar, and that large ignition-delay discrepancies among hydrocarbons are mainly found in the low- and intermediate-temperature regimes. This behavior is depicted in Figure 5.14, which plots calculated ignition delays of the seven fuels tested in this study and neat FACE J. Figure 5.14 shows the large discrepancy in ignition delays that is encountered at low-temperature in addition to the intermediate-temperature NTC behavior that leads to near-convergence of ignition-delay behavior at high-temperature.

While many hydrocarbon fuels exhibit similar auto-ignition behavior at high-temperature, this does not necessarily carry over to other classes of fuels. Specifically, ethanol exhibits higher reactivity and shorter ignition delays at high temperatures than many hydrocarbons found in gasoline. This is why ethanol has a comparatively low MON value; the MON test emphasizes

high-temperature auto-ignition resistance [Leppard 1990], and in this region, ethanol has ignition delays similar to (and sometimes shorter than) typical gasoline components, such as isooctane, toluene, or cyclohexane. However, at low temperatures ethanol has much longer ignition delays than typical alkanes, due to its lack of low-temperature oxidation pathways, and this is reflected in its RON rating. This is also reflected in how ethanol combusts in an HCCI engine. Unlike alkanes, ethanol displays no LTHR, even with high intake pressures. This is due to the fundamental lack of low-temperature chain branching pathways [Sarathy 2014]. Ethanol has also been shown [Vuilleumier 2016 Inves.] to scavenge radicals at low temperatures, converting $OH\cdot$ to H_2O and HO_2 to H_2O_2, which impedes the low-temperature chain branching pathway of the alkanes found in gasoline.

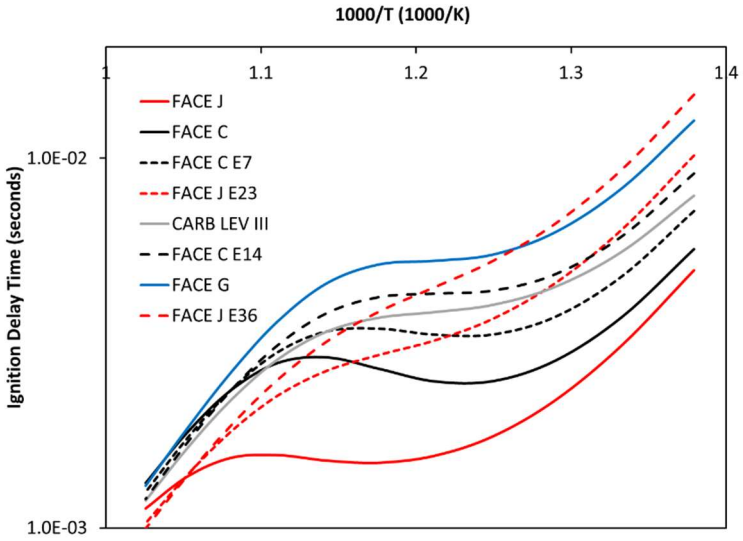

Figure 5.14: Calculated ignition delay times for the seven fuels tested in this study, with the addition of neat FACE J. All calculations made at 40 bar pressure and an equivalence ratio of unity.

Examining the ignition delays shown in Fig. 5.14, it can be seen that the largest discrepancies between fuels tested in this study are the differences in low-temperature reactivity and the temperatures at which NTC behavior begins. This is also the case in the HCCI engine, as the fuels all behave similarly at low pressure and high temperature conditions, but diverge in their performance at the high pressures and lower temperatures at which low-temperature pathways become active for certain fuels. Finally, we can see in Fig. 5.14 that the order of ignition delays at approximately785 K is the same order as the order of lowest achievable loads among the fuels. The ignition delay data, taken together with the HCCI engine data, indicates that the LTHR is likely driving factor between the disparate low-load performance of the 7 tested fuels. Further, as has been discussed, ethanol addition to gasoline suppresses low-temperature reactivity and consequently LTHR. By combining the behavior which has been experimentally observed in the GCI and HCCI engines with the calculated ignition delays of the gasoline fuels, and by combining this information with knowledge of the dominant oxidation pathways for gasoline fuels, the inhibitory chemical effect in the low-temperature regime of ethanol addition to gasoline has been

shown to have a significant influence on the low-load GCI engine performance of gasoline-type fuels.

IV. Conclusions:

In this paper the influences of fuel composition and AKI rating on low-load GCI performance were investigated using 7 gasoline fuels blended with varying levels of ethanol (0-36%), resulting in 3 AKI levels (85, 88, 91). To study this problem, three distinct lines of investigation were carried out. GCI engine experiments were run to empirically understand the problem of GCI auto-ignition at low loads, HCCI engine experiments were used to establish a link to fundamental fuel auto-ignition, and calculated 0-D ignition delays helped link the experimental results to kinetic pathways of fuel oxidation and pyrolysis. Further, the GCI and HCCI experimental results were correlated with the major fuel rating systems, RON, MON, AKI, and OI, in an effort to determine which rating is most suitable for low-load GCI engine operation. The conclusions from these experiments are as follows:

a) GCI Experiments

1. Significant variance was found in the lowest achievable load in a GCI engine for a fixed AKI level.
2. High ethanol content generally, but not always, impedes low-load GCI performance for a given AKI level.
3. AKI does not serve as a sufficient descriptor of low-load GCI performance to be used for this purpose.

b) HCCI Experiments

4. Low Temperature Heat Release significantly changes the intake temperature required to maintain constant combustion phasing.
5. Gasoline mixtures of the same AKI value display significant differences in LTHR onset behavior.
6. All fuels tested behave relatively similarly at low pressures and high temperatures, i.e. naturally aspirated conditions.

c) RON, MON, AKI, OI, and LTHR

7. MON had essentially no correlation with low-load GCI performance; this led to AKI having a poor correlation with said performance.
8. RON had a reasonable correlation with low-load GCI performance, forming the basis for OI, which exhibited the best correlation with low-load GCI performance of the 4 octane ratings.
9. A fuel's LTHR tendency, as described by its critical pressure in an HCCI engine, correlated as well as OI with low-load GCI performance.

d) Fundamental Ignition Delays

10. The primary difference observed between the 7 tested fuels was their reactivity at low and intermediate temperatures.

11. LTHR was found to be the driving factor between the disparate performance of similar gasoline type fuels operated under low-load GCI conditions.
12. Ethanol actively suppresses low-temperature chain-branching pathways, leading to reduced LTHR and longer ignition delays at low temperatures.

Chapter 6:
Multi-Level Computational Exploration of Advanced Combustion Engine Operating Strategies

This article was presented at the 10th Conference on Sustainable Development of Energy, Water and Environment Systems in 2015. It is currently under review for publication in Applied Energy.

David Vuilleumier, Ivan Taritas, Benjamin Wolk, Darko Kozarac, Samveg Saxena, Robert W. Dibble

I. Abstract

Advanced combustion engine (ACE) research is typically carried out on single-cylinder research engines. These engines are designed to tightly control fueling and conditions at intake valve closure (IVC) and to precisely measure in-cylinder conditions and emissions. However, to be able to measure and control engine operation so precisely, these research engines typically do not feature intake and exhaust tracts that resemble those in production engines, specifically in regards to turbomachinery, heat exchangers, and exhaust gas recirculation (EGR) systems. For this reason, these research engines are effective for understanding in-cylinder combustion parameters such as heat release rate, burn duration, combustion efficiency, pollutant formation, and exhaust valve opening (EVO) conditions.

This paper applies high fidelity simulations to determine the feasibility of achieving a chosen single cylinder engine operating point on a production type homogeneous charge compression ignition (HCCI) engine, using a partial fuel stratification (PFS) strategy. To accomplish this, a Converge 3 dimensional (3D) – computational fluid dynamics (CFD) model of the experimental combustion chamber and intake and exhaust runners was created to simulate the experimental engine. This model was used to simulate an operating point achieved experimentally, as well as to determine the sensitivity of the operating point to variations in intake pressure, intake temperature, injection timing, injected mass, and EGR fraction. The results from these simulations were fed into a 1-dimensional engine simulation created in AVL Boost, featuring production-type intake and exhaust systems, including turbomachinery and heat exchanges necessary to create the required IVC conditions. This full engine simulation was used to assess the cycle efficiency of the engine at the experimental operating condition, and to assess whether changes to this operating point in intake temperature, intake pressure, direct injection timing, or fueling are beneficial to the cycle efficiency and engine-out emissions. In addition, the sensitivity of promising engine operating points to injection timing and injection mass are determined to evaluate the potential stability of these operating points.

II. Introduction

The development of an engine operating strategy requires careful balancing of many simultaneously interacting in-cylinder fundamental phenomena that determine overall efficiency, emissions, stability, and noise-vibration-harshness characteristics. In the case of low temperature combustion (LTC) engines, the focus of the present study, important in-cylinder phenomena

include chemical kinetics that determine heat release rates, spatially- and temporally-varying in-cylinder charge conditions, heat transfer, fuel vaporization, and emissions formation [Saxena 2013]. These fundamental phenomena can be affected by several controllable parameters, including fuel type, port and direct injection strategy (including port fuel injection - PFI/direct injection - DI - injection fractions, DI timing, DI duration), intake temperature and pressure, equivalence ratio, EGR dilution, and engine speed. This large number of controllable parameters makes it difficult to identify optimal engine operating conditions across the entire load-speed operating range. Furthermore, in-cylinder operation must be managed to ensure that critical limits are not exceeded, including ringing limits, misfire limits, and stability and cyclic variability limits, while maintaining acceptable overall engine operating efficiency and emissions characteristics [Saxena 2013]. The parameter space of operating variables and interacting fundamental phenomena grows even larger when considering the entire engine system, which includes the aforementioned in-cylinder phenomena, but also the intake and exhaust manifolds, turbocharger, intercooler, and EGR system.

This study aims to predict performance of a gasoline fuelled homogeneous charge compression ignition (HCCI) engine which employs a partial fuel stratification (PFS) operating strategy. Recent studies [Dec 2015, Sjöberg 2006, Dec 2011 Cont., Yang 2011 Proc., Yang 2011 Part., Yang 2011 Exp., Wolk 2014, Wolk 2015] have demonstrated PFS as a promising operating strategy that can extend the operating regime of HCCI engines without exceeding the aforementioned operating limits. Dec et al. [Dec 2015] found that at boosted conditions, PFS operating strategy is effective in increasing thermal efficiency; they increased peak thermal efficiency from 47.8% for premixed fueling to 48.4% with PFS strategy. In [Sjöberg 2006] the authors found that PFS enables staged combustion with reduced pressure rise rate, and therefore offers a potential to increase the high load range of HCCI engine operation. IMEPg increased from 537 to 597 kPa, with NOX emissions under US 2010 standards. In [Dec 2011], Dec et al. found PFS strategy to shift ringing/stability limits and thus allows the maximum IMEPg increase from 11.7 to 13 bar. Yang et al. [Yang 2011 Exp.] found that high load extension in a gasoline HCCI engine that uses PFS strategy is limited by the trade-off between CO (retarded operation) and NOX (advanced operation) emissions. In [Wolk 2014, Wolk 2015 Proc.] the authors used detailed 3-D CFD analysis to study and better explain the in-cylinder phenomena that occurs in HCCI engine that uses a PFS strategy. They found in [Wolk 2014] that occurrence of single- or multi-stage combustion depends on the temperature distribution which is influenced by low temperature heat release (LTHR) and evaporative cooling from the liquid fuel spray. In [Wolk 2015 Proc.] it was found that at 1 bar intake pressure since the premixed portion of the charge ignites before rich regions, the sequential autoignition occurs too fast and there is no reduction in the maximum pressure rise rate compared to HCCI operation. On the other hand, at 2 bar intake pressure the sequential autoignition occurs over a longer period as the premixed portion auto-ignites last, which reduces maximum pressure rise rate compared to HCCI operation.

Given the range of engine operating variables that affect PFS performance, prior studies have focused on in-cylinder operating variables without giving adequate consideration to the engine system. Moreover, the majority of the experimental studies focused solely on extending the high load operation limit, while the numerical ones focused on understanding the fundamental aspect and impact of a PFS strategy on HCCI combustion process. This paper presents a numerical study that focuses on mid-load engine operation, ~10.5 bar indicated mean effective pressure (IMEP), at 1200 RPM. The present study bridges the gap between previous experimental and

numerical studies by investigating an HCCI engine that employs a PFS strategy using a coupling of a detailed 3D-CFD and chemical kinetic combustion chamber model [Babajimopoulos 2005, Embouazza 2002, Wang 2004, Kong 2002] with a 1D multi-cylinder engine system model [Ogink 2001, AVL 2013].

3D-CFD simulations incorporating chemical kinetic combustion models are an established way to study kinetically controlled combustion engines [Zhou 2015, Li 2015]. In the first part of the study, a detailed 3D-CFD simulation was used in performing a detailed parameter sweep to identify the PFS operating parameters leading to optimal engine performance. Operating parameters varied in this numerical study are intake pressure and temperature, DI timing, DI mass fraction, equivalence ratio and EGR fraction. By sweeping through a narrow range of controllable parameters, the sensitivity of engine performance (including efficiency, emissions, ringing intensity (RI), etc.) to many of the operating variables is quantified. After identifying feasible operating points, which resulted in high indicated efficiency and low exhaust gas emissions, a full model cycle-simulation, featuring a detail description of a multi-cylinder engine charging and cooling elements, and entire intake and exhaust flow path, was run in order to assess the overall system efficiency and operating range in terms of intake temperature and engine speed.

III. Methods

a) Combustion Model

3D-CFD simulations in this work were performed using CONVERGE [Richards 2013], a commercially available CFD code. The grid used for all CFD simulations is representative of the Sandia HCCI engine [Dec 2011], as shown in Fig. 6.1. CONVERGE employs a cut-cell Cartesian method for grid generation and generates a grid at each time step given the position of the boundary surfaces. The previous time step solution is mapped onto the new grid before solving for the next time step. This procedure naturally permits the use of moving surfaces, such as the piston and intake/exhaust valves. A uniform grid spacing of 2 mm was used, as this was the finest grid resolution that could be computationally afforded. This resulted in 140,881 in-cylinder cells at bottom dead center (BDC) and 13,859 in-cylinder cells at top dead center (TDC). A non-uniform, adaptive grid may be required to resolve a flame surface. However, a non-uniform grid is not required in this work as there is only sequential auto-ignition without flame propagation.

A schematic of the computational grid is shown in Fig. 6.1 and engine specifications are listed in Table 6.1 (values in parentheses indicate experimental values that differ from the associated values used in the simulations). The geometric compression ratio (CR) of the computational mesh is 13.65:1, which is slightly lower than the 14:1 used in the experiment, in order to match the motored pressure trace as crevices and blow down are not meshed directly.

The engine has two intake ports, one port with a helical geometry and one port with a tangential geometry. The valve lift profiles are set using experimentally measured valve lift values. The piston has a deep central bowl to prevent piston wetting at late direct-injection timings. The head gasket crevice is included in the computational mesh and a piston ring crevice model is used rather than direct meshing of the piston ring crevices. Dimensional information about the piston rings and piston ring cutouts is used as input to the piston ring crevice model.

Simulations are run from 360 ° bTDC to 122 ° aTDC. This encompasses the full intake stroke to part way through the expansion, after combustion has completed and to the point at which the exhaust valve opens. The intake stroke is computed to create realistic thermal stratification and in-cylinder velocity profiles in the premixed intake gas. Chemistry is computed only for cells with temperatures in excess of 600 K and is not computed in the intake or exhaust ports while the respective valves are closed. This helps to reduce the computational cost of the simulations, as the time for computing chemistry accounts for a large fraction of the total computational effort.

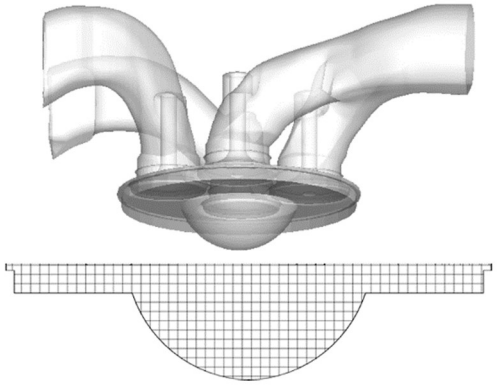

Figure 6.1: Computational surface of Sandia HCCI engine at top dead center. The in-cylinder grid is shown with a grid spacing of 2 mm (the full grid includes the intake and exhaust ports).

Table 6.1. Sandia HCCI engine specifications

Displacement	0.981 L
Bore	102 mm
Stroke	120 mm
Connecting rod	192 mm
Geometric CR	13.65:1 (14:1)
Number of valves	4
IVO	360 °BTDC
IVC	158 °BTDC
EVO	122 °ATDC
EVC	368 °ATDC
Engine speed	1200 rpm
Intake pressure	1.9 – 2.1 bar
Coolant temperature	100 °C

The gasoline used in the experiments by Dec et al. [Dec 2011] and considered in this work is RD387 research grade gasoline, which contains a wide range of molecular components. Although the broad molecular composition has been quantified (i.e. amount of alkanes, aromatics, and olefins), specifying the exact amount of each molecule in RD387 is not feasible. As a result, a surrogate containing a small number of pure components has been formulated by Mehl et al. [Mehl 2011 App.] to mimic major properties of RD387. The targeted properties are the broad molecular composition, the H/C ratio, stoichiometric air-fuel ratio, and anti-knock index (AKI).

In this study, gasoline is modeled by the 4-component surrogate identified by Mehl et al. [Mehl 2011 App.] comprised of 57% isooctane (iC_8H_{18}), 16% n-heptane (nC_7H_{16}), 23% toluene ($C_6H_5CH_3$), and 4% 2-pentene (C_5H_{10}-2) by liquid volume. The chemistry is modeled using a 98-species reduced mechanism for the 4-component gasoline surrogate [Wolk 2015 Thesis] including NO_x formation reactions and a well-mixed sub-grid chemistry model. A well-mixed sub-grid chemistry model indicates that the reaction rates are evaluated at the mean cell temperature (sub-grid temperature fluctuations are ignored). Despite this shortcoming, well-mixed sub-grid chemistry is common among RANS engine codes. Turbulence is modeled using the RNG k-epsilon turbulence model [Orszag 1993].

The fuel injector used in the experiment is an 8-hole gasoline direct injection (GDI) injector that has a hole diameter of 125 μm, included angle of 70°, and injection pressure of 120 bar. The injector is centrally mounted in the combustion chamber and oriented vertically downward. The simulated injection uses a Lagrangian spray model and a stochastic collision model (O'Rourke) with injected droplets following a Rosin-Rammler distribution [Rosin 1993] with a Sauter mean diameter (SMD) of 125 μm, 180 m/s injection velocity, and initial droplet temperature of 300 K. The liquid fuel droplet breakup is modeled using the Kelvin-Helmholtz Rayleigh-Taylor (KHRT) droplet breakup model [Patterson 1998]. The KHRT breakup model evaluates the growth rates of the KH and RT instabilities to determine if a droplet breaks up due to one of these mechanisms during a computational time step.

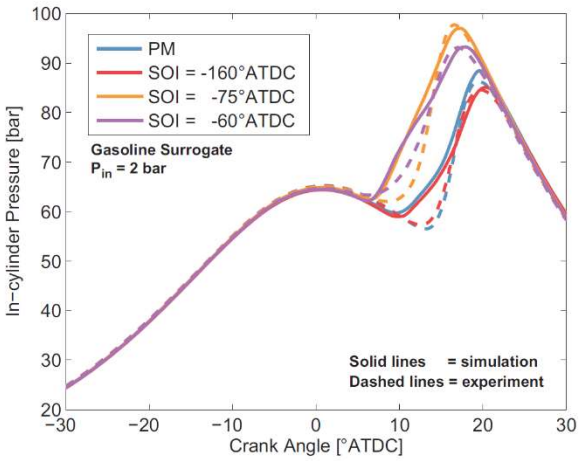

Figure 6.2: Comparison of four experimental and simulated pressure traces at 2 bar intake pressure, for fully premixed (PM) and partially stratified (13% DI) cases at two different combustion phasings [Wolk 2015 Proc.].

The boundary conditions used for solid surfaces are constant temperature. Surface temperatures are set to the coolant temperature, except for the piston and head, which are set to the experimentally measured head temperature. For the intake ports, the initial conditions and the intake inflow compositions are set to the composition of the premixed charge. For the in-cylinder region and exhaust ports, the initial composition is the complete combustion products (CO_2, H_2O, O_2, N_2) of the premixed gas (not including additional DI fuel). The initial temperature of the intake region is the intake temperature, and the initial in-cylinder and exhaust temperatures are the experimental exhaust temperatures. The model used in this paper was previously validated and published in [Wolk 2015 Proc.]. The agreement between experimental and simulated conditions can be seen in Fig. 6.2, Fig. 6.3, and Fig. 6.4. Figure 6.2 shows the agreement of in-cylinder

pressure between the simulation and the experiment for four different injection strategies at 2 bar intake pressure. Figure 6.3 and Fig. 6.4 show the simulated and experimental rates of heat release for the same four operating points. It can be seen from the three figures that generally good agreement exists between the model and the experiment. A more detailed discussion of the operating points and their specific agreements with experiments can be found in [Wolk 2015 Proc.]. For this paper, the model was used nearly unaltered from that presented in [Wolk 2015 Proc.], except for the use of the 98 species kinetic mechanism rather than the 96 species mechanism used in [Wolk 2015 Proc.]. These mechanisms were both reduced from the same detailed mechanism, and have nearly identical behavior, with the primary difference between them being the addition of the species NO and NO_2 to the 98 species mechanism, for the calculation of the concentrations of these pollutants.

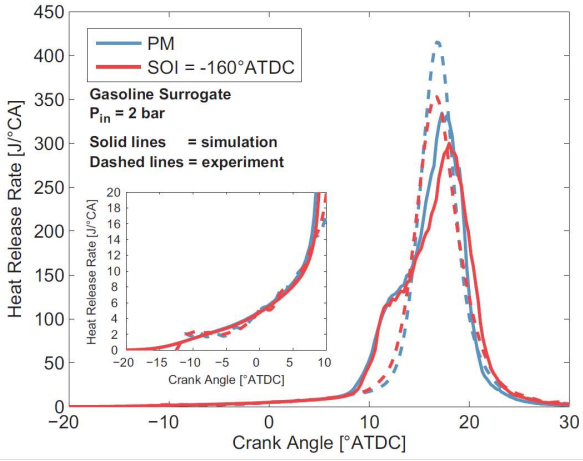

Figure 6.3: Comparison of experimental and simulated rates of heat release at 2 bar intake pressure, for fully premixed (PM) and partially stratified (13% DI) cases [Wolk 2015 Proc.].

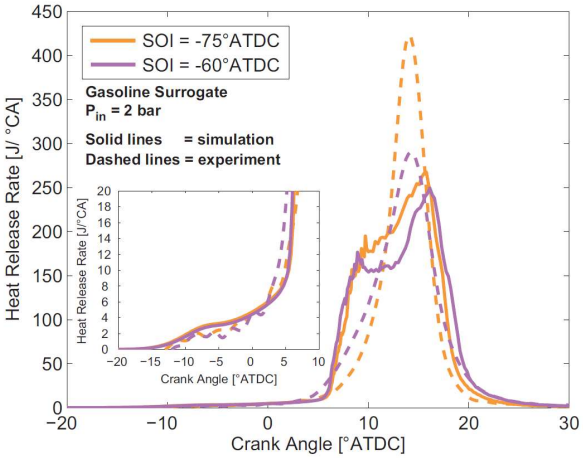

Figure 6.4: Comparisons between experimental and simulated rates of heat release at 2 bar intake pressure for two different injection timings for partially stratified (13% DI) cases [Wolk 2015 Proc.].

a) Cycle-simulation

The simulation of the full engine performance was performed by a cycle–simulation model made in the AVL Boost. In order to obtain simulation results which accurately reflect the operation of the engine, the entire engine layout featuring four cylinders and a detail description of the entire engine flow path was made, as seen in Fig. 6.5. More detailed information on this model can be found in [Taritas 2014].

In the full engine model, combustion was calculated with a table heat release model which enables the calculation of many engine cycles in a reasonable time. These tables were created according to the rate of heat release profiles, obtained from the detailed 3D-CFD simulation. The cylinder was modeled according to the cylinder geometry data, which is given in Table 6.. In the AVL Boost, the effect of two intake and two exhaust valves is taken into account by setting the appropriate value for the scaling factor for the effective intake & exhaust flow area [AVL 2013]. Heat transfer in the combustion chamber was calculated with Woschni's model. More on the heat transfer calculation in the combustion chamber, as well as on the heat transfer and friction calculation in the pipe elements can be found in [AVL 2013].

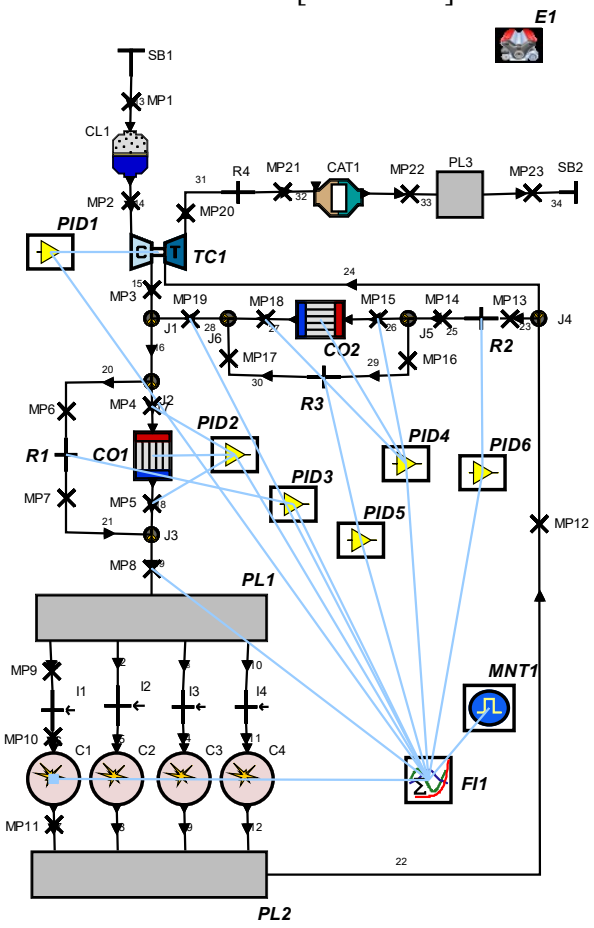

Figure 6.5: Full engine simulation model.

Variable geometry turbocharger (shown in Fig. 6.5 as TC1) performance was calculated with the full model charger calculation, which uses the turbine and compressor static performance maps that were obtained from the manufacturer. As these maps present just a narrow operating range of the charging device, extrapolation of the maps was performed by a BOOST Turbocharger

Tool [AVL 2013]. Vane position was set so that the appropriate pressure at the IVC is obtained. This was controlled automatically by a PID controller (shown in Fig. 6.5 as PID 1*)*.

Besides the charging element, the full engine model features an intake air cooler (shown in Fig. 6.5 as CO1) and a system to bypass it. It also features a high pressure EGR loop with an EGR cooler (shown in Fig. 6.5 as CO2) and a system to bypass it. The intake air cooler is an air to air cooler, while the EGR cooler is an air to water cooler. Cooling performance was calculated with the target efficiency model, which requires the input of the cooler efficiency and the coolant temperature [AVL 2013]. For the air to air cooler, the cooling efficiency was set to 65% [Garrett 2015], and the coolant temperature was set to 25°C, which corresponds to the temperature of the outside air. The air to water cooler efficiency was set to 90% [Garrett 2015], while its coolant temperature was set to 50°C. The cooler outlet temperature was controlled by the PID regulators (shown in Fig. 6.5 as PID 2 and PID 4*,* respectively), which control the flow through the cooler bypass, thus regulating the cooler outlet temperature. Cooler outlet temperature was set so that temperature at IVC matches the one obtained with the detailed 3D-CFD simulation. If no cooling is needed, cooler flow coefficients are set to zero, while the bypass restrictors are kept fully open, which means that the entire charge flows through the bypass. The external EGR loop is also equipped with a controllable valve (shown in Fig. 6.5 as R1) that enables the control of the amount of combustion products that are recirculated back to the intake manifold. The amount of EGR in the intake is controlled by a PID controller (shown in Fig. 6.5 as PID 6), and was set so that it matches the amount that was simulated with a detailed 3D-CFD model.

As classical species transport was used, a 4-component surrogate fuel (details can be found in the previous section) was created with a BOOST Gas Properties Tool [AVL 2013]. The same injection strategy as in the 3D-CFD model was used, where a part of the fuel was injected into the intake port, while the other part was injected into the cylinder during the compression stroke. Fuel evaporation was modeled with a standard evaporation model available in AVL Boost [AVL 2013].

The first set of the full engine simulations was performed to analyze the entire engine performance for the three most interesting points obtained with the 3D-CFD simulation. Operating parameters of these points are given in the next section.

The second set of the full engine simulations was performed to analyze the operability limit in terms of the simulation-boundary intake temperature (SB1 in Fig. 6.5), for the most interesting points simulated with a detailed 3D-CFD model. These simulations were performed in order to determine the lowest and the highest intake temperature that would still be able to achieve the desired intake valve closure (IVC) temperature. The lowest intake temperature case presumes operation with uncooled EGR and intake air charge, while the highest intake temperature presumes the operation with the maximum cooling capacity. Hence, six simulations were run in this set, and the details regarding the operating parameters of these points are given in the next section.

Finally, the third set of the full-engine simulations was performed to analyze the engine's operability range in terms of engine speed (turbocharger matching). Eight simulations were run in this set, and details regarding the operating parameters of these points are given in the next section. Since these operation points were not simulated with a 3D-CFD model, due to lack of validation data, reference rates of heat release were not available. Hence, the combustion was calculated with a Vibe model, whose parameters were tuned so that the ROHR profile has a bell like shape; start of combustion was set to 4.9 degCA ATDC and combustion duration was set to 6.3 degCA. These

values were chosen according to the values obtained in the base operating point at 1200 rpm. Moreover, as there is no data on the fuel mass for these operating points, fueling was set so that the overall charge to fuel ratio (C/F ratio) was approximately 34.5. This C/F ratio was chosen so that it equals the one that was simulated in the base operating point at the engine speed of 1200 rpm. Since there is no data on the EGR fractions for these operating points, simulated EGR fractions were set to 28.57% for the first sweep, and 20% for the second sweep. Also, as there was no data on the IVC pressure and temperature for these operating points, the desired values were set according to the base operating point at 1200 rpm (2.014 bar and 383.95 K).

IV. Results and Discussion

a) Combustion Model Results

Table 6.2. Key engine operation variables.

Variable	Unit	Range
Intake Pressure	Bar	1.9 - 2.1
Intake Temperature	Kelvin	336 - 377
Direct Injection Timing	CAD bTDC	25 - 130
Direct Injection Fraction	-	0.08 - 0.19
Charge-Mass Equivalence Ratio	-	0.4 - 0.45
Exhaust Gas Recirculation Fraction	-	0.2 - 0.4

Table 6.3. Detailed intake parameters and results for five engine operating conditions. Note that points 3 and 4 are only used for Ringing Analysis.

Variable	Unit	Base Case	P1	P2	P3	P4
Intake Temperature	K	359	349	362	372	367
Intake Pressure	Bar	2.00	1.98	1.90	2.10	1.90
Injection Timing	dADTC	-75	-100	-100	-100	-75
EGR	%	29	14	22	29	22
Engine Speed	RPM	1200	1200	1200	1200	1200
IMEP	bar	10.60	10.63	10.60	10.44	9.87
Direct Injected Fraction	-	0.13	0.08	0.20	0.08	0.14
Equivalence Ratio	-	0.43	0.41	0.44	0.40	0.41
UHC	g/kW-hr	0.30	0.27	0.31	0.33	0.34
O2	g/kW-hr	456	730	510	518	586
CO	g/kW-hr	1.68	1.65	1.67	1.82	1.80
CO2	g/kW-hr	968	760	860	982	874
NOx	g/kW-hr	0.98	0.14	2.72	0.14	1.82

Efficiency	-	43.0	43.4	43.2	43.3	43.5
CA10	Degrees	6.8	9.0	7.2	6.8	5.8
CA50	Degrees	11.1	12.7	10.2	9.6	9.5
CA90	Degrees	13.6	15.0	12.8	11.3	11.6
Combustion Duration	Degrees	8.3	9.2	6.9	6.3	7.2
Ringing Intensity	MW/m^2	3.9	4.6	3.7	11.6	6.3
Maximum Cylinder Pressure	Bar	112	109	113	123	112
Maximum Cylinder Temperature	K	2538	2190	2572	2230	2583
Maximum Average Cylinder Temperature	K	1928	1901	1983	1921	1943

The combustion modeling portion of this study focused on conducting a parametric variable sweep around an experimentally-validated simulated engine operating point. Important engine operating parameters, listed in Table 6., were varied in an effort to assess the performance of the original operating point against similar operating points that would provide similar load levels. These operating points characterize mid-load operation (IMEP of approximately 10.5 bar) at low engine speed (1200 RPM). In total, 212 simulations were run, using approximately 150,000 CPU hours.

A primary focus of this study is the closed-cycle efficiency, as this will have a significant influence on efficiency and exhaust gas emissions. In Fig. 6.6 and Fig. 6.7, cycle efficiency is plotted against combustion phasing and combustion duration, respectively. In these figures, three possible operating points are indicated by special markers, while all other operating points are indicated by round black markers. The specific conditions relating to these three operating points, as well as two others that will be discussed later, can be found in Table 6.3. It can be seen from Fig. 6.6 and Fig. 6.7 that the peak efficiencies indicated by the simulations range between 43 – 44%. Also, it can be seen in Fig. 6.6 that a relatively wide range of combustion phasings yield high indicated efficiencies, with phasings ranging from the earliest tested (4 CAD aTDC) to approximately 14 CAD aTDC yielding efficiencies above 42%. This trend of efficiencies is driven by the effects of heat transfer, thermodynamics, and combustion efficiency. In this case, early combustion phasings yielded high combustion efficiency and high thermodynamic efficiency, while not incurring enough of a heat transfer penalty to reduce efficiency. As will be discussed later, earlier combustion phasing was not tested due to ringing limits. At later combustion phasings, there is a thermodynamic penalty on efficiency, as a portion of the expansion stroke is left effectively unused, and this accounts for the majority of the drop in overall efficiency at later combustion phasings. At extremely late combustion phasings, a combustion efficiency penalty may occur as well, though as can be seen in Fig. 6.8 and Fig. 6.9, unburned hydrocarbon (UHC) and carbon monoxide (CO) emissions are similar under most conditions, as cases with partial or full misfires have been omitted from these results as they are unfeasible for engine operation. In the PFS combustion system, and at the mid-load conditions that are studied here, the UHC and CO emissions are primarily from charge that is present in the crevice and near-wall regions during combustion. This can be seen most clearly in Fig. 6.8; as combustion phasing is delayed, a lower

fraction of the charge is present in the crevice and near-wall regions (due to combustion occurring later in the expansion stroke, resulting in a higher combustion chamber volume), resulting in slightly decreased carbon monoxide emissions.

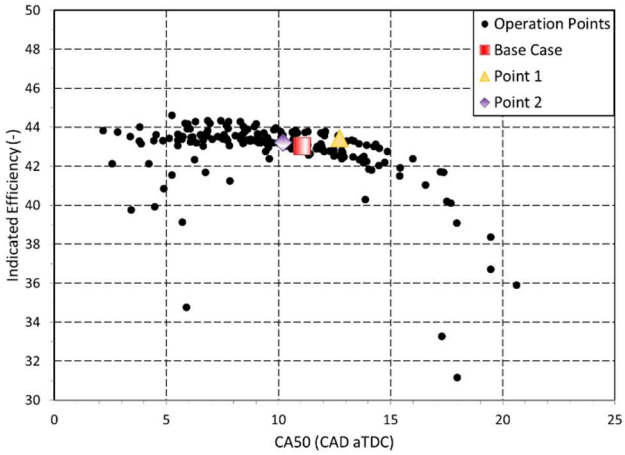

Figure 6.6: Indicated efficiency plotted against combustion phasing for all operating conditions evaluated using the combustion model.

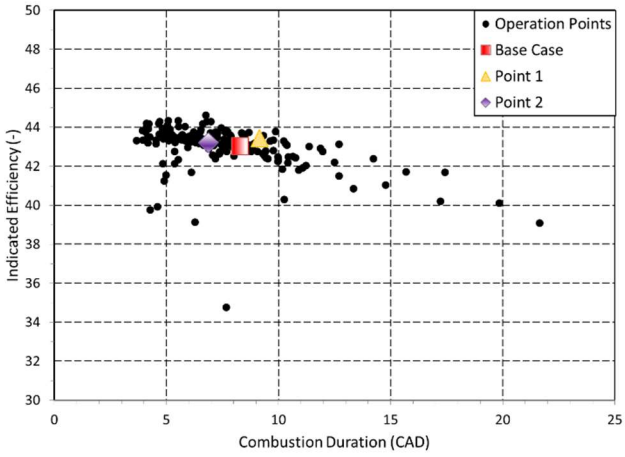

Figure 6.7: Indicated efficiency plotted against combustion duration for all tested operating conditions.

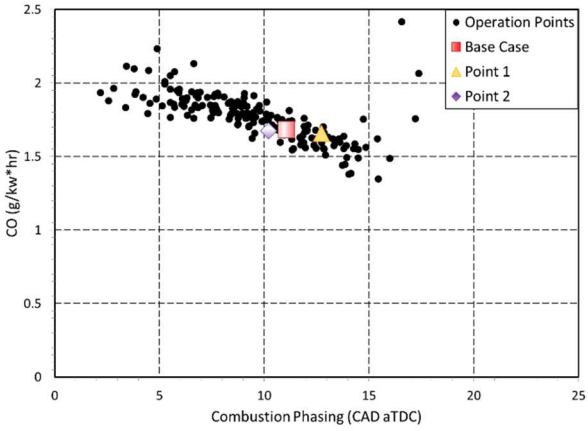

Figure 6.8: Carbon Monoxide (CO) emissions as a function of combustion phasing.

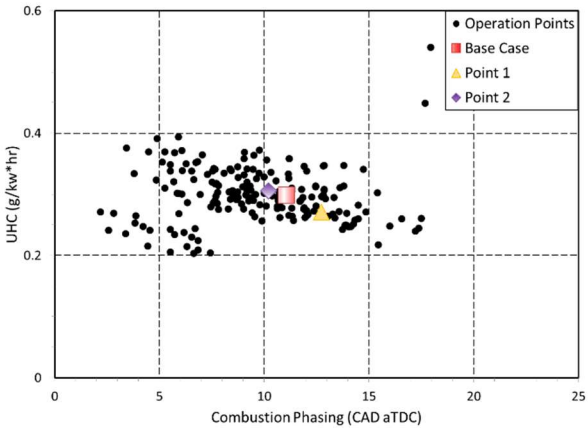

Figure 6.9: Unburned Hydrocarbons (UHC) emissions as a function of combustion phasing.

The sweep of engine operating conditions identified two potential engine operating points in addition to the base case from which the permutations were based on. Point 1 improves upon the base case in the main metrics used for this study: indicated efficiency and NO_x emissions, while maintaining acceptable RI. Thus, Point 1 would be a preferred operating point to the Base Case under most circumstances. Point 2, on the other hand, reduced RI and increased control over combustion phasing at the expense of NO_x production and indicated efficiency. Therefore, this operation point may be favored in an environment in which Point 1 cannot be achieved due to the lower required intake temperature or in which RI must be reduced. From Fig. 6.6 and Fig. 6.7 it can be seen that points exist with greater efficiencies than the three points that were chosen. However, it will be seen in figures presented later in this paper that these points were unsuitable either from a standpoint of RI, or NO_x emissions, or both.

NO_x emissions are a particular problem for lean burn engines that cannot make use of a 3-way catalyst. As seen in Fig. 6.10, NO_x emissions were highly dependent on combustion phasing, and fuel inhomogeneity (in this case a function of DI fractions and injection timings). This trend is easily explained by the thermal dependence of NO_x via the Zeldovich mechanism [Zeldovich 1946]. As seen in Fig. 6.11, the NO_x emissions correspond closely with the peak cell temperature encountered by each operating condition. The peak temperature, in turn, was influenced by both the mixture preparation and the combustion phasing. In general, the higher DI fractions had significantly higher NO_x than the lower DI fractions for a given combustion phasing. This is caused by a larger amount of fuel mass close to stoichiometric conditions at the point of auto-ignition, which results in higher localized post-combustion temperatures. Therefore, to keep NO_x low while using a more aggressive DI strategy (possibly as a control strategy), a later combustion phasing is required. However, combustion phasings late enough to ensure low NO_x also begin to reduce the indicated efficiency of the high pressure cycle, and push the operating point closer to the misfire limit. Therefore, reducing the DI fraction seems more favorable for this mid-load condition.

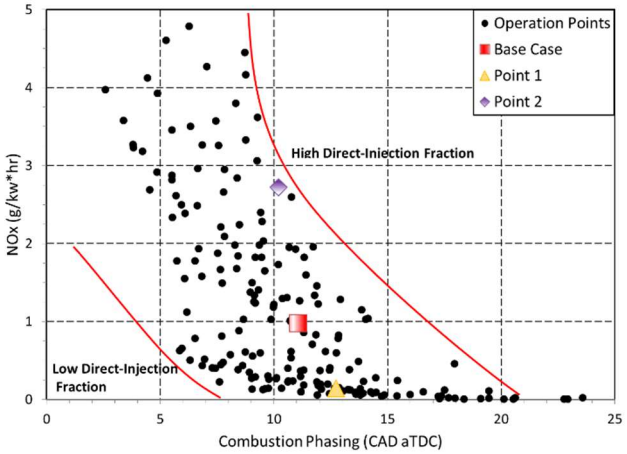

Figure 6.10: Plot of NOx emissions against combustion phasing for all operating points.

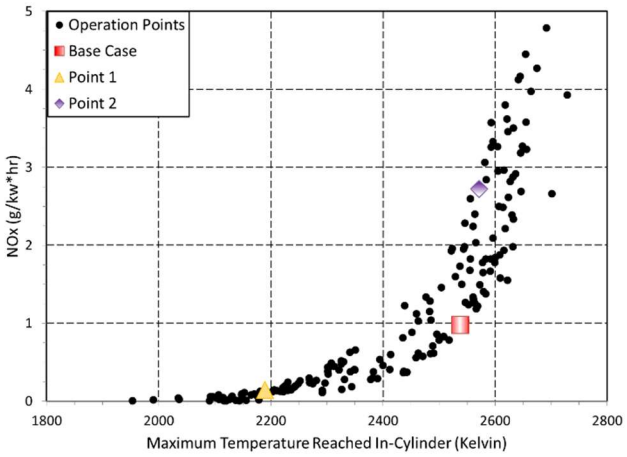

Figure 6.11: Plot of NOx emissions against the maximum temperature reached in the cylinder during the complete engine cycle.

A critical index for safe engine operation of advanced combustion engines (ACE's) is the RI. This parameter quantifies the degree of engine-damaging pressure oscillations that are occurring in the cylinder due to combustion. Figure 6.12 shows the level of ringing that occurs in the simulated engine operating points. In this figure a threshold is marked at 5 MW/m^2, which has become the accepted maximum level of RI for production engines [Dernotte 2014]. From Fig. 6.12 it can be seen that RI is closely related to combustion phasing, with later combustion phasings reducing the RI. Late combustion phasing helps reduce ringing because as phasing is delayed, the piston is more rapidly increasing the volume of the combustion chamber as combustion occurs, which in turn reduces the pressure rise rate and maximum temperature in the cylinder. Figure 6.12 also shows that for a given combustion phasing, RI can vary on the order of 50%, indicating that factors other than combustion phasing can have a large influence on ringing.

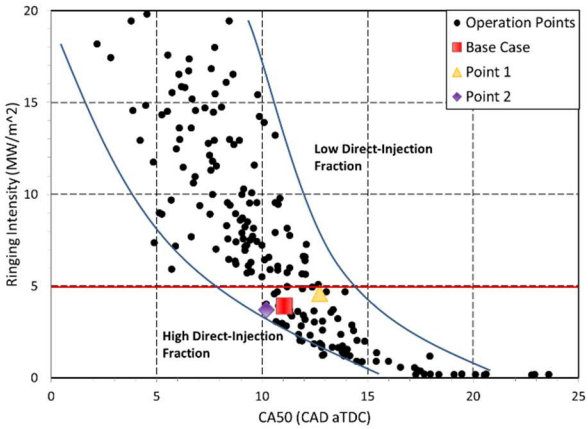

Figure 6.12: Plot of RI against combustion phasing for all operating points. An upper limit of ringing for this engine is shown by the red line.

Figure 6.13 plots the rate of heat release for four cases: the two cases of interest, and two additional cases, Point 3 and Point 4. Point 3 and Point 4 have nearly identical CA50's, of ~ 9 CAD aTDC, however their RI's are 11.6 and 6.3 MW/m^2, respectively. The cause of these radically different RI's can be found in their ROHR profiles, as seen in Fig. 6.13. These figures show the different manners in which Points 3 & 4 burn. Point 4 has a significantly lower peak ROHR; this peak ROHR is caused by the bulk nearly homogenous charge igniting. Point 4 has a smaller bulk charge mass than Point 3. This is due to the greater fuel stratification found in Point 4, which is caused by a later direct injection which contains more fuel than the direct injection strategy employed in Point 3. As seen in Fig. 6.14, the higher peak ROHR results in a higher pressure rise rate, which in turn raises the RI.

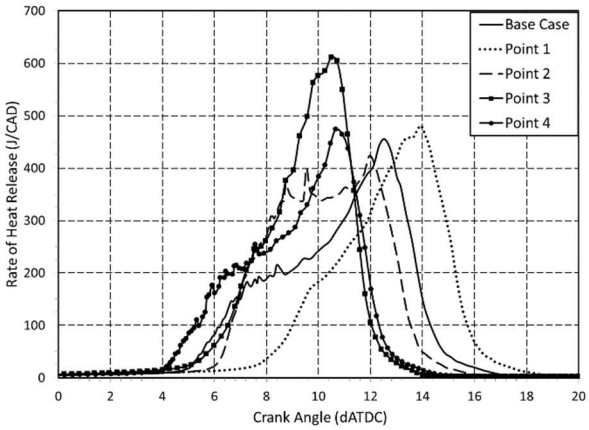

Figure 6.13: Rate of heat release profiles for five operating points.

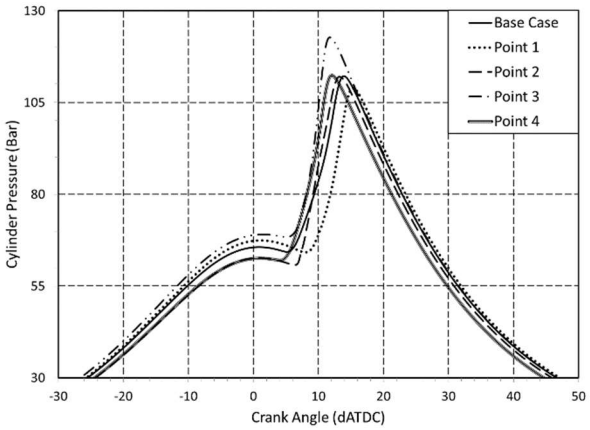

Figure 6.14: In-cylinder pressure traces for five operating points of interest.

Finally, direct-injection timing and mass sweeps were conducted to assess the ability to use the directly-injected fuel to help control combustion phasing during engine operation. Figure 6.15 and Figure 6.16 show the results of these sweeps.

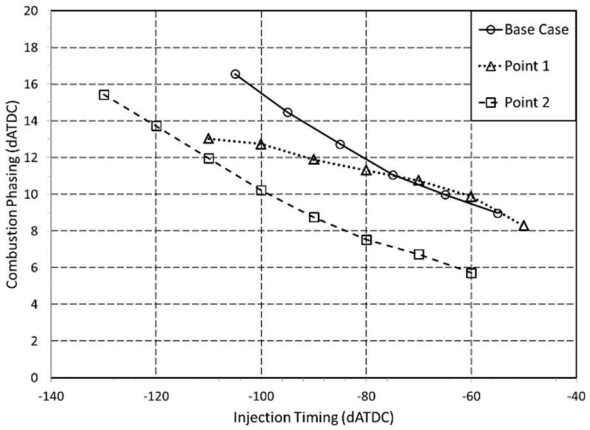

Figure 6.15: Combustion phasing (CA50) plotted against direct injection timing. In this sweep, the mass of both the aspirated and directly injected fuel is held constant for each case.

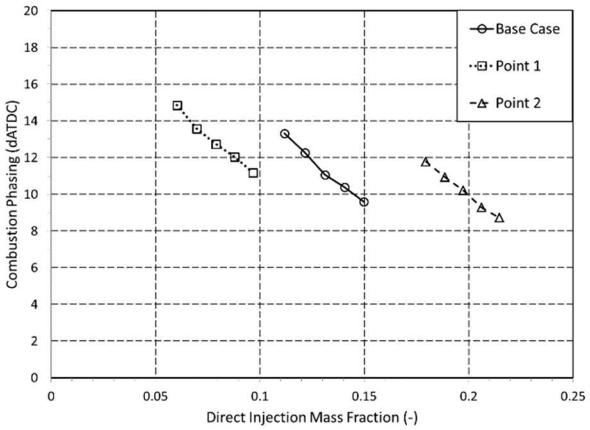

Figure 6.16: Combustion phasing (CA50) plotted against direct injection mass fraction.

In this sweep, the mass of the aspirated fuel is held constant while the mass of the directly injected fuel varies. It can be seen in Fig. 6.16, that the Base Case and Point 2 both demonstrate significant control over combustion phasing with the injection timing sweep. However, Point 1 shows significantly reduced control over combustion phasing relative to the other points, as indicated by the difference in slope of the Point 1 dataset compared to Points 2 and 3. This is likely due to the lower direct-injection mass fraction in Point 1, resulting in a smaller perturbation of the in-cylinder conditions at TDC, reducing the effect on combustion phasing. This effect is obviously nonlinear, as the Base Case and Point 2 show similar control over combustion phasing even though they have different direct-injection mass fractions. However, it can be seen in Fig. 6.16 that when the direct-injection mass fraction is altered, all three points have similar changes in CA50. It should be noted, however, that in the range tested, the timing sweep has a larger effect on CA50 while not altering the fuel energy level, though in the case of Point 1, the timing sweep could not alter the combustion phasing over a wide range.

b) Cycle Simulation Results – Complete Engine Performance

Complete engine performance was estimated for only three operating points (as seen in Table 6.4). In the full engine performance calculation, combustion was calculated with a table heat release model, with tables that were created according to the rate of heat release profiles obtained from the detailed 3D-CFD simulation. Figure 6.17 shows that the there is a good fit between the pressure traces obtained in the 3D-CFD and Boost simulation.

Table 6.4. Simulated key operating points.

Operating Point	Engine Speed (rpm)	Pressure at IVC (bar)	Temperature at IVC (K)	EGR (%)
Base	1200	2.014	383.95	28.57
Point 1	1200	1.994	370.81	20
Point 2	1200	1.933	381.65	20

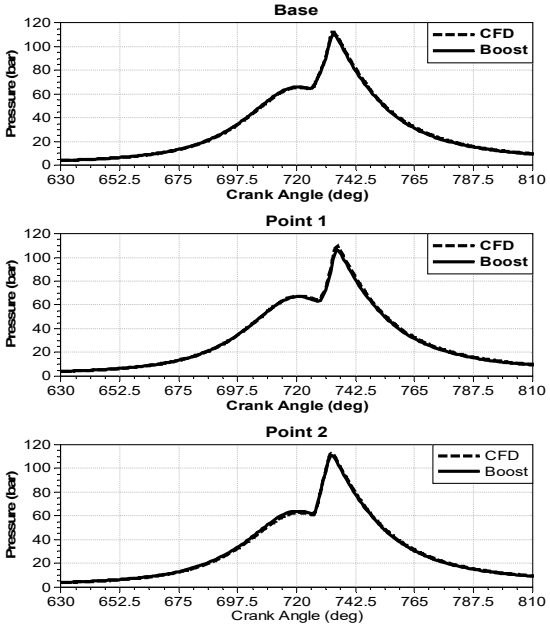

Figure 6.17: Comparison between the CFD and Boost simulation

The variable geometry turbocharger was chosen so that the compressor operates in the optimum area in the engine operating points of interest, as seen in Fig. 6.18. The engine performance results obtained with the full engine simulation are presented in Table 6.5 and

Table **6.6**.

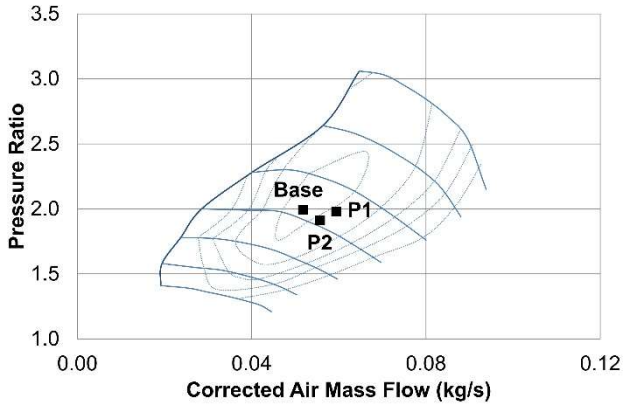

Figure 6.18. Compressor performance map with the referenced operating points plotted in it.

Table 6.5. The engine performance obtained with the full engine simulation (η_E – the engine brake efficiency; p_{INT} – intake pressure; p_{EXH} – exhaust pressure)

Operating Point	BMEP (bar)	η_E (%)	p_{INT} (bar)	p_{EXH} (bar)
Base	9,57	38.96	1,94	2,45

Point 1	9,44	38.8	1,97	2,5
Point 2	9,52	38.96	1,91	2,32

Table 6.6. The system performance obtained with the full engine simulation ($P_{EGR,\ COOLER}$ – the calculated heat flux at EGR cooler; $P_{INTERCOOLER}$ – the calculated heat flux at intercooler

Operating Point	$P_{EGR,COOLER}$ (W)	$P_{INTERCOOLER}$ (W)	T_{EXH} (K)	η_{COMP} (%)	η_{TC} (%)
Base	7486.3	0	789	73.7	39
Point 1	6447.23	933.82	777.3	72.9	37.8
Point 2	4069.4	0	799	73	37.5

The overall turbocharger efficiency was quite high in all three operating points. The base operating point had the highest turbocharger efficiency, which is a result of the position of the turbine stator blade that the turbine was operated at. Point 1 and Point 2 were operated with more opened turbine stator blades which is a result of the lower EGR requirement and hence higher exhausts mass flow at the turbine. Slightly lower turbocharger efficiency in these operating points is a result of the lower turbine efficiency at this stator blade position. Although Point 2 has lower turbocharger efficiency compared to the Base point, this point has the lowest pumping losses, which comes as a result of the highest exhaust (turbine inlet) temperature, which enables the operation with lower exhaust (turbine inlet) pressure.

The highest cooling requirement was in the base operating point, as a result of the highest amount of EGR that had to be cooled. It can be seen that intercooler only had to be applied in the Point 1 operating point. This is a result of low EGR rate (20%) in the combination with a low IVC temperature requirement Table 6.6.

c) Cycle Simulation Results – Engine Operability Range

The low and high intake temperature range was analyzed with a table heat release model at the engine speed of 1200 rpm. The operating points that were analyzed are specified in Table 6.7.

The engine could be operated in all three operating points at -70°C and 70°C. To obtain the desired IVC temperature at -70°C, the EGR cooler had to be engaged, which means that even lower intake temperature could be obtained. However, as such low temperatures are not expected, -70°C was set as a low temperature limit. Also, at 70°C the desired IVC temperature was obtained without the intercooler operating at full capacity, which means that even higher intake temperature could be obtained. However, as such high temperatures are not expected, 70°C was set as a high temperature limit.

Table 6.7. Simulated operating points for high- and low-temperature limits.

Operating Point	Engine Speed (rpm)	Pressure at IVC (bar)	Temperature at IVC (K)	EGR (%)
Base – Low	1200	2.014	383.95	28.57

Base – High	1200	2.014	383.95	28.57
Point 1 – Low	1200	1.994	370.81	20
Point 1 – High	1200	1.994	370.81	20
Point 2 – Low	1200	1.933	381.65	20
Point 2 – High	1200	1.933	381.65	20

The operability limit in terms of the engine speed was analyzed with a Vibe model as 3D-CFD results were not available. These simulations were performed to test if the chosen turbocharger and coolers could accommodate the engine operation at various engine speeds. The tested engine speed range was from 800 rpm to 2400 rpm, which represents the idle and top speed for a common heavy-duty engine. The analyzed operating points are specified in Table 6.8.

As can be seen from the compressor performance map, shown in Fig. 6.18, the engine could be operated in this speed range with a few limitations. At 800 rpm, the desired level of SHP pressure could not be obtained with the both EGR rates, due to the combination of the low exhaust gas enthalpy and low exhaust gas mass flow at the turbine. As expected, higher intake pressure could be obtained with a 20% EGR rate due to higher mass flow at the turbine.

Table 6.8. Simulated operating points for the engine speed range

Operating Point	Engine Speed (rpm)	Pressure at IVC (bar)	Temperature at IVC (K)	EGR (%)
Idle	800	2.014	383.95	28.57
Speed 1	1600	2.014	383.95	28.57
Speed 2	2000	2.014	383.95	28.57
Top Speed	2400	2.014	383.95	28.57
Idle	800	2.014	383.95	20
Speed 1	1600	2.014	383.95	20
Speed 2	2000	2.014	383.95	20
Top Speed	2400	2.014	383.95	20

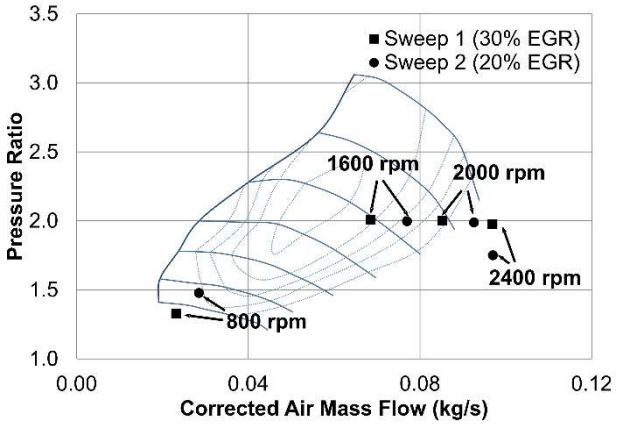

Figure 6.18. Compressor performance map with the referent operating points plotted in it.

On the other side of the engine speed range, at 2400 rpm, the compressor was operated in the low efficiency area which led to a considerable deterioration in the engine breathing (Table 6.9), which can be seen through the increased exhaust backpressure. As can be seen, at 2400 rpm the desired IVC pressure could not be obtained with a 20% EGR rate due to significantly deteriorated compressor efficiency.

Table 6.9. The engine performance obtained in the operability range simulation

Operating Point	Engine speed (rpm)	p_{INT} (bar)	p_{EXH} (bar)	EGR (%)
Idle	800	1.32	1.61	28.57
Speed 1	1600	2	2.58	28.57
Speed 2	2000	2	2.96	28.57
Top Speed	2400	1.98	3.68	28.57
Idle	800	1.48	1.85	28.57
Speed 1	1600	2	2.67	28.57
Speed 2	2000	1.98	3.42	28.57
Top Speed	2400	1.75	3.45	28.57

I. Conclusions

This study used a RANS 3D-CFD model of an experimental medium duty Homogeneous Charge Compression Ignition engine operating with a Partial Fuel Stratification strategy to optimize a mid-load engine operation point at both the combustion and system levels. It was found that relative to a baseline operating point, the closed-cycle engine operation was improved in terms of indicated efficiency (0.4%), NO_x emissions (0.8 g/kw*hr) at the expense of RI (0.7 MW/m^2) by carefully tuning intake and direct injection parameters. A second operating point was identified which increased efficiency (0.2 %) and reduced RI (0.2 MW/m^2) at the cost of NO_x emissions (1.7 g/kw*hr). In assessing the parametric sweep of operating conditions, it was found that the largest influence on combustion system performance came from the combustion phasing of the engine operating point, with late combustion phasing being required to reduce RI and reduce NO_x production. However, excessively late combustion phasing reduced efficiency. Therefore, the three operating conditions that were analyzed achieved good performance metrics in different

ways. The Base Case employed higher EGR and a moderate direct-injection fraction to reduce NO_x and RI at the cost of efficiency, while Point 1 used a reduced direct-injection fraction and EGR fraction coupled with delayed combustion phasing to reduce NO_x while increasing efficiency. Point 2 used a high direct-injection fraction to reduce RI, allowing earlier combustion phasing at the expense of NO_x emissions. The sweep of engine operating points indicated that if NO_x is to be kept at a low level with efficiency kept high, HCCI-like conditions are most desirable. However, these conditions reduce the ability to control combustion phasing with the direct injection. In the case of higher DI fractions, very late combustion phasing was required to keep NO_x low, which reduced efficiency.

Following the optimization of the in-cylinder engine operating point, a 0D/1D engine model was created to determine the feasibility and operability limits of the engine, in regards to turbomachinery and thermal regulation. However, highlighting the importance of a system level approach, the most efficient point over the high-pressure cycle did not result in the highest overall efficiency of the engine at the system level. This was due to the changes to the turbine inlet conditions caused by the reduced use of EGR and lower intake pressure. By reducing EGR and intake pressure, the mass flow through the turbine increased, while the pressure ratio decreased, which moved the turbine into a lower efficiency range. The peak brake efficiency for the engine, when considering turbomachinery sized for operation of the base case between 800 RPM and 2400 RPM, was found to be 39%. For this operating condition, intake temperatures in the range of -70 °C to 70 °C were found to permit the correct IVC conditions through charge and EGR cooling. These results indicate that the engine operating points are viable and competitive with traditional diesel operation, and are more efficient than current spark-ignition operating points at a similar load level.

II. Nomenclature

ACE – advanced combustion engine
aTDC – after top dead center
BDC – bottom dead center
BMEP – brake mean effective pressure
bTDC – before top dead center
CA50 – crank angle at which 50% of total heat release has occurred
CFD – computational fluid dynamics
CO – carbon monoxide
CR – compression ratio
DI – direct injection
EGR – exhaust gas recirculation
GDI – gasoline direct injection
H_2O – water
HC – hydrocarbons
HCCI – homogeneous charge compression ignition
IMEP – indicated mean effective pressure during the closed cycle
$IMEP_{GE}$ – indicated mean effective pressure during the gas exchange phase

IVC – intake valve closure
IVO – intake valve opening
KHRT – Kelvin-Helmholtz Rayleigh-Taylor
LTC – low temperature combustion
N_2 – nitrogen
NO_x – oxides of nitrogen
O_2 – oxygen
OP – operating point
p_{INT} – intake pressure
$P_{EGR,COOLER}$ – required cooling power of the EGR cooler
p_{EXH} – exhaust pressure
PFI – port fuel injection
PFS – partial fuel stratification
PM – fully premixed
RANS – Reynolds averaged Navier Stokes
RPM – revolutions per minute
SHP – start of high pressure cycle
SMD – Sauter mean diameter
TDC – top dead center
T_{EXH} – exhaust gas temperature
VP – turbine vane position
η_E – brake efficiency
η_T – turbine efficiency
η_{TC} – overall variable geometry turbocharger efficiency

Chapter 7:
Conclusions

While detailed conclusions have been presented in each chapter, the highlights are reiterated here.

I. Gasoline Low-Temperature Heat Release

a) Gasoline was found to exhibit single-stage heat release at low-intake pressures, and transition to exhibiting both low- and high-temperature heat release at elevated intake pressures.
b) Gasoline composition had significant effects on the intake pressure level needed to effect the transition to low-temperature heat release, with fuel components such toluene or ethanol inhibiting low-temperature heat release.
c) Low-temperature heat release significantly raised the system reactivity, and in the case of homogeneous charge compression ignition engine experiments, low-temperature heat release rapidly caused the fuels to become too reactive for operation.

II. Ethanol Addition to Gasoline

a) Ethanol addition to gasoline was found to significantly decrease reactivity at conditions which would exhibit low-temperature heat release for neat gasoline.
b) Ethanol was found to reduce the $OH\cdot$ and HO_2 radical pools, inhibiting the low-temperature chain branching pathway.
c) Ethanol addition effects were not found to be captured by the Anti-Knock Index (average of Research Octane Number and Motor Octane Number).

III. Combustion System and Engine System Coupling

a) The partial fuel stratification (PFS) combustion system was found to present tradeoffs between thermal efficiency, NO_2 formation, and ringing.
b) Multiple high-efficiency (>43% indicated) operating points were feasible using a PFS strategy with different combinations of intake pressure, intake temperature, exhaust gas recirculation, and injection timing.
c) The turbocharging system was found to have a significant effect on overall system performance; optimization of the operating point to the turbocharger map changed brake efficiency from 38.8% to 38.96%.
d) The operating point's intake conditions were found to be feasible without external heating for intake temperatures ranging from -70 °C to 70 °C.

IV. Prospects for Future Work

a) The effects of temperature and pressure histories on LTHR magnitude should be investigated. Specifically, how do the competing influences of compression ratio, intake pressure, and intake temperature compare when Top-Dead Center conditions are matched?

b) The relative magnitude of LTHR inhibition in a gasoline fueled HCCI engine by ethanol addition and toluene addition should be measured for low- to moderate-levels of ethanol and toluene (5%, 10%, 20%, and 30% on a volumetric blending basis).
c) The trends of LTHR behavior observed in the HCCI engine for gasoline-type fuels, both neat and blended with ethanol, should be compared to behavior in boosted SI engines. As LTHR has been shown to have a significant influence on gasoline auto-ignition under engine relevant conditions, it is likely that a strong link will be found between HCCI and SI engine behavior.

Chapter 8:
References

1. Aceves, D. Flowers, C. Westbrook, J. Smith and W. Pitz, “A multi-zone model for prediction of HCCI combustion and emissions”, SAE 2000-01-0327, 2000.
2. Aceves, Salvador, et al. *HCCI in a CFR engine: Experiments and detailed kinetic modeling*. SAE International, 2000.
3. Aceves, Salvador M., et al. "HCCI combustion: analysis and experiments."*SAE paper* 2001-01 (2001): 2077.
4. Andrae, Johan CG, and R. A. Head. "HCCI experiments with gasoline surrogate fuels modeled by a semidetailed chemical kinetic model."*Combustion and flame* 156.4 (2009): 842-851.
5. ASTM D613, “Cetane Test.” 2015, http://www.astm.org/Standards/D613.htm
6. ASTM D2699, “Research Octane Number Test.” 2015, http://www.astm.org/Standards/D2699.htm
7. ASTM D2700, “Motor Octane Number Test.” 2015, http://www.astm.org/Standards/D2700.htm
8. ASTM D7668, “Derived Cetane Number Test.” 2015, http://www.astm.org/Standards/D7668.htm
9. AVL Boost v2013.2 - Theory, AVL LIST GmbH, 2013.
10. Babajimopoulos A, Assanis DN, Flowers DL, Aceves SM, Hessel RP. A fully coupled computational fluid dynamics and multi-zone model with detailed chemical kinetics for the simulation of premixed charge compression ignition engines. Int J Engine Res 2005; 6(5): 497-512. http://dx.doi.org/10.1243/146808705X30503.
11. Battin-Leclerc, Frédérique. "Detailed chemical kinetic models for the low-temperature combustion of hydrocarbons with application to gasoline and diesel fuel surrogates." *Progress in Energy and Combustion Science* 34.4 (2008): 440-498.
12. Borgqvist, Patrick, Per Tunestål, and Bengt Johansson. "Gasoline partially premixed combustion in a light duty engine at low load and idle operating conditions." *SAE World Congress & Exhibition*. Society of Automotive Engineers, 2012.
13. Brezinsky, Kenneth. "The high-temperature oxidation of aromatic hydrocarbons." *Progress in Energy and Combustion Science* 12.1 (1986): 1-24.
14. Cai, Liming, and Heinz Pitsch. "Optimized chemical mechanism for combustion of gasoline surrogate fuels." *Combustion and Flame* 162.5 (2015): 1623-1637.
15. CARB, “The California Reformulated Gasoline Regulations.” 2013, http://www.arb.ca.gov/fuels/gasoline/100912CaRFG_regs.pdf
16. CARB, “Key Events in the History of Air Quality in California.” 2016, http://www.arb.ca.gov/html/brochure/history.htm
17. Chang, Junseok, et al. "Enabling high efficiency direct injection engine with naphtha fuel through Partially Premixed Charge Compression Ignition Combustion." *SAE Technical paper* (2012): 01-0677.

18. CHEMKIN-PRO, Reaction Design Inc., San Diego, CA, 2008. URL: www.reactiondesign.com. Version 15101 (13-Sep-2010).
19. Cannella, W., et al. "FACE Gasolines and Blends with Ethanol: Detailed Characterization of Physical and Chemical Properties." *CRC Report No AVFL-24* (2014).
20. Ciatti, Stephen, et al. *Efficiency and emissions performance of multizone stratified compression ignition using different octane fuels*. No. 2013-01-0263. SAE Technical Paper, 2013.
21. Curran, Henry J., et al. "A comprehensive modeling study of n-heptane oxidation." *Combustion and flame* 114.1 (1998): 149-177.
22. Curran, Henry J., et al. "A comprehensive modeling study of isooctane oxidation." *Combustion and flame* 129.3 (2002): 253-280.
23. Dagaut, Philippe, and Casimir Togbé. "Experimental and modeling study of the kinetics of oxidation of ethanol-n-heptane mixtures in a jet-stirred reactor."*Fuel* 89.2 (2010): 280-286.
24. Dahl, Daniel, and Ingemar Denbratt. "HCCI/SCCI load limits and stoichiometric operation in a multicylinder naturally aspirated spark ignition engine operated on gasoline and E85." *International Journal of Engine Research* 12.1 (2011): 58-68.
25. Dec, John E. *A conceptual model of di diesel combustion based on laser-sheet imaging**. No. 970873. SAE technical paper, 1997.
26. Dec, J.E., Sjoberg, M., "Isolating the Effects of Fuel Chemistry on Combustion Phasing in an HCCI Engine and the Potential of Fuel Stratification for Ignition Control," SAE Technical Paper, 2004-01-0557, 2004, doi:10.4271/2004-01-0557.
27. Dec, John E. "Advanced compression-ignition engines—understanding the in-cylinder processes." *Proceedings of the combustion institute* 32.2 (2009): 2727-2742.
28. Dec, John E., and Yi Yang. "Boosted HCCI for high power without engine knock and with ultra-low NOx emissions-using conventional gasoline." *SAE International Journal of Engines* 3.1 (2010): 750-767.
29. Dec, John E., Yi Yang, and Nicolas Dronniou. "Boosted HCCI-controlling pressure-rise rates for performance improvements using partial fuel stratification with conventional gasoline." *SAE International Journal of Engines* 4.1 (2011): 1169-1189.
30. Dec, John E., Yi Yang, and Nicolas Dronniou. "Improving Efficiency and Using E10 for Higher Loads in Boosted HCCI Engines." *SAE International Journal of Engines* 5.3 (2012): 1009-1032.
31. Dec, John E., et al. "Effects of Gasoline Reactivity and Ethanol Content on Boosted, Premixed and Partially Stratified Low-Temperature Gasoline Combustion (LTGC)." *SAE International Journal of Engines* 8.3 (2015): 935-955.
32. Dernotte, Jeremie, John Dec, and Chunsheng Ji. "Investigation of the sources of combustion noise in HCCI engines." *SAE International Journal of Engines* 7.2 (2014): 730-761.
33. DOE, Co-Optimization of Fuels and Engines, 2016, http://www.energy.gov/sites/prod/files/2015/05/f22/optima_sand2015-2142m.PDF

34. Embouazza, M., D. C. Haworth, and N. Darabiha. *Implementation of detailed chemical mechanisms into multidimensional CFD using in situ adaptive tabulation: Application to HCCI engines*. No. 2002-01-2773. SAE Technical Paper, 2002.
35. Eng, James A. *Characterization of pressure waves in HCCI combustion*. No. 2002-01-2859. SAE Technical Paper, 2002.
36. EPA 2013, *Energy Policy Act of 2005*. http://energy.gov/sites/prod/files/2013/10/f3/epact_2005.pdf
37. EPA 2016, *Ethanol Waivers for E10 and E15.* https://www.epa.gov/gasoline-standards/ethanol-waivers-e15-and-e10
38. Flowers, S. M. Aceves, C. K. Westbrook, J.R. Smith, and R. W. Dibble, "Sensitivity of natural gas HCCI combustion to fuel and operating parameters using detailed kinetic modeling," In AES-Vol. 39, "Proceedings of the ASME Advanced Energy Systems Division – 1999," Edited by S.M. Aceves, S. Garimella and R. Peterson, pp. 465-473, 1999.
39. Flowers, Daniel L., et al. "Prediction of carbon monoxide and hydrocarbon emissions in isooctane HCCI engine combustion using multizone simulations." *Proceedings of the Combustion Institute* 29.1 (2002): 687-694.
40. Foong, Tien Mun, et al. "The octane numbers of ethanol blended with gasoline and its surrogates." *Fuel* 115 (2014): 727-739.
41. Garrett Turbochargers, "Intercooler Effectiveness." http://www.turbobygarrett.com/turbobygarrett/intercooler-effectiveness
42. Georgano, George Nicolas. *Cars, 1886-1930*. Colporteur Press, 1985.
43. Government Printing Office (GPO), 2007, *Energy Independence and Security Act*: https://www.gpo.gov/fdsys/pkg/BILLS-110hr6enr/pdf/BILLS-110hr6enr.pdf
44. Haas, Francis M., Marcos Chaos, and Frederick L. Dryer. "Low and intermediate temperature oxidation of ethanol and ethanol–PRF blends: An experimental and modeling study." *Combustion and flame* 156.12 (2009): 2346-2350.
45. Halterman, "Halterman CARB LEV III E10 Certification Fuel Regular Octane Specifications Sheet 2014." See Appendix 3.
46. Heywood, Internal Combustion Engines Fundamentals, McGraw-Hill, 1988.
47. Hwang, Wontae, John Dec, and Magnus Sjöberg. "Spectroscopic and chemical-kinetic analysis of the phases of HCCI autoignition and combustion for single-and two-stage ignition fuels." *Combustion and Flame* 154.3 (2008): 387-409.
48. IEA, "CO2 Emissions from Fuel Combustion Highlights 2013." 2013, http://www.iea.org/publications/freepublications/publication/co2-emissions-from-fuel-combustion-highlights-2015.html
49. IPCC, "Climate Change 2014: Impacts, Adaption, and Vulnerability." 2014 https://www.ipcc.ch/report/ar5/
50. Johnson, Michael V., et al. "A shock tube study of n-and iso-propanol ignition." *Energy & Fuels* 23.12 (2009): 5886-5898.
51. Jun, Daesu, Kazuaki Ishii, and Norimasa Iida. "Combustion analysis of natural gas in a four stroke HCCI engine using experiment and elementary reactions calculation." *2003 SAE World Congress*. 2003.

52. Kalghatgi, Gautam T., Per Risberg, and Hans-Erik Ångström. "Partially pre-mixed auto-ignition of gasoline to attain low smoke and low NOx at high load in a compression ignition engine and comparison with a diesel fuel." *SAE paper* 2007-01 (2007): 0006.
53. Kalghatgi, Gautam, et al. "An alternative method based on toluene/n-heptane surrogate fuels for rating the anti-knock quality of practical gasolines." *SAE International Journal of Fuels and Lubricants* 7.2014-01-2609 (2014): 663-672.
54. Kalghatgi, Gautam, et al. *Knock Prediction Using a Simple Model for Ignition Delay*. No. 2016-01-0702. SAE Technical Paper, 2016.
55. Kamio, Junichi, et al. *Study on HCCI-SI combustion using fuels ethanol containing*. No. 2007-01-4051. SAE Technical Paper, 2007.
56. Kolodziej, Christopher P., et al. *Extension of the lower load limit of gasoline compression ignition with 87 AKI gasoline by injection timing and pressure*. No. 2014-01-1302. SAE Technical Paper, 2014.
57. Kolodziej, Christopher, et al. *Achieving stable engine operation of gasoline compression ignition using 87 AKI gasoline down to idle*. No. 2015-01-0832. SAE Technical Paper, 2015.
58. Kong, Song-Charng, and Rolf D. Reitz. "Application of detailed chemistry and CFD for predicting direct injection HCCI engine combustion and emissions."*Proceedings of the Combustion Institute* 29.1 (2002): 663-669.
59. Johanson 2016 – Typical engine efficiency
60. Leone, Thomas G., et al. "Effects of fuel octane rating and ethanol content on knock, fuel economy, and CO2 for a turbocharged DI engine." *SAE International Journal of Fuels and Lubricants* 7.1 (2014): 9-28.
61. Leppard, William R. *The chemical origin of fuel octane sensitivity*. No. CONF-9010205--. Warrendale, PA (USA); Society of Automotive Engineers, 1990.
62. Lewander, Magnus, et al. "Investigation of the combustion characteristics with focus on partially premixed combustion in a heavy duty engine." *SAE International Journal of Fuels and Lubricants* 1.1 (2009): 1063-1074.
63. Li, J., et al. "Effects of fuel ratio and injection timing on gasoline/biodiesel fueled RCCI engine: A modeling study." *Applied Energy* 155 (2015): 59-67.
64. Van Lipzig, J. P. J., et al. "Laminar burning velocities of n-heptane, isooctane, ethanol and their binary and tertiary mixtures." *Fuel* 90.8 (2011): 2773-2781.
65. LLNL, "n-Heptane, Detailed Mechanism, Version 3.1." 2013, https://www-pls.llnl.gov/?url=science_and_technology-chemistry-combustion-n_heptane_version_3
66. LLNL, "Gasoline Surrogate." 2013, https://www-pls.llnl.gov/?url=science_and_technology-chemistry-combustion-gasoline_surrogate
67. Lü, Xingcai, et al. "Experimental study on the auto-ignition and combustion characteristics in the homogeneous charge compression ignition (HCCI) combustion operation with ethanol/n-heptane blend fuels by port injection."*Fuel* 85.17 (2006): 2622-2631.
68. Lü, Xingcai, et al. "Experimental study and chemical analysis of n-heptane homogeneous charge compression ignition combustion with port injection of reaction inhibitors." *Combustion and flame* 149.3 (2007): 261-270.

69. Machrafi, Hatim, Simeon Cavadias, and Philippe Guibert. "An experimental and numerical investigation on the influence of external gas recirculation on the HCCI autoignition process in an engine: Thermal, diluting, and chemical effects." *Combustion and Flame* 155.3 (2008): 476-489.
70. Mack, John Hunter, et al. "Investigation of HCCI combustion of diethyl ether and ethanol mixtures using carbon 14 tracing and numerical simulations."*Proceedings of the Combustion Institute* 30.2 (2005): 2693-2700.
71. Mahalec I., Lulić Z., Kozarac, D: Internal combustion engines, internal script, FMENA (Faculty of Mechanical Engineering and Naval Architecture), 2013.
72. Marinov, Nick M. "A detailed chemical kinetic model for high temperature ethanol oxidation." *International Journal of Chemical Kinetics* 31.3 (1999): 183-220.
73. Mehl, M., et al. *Detailed kinetic modeling of low-temperature heat release for PRF fuels in an HCCI engine*. No. 2009-01-1806. SAE Technical Paper, 2009.
74. Mehl, W.J. Pitz, M. Sjöberg, J.E. Dec, SAE Paper 2009-01-1806 (2009) doi:10.4271/2009-01-1806.
75. Mehl M, Chen JY, Pitz WJ. An approach for formulating surrogates for gasoline with application towards a reduced surrogate mechanism for CFD engine modeling. Energy Fuels 2011; 25(11): 5215-5223. http://dx.doi.org/10.1021/ef201099y.
76. Mehl M., W.J. Pitz, C.K. Westbrook, H.J. Curran, "Kinetic modeling of gasoline surrogate components and mixtures under engine conditions", *Proceedings of the Combustion Institute* **33**:193-200 (2011).
77. Mehl, Marco, et al. *Detailed kinetic modeling of conventional gasoline at highly boosted conditions and the associated intermediate temperature heat release*. No. 2012-01-1109. SAE Technical Paper, 2012.
78. Mehl, Marco, et al. "Chemical Kinetic Modeling of Surrogate Components and Mixtures to Represent Gasoline and Diesel Fuels." Oral Presentation, Feb. 10th 2015, Advanced Engine Consortium Meeting, Sandia National Laboratory, Livermore, California, USA.
79. Moc, Jerzy, et al. "The Unimolecular Decomposition and H Abstraction Reactions by HO and HO2 from n-Butanol." *COMPUTATIONAL METHODS IN SCIENCE AND ENGINEERING: Advances in Computational Science: Lectures presented at the International Conference on Computational Methods in Sciences and Engineering 2008 (ICCMSE 2008)*. Vol. 1148. No. 1. AIP Publishing, 2009.
80. Musculus, Mark PB, Paul C. Miles, and Lyle M. Pickett. "Conceptual models for partially premixed low-temperature diesel combustion." *Progress in Energy and Combustion Science* 39.2 (2013): 246-283.
81. Naik, C. V., Pitz, W.J., Westbrook, C.K., Sjoberg, M., Dec, J.E., More, J., Curran, H.J., Simmie, J.M., "Detailed Chemical Kinetic Modeling of Surrogate Fuels for Gasoline and Application to an HCCI Engine," SAE Technical Paper 2005-01-3741, 2005, doi: 10.4271/2005-01-3741.
82. Najt, Paul M., and David E. Foster. *Compression-ignited homogeneous charge combustion*. No. 830264. SAE Technical paper, 1983.
83. NIST, "Ethanol," 2016, http://webbook.nist.gov/cgi/cbook.cgi?ID=C64175&Mask=4
84. NHTSA, "CAFE – FUEL ECONOMY." 2016 http://www.nhtsa.gov/fuel-economy

85. Ogink, Roy, and Valeri Golovitchev. *Gasoline HCCI modeling: computer program combining detailed chemistry and gas exchange processes*. No. 2001-01-3614. SAE Technical paper, 2001.
86. OICA, "Production Statistics." 2016 http://www.oica.net/category/production-statistics/
87. Olsson, Jan-Ola, et al. "A turbocharged dual-fuel HCCI engine." *SAE Special Publications* 2001.1627 (2001).
88. Orszag, Steven A., et al. "Renormalization group modeling and turbulence simulations." *Near-wall turbulent flows* (1993): 1031-1046.
89. Patterson, Mark A., and Rolf D. Reitz. *Modeling the effects of fuel spray characteristics on diesel engine combustion and emission*. No. 980131. SAE Technical Paper, 1998.
90. Patzek 2005: Patzek, Tad W., et al. "Ethanol from corn: clean renewable fuel for the future, or drain on our resources and pockets?." *Environment, Development and Sustainability* 7.3 (2005): 319-336.
91. Pilling, Michael J. *Low-temperature combustion and autoignition*. Vol. 35. Elsevier, 1997.
92. Richards KJ, Senecal PK, Pomraning E. CONVERGE 2.1.0. 2013.
93. Risberg, Per, Gautam Kalghatgi, and Hans-Erik Ångström. "Auto-ignition quality of gasoline-like fuels in HCCI engines." *Presented at the SAE Powertrain & Fluid Systems Conference & Exhibition, held October 2003, in Pittsburgh, PA, USA. SAE 2003-01-3215*. 2003.
94. Rosin P, Rammler E. The laws governing the fineness of powdered coal. J Inst of Fuel 1993; 7: 29-36.
95. Saisirirat, Peerawat, et al. "Spectroscopic measurements of low-temperature heat release for homogeneous combustion compression ignition (HCCI) n-heptane/alcohol mixture combustion." *Energy & Fuels* 24.10 (2010): 5404-5409.
96. Saisirirat, Peerawat, et al. "Auto-ignition and combustion characteristics in HCCI and JSR using 1-butanol/n-heptane and ethanol/n-heptane blends."*Proceedings of the Combustion Institute* 33.2 (2011): 3007-3014.
97. Sarathy, S. Mani, et al. "Alcohol combustion chemistry." *Progress in Energy and Combustion Science* 44 (2014): 40-102.
98. Sarathy, S. Mani, et al. "Ignition of alkane-rich FACE gasoline fuels and their surrogate mixtures." *Proceedings of the Combustion Institute* 35.1 (2015): 249-257.
99. Savitzky, Abraham, and Marcel JE Golay. "Smoothing and differentiation of data by simplified least squares procedures." *Analytical chemistry* 36.8 (1964): 1627-1639.
100. Saxena, Samveg, Jyh-Yuan Chen, and Robert Dibble. *Maximizing power output in an automotive scale multi-cylinder homogeneous charge compression ignition (HCCI) engine*. No. 2011-01-0907. SAE Technical Paper, 2011.
101. Saxena, S., Bedoya, I.D., Shah, N., and Phadke, A., "Understanding loss mechanisms and identifying areas of improvement for HCCI engines using detailed exergy analysis," *ASME Journal for Engineering for Gas Turbines and Power* (2013): GTP-13-1102.
102. Saxena, Samveg, and Iván D. Bedoya. "Fundamental phenomena affecting low temperature combustion and HCCI engines, high load limits and strategies for extending these limits." *Progress in Energy and Combustion Science* 39.5 (2013): 457-488.

103. Sellnau, Mark C., et al. "Full-Time Gasoline Direct-Injection Compression Ignition (GDCI) for High Efficiency and Low NOx and PM." *SAE International Journal of Engines* 5.2012-01-0384 (2012): 300-314.
104. Sellnau, Mark C., et al. *Part-load operation of gasoline direct-injection compression ignition (GDCI) engine*. No. 2013-01-0272. SAE Technical Paper, 2013.
105. Sellnau, Mark, et al. "GDCI multi-cylinder engine for high fuel efficiency and low emissions." *SAE International Journal of Engines* 8.2 (2015): 775-790.
106. Shahlari, Arsham J., et al. "Comparison of compression ignition engine noise metrics in low-temperature combustion regimes." *SAE International Journal of Engines* 6.1 (2013): 541-552.
107. Shi, Xian, Jyh-Yuan Chen, and Zheng Chen. "Numerical study of laminar flame speed of fuel-stratified hydrogen/air flames." *Combustion and Flame*163 (2016): 394-405.
108. Silke, E.J., Pitz, W.J., Westbrook, C.W., Sjoberg, M., Dec, J.E., "Understanding the Chemical Effects of Increased Boost Pressure under HCCI Conditions," SAE Int. J. Fuels and Lubr. 1(1):12-25, 2009, doi:10.4271/2008-01-0019.
109. Simmie, John M. "Detailed chemical kinetic models for the combustion of hydrocarbon fuels." *Progress in energy and combustion science* 29.6 (2003): 599-634.
110. Sjöberg, Magnus, et al. "Comparing enhanced natural thermal stratification against retarded combustion phasing for smoothing of HCCI heat-release rates." *SAE transactions* 113.3 (2004): 1557-1575.
111. Sjöberg, Magnus, and John E. Dec. *Smoothing HCCI heat-release rates using partial fuel stratification with two-stage ignition fuels*. No. 2006-01-0629. SAE Technical Paper, 2006.
112. Sjöberg, Magnus, and John E. Dec. "Comparing late-cycle autoignition stability for single-and two-stage ignition fuels in HCCI engines." *Proceedings of the combustion institute* 31.2 (2007): 2895-2902.
113. Sjöberg, Magnus, and John E. Dec. *EGR and intake boost for managing HCCI low-temperature heat release over wide ranges of engine speed*. No. 2007-01-0051. SAE Technical Paper, 2007.
114. Sjoberg, Magnus, and John E. Dec. "Ethanol autoignition characteristics and HCCI performance for wide ranges of engine speed, load and boost." *SAE International Journal of Engines* 3.1 (2010): 84-106.
115. Shibata, G., Oyama, K., Urushihara, T., and Nakano, T., "Correlation of Low Temperature Heat Release With Fuel Composition and HCCI Engine Combustion," SAE Technical Paper 2005-01-0138, 2005, doi:10.4271/2005-01-0138.
116. Shibata, G. and Urushihara, T., "Auto-Ignition Characteristics of Hydrocarbons and Development of HCCI Fuel Index," SAE Technical Paper 2007-01-0220, 2007, doi:10.4271/2007-01-0220.
117. Smit, Berend, et al. *Introduction to Carbon Capture and Sequestration*. Vol. 1. World Scientific, 2014.
118. Sluder, C. Scott, et al. "Exploring the Relationship Between Octane Sensitivity and Heat-of-Vaporization." *SAE International Journal of Fuels and Lubricants* 9.2016-01-0836 (2016): 80-90.

119. Splitter, Derek, Rolf Reitz, and Reed Hanson. "High efficiency, low emissions RCCI combustion by use of a fuel additive." *SAE International Journal of Fuels and Lubricants* 3.2 (2010): 742-756.
120. Stein, Robert A., et al. "Effect of Heat of Vaporization, Chemical Octane, and Sensitivity on Knock Limit for Ethanol-Gasoline Blends." *SAE International Journal of Fuels and Lubricants* 5.2 (2012): 823-843.
121. Tanaka, Shigeyuki, et al. "Two-stage ignition in HCCI combustion and HCCI control by fuels and additives." *Combustion and flame* 132.1 (2003): 219-239.
122. Taritas, Ivan, Darko Kozarac, and Momir Sjeric. *Numerical Study of Boosting Configurations and Valve Strategies for High Load HCCI Engine in Wide Range of Engine Speed*. No. 2014-01-1267. SAE Technical Paper, 2014.
123. Truedsson, Ida, et al. *Development of new test method for evaluating HCCI fuel performance*. No. 2014-01-2667. SAE Technical Paper, 2014.
124. Tsujimura, Taku, et al. "Development of isopentanol reaction mechanism reproducing autoignition character at high and low temperatures." *Energy & Fuels* 26.8 (2012): 4871-4886.
125. Vibe, Ivan I., and Franz Meißner. *Brennverlauf und kreisprozess von verbrennungsmotoren*. Verlag Technik, 1970.
126. Vuilleumier, D., Kozarac, D., Mehl, M., Pitz, W.J., et al., "Intermediate temperature heat release in an HCCI engine fueled by ethanol / n-heptane mixtures: an experimental and modeling study," *Combustion and Flame* (2013): CNF-D-13-00131.
127. Vuilleumier, David, et al. *Exploration of heat release in a homogeneous charge compression ignition engine with primary reference fuels*. No. 2013-01-2622. SAE Technical Paper, 2013.
128. Vuilleumier, David, et al. "Multi-Level Computational Exploration of Advanced Combustion Engine Operating Strategies." *10th Conference on Sustainable Development of Energy, Water and Environment Systems*. 2015.
129. Vuilleumier, David, et al., "Investigation of the influence of intake pressure and fuel composition on Low-Temperature Heat Release in a gasoline fueled HCCI engine," in preparation for review, *Fuel*.
130. Vuilleumier, David, et al., "The effects of fuel composition and ethanol content on lowest stable load in a Gasoline Compression Ignition engine: An Experimental and Modeling Study," in preparation for review, *Fuel.*
131. Wang, Zhi, et al. "Numerical simulation of HCCI engine with multi-stage gasoline direct injection using 3D-CFD with detailed chemistry." *SAE transactions* 113.3 (2004): 367-380.
132. Westbrook, CK., Pitz, WJ., and Curran, H.J., "Auto-ignition and chemical kinetic mechanisms of HCCI combustion," In: HCCI and CAI engines for the automotive industry, Zhao H., editor, Boca Raton: Woodhead Publishing; 2007, p. 433- 445.
133. Westbrook, Charles, "Chemical Kinetic Origins of Octane Sensitivity." Oral Presentation, Feb. 8th 2016, Advanced Engine Consortium Meeting, Sandia National Laboratory, Livermore, California, USA.

134. Wolk, Benjamin, and Jyh-Yuan Chen. "Computational Study of Partial Fuel Stratification for HCCI Engines Using Gasoline Surrogate Reduced Mechanism." *Combustion Science and Technology* 186.3 (2014): 332-354.
135. Wolk, Benjamin, Jyh-Yuan Chen, and John E. Dec. "Computational study of the pressure dependence of sequential auto-ignition for partial fuel stratification with gasoline." *Proceedings of the Combustion Institute* 35.3 (2015): 2993-3000.
136. Wolk 2015 – AEC
137. Wolk BM. *Fundamental interactions in gasoline compression ignition engines with fuel stratification* (Doctoral dissertation, UNIVERSITY OF CALIFORNIA, BERKELEY).
138. Woschni, Gerhard. *A universally applicable equation for the instantaneous heat transfer coefficient in the internal combustion engine*. No. 670931. SAE Technical paper, 1967.
139. Yang, Dong-bo, et al. "Experimental study of fuel stratification for HCCI high load extension." *Applied Energy* 88.9 (2011): 2949-2954.
140. Yang, Yi, et al. "Characteristics of isopentanol as a fuel for HCCI engines."*SAE International Journal of Fuels and Lubricants* 3.2 (2010): 725-741.
141. Yang, Dong-bo, et al. "Experimental study of fuel stratification for HCCI high load extension." *Applied Energy* 88.9 (2011): 2949-2954.
142. Yang, Yi, et al. "Partial fuel stratification to control HCCI heat release rates: fuel composition and other factors affecting pre-ignition reactions of two-stage ignition fuels." *SAE International Journal of Engines* 4.1 (2011): 1903-1920.
143. Yang, Yi, et al. "Tailoring HCCI heat-release rates with partial fuel stratification: Comparison of two-stage and single-stage-ignition fuels."*Proceedings of the Combustion Institute* 33.2 (2011): 3047-3055.
144. Yang, Yi, et al. "Boosted HCCI combustion using low-octane gasoline with fully premixed and partially stratified charges." *SAE International Journal of Engines* 5.3 (2012): 1075-1088.
145. Yao, Mingfa, Zhaolei Zheng, and Haifeng Liu. "Progress and recent trends in homogeneous charge compression ignition (HCCI) engines." *Progress in Energy and Combustion Science* 35.5 (2009): 398-437.
146. Yates, Andy, Arthur Bell, and Andre Swarts. "Insights relating to the autoignition characteristics of alcohol fuels." *Fuel* 89.1 (2010): 83-93.
147. Zeldovich, Ya B. "The oxidation of nitrogen in combustion and explosions."*Acta Physicochim. URSS* 21.4 (1946): 577-628.
148. Zhang, Yu, Yi Yang, and André L. Boehman. "Premixed ignition behavior of C 9 fatty acid esters: a motored engine study." *Combustion and Flame* 156.6 (2009): 1202-1213.
149. Zhang, Yu, and André L. Boehman. "Oxidation of 1-butanol and a mixture of n-heptane/1-butanol in a motored engine." *Combustion and Flame* 157.10 (2010): 1816-1824.
150. Zhang, Yu, and André L. Boehman. "Autoignition of binary fuel blends of n-heptane and C 7 esters in a motored engine." *Combustion and Flame* 159.4 (2012): 1619-1630.
151. Zhou, D. Z., et al. "Application of CFD-chemical kinetics approach in detecting RCCI engine knocking fuelled with biodiesel/methanol." *Applied Energy* 145 (2015): 255-264.

Appendix 1:
Supplementary Figures from Chapter 2

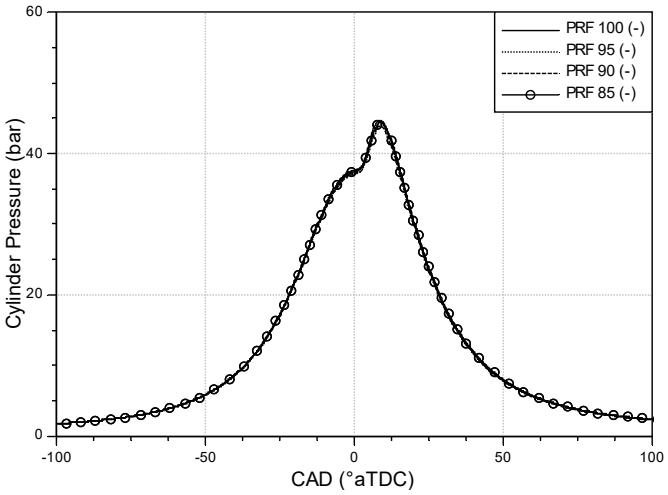

Appendix 1 Figure 1. Pressure traces for various fuels at 1.0 bar intake pressure, ϕ = 0.4.

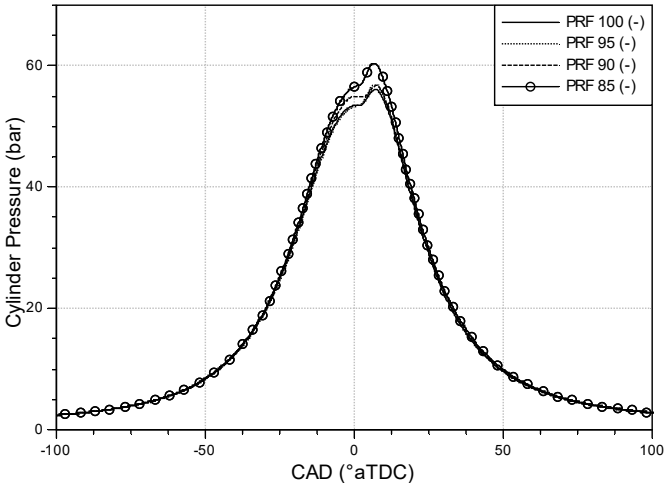

Appendix 1 Figure 2. Pressure traces for various fuels at 1.4 bar intake pressure, ϕ = 0.3.

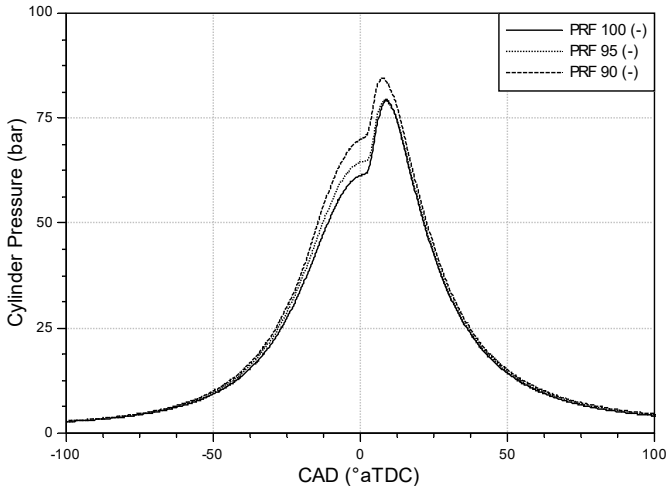

Appendix 1 Figure 3. Pressure traces for various fuels at 1.6 bar intake pressure, ϕ = 0.4.

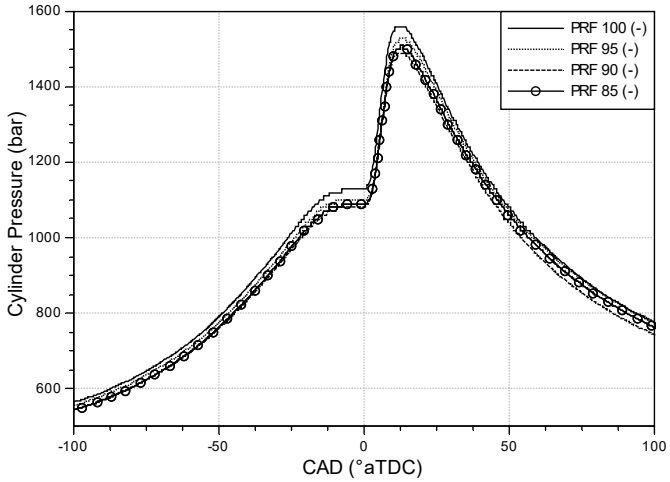

Appendix 1 Figure 4. Temperature profiles for various fuels at 1.0 bar intake pressure, ϕ = 0.4.

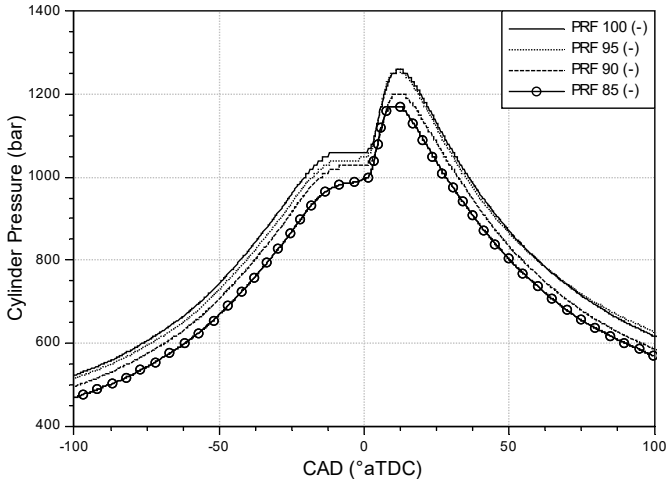

Appendix 1 Figure 5. Temperature profiles for various fuels at 1.4 bar intake pressure, ϕ = 0.3.

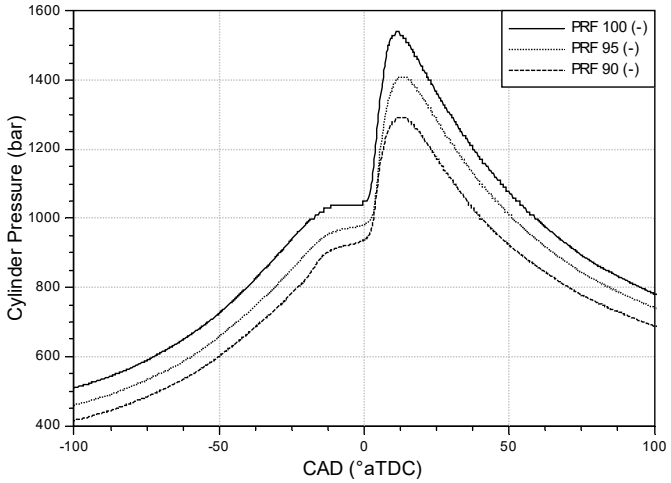

Appendix 1 Figure 6. Temperature profiles for various fuels at 1.6 bar intake pressure, ϕ = 0.4.

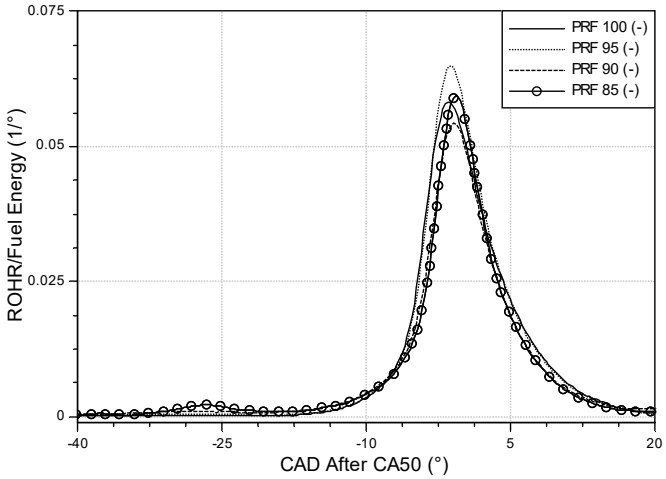

Appendix 1 Figure 7. Heat release profiles for various fuels at 1.4 bar intake pressure, ϕ = 0.3.

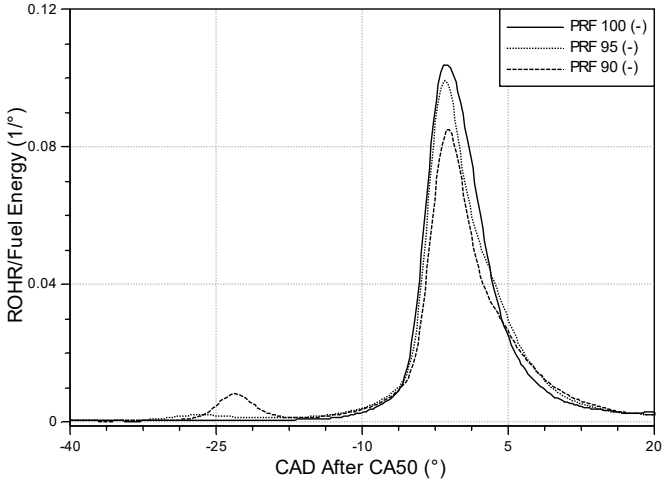

Appendix 1 Figure 8. Heat release profiles for various fuels at 1.6 bar intake pressure, ϕ = 0.4.

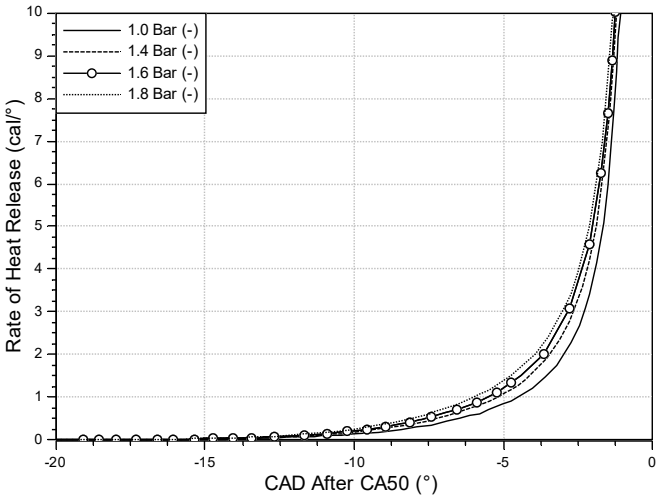

Appendix 1 Figure 9. Simulated heat release profiles for PRF95 under different inlet pressures, constant CA50 = 6 °aTDC, ϕ = 0.4.

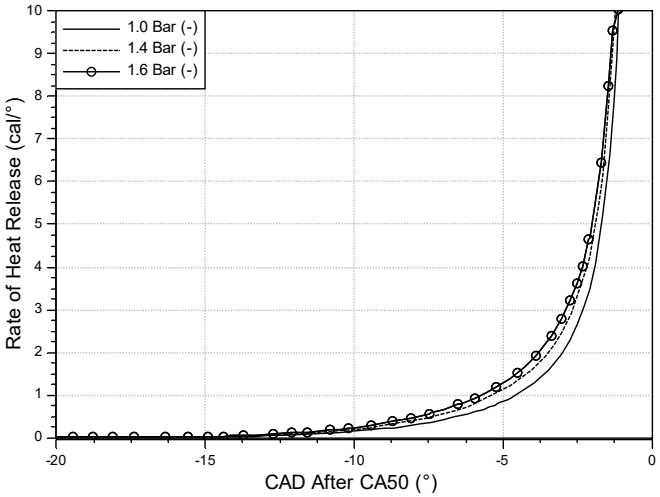

Appendix 1 Figure 10. Simulated heat release profiles for PRF90 under different inlet pressures, constant CA50 = 6 °aTDC, ϕ = 0.4.

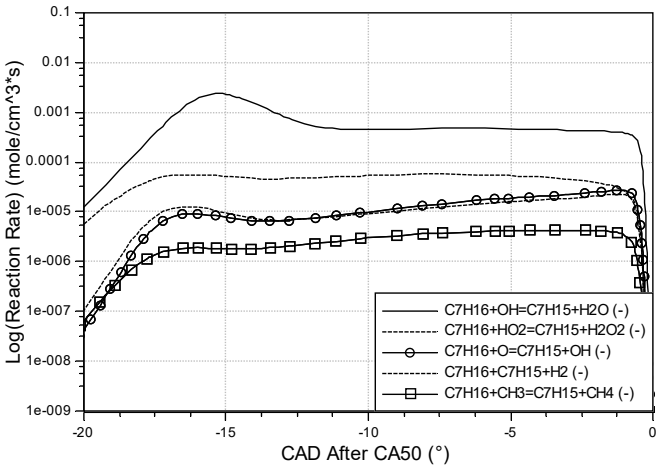

Appendix 1 Figure 11. Reaction rate of hydrogen abstraction elementary reactions, PRF85 at 2.2 bar intake pressure, ϕ = 0.4.

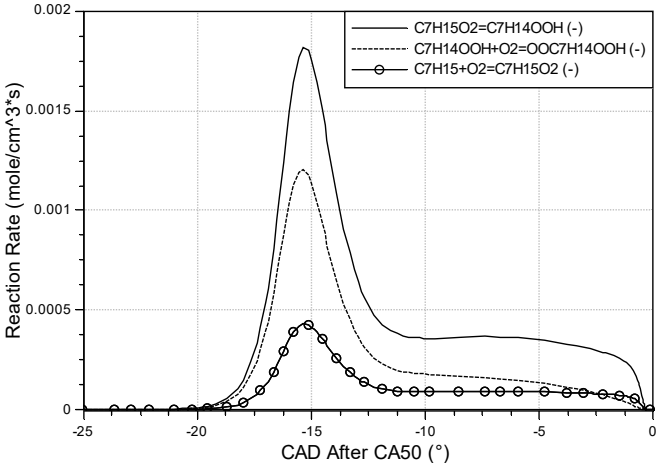

Appendix 1 Figure 12. Reaction rates of alkyl group isomerization elementary reactions, PRF85 at 2.2 bar intake pressure, ϕ = 0.4.

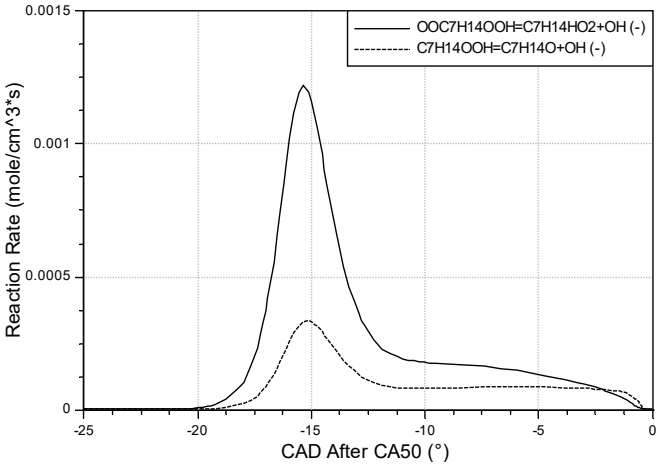

Appendix 1 Figure 13. Reaction rates of hydroxyl radical release and formation of ketones and cyclic ethers elementary reactions, PRF85 at 2.2 bar intake pressure, ϕ = 0.4.

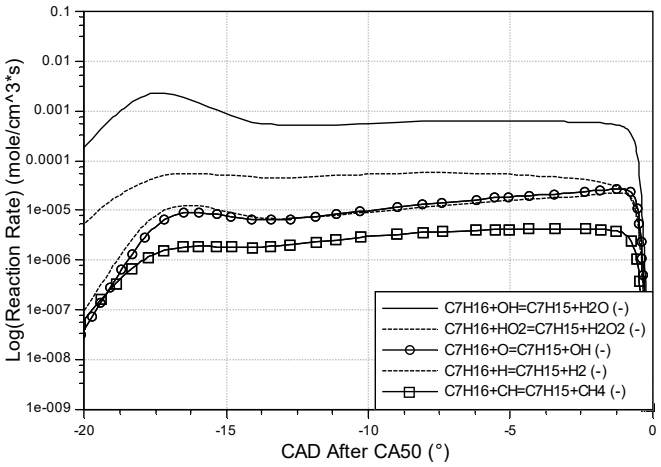

Appendix 1 Figure 14. Reaction rate of hydrogen abstraction elementary reactions, PRF70 at 2.2 bar intake pressure, ϕ = 0.4.

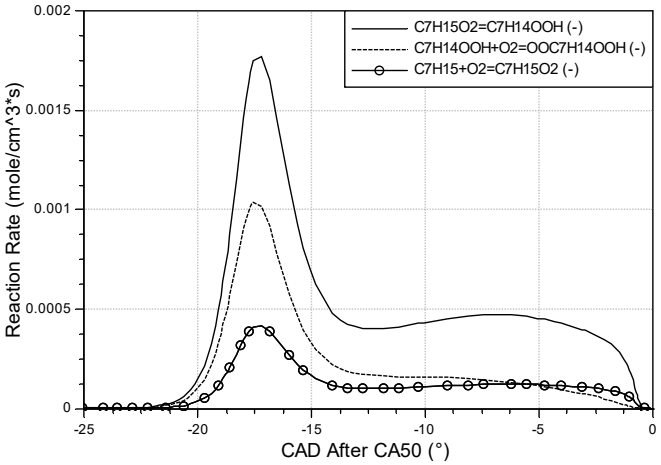

Appendix 1 Figure 15. Reaction rates of alkyl group isomerization elementary reactions, PRF70 at 2.2 bar intake pressure, ϕ = 0.4.

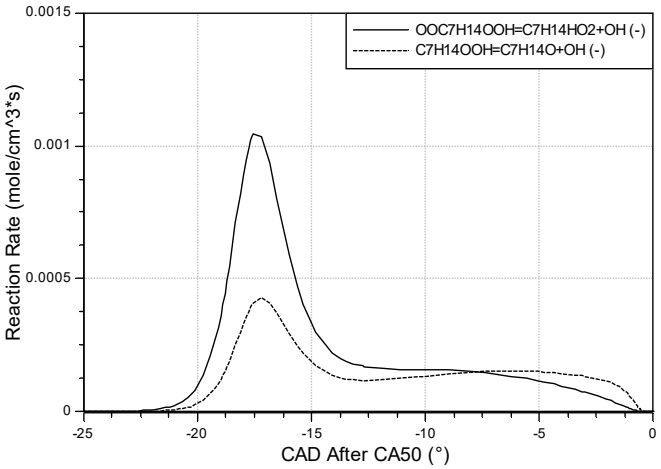

Appendix 1 Figure 16. Reaction rates of hydroxyl radical release and formation of ketones and cyclic ethers elementary reactions, PRF70 at 2.2 bar intake pressure, ϕ = 0.4.

Appendix 2:
Converge Post-Processing Code

"Main_Converge_Function1.m"

```
%This is the main program
function Main_Converge_Function1()
close all
clear all


% Constants:

Fuel_LHV=44; % MJ/kg
nr=2; % number of cycles per power stroke
AFR_Stoich=14.7; % stoichiometric AFR
R_uni=8314; %J/kmol-K

%-------------------------------------------------------------------
-------------------------
%-------Load In-Cylinder Thermo File
%-------------------------------------------------------------------
-------------------------

Thermo_File_Name=['thermo_region0.out'];
fileID=fopen(Thermo_File_Name,'r');
delimiter = '\t';
startRow = 5;
formatSpec =
'%16f%17f%17f%17f%17f%17f%17f%17f%17f%17f%17f%17f%17f%17f%17f%17
f%f%[^\n\r]';
dataArray = textscan(fileID, formatSpec, 'Delimiter', delimiter,
'EmptyValue' ,NaN,'HeaderLines' ,startRow-1, 'ReturnOnError',
false);
fclose(fileID);

Thermo_Data = [dataArray{1:end-1}];


Thermo_Matrix_Size=size(Thermo_Data);

Thermo_Data(:,2)=Thermo_Data(:,2)*10; % Convert MPa to Bar
```

```
Thermo_Data(:,3)=Thermo_Data(:,3)*10; % Convert MPa to Bar
Thermo_Data(:,4)=Thermo_Data(:,4)*10; % Convert MPa to Bar




%-------------------------------------------------------------------
-------------------------
%-------Thermo File Indexes
%-------------------------------------------------------------------
-------------------------

idx_CA=1; % Crank Angle
idx_Press=2;
idx_Max_Press=3;
idx_Min_Press=4;
idx_Temp=5;
idx_Max_Temp=6;
idx_Min_Temp=7;
idx_Volume=8;
idx_Mass=9;
idx_Density=10;
idx_Cum_ROHR=11;
idx_ROHR=12;
idx_C_p=13;
idx_C_v=14;
idx_gamma=15;
idx_kin_vis=16;
idx_dyn_vis=17;
idx_Cum_Norm_ROHR=18;


%-------------------------------------------------------------------
-------------------------
%-------Load Engine Inputs File
%-------------------------------------------------------------------
-------------------------

Engine_File_Name=['engine.in'];
file_id=fopen(Engine_File_Name,'r');
delimiter = {',',' '};
startRow = 3;
formatSpec =
'%f%*s%*s%*s%*s%*s%*s%*s%*s%*s%*s%*s%*s%*s%*s%*s%*s%*s%*s%*s%*s%*s%*s%*s%
*s%*s%*s%*s%*s%*s%*s%*s%*s%*s%*s%*s%*s%*s%*s%*s%*s%*s%*s%*s%*s%*s%*s%*s%*
s%*s%*s%*s%*s%*s%*s%*s%[^\n\r]';
```

```
textscan(file_id, '%[^\n\r]', startRow-1, 'ReturnOnError',
false);
dataArray = textscan(file_id, formatSpec, 'Delimiter',
delimiter, 'ReturnOnError', false);
fclose(file_id);

Engine_Data = dataArray{:, 1};




Engine_Matrix_Size=size(Engine_Data);

Bore=Engine_Data(1); % m

Stroke=Engine_Data(2); % m

Displacement=pi*(Bore/2)^2*Stroke; % m^3

idx_rpm=6;

RPM=Engine_Data(idx_rpm); % rpm

CA_to_S=((RPM/60)*360)^-1;



%-------------------------------------------------------------------
-------------------------
%-------Load Valve Timing
%-------------------------------------------------------------------
-------------------------

Events_File_Name = 'events.in';
delimiter = ' ';
startRow = 6;

formatSpec = '%*s%*s%*s%f%*s%*s%*s%[^\n\r]';

fileID = fopen(Events_File_Name,'r');

textscan(fileID, '%[^\n\r]', startRow-1, 'ReturnOnError',
false);
dataArray = textscan(fileID, formatSpec, 'Delimiter', delimiter,
'MultipleDelimsAsOne', true, 'ReturnOnError', false);
fclose(fileID);
```

```
Valve_Timing = [dataArray{1:end-1}];

IVO= 1 ; % subtract 720 degrees
IVC= 2 ; % Intake Valve Closure, subtract 720 degrees
EVO= 4 ; % Exhaust Valve Opening, subtract 720 degrees
EVC= 3 ; % subtract 720 degrees

EVO_CA=Valve_Timing(EVO);
IVC_CA=Valve_Timing(IVC)-720;

idx_IVC=1;
Crank=-360;
while Crank<=IVC_CA
    Crank=Thermo_Data(idx_IVC,idx_CA);
    idx_IVC=idx_IVC+1;
end

idx_EVO=Thermo_Matrix_Size(1);
Crank=360;
while Crank>=EVO_CA
    Crank=Thermo_Data(idx_EVO,idx_CA);
    idx_EVO=idx_EVO-1;
end



%-------------------------------------------------------------------
-------------------------
%-------Load Initialization File
%-------------------------------------------------------------------
-------------------------

filename = 'initialize.in';
delimiter = {'     ',','};
startRow = 10;
endRow = 54;
formatSpec = '%s%s%[^\n\r]';
fileID = fopen(filename,'r');
textscan(fileID, '%[^\n\r]', startRow-1, 'ReturnOnError',
false);
dataArray = textscan(fileID, formatSpec, endRow-startRow+1,
'Delimiter', delimiter, 'ReturnOnError', false);

fclose(fileID);

raw = repmat({''},length(dataArray{1}),length(dataArray)-1);
```

```
for col=1:length(dataArray)-1
    raw(1:length(dataArray{col}),col) = dataArray{col};
end
numericData = NaN(size(dataArray{1},1),size(dataArray,2));

for col=[1,2]
    % Converts strings in the input cell array to numbers.
Replaced non-numeric
    % strings with NaN.
    rawData = dataArray{col};
    for row=1:size(rawData, 1);
        % Create a regular expression to detect and remove non-
numeric prefixes and
        % suffixes.
        regexstr = '(?<prefix>.*?)(?<numbers>([-
]*(\d+[\,]*)+[\.]{0,1}\d*[eEdD]{0,1}[-+]*\d*[i]{0,1})|([-
]*(\d+[\,]*)*[\.]{1,1}\d+[eEdD]{0,1}[-
+]*\d*[i]{0,1}))(?<suffix>.*)';
        try
            result = regexp(rawData{row}, regexstr, 'names');
            numbers = result.numbers;

            % Detected commas in non-thousand locations.
            invalidThousandsSeparator = false;
            if any(numbers==',');
                thousandsRegExp = '^\d+?(\,\d{3})*\.{0,1}\d*$';
                if isempty(regexp(thousandsRegExp, ',',
'once'));
                    numbers = NaN;
                    invalidThousandsSeparator = true;
                end
            end
            % Convert numeric strings to numbers.
            if ~invalidThousandsSeparator;
                numbers = textscan(strrep(numbers, ',', ''),
'%f');
                numericData(row, col) = numbers{1};
                raw{row, col} = numbers{1};
            end
        catch me
        end
    end
end

R = cellfun(@(x) ~isnumeric(x) && ~islogical(x),raw); % Find
non-numeric cells
raw(R) = {NaN}; % Replace non-numeric cells
```

```
Initial_Data = cell2mat(raw);
clearvars filename delimiter startRow endRow formatSpec fileID
dataArray ans raw col numericData rawData row regexstr result
numbers invalidThousandsSeparator thousandsRegExp me R;


Intake_Temp=Initial_Data(17,1); % K
Intake_Press=Initial_Data(18,1)/10^5; % Bar
Intake_O2=Initial_Data(23,2); % Mass Fraction

EGR=100*(0.232-Intake_O2)/0.232; % Calculate EGR using mass
fraction of air in atmosphere

Exhaust_O2=Initial_Data(42,2);
Exhaust_N2=Initial_Data(43,2);
Exhaust_H2O=Initial_Data(44,2);
Exhaust_CO2=Initial_Data(45,2);


%-------------------------------------------------------------------
-------------------------
%-------Load Cycle Mass Flows
%-------------------------------------------------------------------
-------------------------

% filename = 'mass_avg_flow.out';
% startRow = 6;
% formatSpec =
'%*16s%17s%17s%17s%17s%17s%17s%17s%17s%17s%17s%17s%17s%17s%17s%1
7s%17s%17s%17s%17s%s%[^\n\r]';
% fileID = fopen(filename,'r');
% dataArray = textscan(fileID, formatSpec, 'Delimiter', '',
'WhiteSpace', '', 'HeaderLines' ,startRow-1, 'ReturnOnError',
false);
% fclose(fileID);
% raw = repmat({''},length(dataArray{1}),length(dataArray)-1);
% for col=1:length(dataArray)-1
%     raw(1:length(dataArray{col}),col) = dataArray{col};
% end
% numericData = NaN(size(dataArray{1},1),size(dataArray,2));
%
% for col=[1,2,3,4,5,6,7,8,9,10,11,12,13,14,15,16,17,18,19,20]
%     % Converts strings in the input cell array to numbers.
Replaced non-numeric
%     % strings with NaN.
%     rawData = dataArray{col};
%     for row=1:size(rawData, 1);
```

```
%         % Create a regular expression to detect and remove
non-numeric prefixes and
%         % suffixes.
%         regexstr = '(?<prefix>.*?)(?<numbers>([-
]*(\d+[\,]*)+[\.]{0,1}\d*[eEdD]{0,1}[-+]*\d*[i]{0,1})|([-
]*(\d+[\,]*)*[\.]{1,1}\d+[eEdD]{0,1}[-
+]*\d*[i]{0,1}))(?<suffix>.*)';
%         try
%             result = regexp(rawData{row}, regexstr, 'names');
%             numbers = result.numbers;
%
%             % Detected commas in non-thousand locations.
%             invalidThousandsSeparator = false;
%             if any(numbers==',');
%                 thousandsRegExp =
'^\d+?(\,\d{3})*\.{0,1}\d*$';
%                 if isempty(regexp(thousandsRegExp, ',',
'once'));
%                     numbers = NaN;
%                     invalidThousandsSeparator = true;
%                 end
%             end
%             % Convert numeric strings to numbers.
%             if ~invalidThousandsSeparator;
%                 numbers = textscan(strrep(numbers, ',', ''),
'%f');
%                 numericData(row, col) = numbers{1};
%                 raw{row, col} = numbers{1};
%             end
%         catch me
%         end
%     end
% end
% R = cellfun(@(x) ~isnumeric(x) && ~islogical(x),raw); % Find
non-numeric cells
% raw(R) = {NaN}; % Replace non-numeric cells
% Mass_Flow_Data = cell2mat(raw);
% clearvars filename startRow formatSpec fileID dataArray ans
raw col numericData rawData row regexstr result numbers
invalidThousandsSeparator thousandsRegExp me R;
%
% idx_bound_5_flow=2; % Exhaust Port boundary, kg/s
% idx_bound_9_flow=9; % Main Intake Port boundary, kg/s
% idx_bound_17_flow=15; % Swirl Port bounday, kg/s
%
% Exhaust_Flow=0;
% Main_Intake_Flow=0;
```

```
% Swirl_Flow=0;
%
% for i=1:Thermo_Matrix_Size(1)-1
%
Exhaust_Flow=Exhaust_Flow+Mass_Flow_Data(i,idx_bound_5_flow)*(Ma
ss_Flow_Data(i+1,idx_CA)-Mass_Flow_Data(i,idx_CA))*CA_to_S;
%
Main_Intake_Flow=Main_Intake_Flow+Mass_Flow_Data(i,idx_bound_9_f
low)*(Mass_Flow_Data(i+1,idx_CA)-
Mass_Flow_Data(i,idx_CA))*CA_to_S;
%
Swirl_Flow=Swirl_Flow+Mass_Flow_Data(i,idx_bound_17_flow)*(Mass_
Flow_Data(i+1,idx_CA)-Mass_Flow_Data(i,idx_CA))*CA_to_S;
% end
%
% Total_Massflow=Swirl_Flow+Main_Intake_Flow+Exhaust_Flow;



%-------------------------------------------------------------------
-------------------------
%-------Calculate IMEP gross
%-------------------------------------------------------------------
-------------------------

filename = 'boundary.in';
delimiter = ' ';
startRow = 233;
endRow = 240;
formatSpec = '%*s%f%*s%*s%*s%*s%*s%[^\n\r]';

fileID = fopen(filename,'r');

textscan(fileID, '%[^\n\r]', startRow-1, 'ReturnOnError',
false);
dataArray = textscan(fileID, formatSpec, endRow-startRow+1,
'Delimiter', delimiter, 'MultipleDelimsAsOne', true,
'ReturnOnError', false);

fclose(fileID);

boundary = [dataArray{1:end-1}];

clearvars filename delimiter startRow endRow formatSpec fileID
dataArray ans;
```

```
Int_Iso_Oct=boundary(1);
Int_O2=boundary(2);
Int_N2=boundary(3);
Int_H2O=boundary(4);
Int_CO2=boundary(5);
Int_N_Hept=boundary(6);
Int_C5H10_2=boundary(7);
Int_C6H5CH3=boundary(8);


%---------------------------------------------------------------
--------------------------
%-------Load Species Data and Save EVO Emissions and IVC Fuel
%---------------------------------------------------------------
--------------------------

Exhaust_File_Name=['species_region0.out'];
fileID=fopen(Exhaust_File_Name,'r');
delimiter = '\t';
startRow = 5;
formatSpec =
'%f%f%f%f%f%f%f%f%f%f%f%f%f%f%f%f%f%f%f%f%f%f%f%f%f%f%f%f%f%f%f%
f%f%f%f%f%f%f%f%f%f%f%f%f%f%f%f%f%f%f%f%f%f%f%f%f%f%f%f%f%f%f%f%
f%f%f%f%f%f%f%f%f%f%f%f%f%f%f%f%f%f%f%f%f%f%f%f%f%f%f%f%f%f%f%f%
f%f%f%f%*s%*s%*s%*s%*s%*s%*s%*s%*s%*s%*s%*s%*s%*s%*s%*s%*s%*s%*s
%*s%*s%*s%*s%*s%*s%*s%*s%*s%*s%*s%*s%*s%*s%*s%*s%*s%*s%*s%*s%*s%
*s%*s%*s%*s%*s%*s%*s%*s%*s%*s%*s%*s%*s%*s%*s%*s%*s%*s%*s%*s%*s%*
s%*s%*s%*s%*s%*s%*s%*s%*s%*s%*s%*s%*s%*s%*s%*s%*s%*s%*s%*s%*s%*s
%*s%*s%*s%*s%*s%*s%*s%*s%*s%*s%*s%*s%*s%*s%*s%*s%*s%*s%*s%*s%*s%
*s%*s%*s%*s%*s%*s%*s%*s%*s%*s%*s%*s%*s%*s%*s%*s%*s%*s%*s%*s%*s%*
s%*s%*s%*s%*s%*s%*s%*s%*s%*s%*s%*s%*s%*s%*s%*s%*s%*s%*s%*s%*s%*s
%*s%*s%*s%*s%*s%*s%*s%*s%*s%*s%*s%*s%*s%*s%*s%*s%*s%*s%*s%*s%*s%
*s%*s%*s%*s%*s%*s%*s%*s%*s%*s%*s%*s%*s%*s%*s%*s%*s%*s%*s%*s%*s%*
s%*s%*s%*s%*s%*s%*s%*s%*s%*s%*s%*s%[^\n\r]';
dataArray = textscan(fileID, formatSpec, 'Delimiter', delimiter,
'EmptyValue' ,NaN,'HeaderLines' ,startRow-1, 'ReturnOnError',
false);
fclose(fileID);
Exhaust_Data = [dataArray{1:end-1}];


Exhaust_Matrix_Size=size(Exhaust_Data);

idx_IC8H18=2; % Isooctane
idx_NC7H16=7; % N-Heptane
idx_C5H10_2=8; % Fuel Component
idx_C6H5CH3=9; % Fuel Component
```

```
idx_CO=16;
idx_CO2=5;
idx_O2=3;
idx_NO=98;
idx_NO2=99;



Total_Mass_IVC=sum(Exhaust_Data(idx_IVC,2:end)); % Mass of all
species at EVO
Total_Mass_EVO=sum(Exhaust_Data(idx_EVO,2:end)); % Mass of all
species at EVO


IC8H18_IVC=Exhaust_Data(idx_IVC,idx_IC8H18); % kg Isooctane
NC7H16_IVC=Exhaust_Data(idx_IVC,idx_NC7H16); % kg N-Heptane
C5H10_2_IVC=Exhaust_Data(idx_IVC,idx_C5H10_2); % Fuel Component
C6H5CH3_IVC=Exhaust_Data(idx_IVC,idx_C6H5CH3); % Fuel Component

Aspirated_Fuel=IC8H18_IVC+NC7H16_IVC+C5H10_2_IVC+C6H5CH3_IVC; %
kg of aspirated fuel


IC8H18=Exhaust_Data(idx_EVO,idx_IC8H18)/Total_Mass_EVO; % Mass
fractions Isooctane
NC7H16=Exhaust_Data(idx_EVO,idx_NC7H16)/Total_Mass_EVO; % Mass
Fraction N-Heptane
C5H10_2=Exhaust_Data(idx_EVO,idx_C5H10_2)/Total_Mass_EVO; % Fuel
Component
C6H5CH3=Exhaust_Data(idx_EVO,idx_C6H5CH3)/Total_Mass_EVO; % Fuel
Component
CO=Exhaust_Data(idx_EVO,idx_CO)/Total_Mass_EVO;
CO2=Exhaust_Data(idx_EVO,idx_CO2)/Total_Mass_EVO;
O2=Exhaust_Data(idx_EVO,idx_O2)/Total_Mass_EVO;
NOx=(Exhaust_Data(idx_EVO,idx_NO)+Exhaust_Data(idx_EVO,idx_NO2))
/Total_Mass_EVO;

UHC=IC8H18+NC7H16+C5H10_2+C6H5CH3; % Mass fraction unburned fuel




%-----------------------------------------------------------------
-------------------------
%-------Load Spray File
%-----------------------------------------------------------------
-------------------------
```

```
Spray_File_Name = 'spray.in';
delimiter = ',';

formatSpec = '%s%[^\n\r]';
fileID = fopen(Spray_File_Name,'r');
dataArray = textscan(fileID, formatSpec, 'Delimiter', delimiter,
'ReturnOnError', false);
fclose(fileID);

% Replace non-numeric strings with NaN.
raw = repmat({''},length(dataArray{1}),length(dataArray)-1);
for col=1:length(dataArray)-1
    raw(1:length(dataArray{col}),col) = dataArray{col};
end
numericData = NaN(size(dataArray{1},1),size(dataArray,2));

% Converts strings in the input cell array to numbers. Replaced
non-numeric
% strings with NaN.
rawData = dataArray{1};
for row=1:size(rawData, 1);
    % Create a regular expression to detect and remove non-
numeric prefixes and
    % suffixes.
    regexstr = '(?<prefix>.*?)(?<numbers>([-
]*(\d+[\,]*)+[\.]{0,1}\d*[eEdD]{0,1}[-+]*\d*[i]{0,1})|([-
]*(\d+[\,]*)*[\.]{1,1}\d+[eEdD]{0,1}[-
+]*\d*[i]{0,1}))(?<suffix>.*)';
    try
        result = regexp(rawData{row}, regexstr, 'names');
        numbers = result.numbers;

        % Detected commas in non-thousand locations.
        invalidThousandsSeparator = false;
        if any(numbers==',');
            thousandsRegExp = '^\d+?(\,\d{3})*\.{0,1}\d*$';
            if isempty(regexp(thousandsRegExp, ',', 'once'));
                numbers = NaN;
                invalidThousandsSeparator = true;
            end
        end
        % Convert numeric strings to numbers.
        if ~invalidThousandsSeparator;
            numbers = textscan(strrep(numbers, ',', ''), '%f');
            numericData(row, 1) = numbers{1};
            raw{row, 1} = numbers{1};
        end
```

```
    catch me
    end
end


R = cellfun(@(x) ~isnumeric(x) && ~islogical(x),raw); % Find
non-numeric cells
raw(R) = {NaN}; % Replace non-numeric cells

Spray_Data = cell2mat(raw);
Inject_Timing=Spray_Data(52);
Inject_Duration=Spray_Data(53); % CAD
Injected_Mass=Spray_Data(55);
Fuel=Aspirated_Fuel+Injected_Mass; % Total mass of fuel used
Injected_Fraction=Injected_Mass/Fuel; % Injected Fraction
AFR=(Total_Mass_IVC-Aspirated_Fuel)/Fuel;
Equivalence_Ratio=1/(AFR/AFR_Stoich); % Does not include EGR
effects

Blow_By=(Total_Mass_IVC+Injected_Mass-
Total_Mass_EVO)/Total_Mass_IVC; % Percentage of total intake
charge



%-------------------------------------------------------------------
-------------------------
%-------Calculate IMEP gross
%-------------------------------------------------------------------
-------------------------

for i=idx_IVC:idx_EVO-1

IMEP_Partial(i)=((Thermo_Data(i,idx_Press)+Thermo_Data(i+1,idx_P
ress))/2)*(Thermo_Data(i+1,idx_Volume)-
Thermo_Data(i,idx_Volume));
end


%
IMEP_Partial(size(IMEP_Partial)+1)=((Thermo_Data(1,idx_Press)+Th
ermo_Data(Thermo_Matrix_Size(1),idx_Press))/2)*(Thermo_Data(1,id
x_Volume)-Thermo_Data(Thermo_Matrix_Size(1),idx_Volume));


IMEP=sum(IMEP_Partial)/Displacement;
```

```
Torque=IMEP*100*Displacement*1000/(nr*6.28); % In N*m, page 50
Heywood

Power=IMEP*100*Displacement*1000*(RPM/60)/(nr*10^3); % In kW,
page 50 Heywood

Work=Power*nr/(RPM/60); % (kj) Heywood pg 50

Efficiency=100*Work/(Fuel*Fuel_LHV*1000); % Work out / Fuel
Energy in


%-------------------------------------------------------------
-------------------------
%-------Calculate IVC and EVO Conditions
%-------------------------------------------------------------
-------------------------


IVC_Temp=Thermo_Data(idx_IVC,idx_Temp);
IVC_Press=Thermo_Data(idx_IVC,idx_Press);
EVO_Temp=Thermo_Data(idx_EVO,idx_Temp);
EVO_Press=Thermo_Data(idx_EVO,idx_Press);



%-------------------------------------------------------------
-------------------------
%-------Trace Analysis
%-------------------------------------------------------------
-------------------------
CA5=0;
CA10=0;
CA50=0;
CA90=0;
CA95=0;
Press_Max=0;
Temp_Max=0;


% Calculate Heat Release Progress
for i=1:Thermo_Matrix_Size(1)

Thermo_Data(i,idx_Cum_Norm_ROHR)=Thermo_Data(i,idx_Cum_ROHR)/The
rmo_Data(Thermo_Matrix_Size(1),idx_Cum_ROHR);
end
```

```
idx_CA0=1;
Heat=0;
while Heat<=0.01
    Heat=Thermo_Data(idx_CA0,idx_Cum_Norm_ROHR);
    idx_CA0=idx_CA0+1;
end

idx_CA95=Thermo_Matrix_Size(1);
Heat=1;
while Heat>=0.95
    Heat=Thermo_Data(idx_CA95,idx_Cum_Norm_ROHR);
    idx_CA95=idx_CA95-1;
end



CA5=interp1(Thermo_Data(idx_CA0:idx_CA95,idx_Cum_Norm_ROHR),Ther
mo_Data(idx_CA0:idx_CA95,idx_CA),0.05);
CA10=interp1(Thermo_Data(idx_CA0:idx_CA95,idx_Cum_Norm_ROHR),The
rmo_Data(idx_CA0:idx_CA95,idx_CA),0.1);
CA50=interp1(Thermo_Data(idx_CA0:idx_CA95,idx_Cum_Norm_ROHR),The
rmo_Data(idx_CA0:idx_CA95,idx_CA),0.5);
CA90=interp1(Thermo_Data(idx_CA0:idx_CA95,idx_Cum_Norm_ROHR),The
rmo_Data(idx_CA0:idx_CA95,idx_CA),0.90);

CA0=Thermo_Data(idx_CA0,idx_CA);
CA95=Thermo_Data(idx_CA95,idx_CA);

Combust_Duration=CA95-CA5;


Press_Max=max(Thermo_Data(:,idx_Press)); % Bar
Temp_Max_mean=max(Thermo_Data(:,idx_Temp));  % K
Temp_Max_max=max(Thermo_Data(:,idx_Max_Temp));  % K

%-----------------------------------------------------------------
-------------------------
%--------Ringing Intensity
%-----------------------------------------------------------------
-------------------------


[maxROHR,I]=max(Thermo_Data(:,idx_ROHR)); %finds max ROHR and
index at which this occurs
beta = 0.05;
dP=diff(Thermo_Data(:,idx_Press)*10^5);
```

```
[max_dp,I1]=max(dP);
[TempCylMax,idxTcylMax]=max(Thermo_Data(:,idx_Temp));
dt=((Thermo_Data(I1+1,idx_CA)-Thermo_Data(I1-
1,idx_CA))/2)*CA_to_S*1000;
MM=R_uni/(Thermo_Data(I1,idx_C_p)-Thermo_Data(I1,idx_C_v));
R_spec=R_uni/MM;
gamma_RI=Thermo_Data(I1,idx_gamma);

RI =
((1/(2*gamma_RI))*(((beta*(max_dp/1000)/dt)^2)/(Press_Max*10^5/1
000))...
          *sqrt(R_spec*gamma_RI*TempCylMax))/1000;  % MW/m^2,
pressure must be in Pa (it is from Main)

%-------------------------------------------------------------
-------------------------
%--------Calculate Emissions in g/kW-hr
%-------------------------------------------------------------
-------------------------


IC8H18_mass=Exhaust_Data(idx_EVO,idx_IC8H18); % Mass (kg)
Isooctane
NC7H16_mass=Exhaust_Data(idx_EVO,idx_NC7H16); % Mass (kg) N-
Heptane
C5H10_2_mass=Exhaust_Data(idx_EVO,idx_C5H10_2); % Fuel Component
C6H5CH3_mass=Exhaust_Data(idx_EVO,idx_C6H5CH3); % Fuel Component
CO_mass=Exhaust_Data(idx_EVO,idx_CO);
CO2_mass=Exhaust_Data(idx_EVO,idx_CO2);
O2_mass=Exhaust_Data(idx_EVO,idx_O2);
NOx_mass=Exhaust_Data(idx_EVO,idx_NO)+Exhaust_Data(idx_EVO,idx_N
O);
UHC_mass=IC8H18_mass+NC7H16_mass+C5H10_2_mass+C6H5CH3_mass; %
Mass (kg) unburned fuel



CO_gkwhr=CO_mass*1000/(Work*0.00027777777777778); % emissions in
grams/kw-hr

%CO_gkwhr=(CO_mass*1000*(RPM/2)*60)/(Work*30*60);  kg/cycle *
grams/kg *
%cycles/minute * minutes/hour / ( kj/cycle * cycles/minute *
minutes/hour
%==> grams/hour / (kj/hour)
```

```
% CO_gkwhr=CO_mass*1000/(Work/3600); % emissions in grams/kw-hr
===> 3.6 Mj
% = 1 kw*hr  ==> 1/3600*0.00277....


CO2_gkwhr=CO2_mass*1000/(Work*0.00027777777777778);
O2_gkwhr=O2_mass*1000/(Work*0.00027777777777778);
NOx_gkwhr=NOx_mass*1000/(Work*0.00027777777777778);
UHC_gkwhr=UHC_mass*1000/(Work*0.00027777777777778); % Mass
unburned fuel



%-------------------------------------------------------------------
-------------------------
%--------Saving Traces in Excell
%-------------------------------------------------------------------
-------------------------


Excell_Output_Trace={'Crank Angle', 'Pressure Ave', 'Pressure
Max', 'Pressure Min', 'Temperature Ave',...
    'Temperature Max', 'Temperature Min', 'Volume', 'Mass',
'Density', 'Cumulative ROHR', 'ROHR', 'C_p',...
    'C_v', 'Gamma', 'Kinematic Viscosity', 'Dynamic Viscosity',
'Normalized Cumulative ROHR','NOx';...
    'Degrees',  'Bar', 'Bar', 'Bar', 'Kelvin', 'Kelvin',
'Kelvin', 'm^3', 'kg', 'kg/m^3',...
    'J', 'J/Degree',  'J/kg-K', 'J/kg-K', '-', 'm^2/s', 'm^2/s',
'-','-'};

for i=1:Thermo_Matrix_Size(1)
    for j=1:18
        Excell_Output_Trace(i+3,j)={Thermo_Data(i,j)};
    end
end

for i=1:Thermo_Matrix_Size(1)

Excell_Output_Trace(i+3,19)={Exhaust_Data(i,idx_NO)+Exhaust_Data
(i,idx_NO2)};
end

Output_FileName=['Analysis.xls'];
TEST = xlswrite(Output_FileName, Excell_Output_Trace,
'Final_Trace_Data', 'A1');
```

```
%-------------------------------------------------------------------
-------------------------
%--------Saving Cycle Data in Excell
%-------------------------------------------------------------------
-------------------------

Excell_Output={'Intake Temperature', 'Intake
Pressure','Injection Timing','EGR','Torque', 'Power', 'Engine
Speed', 'IMEP',...
    'Injected Fuel Mass','Injection Duration','Aspirated Fuel
Mass','Total Fuel Mass', 'Injected Fraction','Equivalence
Ratio', 'Air-Fuel Ratio','Unburned Fuel',...
    'O2', 'CO', 'CO2', 'NOx','UHC','O2', 'CO', 'CO2', 'NOx',...
    'Efficiency', 'CA5', 'CA10', 'CA50', 'CA90', 'CA95',
'Combustion Duration', 'Ringing Intensity', 'Maximum Cylinder
Pressure',...
    'Maximum Cylinder Temperature','Maximum Average Cylinder
Temperature','Blow By','IVC Temperature', 'IVC Pressure',
'Exhaust Temperature',...
    'Exhaust Pressure', 'EVO Temperature', 'EVO
Pressure','Intake Isooctane','Intake O2','Intake N2','Intake
H20','Intake CO2','Intake N-Heptane','Intake C5H10_2','Intake
C6H5CH3',...
    'Exhaust O2', 'Exhaust N2', 'Exhaust H2O', 'Exhaust CO2';
'K', 'Bar', 'dADTC','%','N*m',  'kW','RPM', 'bar',
'kg','CAD','kg','kg', '-', '-','-','Mass Fraction','Mass
Fraction','Mass Fraction', 'Mass Fraction',...
    'Mass Fraction','g/kW-hr','g/kW-hr','g/kW-hr','g/kW-
hr','g/kW-hr','-
','Degrees','Degrees','Degrees','Degrees','Degrees','Degrees','M
W/m^2','Bar','K','K','%','K', 'Bar', 'K', 'Bar', 'K', 'Bar',...
    '-','-','-','-','-','-','-','-','-','-','-','-'};



Exhaust_Temp=EVO_Temp;
Exhaust_Press=EVO_Press;

line_num=1;

Excell_Output(3,line_num)={Intake_Temp};
line_num=line_num+1;
Excell_Output(3,line_num)={Intake_Press};
line_num=line_num+1;
Excell_Output(3,line_num)={Inject_Timing};
```

```
line_num=line_num+1;
Excell_Output(3,line_num)={EGR};
line_num=line_num+1;
Excell_Output(3,line_num)={Torque};
line_num=line_num+1;
Excell_Output(3,line_num)={Power};
line_num=line_num+1;
Excell_Output(3,line_num)={RPM};
line_num=line_num+1;
Excell_Output(3,line_num)={IMEP};
line_num=line_num+1;
Excell_Output(3,line_num)={Injected_Mass};
line_num=line_num+1;
Excell_Output(3,line_num)={Inject_Duration};
line_num=line_num+1;
Excell_Output(3,line_num)={Aspirated_Fuel};
line_num=line_num+1;
Excell_Output(3,line_num)={Fuel};
line_num=line_num+1;
Excell_Output(3,line_num)={Injected_Fraction};
line_num=line_num+1;
Excell_Output(3,line_num)={Equivalence_Ratio};
line_num=line_num+1;
Excell_Output(3,line_num)={AFR};
line_num=line_num+1;
Excell_Output(3,line_num)={UHC};
line_num=line_num+1;
Excell_Output(3,line_num)={O2};
line_num=line_num+1;
Excell_Output(3,line_num)={CO};
line_num=line_num+1;
Excell_Output(3,line_num)={CO2};
line_num=line_num+1;
Excell_Output(3,line_num)={NOx};
line_num=line_num+1;
Excell_Output(3,line_num)={UHC_gkwhr};
line_num=line_num+1;
Excell_Output(3,line_num)={O2_gkwhr};
line_num=line_num+1;
Excell_Output(3,line_num)={CO_gkwhr};
line_num=line_num+1;
Excell_Output(3,line_num)={CO2_gkwhr};
line_num=line_num+1;
Excell_Output(3,line_num)={NOx_gkwhr};
line_num=line_num+1;
Excell_Output(3,line_num)={Efficiency};
line_num=line_num+1;
```

```
Excell_Output(3,line_num)={CA5};
line_num=line_num+1;
Excell_Output(3,line_num)={CA10};
line_num=line_num+1;
Excell_Output(3,line_num)={CA50};
line_num=line_num+1;
Excell_Output(3,line_num)={CA90};
line_num=line_num+1;
Excell_Output(3,line_num)={CA95};
line_num=line_num+1;
Excell_Output(3,line_num)={Combust_Duration};
line_num=line_num+1;
Excell_Output(3,line_num)={RI};
line_num=line_num+1;
Excell_Output(3,line_num)={Press_Max};
line_num=line_num+1;
Excell_Output(3,line_num)={Temp_Max_max};
line_num=line_num+1;
Excell_Output(3,line_num)={Temp_Max_mean};
line_num=line_num+1;
Excell_Output(3,line_num)={Blow_By};
line_num=line_num+1;
Excell_Output(3,line_num)={IVC_Temp};
line_num=line_num+1;
Excell_Output(3,line_num)={IVC_Press};
line_num=line_num+1;
Excell_Output(3,line_num)={Exhaust_Temp};
line_num=line_num+1;
Excell_Output(3,line_num)={Exhaust_Press};
line_num=line_num+1;
Excell_Output(3,line_num)={EVO_Temp};
line_num=line_num+1;
Excell_Output(3,line_num)={EVO_Press};
line_num=line_num+1;
Excell_Output(3,line_num)={Int_Iso_Oct};
line_num=line_num+1;
Excell_Output(3,line_num)={Int_O2};
line_num=line_num+1;
Excell_Output(3,line_num)={Int_N2};
line_num=line_num+1;
Excell_Output(3,line_num)={Int_H2O};
line_num=line_num+1;
Excell_Output(3,line_num)={Int_CO2};
line_num=line_num+1;
Excell_Output(3,line_num)={Int_N_Hept};
line_num=line_num+1;
Excell_Output(3,line_num)={Int_C5H10_2};
```

```
line_num=line_num+1;
Excell_Output(3,line_num)={Int_C6H5CH3};
line_num=line_num+1;
Excell_Output(3,line_num)={Exhaust_O2};
line_num=line_num+1;
Excell_Output(3,line_num)={Exhaust_O2};
line_num=line_num+1;
Excell_Output(3,line_num)={Exhaust_H2O};
line_num=line_num+1;
Excell_Output(3,line_num)={Exhaust_CO2};



Output_FileName=['Transient.xls'];
TEST = xlswrite(Output_FileName, Excell_Output,
'Final_Transient_Data', 'A1');

end
```

"List_of_folders_Converge.m"

```
A=fopen('Input_file_folders.dat','w');
List_of_Folders=dir;
Rows=size(List_of_Folders);
for i=1:Rows
    if List_of_Folders(i,1).isdir
        test=List_of_Folders(i,1).name=='.';
        if ~test(1)
            folder_line=List_of_Folders(i,1).name;
            fprintf(A,'%s\n',folder_line);
        end
    end
end
fclose('all');
```

"Run_all_calculations_Converge.m"

```
clear all
close all
clc
```

```
filename = 'Input_file_folders.dat';
delimiter = '';
formatSpec = '%s%[^\n\r]';
fileID = fopen(filename,'r');
dataArray = textscan(fileID, formatSpec, 'Delimiter', delimiter,
'ReturnOnError', false);
fclose(fileID);
folders = dataArray{:, 1};
clearvars filename delimiter formatSpec fileID dataArray ans;

for i=1:length(folders)
    cd(folders{i})
    disp('Calculation of folder')
    disp(folders(i))
    Main_Converge_Function1()
    cd ..

end
fclose('all');
```

"Summ_Single_Case_Converge.m"

```
function Excell_Output=Summ_Single_Case(input)
i_FileWithNames = fopen('Input_file_names.txt','r');
i_snap_no=0;
while 1
     c_single_line=fgetl(i_FileWithNames);
     if ~ischar(c_single_line)
        break
     end
     i_snap_no=i_snap_no+1;
     i_InFileLength=length(c_single_line);
     Excell_File_Name=[c_single_line(1:(i_InFileLength-4)),
'_Analysis.xls'];
     [Values_Thermo(i_snap_no,:),
Labels_Thermo]=xlsread(Excell_File_Name,'Final_Transient_Data');
%      [Values_ROHR_TMP,
Labels_ROHR_TEMP]=xlsread(Excell_File_Name,'ROHR_analysis');
%      Values_ROHR(i_snap_no,:)=Values_ROHR_TMP(1,:);
```

```
%
Labels_ROHR=Labels_ROHR_TEMP(1:2,2:size(Labels_ROHR_TEMP,2));
     FileLabel(i_snap_no)={c_single_line(1:(i_InFileLength-
13))};
end

for i_loop_2=1:size(Values_Thermo,1)
    Excell_Output(2+i_loop_2,1)=FileLabel(i_loop_2);
end

for i_loop_1=1:(size(Values_Thermo,2))
   Excell_Output(1,i_loop_1+1)=Labels_Thermo(1,i_loop_1);
   Excell_Output(2,i_loop_1+1)=Labels_Thermo(2,i_loop_1);
   for i_loop_2=1:size(Values_Thermo,1)

Excell_Output(2+i_loop_2,i_loop_1+1)={Values_Thermo(i_loop_2,i_l
oop_1)};
   end
end
% for i_loop_1=1:(size(Values_ROHR,2))
%
Excell_Output(1,i_loop_1+1+size(Values_Thermo,2))=Labels_ROHR(1,
i_loop_1);
%
Excell_Output(2,i_loop_1+1+size(Values_Thermo,2))=Labels_ROHR(2,
i_loop_1);
%    for i_loop_2=1:size(Values_ROHR,1)
%
Excell_Output(2+i_loop_2,i_loop_1+1+size(Values_Thermo,2))={Valu
es_ROHR(i_loop_2,i_loop_1)};
%     end
% end

fclose(i_FileWithNames);
```

“Summing_up_of_Excell_Files_Converge.m”

```
clear all
close all
clc
```

```
filename = 'Input_file_folders.dat';
delimiter = '';
formatSpec = '%s%[^\n\r]';
fileID = fopen(filename,'r');
dataArray = textscan(fileID, formatSpec, 'Delimiter', delimiter,
'ReturnOnError', false);
fclose(fileID);
folders = dataArray{:, 1};
clearvars filename delimiter formatSpec fileID dataArray ans;

for i=1:length(folders)
    cd(folders{i})
    disp('Calculation of folder')
    disp(folders(i))
    Excell_File_Name=['Transient.xls'];
    [Values_Thermo(i,:),
Labels_Thermo]=xlsread(Excell_File_Name,'Final_Transient_Data');
    FileLabel(i)={folders{i}};
    Excell_Output(2+i,1)=FileLabel(i);


    if i==1
        for i_loop_1=1:(size(Labels_Thermo,2))

Excell_Output(1,i_loop_1+1)=Labels_Thermo(1,i_loop_1);

Excell_Output(2,i_loop_1+1)=Labels_Thermo(2,i_loop_1);
        end
    end

    for j=1:size(Values_Thermo,2)
                Excell_Output(2+i,j+1)={Values_Thermo(i,j)};
    end

    cd ..

end
TEST = xlswrite('Trace_Data_summ', Excell_Output, 'All_results',
'A2');

fclose('all');
clear all
```

Appendix 3:

Halterman CARB LEV III E10 Certification Fuel Regular Octane Specifications Sheet

haltermannsolutions

Product Information

Telephone: (800) 969-2542 **FAX: (281) 457-1469**

Johann Haltermann Ltd.

PRODUCT: CARB LEV III E10 Certification Fuel Regular Octane

PRODUCT CODE: HF0892

Batch No.: BC0621GP01

Tank No.: 58

Date: 3/20/2013

TEST	METHOD	UNITS	SPECIFICATIONS			RESULTS
			MIN	TARGET	MAX	
Distillation - IBP	ASTM D86	°F				106
5%		°F				132
10%		°F	130		150	138
20%		°F				145
30%		°F				151
40%		°F				166
50%		°F	205		215	215
60%		°F				241
70%		°F				264
80%		°F				290
90%		°F	310		320	317
95%		°F				329
Distillation - EP		°F			390	349
Recovery		vol %		Report		97.5
Residue		vol %			2.0	1.0
Loss		vol %		Report		1.5
Gravity @ 60° F	ASTM D4052	°API		Report		57.6
Specific Gravity	ASTM D4052	-		Report		0.7483
Reid Vapor Pressure	ASTM D5191	psi	6.9		7.2	7.2
Carbon	ASTM D5291	wt%		Report		82.60
Hydrogen	ASTM D5291	wt%		Report		13.74
Hydrogen/Carbon ratio	ASTM D5291	mole/mole		Report		1.982
Oxygen	ASTM D4815	wt %	3.3		3.7	3.7
Ethanol content	ASTM D4815	vol %	9.8		10.2	10.0
MTBE content	ASTM D4815	vol %			0.05	None detected
Sulfur	ASTM D5453	ppm wt	8		11	10
Phosphorus	ASTM D3231	g/gal			0.005	None detected
Lead	ASTM D3237	g/gal			0.01	None detected
Composition, aromatics	ASTM D5580	vol %	19.5		22.5	22.5
Composition, olefins	ASTM D6550	vol %	4.0		6.0	5.7
Multisubstituted Alkyl Aromatics	ASTM D5769	vol %	13		15	14
Benzene	ASTM D5580	vol %	0.6		0.8	0.8
Oxidation Stability	ASTM D525	minutes	1000			1000+
Copper Corrosion	ASTM D130				1	1a
Existent gum, washed	ASTM D381	mg/100mls			3.0	<0.5
Existent gum, unwashed	ASTM D381	mg/100mls		Report		18.5
Research Octane Number	ASTM D2699			Report		91.0
Motor Octane Number	ASTM D2700			Report		83.4
R+M/2	D2699/2700		87.0		88.4	87.2
Sensitivity	D2699/2700		7.5			7.6
Net Heat of Combustion	ASTM D240	BTU/lb		Report		18024
Deposit Control Additive	Calculated	ptb active		75		75

APPROVED BY: